ADHESION MOLECULES AND AUTOIMMUNE DISEASES

EDITED BY: Hao Sun, Frederic Lagarrigue, Zhichao Fan and Jianfeng Chen
PUBLISHED IN: Frontiers in Immunology

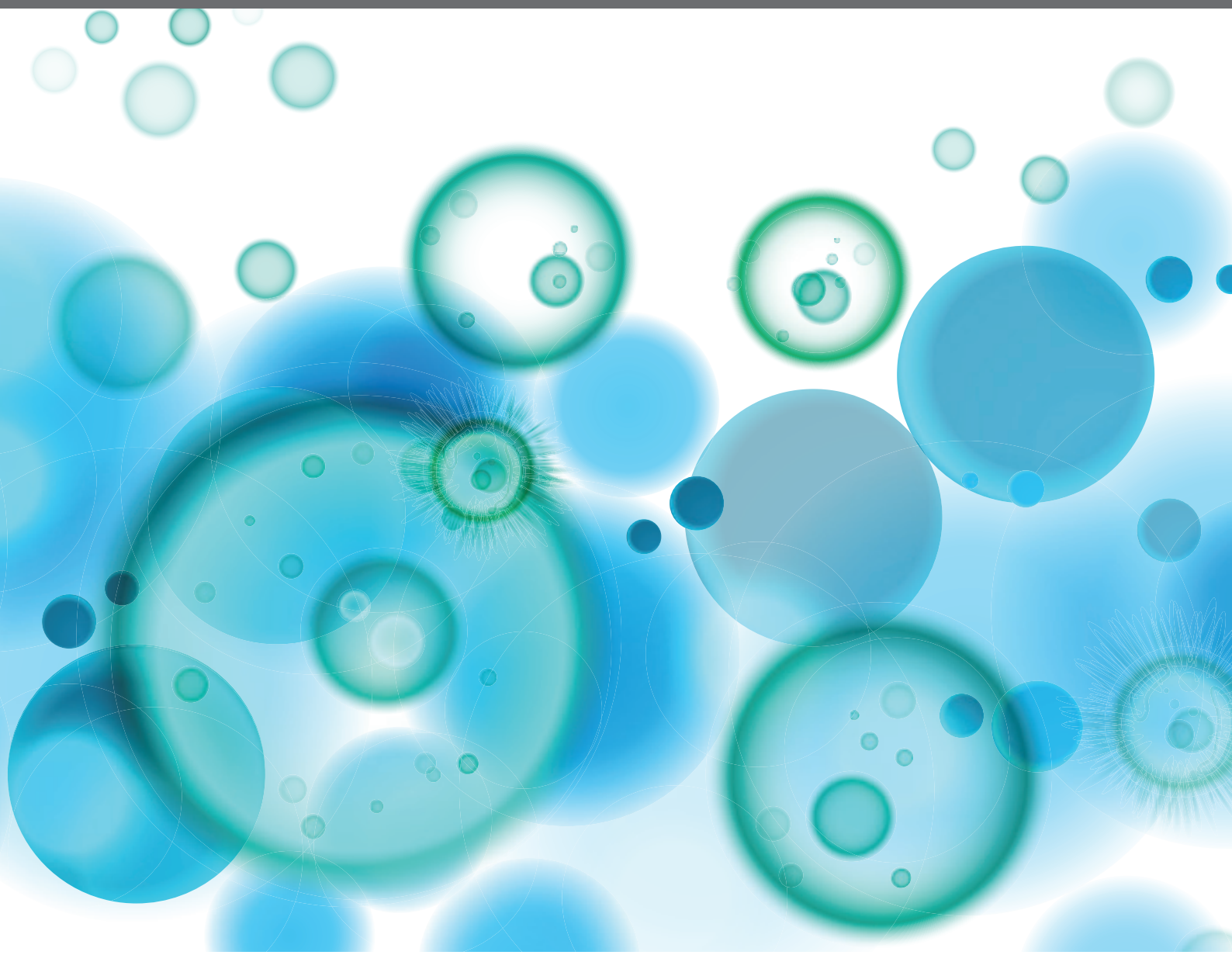

frontiers Research Topics

frontiers

ISSN 1664-8714
ISBN 978-2-88976-996-4
DOI 10.3389/978-2-88976-996-4

About Frontiers

Frontiers is more than just an open-access publisher of scholarly articles: it is a pioneering approach to the world of academia, radically improving the way scholarly research is managed. The grand vision of Frontiers is a world where all people have an equal opportunity to seek, share and generate knowledge. Frontiers provides immediate and permanent online open access to all its publications, but this alone is not enough to realize our grand goals.

Frontiers Journal Series

The Frontiers Journal Series is a multi-tier and interdisciplinary set of open-access, online journals, promising a paradigm shift from the current review, selection and dissemination processes in academic publishing. All Frontiers journals are driven by researchers for researchers; therefore, they constitute a service to the scholarly community. At the same time, the Frontiers Journal Series operates on a revolutionary invention, the tiered publishing system, initially addressing specific communities of scholars, and gradually climbing up to broader public understanding, thus serving the interests of the lay society, too.

Dedication to Quality

Each Frontiers article is a landmark of the highest quality, thanks to genuinely collaborative interactions between authors and review editors, who include some of the world's best academicians. Research must be certified by peers before entering a stream of knowledge that may eventually reach the public - and shape society; therefore, Frontiers only applies the most rigorous and unbiased reviews.
Frontiers revolutionizes research publishing by freely delivering the most outstanding research, evaluated with no bias from both the academic and social point of view. By applying the most advanced information technologies, Frontiers is catapulting scholarly publishing into a new generation.

What are Frontiers Research Topics?

Frontiers Research Topics are very popular trademarks of the Frontiers Journals Series: they are collections of at least ten articles, all centered on a particular subject. With their unique mix of varied contributions from Original Research to Review Articles, Frontiers Research Topics unify the most influential researchers, the latest key findings and historical advances in a hot research area! Find out more on how to host your own Frontiers Research Topic or contribute to one as an author by contacting the Frontiers Editorial Office: frontiersin.org/about/contact

ADHESION MOLECULES AND AUTOIMMUNE DISEASES

Topic Editors:
Hao Sun, University of California, San Diego, United States
Frederic Lagarrigue, UMR5089 Institut de Pharmacologie et de Biologie Structurale (IPBS), France
Zhichao Fan, UCONN Health, United States
Jianfeng Chen, Shanghai Institute of Biochemistry and Cell Biology, Chinese Academy of Sciences (CAS), China

Citation: Sun, H., Lagarrigue, F., Fan, Z., Chen, J., eds. (2022). Adhesion Molecules and Autoimmune Diseases. Lausanne: Frontiers Media SA.
doi: 10.3389/978-2-88976-996-4

Table of Contents

frontiers | Frontiers in Immunology

TYPE Editorial
PUBLISHED 18 August 2022
DOI 10.3389/fimmu.2022.1009708

OPEN ACCESS

EDITED BY
Yoshishige Miyabe,
St. Marianna University School of Medicine, Japan

REVIEWED BY
Tadashi Hosoya,
Tokyo Medical and Dental University, Japan

*CORRESPONDENCE
Hao Sun
has073@ucsd.edu
Zhichao Fan
zfan@uchc.edu

SPECIALTY SECTION
This article was submitted to Autoimmune and Autoinflammatory Disorders: Autoinflammatory Disorders, a section of the journal Frontiers in Immunology

RECEIVED 02 August 2022
ACCEPTED 08 August 2022
PUBLISHED 18 August 2022

CITATION
Fan Z and Sun H (2022) Editorial: Adhesion molecules and autoimmune diseases.
Front. Immunol. 13:1009708.
doi: 10.3389/fimmu.2022.1009708

Editorial: Adhesion molecules and autoimmune diseases

Zhichao Fan[1]* and Hao Sun[2]*

[1]Department of Immunology, School of Medicine, UConn Health, Farmington, CT, United States, [2]Department of Medicine, University of California San Diego, La Jolla, CA, United States

KEYWORDS

adhesion molecules, integrin, autoimmune diseases, migration, recruitment

Editorial on the Research Topic
Adhesion molecules and autoimmune diseases

A large number of associations proceed between immune cells and the endothelium, extracellular matrix, and tissue during the development of autoimmune diseases. These interactions are mediated by adhesion molecules that promote leukocyte adhesion and extravasation from the blood into inflamed tissues. Immune cell activation and trafficking to the site of inflammation depend on their adhesion molecules' interaction with the ligands expressed on other immune cells or the extracellular matrix. Leukocyte adhesion molecules, such as integrins, immunoglobulin superfamily, cadherins and selectins, play key roles in modulating these vital life processes. Integrins, in particular, play critical roles in regulating all aspects of immune cell function, including leukocyte activation, homing, circulation, transendothelial migration, and proliferation.

The Frontiers Research Topic "Adhesion Molecules and Autoimmune Diseases" highlights 10 recent studies that investigate the function of the adhesion molecules, regulation of immune cell adhesion, trafficking and recruitment, and characterization of adhesion receptors in autoimmune diseases.

Integrin activation in leukocytes is a central event in many leukocyte processes. Leukocyte integrins are key elements for both innate and adaptive immune responses, which have emerged as promising therapeutic targets for patients with inflammation and autoimmune diseases. Among them, β2 integrins have attracted more and more attention as a therapeutic target for autoimmune diseases. An antibody (Efalizumab) that blocks the interaction between β2 integrins and ligands has shown significant efficacy in autoimmune psoriasis. However, Efalizumab was withdrawn later due to JC virus reactivation in some patients; therefore, better understanding the roles of β2 integrins may help guide more effective therapeutics. In a comprehensive overview, Carla Guenther (1) depicted the role of β2 integrins in leukocyte recruitment. This review summarized the involvement of β2 integrins in the migration of each type of leukocyte with a view on signaling, what mode of migration has been described in which context, and their binding partners. In an original research article, Casteel et al. (2) proposed a potential mechanism that regulates macrophage functions in inflamed tissue mediated by integrin αDβ2. Carboxyethylpyrrole (CEP), which is the end-product produced by

oxidation of DHA, modifies proteins serving as novel adhesion factors for integrin αDβ2. This also applies to primary ligands for αDβ2 and has potential implications for leukocyte recruitment during inflammation/oxidation.

Recently, much attention has been drawn to the miRNAs in the progression of autoimmune diseases. MicroRNAs (miRNAs) are small non-coding RNAs that modulating gene expression. Various miRNA genes are expressed in immune cells and other inflammatory cells in patients with rheumatoid arthritis (RA) and systemic lupus erythematosus (SLE). The research article by Chang et al. (3) highlights the role of Apelin in RA by connecting it to angiogenesis. Apelin increased Ang1 expression and facilitated Ang1-dependent EPC angiogenesis by suppressing miR-525-5p synthesis *via* PLCγ and PKCα signaling. This provides a new therapeutic target for the treatment of RA. Along the same line, a recent study by Yang et al. (4) evaluated the role of miR-4512 in SLE. The abnormal down-regulation of miR-4512 found in monocytes and macrophages in SLE patients promotes the formation of SLE neutrophil extracellular traps by reducing the targeted inhibition of CXCL2 and TLR4. In addition, this study further validated the therapeutic effect of CXCL2 in animal models of SLE, suggesting that chemokines and cytokines – which regulate the recruitment, survival, expansion, and effector function of lymphocytes in autoimmunity – play pivotal roles in the pathogenesis of autoimmune diseases. This particular topic of the importance of chemokines and cytokines is emphasized in the research article by Feng et al. (5), which focused on the IL-35 single nucleotide polymorphism (SNP) in two types of non-infectious uveitis, including Behçet's disease (BD) and Vogt-Koyanagi-Harada (VKH) syndrome. Their findings suggest that uveitis may be the result of the interaction between the genetic and immune environments, which may provide a new basis for the diagnosis and treatment. In another original work, Huang et al. (6) focused on the relationship between autoimmune thyroiditis (AIT), a chronic disorder that leads to immunological abnormalities, and infertility. They collected follicular fluids from 122 patients and found that IFN-γ levels were significantly elevated in the follicular fluids of patients who concomitantly had AIT. The increased IFN-γ led to the production of CXCL9/10/11 by primary granulosa cells and subsequent enrichment of CXCR3+ T cells in the follicular fluids.

In the report on children with an anti-neutrophil cytoplasmic antibody (ANCA)-associated vasculitis (AAV), Yang et al. (7) collected the clinical data from 48 patients and analyzed the potential parameters related to the remission-induction treatment response and progression. The majority of patients had microscopic polyangiitis (MPA) and the presence of myeloperoxidase (MPO)-ANCA. The observations by Ye et al. (8) on digital spatial profiling of individual glomeruli from patients with ANCA-associated glomerulonephritis are very intriguing, which identified mRNA and protein profiles in the individual glomeruli affected differently by the disease processes. The authors use spatial profiling to attempt to determine the mechanism behind Bowman's capsule rupture and the immune cells that may be present and contribute to the underlying pathology that causes the crescent formation and Bowman's capsule rupture.

The TIM family proteins recognize phosphatidylserine (PS) and play a critical role in the regulation of immune responses, including autoimmunity, allergy, asthma, tolerance in transplantation, and tumorigenesis. In the last twenty years, increasing evidence has indicated that the function of TIMs correlates with susceptibility and development of multiple autoimmune diseases, while the underlying molecular mechanism remains unclear. Liu Y et al. (9) discuss the potential function of TIMs in typical autoimmune diseases, including multiple sclerosis (MS), RA, SLE, and type 1 diabetes (T1D). As a better understanding of the molecular function of Tim proteins is important for the improvement in diagnosis and therapeutics of autoimmune diseases, this minireview is expected to be of high interest to the audience. In an article focusing on the pathogenesis of RA, Chen et al. (10) illustrated the central role of HAPLN1 function in promoting proliferation and pro-inflammatory phenotype of RA-FLSs, which in turn could contribute to RA pathogenesis, suggesting that HAPLN1 may be utilized as a diagnostic marker and therapeutic target.

In general, the Research Topic investigates the regulatory roles and molecular mechanisms of adhesion molecules in autoimmune diseases. We would like to thank all the authors for entrusting us with their discoveries, and all the referees for their careful and insightful review. We believe that all the articles included in the topic will be of interest to all researchers studying the role of adhesion molecules in autoimmune diseases and will make them aware of how a clearer understanding of these mechanisms can inform treatment and diagnosis.

Author contributions

ZF and HS conceived the idea, designed and edited the manuscript. All authors listed have approved the work for publication.

Funding

This work was supported by the Crohn's & Colitis Foundation Career Development Award 902590 (H.S.), and HL145454 (Z.C.F.).

Acknowledgments

We would like to thank the authors, reviewers, and editors for their essential contribution to this exciting and unexplored Research Topic, as well as of the members of the Frontiers in Immunology Editorial Office. We acknowledge Dr. Geneva

Hargis from UConn Health School of Medicine for their help in the scientific writing and editing of this manuscript.

Conflict of interest

The authors declare that the research was conducted in the absence of any commercial or financial relationships that could be construed as a potential conflict of interest.

Publisher's note

References

1. Guenther C. beta2-integrins - regulatory and executive bridges in the signaling network controlling leukocyte trafficking and migration. *Front Immunol* (2022) 13:809590. doi: 10.3389/fimmu.2022.809590

2. Casteel JL, Keever KR, Ardell CL, Williams DL, Gao D, Podrez EA, et al. Modification of extracellular matrix by the product of DHA oxidation switches macrophage adhesion patterns and promotes retention of macrophages during chronic inflammation. *Front Immunol* (2022) 13:867082. doi: 10.3389/fimmu.2022.867082

3. Chang TK, Zhong YH, Liu SC, Huang CC, Tsai CH, Lee HP, et al. Apelin promotes endothelial progenitor cell angiogenesis in rheumatoid arthritis disease *via* the miR-525-5p/Angiopoietin-1 pathway. *Front Immunol* (2021) 12:737990. doi: 10.3389/fimmu.2021.737990

4. Yang B, Huang X, Xu S, Li L, Wu W, Dai Y, et al. Decreased miR-4512 levels in monocytes and macrophages of individuals with systemic lupus erythematosus contribute to innate immune activation and neutrsophil NETosis by targeting TLR4 and CXCL2. *Front Immunol* (2021) 12:756825. doi: 10.3389/fimmu.2021.756825

5. Feng M, Zhou S, Liu T, Yu Y, Su Q, Li X, et al. Association between interleukin 35 gene single nucleotide polymorphisms and the uveitis immune status in a Chinese han population. *Front Immunol* (2021) 12:758554. doi: 10.3389/fimmu.2021.758554

6. Huang N, Liu D, Lian Y, Chi H, Qiao J. Immunological microenvironment alterations in follicles of patients with autoimmune thyroiditis. *Front Immunol* (2021) 12:770852. doi: 10.3389/fimmu.2021.770852

7. Yang J, Yang Y, Xu Y, Zhou L, Yin X, Pu J, et al. Clinical and renal histology findings and different responses to induction treatment affecting the long-term renal outcomes of children with ANCA-associated vasculitis: A single-center cohort analysis. *Front Immunol* (2022) 13:857813. doi: 10.3389/fimmu.2022.857813

8. Ye L, Liu Y, Zhu X, Duan T, Wang C, Fu X, et al. Digital spatial profiling of individual glomeruli from patients with anti-neutrophil cytoplasmic autoantibody-associated glomerulonephritis. *Front Immunol* (2022) 13:831253. doi: 10.3389/fimmu.2022.831253

9. Liu Y, Chen H, Chen Z, Qiu J, Pang H, Zhou Z. Novel roles of the Tim family in immune regulation and autoimmune diseases. *Front Immunol* (2021) 12:748787. doi: 10.3389/fimmu.2021.748787

10. Chen Y, Wang B, Wu Q, Lai WF, Wei L, Nandakumar KS, et al. HAPLN1 affects cell viability and promotes the pro-inflammatory phenotype of fibroblast-like synoviocytes. *Front Immunol* (2022) 13:888612. doi: 10.3389/fimmu.2022.888612

frontiers in Immunology

REVIEW
published: 17 September 2021
doi: 10.3389/fimmu.2021.748787

Novel Roles of the Tim Family in Immune Regulation and Autoimmune Diseases

*Yikai Liu, Hongzhi Chen, Zhiying Chen, Junlin Qiu, Haipeng Pang and Zhiguang Zhou**

National Clinical Research Center for Metabolic Diseases, Key Laboratory of Diabetes Immunology, Ministry of Education, and Department of Metabolism and Endocrinology, The Second Xiangya Hospital of Central South University, Changsha, China

T cell Ig and mucin domain (Tim) protein family members were identified to be important regulators of the immune response. As their name indicates, Tim proteins were originally considered a T cell-specific markers, and they mainly regulate the responses of T helper cells. However, accumulating evidence indicates that Tims are also expressed on antigen-presenting cells (APCs), such as monocytes, macrophages, dendritic cells (DCs) and B cells, and even plays various roles in natural killer cells (NKs) and mast cells. In recent years, the expression and function of Tims on different cells and the identification of new ligands for the Tim family have suggested that the Tim family plays a crucial role in immune regulation. In addition, the relationship between Tim family gene polymorphisms and susceptibility to several autoimmune diseases has expanded our knowledge of the role of Tim proteins in immune regulation. In this review, we discuss how the Tim family affects immunomodulatory function and the potential role of the Tim family in typical autoimmune diseases, including multiple sclerosis (MS), rheumatoid arthritis (RA), systemic lupus erythematosus (SLE) and type 1 diabetes (T1D). A deeper understanding of the immunoregulatory mechanism of the Tim family might provide new insights into the clinical diagnosis and treatment of autoimmune diseases.

Keywords: Tim, autoimmune diseases, multiple sclerosis, rheumatoid arthritis, systemic lupus erythematosus, type 1 diabetes

OPEN ACCESS

Edited by:
Zhichao Fan,
UCONN Health, United States

Reviewed by:
Yi Zhang,
Fudan University, China
Bo Liu,
Institut Pasteur of Shanghai (CAS), China

***Correspondence:**
Zhiguang Zhou
zhouzhiguang@csu.edu.cn

Specialty section:
This article was submitted to Autoimmune and Autoinflammatory Disorders, a section of the journal Frontiers in Immunology

Received: *28 July 2021*
Accepted: *02 September 2021*
Published: *17 September 2021*

Citation:
Liu Y, Chen H, Chen Z, Qiu J, Pang H and Zhou Z (2021) Novel Roles of the Tim Family in Immune Regulation and Autoimmune Diseases. Front. Immunol. 12:748787. doi: 10.3389/fimmu.2021.748787

INTRODUCTION

Autoimmune diseases are characterized by abnormal tolerance to self-antigens that cause damage to body tissues (1). The etiology of autoimmune diseases is multifactorial and includes infection, environment and genetics (2–6). Most of these factors have been reported to be associated with immune disorders. Therefore, a better understanding of autoimmune disease pathogenesis is needed to identify better treatments.

T cell Ig and mucin domain (Tim), a transmembrane glycoprotein, has been identified as one of the three human Tim family members (Tim-1, Tim-3, and Tim-4) that play a key role in regulating immunity in conditions such as allergies, asthma, virus infection and transplant tolerance (7–11). In the immune system, Tim-1 has been reported to be preferentially expressed on T helper type 2 (Th2) cells, where it serves as an effective costimulatory molecule for T cell activation (12). Tim-3 was first identified as being expressed on interferon-γ (IFN-γ)-producing Th1 cells. As an inhibitor of inflammatory Th1 cells, Tim-3 interacts with its ligand to cause the death of Th1 cells, thereby reducing IFN-γ production (13). Tim-4 is a natural ligand of Tim-1. Tim-4 is mainly expressed on antigen-presenting cells (APCs), but not on T cells (14), and it participates in autoimmune diseases by regulating the proliferation of T cells (15). However, in recent studies, Tims were shown to be expressed on other immune cell types, such as macrophages, dendritic cells (DCs), natural killer cells (NKs) and B cells (16–19), and may play a critical role in maintaining immune homeostasis. These findings allow us to improve our knowledge of the role of Tims in the immune system. In this review, we focus on the expression and function of Tims on different immune cells, discuss recent studies examining the role of Tims in autoimmune diseases in both animal models and humans, and provide useful insights into the identification of new therapeutic targets.

THE EXPRESSION AND FUNCTION OF TIMS ON DIFFERENT CELL TYPES

Since the discovery of Tims in 2001, major progress has been achieved in terms of elucidating their characteristics and immunological functions (**Table 1**). In mice, the Tim family is composed of eight members (Tim-1 to Tim-8), and the genes that encode them are located on chromosome 11B1.1. In humans, three members (Tim-1, Tim-3, and Tim-4) have been identified, and the genes are located on chromosome 5q33.2 (**Figure 1**) (20). These three human Tim genes are most homologous to mouse Tim-1, Tim-3 and Tim-4, which are associated with allergic diseases. All Tim molecules are type I glycosylated proteins. Tim proteins contain an IgV domain, a mucin domain, a transmembrane domain, and an intracellular domain (**Figure 2**). Tim-1 and Tim-3 contain a tyrosine phosphorylation motif in the intracellular domain. Tim-3 has the shortest mucin domain and fewest predicted glycosylation sites. Tim-4 differs from the other family members, and it contains a short intracellular tail without a tyrosine phosphorylation motif. In addition, Tim-4 possesses an

TABLE 1 | Known features of the Tim family.

Molecule	Expressing cells	Ligand(s)	Function	Disease	Ref
Tim-1	Activated Th2 cells, Bregs	Tim-4 PS	Costimulation of T cell activation, modulation of Treg function, maintenance and induction of Bregs	Autoimmune diseases, infection, asthma, allergy	(12, 20)
Tim-3	Th1 cells, innate immune cells	Gal-9 HMGB1 Ceacam1 PS	Suppression of the Th1 response, increased activation of signaling pathways leading to T cell activation	Autoimmune diseases, infection, cancer	(13, 21)
Tim-4	APCs	Tim-1 PS	Regulation of T cell proliferation, clearance of apoptotic cells	Autoimmune diseases, chronic metabolic disease, infection, allergy	(15, 22)

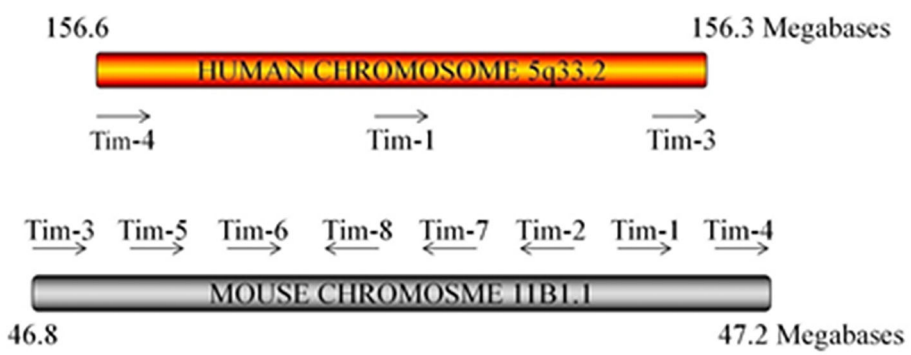

FIGURE 1 | Tim locus. The arrangement of the three Tim genes on human chromosome 5 and the 8 Tim genes on mouse chromosome 11 is shown. Mouse Tim-5–8 are predicted genes. The arrow indicates the direction of mRNA transcription.

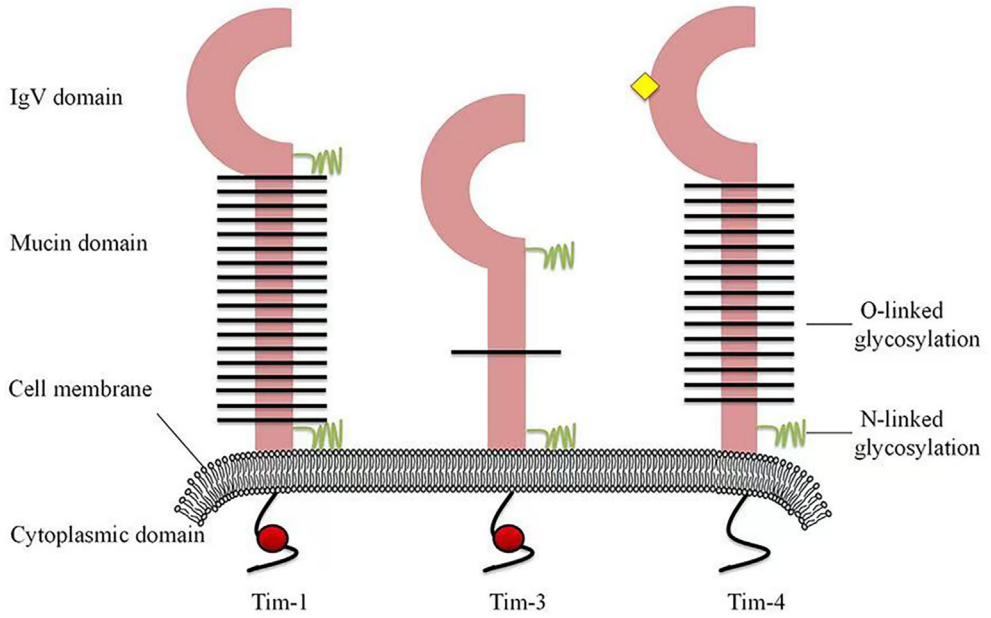

FIGURE 2 | Structures of human Tim family members. Tim proteins contain an IgV domain, a mucin domain, a transmembrane domain and an intracellular domain. Tim-3 has the shortest mucin domain and fewest predicted glycosylated site of the Tims. Tim-4 contains an arginine-glycine-aspartic acid (RGD) motif (yellow diamond), which is present in many ligands that bind to integrins. However, Tim-4 has no tyrosine phosphorylation site (red circle).

arginine-glycine-aspartic acid (RGD) motif, which is present in many ligands that bind to integrins (20). Therefore, Tim-4 may also act as a decoy receptor. Variations in the structures and motifs of Tim family members indicate that individual Tim proteins may have different roles in signal transduction.

Tim-1

The expression of Tim-1, also known as kidney injury molecule-1 (Kim-1), is highly upregulated on the surface of injured kidney epithelial cells (23). Its expression is increased in urine samples from patients with chronic kidney disease (24). Tim-1 has been used as a biomarker to assess the degree of injury in individuals with acute tubular necrosis. In addition to its role in kidney injury, Tim-1 was also detected in African green monkey kidney cells (6) and later identified in humans as a cellular receptor for hepatitis A virus, called HAVCR-1 (25).

Interestingly, Tim-1 is present on activated but not naive $CD4^+$ T cells. Moreover, it is preferentially expressed on activated Th2 cells, but not Th1 cells (12). Tim-1 is a highly effective costimulatory molecule that promotes the formation of T cell receptors (TCRs) through agonistic anti-Tim-1 antibodies, which increase the proliferation of $CD4^+$ T cells (12). According to recent studies, Tim-1 has a dual function as a T cell costimulator; it positively or negatively costimulates the T cell response according to the way it engages with T cells during T cell activation (26). Researchers tested a series of monoclonal antibodies (mAbs) against Tim-1 and identified two antibodies targeting Tim-1 that display distinct effects. One agonistic mAb (3B3) increases the production of the proinflammatory cytokines IFN-γ and IL-17, increasing the severity of experimental autoimmune encephalomyelitis (EAE). In contrast, the antagonistic mAb RMT1-10 inhibits IFN-γ and IL-17 production, alleviates the development of autoimmunity (26).

In addition to exerting regulatory effects on Th cells, Tim-1 is also vital for the function and development of regulatory T cells (Tregs). The anti-Tim-1 mAb 3B3 reduces forkhead box protein P3 (Foxp3) expression, prevents effector T cells (Teffs) from differentiating into Tregs and regulates the suppressive ability of Tregs, thereby preventing transplantation tolerance in mice (11). Tim-1 signaling in B cells plays an important role in maintaining the stability of the immune system and inhibiting autoimmune diseases. Recently, researchers generated Tim-1-mutant [Tim-1 (Δmucin)] mice. Notably, the ability of regulatory B cells (Bregs) to produce IL-10 was compromised in these mutant mice (27). B cells with defective Tim-1 or Tim-1 mutations show reduced IL-10 production and increased production of proinflammatory cytokines (28). Based on these studies, Tim-1 expressed in B cells participates in suppressing immune rejection. Other studies have also found that the expression of Tim-3 and Tim-1 on the surface of mouse mast cells promotes the secretion of the inflammatory factors IL-13, IL-6 and IL-4 (29). Thus, Tim-1 plays wide-ranging roles in various cells to regulate the immune system.

Tim-3

Tim-3 was first reported to be expressed on IFN-γ-producing Th1 cells (21). Binding of Tim-3 to its ligand terminates Th1 immune responses, and Tim-3 expression is regulated by the transcription factor T-bet (30). Human Tim-3 shares 63% amino acid homology with mouse Tim-3. Mouse Tim-3 consists of 281

amino acid residues, while its human homolog consists of 302 amino acid residues (31). The membrane-bound form of Tim-3 includes an N-terminal IgV domain, a mucin domain, a transmembrane domain and a short cytoplasmic tail.

To date, Tim-3 expression has been detected on both innate and adaptive immune cells, such as DCs (32), mast cells (29), macrophages (33), NK cells (34), and $CD4^+$ T and $CD8^+$ T cells (35). In addition, Tim-3 may be expressed on Th17 cells, although at lower levels than in Th1 cells (36). Subsequently, Tim-3 was also shown to be expressed on Tregs and participate in immune regulation (37). The differential expression of Tim-3 on both innate and adaptive immune cells suggests that Tim-3 exerts different effects on the functions of these cells. In a published study, an anti-Tim-3 Ab was used to block Tim-3 signaling in a mouse model of autoimmune heart disease. The decreased expression of Tim-3 and CD80 on mast cells and macrophages reduces the level of cytotoxic T lymphocyte-associated protein 4 (CTLA-4) on the surface of $CD4^+$ T cells, resulting in a decrease in the number of Treg cells and aggravated myocarditis (38). These studies indicate that the Tim-3 signaling pathway affects the adaptive immune system by influencing the innate immune system.

Tim-4

Tim-4 contains an extracellular IgV domain, a glycosylated mucin domain and an intracellular tail, and it is mainly expressed on APCs, including DCs, NKT cells, B1 cells and macrophages (22).

According to the current knowledge of Tim-4, the interaction between Tim-4 and its ligand plays an important role in the initiation of Th2 polarization. In DCs exposed to cholera toxin (CT) or/and peanut extract (PE), Tim-4 expression is increased and participates in triggering specific Th2 polarization and intestinal allergies (39, 40). Tim-4 is a natural ligand for Tim-1, and emerging evidence suggests that the binding of Tim-1 to Tim-4 is involved in regulating T cell proliferation (41). Interestingly, the dose of Tim-4 is very important for the fate of T cells. High doses of Tim-4 promote T cell proliferation, while low doses exert the opposite effect. The explanation for these effects may be that Tim-4 binds unknown ligands with higher affinity than Tim-1 on T cells, transmitting negative signals. Alternatively, the interaction of Tim-1-Tim-4 may transmit a negative signal at a lower ligand density, similar to the agonist-antagonist phenomenon observed when peptide ligands are changed, and this inhibition is reversed by higher Tim-4 concentrations (41, 42). Another study showed that Tim-4 inhibits the activation of naive rather than activated T cells. Since Tim-1 is not expressed on naive T cells, the inhibitory effect of Tim-4 may depend on unknown ligands other than Tim-1. Thus, Tim-4 has at least two types of ligands: one that promotes T cell activation and another that inhibits T cell activation. These results suggested that Tim-4 might regulate T cell depending on the activation status of T cells, probably by binding different ligands (14). A recent study reported that Tim-4 inhibits the production of nitric oxide (NO) and cytokines in LPS-treated macrophages by inhibiting the nuclear factor kappa B (NF-κB) pathway or janus activating kinase 2 (Jak2)/signal transducer and activator of transcription 1 (STAT1) signaling (43). In summary, Tim-4 is expressed on different cell types and plays various roles in regulating immunity.

THE LIGANDS OF TIMS

Published studies have shown that the soluble Tim-4-Ig fusion protein specifically binds to Tim-1-transfected cells, while the soluble Tim-1-Ig fusion protein also specifically binds to Tim-4-transfected cells. These studies confirm the interaction between Tim-4 and Tim-1. In addition, Tim-4-Ig binds to activated T cells that express Tim-1 at high levels, and this binding is blocked by anti-Tim antibodies. Thus, Tim-4 is indeed the natural ligand of Tim-1 (41). Another study showed that Tim-4 binds to (phosphatidylserine) PS exposed on the surface of apoptotic cells. Hence, PS was identified as another ligand of Tim-4 (44). However, a recent study failed to detect a direct interaction between Tim-1 and Tim-4 (45). Miyanishi et al. showed that Ba/F3 B cells expressing Tim-1 or Tim-4 bind to exosomes through PS. PS is present on the surface of exosomes and is involved in signal transduction between cells (44). This finding indicates that the Tim-1-Tim-4 interaction occurs through the PS bridge. Therefore, the interaction between Tim-1 and Tim-4 is indirect.

Adequate research has confirmed that Galectin-9 (Gal-9) is recognized as a ligand of Tim-3. It binds to the carbohydrate structure of the IgV domain of Tim-3, which contains two N-glycosylation sites. The interaction between Gal-9 and Tim-3 triggers the death of Th1 cells, thereby inhibiting tissue inflammation and inhibiting the progression of EAE (13). Carcinoembryonic antigen cell adhesion molecule 1 (Ceacam1), with a molecular weight of 60 kDa, was recently characterized as another candidate Tim-3 ligand that binds to the Tim-3 IgV domain (46). Ceacam1 is expressed on activated T cells and involved in T cell suppression (47). Tim-3 and Ceacam1 are coexpressed and form a heterodimer. This coexpression is necessary for the inhibitory function of Tim-3. Ceacam1 forms heterodimer interactions in cis or in trans through its N-terminal domains, and both cis and trans interactions between Ceacam1 and Tim-3 affect the immune tolerance of T cells (46). In addition, high-mobility group box 1 (HMGB1) and PS have also been identified as Tim-3 ligands. HMGB1 is mainly related to inhibition of the innate immune response, while PS is related to the clearance of apoptotic cells (48, 49). An understanding of how these ligands coordinate their interactions with Tim-3 and regulate immunity is important.

As discussed above, PS has been identified as a ligand of Tim-4. The crystal structure of Tim-4 showed that the CC' and FG loops in the IgV domain of Tim-4 create a narrow cavity. A metal ion-dependent ligand binding site (MILIBS) is specifically responsible for the recognition of PS (50). The hydrophilic head of PS penetrates into the MILIBS, its acidic phosphate group is coordinated with metal ions, and the fatty acid tail of PS interacts with the aromatic residues of the FG loop. The hydrophobic residues in the FG loop are essential for PS recognition (51). The single deletion of aromatic residues in

the FG loop reduces the binding of the Tim protein to PS in liposomes by approximately 70%, while the double mutation completely eliminates PS binding (50).

In addition, PS is a phospholipid present on dying cells and is a typical "eat me" signal. Tim-4 specifically bind to PS exposed on the surface of apoptotic bodies (AB) *via* the IgV domain, and then mediate engulfment by macrophages (44). Effective clearance of apoptotic bodies maintains normal tissue homeostasis in organisms. The blockade of Tim-4 binding to PS leads to deficient clearance of apoptotic cells and results in systemic autoimmunity.

TIM FAMILY IN AUTOIMMUNE DISEASE

The Tim family plays an important role in regulating immunity. The Tim family has also been reported to exert immunomodulatory effects on many autoimmune diseases. Here, we use multiple sclerosis (MS), rheumatoid arthritis (RA), systemic lupus erythematosus (SLE) and type 1 diabetes (T1D) as examples to summarize the roles of the Tim family in autoimmune diseases (summarized in **Table 2**).

The Signaling Pathway of Tims

Tim-1 antibodies were used to identify the signaling pathway by which Tim-1 activates T cells. Overexpression of Tim-1 leads to nuclear factor of activated T-cells (NFAT)/activatorprotein-1 (AP-1) transcriptional activation, which depends on Y276 in the cytoplasmic tail of Tim-1 (63). In addition, Tim-1 is recruited to the TCR signaling complex in human T cells through its interaction with CD3. The increase in signaling events related to TCRs include the phosphorylation of Zap70 and IL-2 inducible T cell kinase (ITK). In addition, ITK and phosphoinositide 3-kinase (PI3K) complexes are recruited to the TCR signaling complex (64). After a tyrosine in Tim-1 is phosphorylated in a Lck-dependent manner, the p85 linker subunit of PI3K is directly recruited, leading to PI3K activation (65). Based on these studies, Tim-1-mediated T cell activation may require PI3K activation.

Tim-3 was identified as specifically expressed on the surface of $CD4^+$ and $CD8^+$ T cells. Studies have found that the tyrosine residues in the cytoplasmic region of Tim-3 are related to T cell signaling (31). When Tim-3 does not bind to its ligand, Tyr256/Tyr263 in the cytoplasmic region of Tim-3 interacts with HLA-B associated transcript 3 (Bat3), and Bat3 recruits the tyrosine kinases Lck to maintains T cell activation (66). However, when Tim-3 binds to the Gal-9, the phosphorylation of Tyr256 and Tyr263 is triggered by ITK (67), then releases Bat3 from Tim-3 and inhibits the T cell signaling by tyrosine kinase Fyn recruitment (68).

Tim-4 has been shown to increase the levels of p-extracellular regulated kinase (ERK) 1/2 and p-Akt in $CD3^+$ T cells by cross-linking with Tim-1. Treatment of naive T cells with inhibitory Tim-4-Ig reduces the phosphorylation of linker for activation of T cells (LAT) and ERK 1/2 (14). In addition, Tim-4 inhibits the mitogen-activated protein kinase (MAPK) pathway in T cells.

In summary, Tim proteins participate in the regulation of many signaling pathways, most of which are related to the pathogenesis of autoimmune diseases. Therefore, an understanding of the role of Tims in different autoimmune diseases and their possible signaling pathways and mechanisms will provide new insights to improve immunotherapy. However, the mechanisms by which Tims regulate autoimmune diseases through these signaling pathways are not yet fully understood, and more research is needed to achieve continuous improvements before clinical treatment.

Tims and MS

Most evidence for the roles of Tims in autoimmune diseases has been derived from studies of mouse EAE models. The findings from these studies enable us to understand the effect of

TABLE 2 | Studies examining the roles of Tim family members in autoimmune diseases.

Tim	Autoimmune disease	Conclusion	Ref
Tim-1	MS	Tim-$1^{-/-}$ B cell mice developed more severe EAE. Transfer of Tim-1^+ B cells reduced the severity of EAE in mice.	(28)
	RA	A polymorphism in the Tim-1 gene was related to RA in a Chinese Hui population, and a polymorphism of the Tim-1 promoter region may be related to the susceptibility to RA in Korean populations.	(52, 53)
	SLE	Tim-1 expression in PBMCs was increased in patients with SLE compared with healthy controls and was positively correlated with IL-10 expression.	(54)
	T1D	The numbers of Tim-1^+ Tregs and Tim-4^+ Tregs in patients with T1D and NOD mice were significantly reduced.	(55)
Tim-3	MS	Tim-3 expression in PBMCs from patients with MS helped predict the prognosis of the disease. Higher Tim-3 expression was associated with a better prognosis than lower Tim-3 expression.	(56)
	RA	Increased expression of Tim-3 in peripheral blood T cells from patients with RA was negatively correlated with the DAS28 and plasma TNF-α levels.	(57)
	SLE	The expression of Tim-3 and Gal-9 in T cells was increased in patients with SLE compared with healthy controls.	(58)
	T1D	In mice treated with a Gal-9 plasmid, inflammation of the pancreatic islets was reduced, and the number of Th1 cells was significantly reduced.	(59)
Tim-4	MS	Tim-4 has been shown to play a critical role in the T cell-mediated immune response.	(14, 60)
	RA	Increased expression of Tim-3 in peripheral blood T cells from patients with RA was negatively correlated with the DAS28 and plasma TNF-α levels.	(61)
	SLE	The Tim-4 mRNA was expressed at significantly higher levels in PBMCs from patients with SLE than in PBMCs from healthy controls and was positively correlated with Tim-1 mRNA and serum TNF-α levels.	(62)
	T1D	The numbers of Tim-1^+ Tregs and Tim-4^+ Tregs in patients with T1D and NOD mice were significantly reduced.	(55)

autoimmune pathology, especially regarding the T cell inflammatory response in the central nervous system (CNS) (69). MS is an autoimmune disease characterized by inflammation of the white matter in the CNS. This disease most commonly affects the white matter around the ventricle, optic nerve, spinal cord, brain stem and cerebellum (70). EAE is a mouse model of MS. The pathogenesis of EAE is similar to that of MS, which provides new insights into the pathology of MS.

Xiao showed that a Tim-1 deficiency in B lymphocytes disrupts the balance between regulatory and proinflammatory cytokines in B cells. Mice with Tim-$1^{-/-}$ B cells exhibit an enhanced pathogenic Th1/Th17 response, a decreased number of $Foxp3^+$ Tregs and reduced IL-10 expression in CNS-derived T cells, resulting in a worse EAE clinical score (28). In addition, the adoptive transfer of Tim-1+ B cells not only alleviates EAE in wild-type mice but also decreases the severity of EAE in the Tim-$1^{-/-}$ B cell mouse model, showing that Tim-1 is associated with the severity of EAE by regulating the balance between pathogenic T cells and protective Tregs. Tim-4 has been shown to play a critical role in the T cell-mediated immune response. On the one hand, treatment with a Tim-4 blocking antibody *in vivo* reduces the T cell-mediated inflammatory response produced in EAE mice (14). On the other hand, the Tim-4-Fc fusion protein inhibits the activation of naive T cells *in vitro* by inhibiting the activation of the MAPK pathway, inhibits the differentiation of Th17 cells and prevents IL-17 production. Notably, the inhibitory effect of the Tim-4-Fc fusion protein is independent of Tim-1 and requires IgV and mucin domains (60). Based on these studies, Tim-4 has a bimodal regulatory function that depends on the activation status of T cells: an inhibitory effect of Tim-4 on naive T cells and a positive regulatory effect on activated T cells.

Tim-3 is expressed on $CD4^+$ Th1 cells that secrete IFN-γ (21). It also ameliorates the symptoms of EAE by inducing the death of pathogenic Th1 cells, and inhibition of Tim-3 aggravates the symptoms of EAE. The expression of both Gal-9 and Tim-3 on Th1 cells *in vitro* induces Th1 cell death and ameliorates EAE (13). During the induction of EAE, the administration of Gal-9 *in vivo* reduces T cell proliferation and IFN-γ production, changes related to reductions in disease morbidity and mortality. In contrast, inhibition of Gal-9 *in vivo* with an siRNA exacerbates the development of EAE. Dysregulation of Tim-3 expression in MS has been reported in clinical studies. Koguchi et al. studied $CD4^+$ T cell clones isolated from the CSF of patients with MS. Compared with $CD4^+$ T cells from healthy controls, $CD4^+$ T cells from patients with MS express lower levels of Tim-3 and produce more IFN-γ (71). Tim-3 signaling also induces the death of specific $CD8^+$ T cells, and the use of Tim-3-blocking antibodies exacerbates $CD8^+$ T cell-mediated EAE (72). Yang et al. examined Tim-3 function on $CD4^+$ T cells isolated from the circulatory system of healthy controls and patients with MS. Blocking Tim-3 during T cell stimulation significantly promotes the secretion of IFN-γ in healthy controls. Tim-3 inhibition has no effect on treated patients, suggesting that patients with MS have defects in Tim-3-mediated immunoregulation (73). According to recent studies, the expression levels of Tim-3 on peripheral blood mononuclear cells (PBMCs) from patients with MS help predict the prognosis of the disease. Lower expression levels of Tim-3 on PBMCs are associated with an increased possibility of progression to secondary progressive multiple sclerosis (SPMS), while higher Tim-3 expression levels on PBMCs are associated with a benign prognosis 10 years later (56).

Tims and RA

RA is a systemic inflammatory autoimmune disease characterized by joint pain and swelling. In severe cases, it can lead to joint deformities and loss of function (74). RA affects 0.5–1% of the adult population and is more common in women (75). Although the pathogenesis of RA remains elusive, multiple factors are widely accepted to be involved. Genetic, environmental and hormonal factors may all contribute to the pathogenesis of RA (76, 77).

Recently, polymorphisms in Tim genes were reported to be potential risk factors for RA. Xu et al. reported that Tim-1 (-1637A>G, -232A>G), Tim-3 (-1541C>T, +4259G>T) and Tim-4 (SNP rs7700944) gene polymorphisms are related to RA susceptibility in the Chinese Hui population (52, 78, 79). Similar results were also reported for other national populations (53, 80). Tim-4 is involved in the immunoregulation of collagen-induced arthritis (CIA), and it exhibits dual functions, depending on the phase of CIA. During the induction phase, treatment with anti-Tim-4 monoclonal antibodies exacerbates the development of CIA in mice. In contrast, during the effector phase, treatment with anti-Tim-4 monoclonal antibodies reduces proinflammatory cytokine levels in the ankle joint, significantly inhibiting the progression of CIA (61).

Tim-3 may be a potential new marker for assessing the severity of RA. The expression levels of Tim-3 on PBMCs from patients with RA have been reported. Liu et al. showed increased expression of Tim-3 on peripheral blood $CD4^+$ T cells, $CD8^+$ T cells, NKT cells and monocytes from patients with RA. The percentage of Tim-3^+ cells is negatively correlated with the 28-joint disease activity score (DAS28) and plasma tumor necrosis factor alpha (TNF-α) levels (57). In another study, Tim-3 expression on $CD4^+$ and $CD8^+$ T cells was shown to be negatively correlated with the progression of RA (81). In addition, the number of Tim-3^+ $Foxp3^+$ Tregs is decreased in patients with RA and is negatively correlated with RA disease activity (82). Based on accumulating evidence, the Tim-3-Gal-9 pathway may play an essential role in the induction and development of RA, and it may be a clinical target for the treatment and alleviation of RA. In an animal model, treatment with Gal-9 was shown to induce naive T cells to differentiate into Tregs, not only reducing the production of proinflammatory cytokines in mouse joints but also decreasing the number of Tim-3^+ $CD4^+$ T cells in the peripheral blood (83). In a clinical study, significantly higher Gal-9 expression in several T cell subsets and plasma was observed in patients with RA than in healthy controls. After 12 weeks of treatment with a calcineurin inhibitor, Gal-9 expression levels in individuals with a good therapeutic response were significantly lower than in

those with a poor therapeutic response (84). Tim-3 is considered a useful biomarker for determining disease activity and progression. However, the current knowledge on Tim-3-targeted therapy for RA is still limited, and more studies in humans are required to provide further evidence (85).

Tims and SLE

SLE is an autoimmune disease with diverse clinical manifestations involving multiple organs. Its etiology is unclear, and it is related to various factors, including genetic, immune, and hormonal factors (86–89).

Lupus nephritis is the main risk factor for the overall morbidity and mortality of SLE and is related to the dysregulation of Th1 and Th2 responses (90). Tim-1 has an important role in regulating the Th1/Th2 response (91). Studies of mouse models of nephritis have suggested that when an inhibitory anti-Tim-1 antibody (RMT1-10) is administered to mice with nephritis, $Foxp3^+$ T cells accumulate in the mice, and the expression of the IL-10 mRNA increases. RMT1-10 treatment reduces the urinary excretion and renal expression of Tim-1, reflecting an alleviation of interstitial injury (92). Previous studies have suggested that patients with SLE show increased expression of Tim-1 in PBMCs compared with healthy people, and Tim-1 expression is positively correlated with IL-10 expression. Moreover, this study also found significantly increased levels of the Tim-1 mRNA in patients with active SLE (SLE disease activity index (SLEDAI)>6), which indicates that Tim-1 mRNA expression in PBMCs is related to the disease activity of patients with SLE (54). Interestingly, in another study, researchers found that the mRNA expression levels of Tim-4 and Tim-1 were positively correlated in patients with SLE, but this correlation was not obvious in healthy controls. However, the authors failed to detect a significant difference in the Tim-1 mRNA expression levels between patients with SLE and healthy controls. This difference may be due to the distinctive SLEDAI of the subjects participating in each study (62). In summary, unlike other Tim molecules, research on the role of Tim-1 in SLE is still limited, and more research is needed to explore this protein in the future.

Th1 and Th17 immune dysregulation is one of the causes of SLE (93). Tim-3 was initially identified on activated Th1 and Th17 cells and induced T cell death after binding to its ligand, Gal-9 (94). Jiao et al. investigated the expression of Tim-3 and Gal-9 in patients with SLE and healthy controls. The expression of Tim-3 and Gal-9 on various T cells (including $CD4^+$ T cells, $CD8^+$ T cells, and $CD56^+$ T cells) was significantly higher in patients with SLE than in healthy controls (58). Another study indicated that the plasma level of soluble Tim-3 (sTim-3) was increased in patients with SLE and positively correlated with anti-dsDNA antibodies, SLEDAI score, erythrocyte sedimentation rate (ESR), and urine albumin levels (95). All these studies illustrated that Tim-3 is potentially useful as an effective biomarker for evaluating indicators of SLE disease activity.

Similar to RA, insufficient clearance of AB is also a cause of SLE. If ABs are not engulfed by macrophages or DCs, the antigens and harmful substances from ABs will trigger an immune response, thereby promoting the progression of SLE (96, 97). The elimination of ABs is a key mechanism for maintaining normal tissue homeostasis in multicellular organisms. Tim-4 binds to PS and exposes it on the surface of ABs, presenting a signal to macrophages to trigger engulfment. Tim-4 mediates the clearance of ABs by macrophages. The mechanism of apoptotic cell phagocytosis is as follows: Ba/F3 transformants expressing the Tim-4 complex and integrin $\alpha(v)\beta$ (3) bind to and phagocytose apoptotic cells in the presence of milk fat globular epidermal growth factor VIII (MFG-E8) (98). A recent study showed that mice lacking Tim-4 or MFG-E8 rarely develop antibodies (99). In contrast, mice lacking both Tim-4 and MFG-E8 produce high levels of anti-dsDNA antibodies, indicating that Tim-4 and MFG-E8 mediates the clearance of apoptotic bodies, and involved in pathogenesis of SLE (15). In a human study, Zhao et al. observed significantly higher Tim-4 mRNA levels in the PBMCs from patients with SLE, especially those in the active phase of the disease, than those in healthy controls. Moreover, the level of the Tim-4 mRNA in PBMCs from patients with SLE positively correlated with the expression of the Tim-1 mRNA and serum TNF-α levels (62). Overexpressed Tim-4 may bind to Tim-1 and promote a Th2-mediated immune response, especially in patients with SLE. TNF-α is mainly secreted by activated macrophages and may induce an increase in Tim-4 expression, thereby promoting the proliferation of Th2 cells by binding to Tim-1. These findings imply that Tim-4 exerts a regulatory function in the pathogenesis of SLE.

Tims and T1D

T1D is a chronic autoimmune disease that is mainly caused by the destruction of islet β cells mediated by T lymphocytes (100). Due to the continuous destruction of insulin-producing islet β cells, insulin deficiency and hyperglycemia occur. Patients with an uncontrolled disease may suffer from ketoacidosis, which can be life-threatening (101). Noninsulin-based treatment strategies, such as delaying β cell failure, stem cell treatment, and islet transplantation, would be optimal to ameliorate T1D in patients and prevent its complications (102–104).

Research by Shimokawa confirmed that $CD8^+$ Tregs are essential for preventing autoimmune diabetes. Notably, compared with healthy individuals, patients with T1D have fewer $CD8^+$ Tregs (105). Tim-1 and Tim-4 are considered essential for the activation and differentiation of T lymphocytes. Guo et al. evaluated the expression of Tim-1 and Tim-4 in Tregs and found that the numbers of $Tim\text{-}1^+$ Tregs and $Tim\text{-}4^+$ Tregs were significantly decreased in both patients with T1D and no obesity diabetes (NOD) mice (55).

The Tim-3 pathway represents an important mechanism for downregulating Th1-mediated autoimmune diseases and promoting the development of immune tolerance. A previous study showed that treating recipient mice with a Tim-3-specific monoclonal antibody accelerated the occurrence of autoimmune diabetes in an adoptive transfer NOD model. In addition, similar results were obtained when researchers treated recipient mice with the Tim-3-Ig fusion protein, which disrupts the integrity of the inhibitory interaction between Tim-3 and its ligand on T cells (106).

Blockade of the Tim-3 pathway accelerates diabetes in NOD mice. This effect may be mediated by inhibiting the immunosuppressive function of Tregs. Furthermore, Gal-9 was identified as a ligand for Tim-3 and shown to suppress the Th1 immune response in the development of T1D (107). Compared with control mice, NOD mice overexpressing the Gal-9 were significantly protected from T1D and showed less inflammation of pancreatic islets (59). Many studies have shown that the Tim-3 pathway is involved in Th1-mediated disease, and blocking the signaling by Tim-3 and its ligand Gal-9 may aggravate autoimmune diseases, including T1D (108).

CONCLUSIONS

Considerable progress has been achieved in understanding the expression and function of the Tim family in autoimmune diseases. Tim proteins are intimately involved in immunoregulation and participate in many diseases, such as allergies, infections, and cancers, by influencing the immune system. The data on the Tim family also provide us with insights into the design of selective targeted therapeutics. Clearly, the expression of Tim molecules is not limited to T cells, indicating that they perform different functions in a variety of cells to modulate immune responses. Emerging evidence suggests that Tim-1 has a potential role in the maintenance and regulation of Bregs. Tim-3 negatively regulates the response of Th1 cells and inhibits the production of inflammatory factors. Similarly, Tim-4 seems to play a positive role in clearing apoptotic cells and might participate in systemic autoimmune diseases. Therefore, future research on the Tim family is expected to provide new strategies for autoimmune treatment.

AUTHOR CONTRIBUTIONS

YL searched the references, wrote the first draft of the paper and revised the text. HC, ZC, JQ, and HP critically revised the text and provided substantial scientific contributions. ZZ proposed the project and revised the manuscript. All authors contributed to the article and approved the submitted version.

FUNDING

This study was supported by the National Natural Science Foundation of China (grant numbers 8181001262 and 81970746) and the Natural Science Foundation of China (grant number 82000748).

REFERENCES

1. Wang L, Wang FS, Gershwin ME. Human Autoimmune Diseases: A Comprehensive Update. *J Intern Med* (2015) 278(4):369–95. doi: 10.1111/joim.12395
2. Hemmer B, Kerschensteiner M, Korn T. Role of the Innate and Adaptive Immune Responses in the Course of Multiple Sclerosis. *Lancet Neurol* (2015) 14(4):406–19. doi: 10.1016/S1474-4422(14)70305-9
3. Mu Q, Zhang H, Luo XM. SLE: Another Autoimmune Disorder Influenced by Microbes and Diet? *Front Immunol* (2015) 6:608. doi: 10.3389/fimmu.2015.00608
4. Maria AT, Maumus M, Le Quellec A, Jorgensen C, Noël D, Guilpain P. Adipose-Derived Mesenchymal Stem Cells in Autoimmune Disorders: State of the Art and Perspectives for Systemic Sclerosis. *Clin Rev Allergy Immunol* (2017) 52(2):234–59. doi: 10.1007/s12016-016-8552-9
5. DiMeglio LA, Evans-Molina C, Oram RA. Type 1 Diabetes. *Lancet* (2018) 391(10138):2449–62. doi: 10.1016/S0140-6736(18)31320-5
6. Gilhus NE. Myasthenia Gravis. *N Engl J Med* (2016) 375(26):2570–81. doi: 10.1056/NEJMra1602678
7. Kuchroo VK, Dardalhon V, Xiao S, Anderson AC. New Roles for TIM Family Members in Immune Regulation. *Nat Rev Immunol* (2008) 8(8):577–80. doi: 10.1038/nri2366
8. Meyers JH, Sabatos CA, Chakravarti S, Kuchroo VK. The TIM Gene Family Regulates Autoimmune and Allergic Diseases. *Trends Mol Med* (2005) 11 (8):362–9. doi: 10.1016/j.molmed.2005.06.008
9. Sonar SS, Hsu YM, Conrad ML, Majeau GR, Kilic A, Garber E, et al. Antagonism of TIM-1 Blocks the Development of Disease in a Humanized Mouse Model of Allergic Asthma. *J Clin Invest* (2010) 120(8):2767–81. doi: 10.1172/JCI39543
10. Wang J, Qiao L, Hou Z, Luo G. TIM-1 Promotes Hepatitis C Virus Cell Attachment and Infection. *J Virol* (2017) 91(2):e01583–16. doi: 10.1128/JVI.01583-16
11. Degauque N, Mariat C, Kenny J, Zhang D, Gao W, Vu MD, et al. Immunostimulatory Tim-1-Specific Antibody Deprograms Tregs and Prevents Transplant Tolerance in Mice. *J Clin Invest* (2008) 118(2):735–41. doi: 10.1172/JCI32562
12. Umetsu SE, Lee W-L, McIntire JJ, Downey L, Sanjanwala B, Akbari O, et al. TIM-1 Induces T Cell Activation and Inhibits the Development of Peripheral Tolerance. *Nat Immunol* (2005) 6(5):447–54. doi: 10.1038/ni1186
13. Zhu C, Anderson AC, Schubart A, Xiong H, Imitola J, Khoury SJ, et al. The Tim-3 Ligand Galectin-9 Negatively Regulates T Helper Type 1 Immunity. *Nat Immunol* (2005) 6(12):1245–52. doi: 10.1038/ni1271
14. Mizui M, Shikina T, Arase H, Suzuki K, Yasui T, Rennert PD, et al. Bimodal Regulation of T Cell-Mediated Immune Responses by TIM-4. *Int Immunol* (2008) 20(5):695–708. doi: 10.1093/intimm/dxn029
15. Fang XY, Xu WD, Pan HF, Leng RX, Ye DQ. Novel Insights Into Tim-4 Function in Autoimmune Diseases. *Autoimmunity* (2015) 48(4):189–95. doi: 10.3109/08916934.2014.983266
16. Xiao S, Zhu B, Jin H, Zhu C, Umetsu DT, DeKruyff RH, et al. Tim-1 Stimulation of Dendritic Cells Regulates the Balance Between Effector and Regulatory T Cells. *Eur J Immunol* (2011) 41(6):1539–49. doi: 10.1002/eji.201040993
17. Yeung MY, Ding Q, Brooks CR, Xiao S, Workman CJ, Vignali DA, et al. TIM-1 Signaling Is Required for Maintenance and Induction of Regulatory B Cells. *Am J Transplant* (2015) 15(4):942–53. doi: 10.1111/ajt.13087
18. Hein RM, Woods ML. TIM-1 Regulates Macrophage Cytokine Production and B7 Family Member Expression. *Immunol Lett* (2007) 108(1):103–8. doi: 10.1016/j.imlet.2006.11.004
19. So EC, Khaladj-Ghom A, Ji Y, Amin J, Song Y, Burch E, et al. NK Cell Expression of Tim-3: First Impressions Matter. *Immunobiology* (2019) 224 (3):362–70. doi: 10.1016/j.imbio.2019.03.001
20. Kuchroo VK, Umetsu DT, DeKruyff RH, Freeman GJ. The TIM Gene Family: Emerging Roles in Immunity and Disease. *Nat Rev Immunol* (2003) 3(6):454–62. doi: 10.1038/nri1111
21. Monney L, Sabatos CA, Gaglia JL, Ryu A, Waldner H, Chernova T, et al. Th1-Specific Cell Surface Protein Tim-3 Regulates Macrophage Activation and Severity of an Autoimmune Disease. *Nature* (2002) 415(6871):536–41. doi: 10.1038/415536a
22. Liu W, Xu L, Liang X, Liu X, Zhao Y, Ma C, et al. Tim-4 in Health and Disease: Friend or Foe? *Front Immunol* (2020) 11:537. doi: 10.3389/fimmu.2020.00537

23. Ichimura T, Asseldonk EJPV, Humphreys BD, Gunaratnam L, Duffield JS, Bonventre JV. Kidney Injury Molecule-1 Is a Phosphatidylserine Receptor That Confers a Phagocytic Phenotype on Epithelial Cells. *J Clin Invest* (2008) 118(5):1657–68. doi: 10.1172/JCI34487
24. Nauta FL, Boertien WE, Bakker SJL, van Goor H, van Oeveren W, de Jong PE, et al. Glomerular and Tubular Damage Markers Are Elevated in Patients With Diabetes. *Diabetes Care* (2011) 34(4):975–81. doi: 10.2337/dc10-1545
25. Feigelstock D, Thompson P, Mattoo P, Zhang Y, Kaplan GG. The Human Homolog of HAVcr-1 Codes for a Hepatitis A Virus Cellular Receptor. *J Virol* (1998) 72(8):6621–8. doi: 10.1128/JVI.72.8.6621-6628.1998
26. Xiao S, Najafian N, Reddy J, Albin M, Zhu C, Jensen E, et al. Differential Engagement of Tim-1 During Activation can Positively or Negatively Costimulate T Cell Expansion and Effector Function. *J Exp Med* (2007) 204(7):1691–702. doi: 10.1084/jem.20062498
27. Xiao S, Brooks CR, Zhu C, Wu C, Sweere JM, Petecka S, et al. Defect in Regulatory B-Cell Function and Development of Systemic Autoimmunity in T-Cell Ig Mucin 1 (Tim-1) Mucin Domain-Mutant Mice. *Proc Natl Acad Sci USA* (2012) 109(30):12105–10. doi: 10.1073/pnas.1120914109
28. Xiao S, Brooks CR, Sobel RA, Kuchroo VK. Tim-1 Is Essential for Induction and Maintenance of IL-10 in Regulatory B Cells and Their Regulation of Tissue Inflammation. *J Immunol* (2015) 194(4):1602–8. doi: 10.4049/jimmunol.1402632
29. Nakae S, Iikura M, Suto H, Akiba H, Umetsu DT, Dekruyff RH, et al. TIM-1 and TIM-3 Enhancement of Th2 Cytokine Production by Mast Cells. *Blood* (2007) 110(7):2565–8. doi: 10.1182/blood-2006-11-058800
30. Anderson AC, Lord GM, Dardalhon V, Lee DH, Sabatos-Peyton CA, Glimcher LH, et al. T-Bet, A Th1 Transcription Factor Regulates the Expression of Tim-3. *Eur J Immunol* (2010) 40(3):859–66. doi: 10.1002/eji.200939842
31. Das M, Zhu C, Kuchroo VK. Tim-3 and Its Role in Regulating Anti-Tumor Immunity. *Immunol Rev* (2017) 276(1):97–111. doi: 10.1111/imr.12520
32. Anderson AC, Anderson DE, Bregoli L, Hastings WD, Kassam N, Lei C, et al. Promotion of Tissue Inflammation by the Immune Receptor Tim-3 Expressed on Innate Immune Cells. *Science (New York NY)* (2007) 318 (5853):1141–3. doi: 10.1126/science.1148536
33. Ocaña-Guzman R, Torre-Bouscoulet L, Sada-Ovalle I. TIM-3 Regulates Distinct Functions in Macrophages. *Front Immunol* (2016) 7:229. doi: 10.3389/fimmu.2016.00229
34. Tan S, Xu Y, Wang Z, Wang T, Du X, Song X, et al. Tim-3 Hampers Tumor Surveillance of Liver-Resident and Conventional NK Cells by Disrupting PI3K Signaling. *Cancer Res* (2020) 80(5):1130–42. doi: 10.1158/0008-5472.Can-19-2332
35. Hastings WD, Anderson DE, Kassam N, Koguchi K, Greenfield EA, Kent SC, et al. TIM-3 Is Expressed on Activated Human CD4+ T Cells and Regulates Th1 and Th17 Cytokines. *Eur J Immunol* (2009) 39(9):2492–501. doi: 10.1002/eji.200939274
36. Nakae S, Iwakura Y, Suto H, Galli SJ. Phenotypic Differences Between Th1 and Th17 Cells and Negative Regulation of Th1 Cell Differentiation by IL-17. *J leukocyte Biol* (2007) 81(5):1258–68. doi: 10.1189/jlb.1006610
37. Liu Z, McMichael EL, Shayan G, Li J, Chen K, Srivastava R, et al. Novel Effector Phenotype of Tim-3(+) Regulatory T Cells Leads to Enhanced Suppressive Function in Head and Neck Cancer Patients. *Clin Cancer Res* (2018) 24(18):4529–38. doi: 10.1158/1078-0432.CCR-17-1350
38. Frisancho-Kiss S, Nyland JF, Davis SE, Barrett MA, Gatewood SJ, Njoku DB, et al. Cutting Edge: T Cell Ig Mucin-3 Reduces Inflammatory Heart Disease by Increasing CTLA-4 During Innate Immunity. *J Immunol* (2006) 176 (11):6411–5. doi: 10.4049/jimmunol.176.11.6411
39. Yang PC, Xing Z, Berin CM, Soderholm JD, Feng BS, Wu L, et al. TIM-4 Expressed by Mucosal Dendritic Cells Plays a Critical Role in Food Antigen-Specific Th2 Differentiation and Intestinal Allergy. *Gastroenterology* (2007) 133(5):1522–33. doi: 10.1053/j.gastro.2007.08.006
40. Feng BS, Chen X, He SH, Zheng PY, Foster J, Xing Z, et al. Disruption of T-Cell Immunoglobulin and Mucin Domain Molecule (TIM)-1/TIM4 Interaction as a Therapeutic Strategy in a Dendritic Cell-Induced Peanut Allergy Model. *J Allergy Clin Immunol* (2008) 122(1):55–61, 61.e1-7. doi: 10.1016/j.jaci.2008.04.036
41. Meyers JH, Chakravarti S, Schlesinger D, Illes Z, Waldner H, Umetsu SE, et al. TIM-4 Is the Ligand for TIM-1, and the TIM-1-TIM-4 Interaction Regulates T Cell Proliferation. *Nat Immunol* (2005) 6(5):455–64. doi: 10.1038/ni1185
42. Racioppi L, Ronchese F, Matis LA, Germain RN. Peptide-Major Histocompatibility Complex Class II Complexes With Mixed Agonist/Antagonist Properties Provide Evidence for Ligand-Related Differences in T Cell Receptor-Dependent Intracellular Signaling. *J Exp Med* (1993) 177 (4):1047–60. doi: 10.1084/jem.177.4.1047
43. Xu LY, Qi JN, Liu X, Ma HX, Yuan W, Zhao PQ, et al. Tim-4 Inhibits NO Generation by Murine Macrophages. *PLoS One* (2015) 10(4):e0124771. doi: 10.1371/journal.pone.0124771
44. Miyanishi M, Tada K, Koike M, Uchiyama Y, Kitamura T, Nagata S. Identification of Tim4 as a Phosphatidylserine Receptor. *Nature* (2007) 450(7168):435–9. doi: 10.1038/nature06307
45. Sizing ID, Bailly V, McCoon P, Chang W, Rao S, Pablo L, et al. Epitope-Dependent Effect of Anti-Murine TIM-1 Monoclonal Antibodies on T Cell Activity and Lung Immune Responses. *J Immunol* (2007) 178(4):2249–61. doi: 10.4049/jimmunol.178.4.2249
46. Huang YH, Zhu C, Kondo Y, Anderson AC, Gandhi A, Russell A, et al. CEACAM1 Regulates TIM-3-Mediated Tolerance and Exhaustion. *Nature* (2015) 517(7534):386–90. doi: 10.1038/nature13848
47. Chen L, Chen Z, Baker K, Halvorsen EM, da Cunha AP, Flak MB, et al. The Short Isoform of the CEACAM1 Receptor in Intestinal T Cells Regulates Mucosal Immunity and Homeostasis via Tfh Cell Induction. *Immunity* (2012) 37(5):930–46. doi: 10.1016/j.immuni.2012.07.016
48. DeKruyff RH, Bu X, Ballesteros A, Santiago C, Chim YL, Lee HH, et al. T Cell/Transmembrane, Ig, and Mucin-3 Allelic Variants Differentially Recognize Phosphatidylserine and Mediate Phagocytosis of Apoptotic Cells. *J Immunol* (2010) 184(4):1918–30. doi: 10.4049/jimmunol.0903059
49. Tang D, Lotze MT. Tumor Immunity Times Out: TIM-3 and HMGB1. *Nat Immunol* (2012) 13(9):808–10. doi: 10.1038/ni.2396
50. Santiago C, Ballesteros A, Martínez-Muñoz L, Mellado M, Kaplan GG, Freeman GJ, et al. Structures of T Cell Immunoglobulin Mucin Protein 4 Show a Metal-Ion-Dependent Ligand Binding Site Where Phosphatidylserine Binds. *Immunity* (2007) 27(6):941–51. doi: 10.1016/j.immuni.2007.11.008
51. Kobayashi N, Karisola P, Peña-Cruz V, Dorfman DM, Jinushi M, Umetsu SE, et al. TIM-1 and TIM-4 Glycoproteins Bind Phosphatidylserine and Mediate Uptake of Apoptotic Cells. *Immunity* (2007) 27(6):927–40. doi: 10.1016/j.immuni.2007.11.011
52. Xu JR, Yang Y, Liu XM, Sun JY, Wang YJ. Polymorphisms of the TIM-1 Gene Are Associated With Rheumatoid Arthritis in the Chinese Hui Minority Ethnic Population. *Genet Mol Res GMR* (2012) 11(1):61–9. doi: 10.4238/2012.January.9.7
53. Chae SC, Park YR, Song JH, Shim SC, Yoon KS, Chung HT. The Polymorphisms of Tim-1 Promoter Region Are Associated With Rheumatoid Arthritis in a Korean Population. *Immunogenetics* (2005) 56 (10):696–701. doi: 10.1007/s00251-004-0743-5
54. Wang Y, Meng J, Wang X, Liu S, Shu Q, Gao L, et al. Expression of Human TIM-1 and TIM-3 on Lymphocytes From Systemic Lupus Erythematosus Patients. *Scand J Immunol* (2008) 67(1):63–70. doi: 10.1111/j.1365-3083.2007.02038.x
55. Guo H, Shen Y, Kong YH, Li S, Jiang R, Liu C, et al. The Expression of Tim-1 and Tim-4 Molecules in Regulatory T Cells in Type 1 Diabetes. *Endocrine* (2020) 68(1):64–70. doi: 10.1007/s12020-019-02173-8
56. Lavon I, Heli C, Brill L, Charbit H, Vaknin-Dembinsky A. Blood Levels of Co-Inhibitory-Receptors: A Biomarker of Disease Prognosis in Multiple Sclerosis. *Front Immunol* (2019) 10:835. doi: 10.3389/fimmu.2019.00835
57. Liu Y, Shu Q, Gao L, Hou N, Zhao D, Liu X, et al. Increased Tim-3 Expression on Peripheral Lymphocytes From Patients With Rheumatoid Arthritis Negatively Correlates With Disease Activity. *Clin Immunol* (2010) 137(2):288–95. doi: 10.1016/j.clim.2010.07.012
58. Jiao Q, Qian Q, Zhao Z, Fang F, Hu X, An J, et al. Expression of Human T Cell Immunoglobulin Domain and Mucin-3 (TIM-3) and TIM-3 Ligands in Peripheral Blood From Patients With Systemic Lupus Erythematosus. *Arch Dermatol Res* (2016) 308(8):553–61. doi: 10.1007/s00403-016-1665-4
59. Chou FC, Kuo CC, Wang YL, Lin MH, Linju Yen B, Chang DM, et al. Overexpression of Galectin-9 in Islets Prolongs Grafts Survival via

Downregulation of Th1 Responses. *Cell Transplant* (2013) 22(11):2135–45. doi: 10.3727/096368912X657891
60. Cao W, Ryan M, Buckley D, O'Connor R, Clarkson MR. Tim-4 Inhibition of T-Cell Activation and T Helper Type 17 Differentiation Requires Both the Immunoglobulin V and Mucin Domains and Occurs via the Mitogen-Activated Protein Kinase Pathway. *Immunology* (2011) 133(2):179–89. doi: 10.1111/j.1365-2567.2011.03424.x
61. Abe Y, Kamachi F, Kawamoto T, Makino F, Ito J, Kojima Y, et al. TIM-4 has Dual Function in the Induction and Effector Phases of Murine Arthritis. *J Immunol* (2013) 191(9):4562–72. doi: 10.4049/jimmunol.1203035
62. Zhao P, Xu L, Wang P, Liang X, Qi J, Liu P, et al. Increased Expression of Human T-Cell Immunoglobulin- and Mucin-Domain-Containing Molecule-4 in Peripheral Blood Mononuclear Cells From Patients With System Lupus Erythematosus. *Cell Mol Immunol* (2010) 7(2):152–6. doi: 10.1038/cmi.2009.118
63. de Souza AJ, Oriss TB, O'Malley KJ, Ray A, Kane LP. T Cell Ig and Mucin 1 (TIM-1) Is Expressed on *In Vivo*-Activated T Cells and Provides a Costimulatory Signal for T Cell Activation. *Proc Natl Acad Sci USA* (2005) 102(47):17113–8. doi: 10.1073/pnas.0508643102
64. Binné LL, Scott ML, Rennert PD. Human TIM-1 Associates With the TCR Complex and Up-Regulates T Cell Activation Signals. *J Immunol* (2007) 178 (7):4342–50. doi: 10.4049/jimmunol.178.7.4342
65. de Souza AJ, Oak JS, Jordanhazy R, DeKruyff RH, Fruman DA, Kane LP. T Cell Ig and Mucin Domain-1-Mediated T Cell Activation Requires Recruitment and Activation of Phosphoinositide 3-Kinase. *J Immunol* (2008) 180(10):6518–26. doi: 10.4049/jimmunol.180.10.6518
66. Rangachari M, Zhu C, Sakuishi K, Xiao S, Karman J, Chen A, et al. Bat3 Promotes T Cell Responses and Autoimmunity by Repressing Tim-3–Mediated Cell Death and Exhaustion. *Nat Med* (2012) 18(9):1394–400. doi: 10.1038/nm.2871
67. van de Weyer PS, Muehlfeit M, Klose C, Bonventre JV, Walz G, Kuehn EW. A Highly Conserved Tyrosine of Tim-3 Is Phosphorylated Upon Stimulation by Its Ligand Galectin-9. *Biochem Biophys Res Commun* (2006) 351(2):571–6. doi: 10.1016/j.bbrc.2006.10.079
68. Lee J, Su EW, Zhu C, Hainline S, Phuah J, Moroco JA, et al. Phosphotyrosine-Dependent Coupling of Tim-3 to T-Cell Receptor Signaling Pathways. *Mol Cell Biol* (2011) 31(19):3963–74. doi: 10.1128/MCB.05297-11
69. Rangachari M, Kuchroo VK. Using EAE to Better Understand Principles of Immune Function and Autoimmune Pathology. *J Autoimmun* (2013) 45:31–9. doi: 10.1016/j.jaut.2013.06.008
70. Frohman EM, Racke MK, Raine CS. Multiple Sclerosis–the Plaque and Its Pathogenesis. *N Engl J Med* (2006) 354(9):942–55. doi: 10.1056/NEJMra052130
71. Koguchi K, Anderson DE, Yang L, O'Connor KC, Kuchroo VK, Hafler DA. Dysregulated T Cell Expression of TIM3 in Multiple Sclerosis. *J Exp Med* (2006) 203(6):1413–8. doi: 10.1084/jem.20060210
72. Lee SY, Goverman JM. The Influence of T Cell Ig Mucin-3 Signaling on Central Nervous System Autoimmune Disease Is Determined by the Effector Function of the Pathogenic T Cells. *J Immunol* (2013) 190(10):4991–9. doi: 10.4049/jimmunol.1300083
73. Yang L, Anderson DE, Kuchroo J, Hafler DA. Lack of TIM-3 Immunoregulation in Multiple Sclerosis. *J Immunol* (2008) 180(7):4409–14. doi: 10.4049/jimmunol.180.7.4409
74. Sparks JA. Rheumatoid Arthritis. *Ann Internal Med* (2019) 170(1):Itc1–itc16. doi: 10.7326/AITC201901010
75. Batko B, Stajszczyk M, Świerkot J, Urbański K, Raciborski F, Jędrzejewski M, et al. Prevalence and Clinical Characteristics of Rheumatoid Arthritis in Poland: A Nationwide Study. *Arch Med Sci AMS* (2019) 15(1):134–40. doi: 10.5114/aoms.2017.71371
76. Viatte S, Barton A. Genetics of Rheumatoid Arthritis Susceptibility, Severity, and Treatment Response. *Semin Immunopathology* (2017) 39(4):395–408. doi: 10.1007/s00281-017-0630-4
77. Alpízar-Rodríguez D, Finckh A. Environmental Factors and Hormones in the Development of Rheumatoid Arthritis. *Semin Immunopathology* (2017) 39(4):461–8. doi: 10.1007/s00281-017-0624-2
78. Xu J, Yang Y, Liu X, Wang Y. The -1541 C>T and +4259 G>T of TIM-3 Polymorphisms Are Associated With Rheumatoid Arthritis Susceptibility in a Chinese Hui Population. *Int J immunogenetics* (2011) 38(6):513–8. doi: 10.1111/j.1744-313X.2011.01046.x
79. Xu J, Yang Y, Liu X, Wang Y. Genetic Variation and Significant Association of Polymorphism Rs7700944 G>A of TIM-4 Gene With Rheumatoid Arthritis Susceptibility in Chinese Han and Hui Populations. *Int J Immunogenetics* (2012) 39(5):409–13. doi: 10.1111/j.1744-313X.2012.01103.x
80. Mosaad YM, El-Bassiony SR, El-Ghaweet AE, Elhindawy MM, El-Deek BS, Sultan WA. TIM-1 Rs41297579 G>A (-1454) and TIM-4 Rs7700944 Gene Polymorphisms as Possible Risk Factor for Rheumatoid Arthritis: Relation to Activity and Severity. *Int J immunogenetics* (2015) 42(4):254–64. doi: 10.1111/iji.12201
81. Li S, Peng D, He Y, Zhang H, Sun H, Shan S, et al. Expression of TIM-3 on CD4+ and CD8+ T Cells in the Peripheral Blood and Synovial Fluid of Rheumatoid Arthritis. *APMIS Acta Pathologica Microbiologica Immunologica Scandinavica* (2014) 122(10):899–904. doi: 10.1111/apm.12228
82. Sun H, Gao W, Pan W, Zhang Q, Wang G, Feng D, et al. Tim3(+) Foxp3 (+) Treg Cells Are Potent Inhibitors of Effector T Cells and Are Suppressed in Rheumatoid Arthritis. *Inflammation* (2017) 40(4):1342–50. doi: 10.1007/s10753-017-0577-6
83. Seki M, Oomizu S, Sakata KM, Sakata A, Arikawa T, Watanabe K, et al. Galectin-9 Suppresses the Generation of Th17, Promotes the Induction of Regulatory T Cells, and Regulates Experimental Autoimmune Arthritis. *Clin Immunol* (2008) 127(1):78–88. doi: 10.1016/j.clim.2008.01.006
84. Sun J, Sui Y, Wang Y, Song L, Li D, Li G, et al. Galectin-9 Expression Correlates With Therapeutic Effect in Rheumatoid Arthritis. *Sci Rep* (2021) 11(1):5562. doi: 10.1038/s41598-021-85152-2
85. Li X, Zhao YQ, Li CW, Yuan FL. T Cell Immunoglobulin-3 as a New Therapeutic Target for Rheumatoid Arthritis. *Expert Opin Ther Targets* (2012) 16(12):1145–9. doi: 10.1517/14728222.2012.726616
86. Tsokos GC, Lo MS, Costa Reis P, Sullivan KE. New Insights Into the Immunopathogenesis of Systemic Lupus Erythematosus. *Nat Rev Rheumatol* (2016) 12(12):716–30. doi: 10.1038/nrrheum.2016.186
87. Ghodke-Puranik Y, Niewold TB. Immunogenetics of Systemic Lupus Erythematosus: A Comprehensive Review. *J Autoimmun* (2015) 64:125–36. doi: 10.1016/j.jaut.2015.08.004
88. Surace AEA, Hedrich CM. The Role of Epigenetics in Autoimmune/Inflammatory Disease. *Front Immunol* (2019) 10:1525. doi: 10.3389/fimmu.2019.01525
89. Barbhaiya M, Costenbader KH. Environmental Exposures and the Development of Systemic Lupus Erythematosus. *Curr Opin Rheumatol* (2016) 28(5):497–505. doi: 10.1097/BOR.0000000000000318
90. Almaani S, Meara A, Rovin BH. Update on Lupus Nephritis. *Clin J Am Soc Nephrol CJASN* (2017) 12(5):825–35. doi: 10.2215/CJN.05780616
91. Du P, Xiong R, Li X, Jiang J. Immune Regulation and Antitumor Effect of TIM-1. *J Immunol Res* (2016) 2016:8605134. doi: 10.1155/2016/8605134
92. Nozaki Y, Nikolic-Paterson DJ, Snelgrove SL, Akiba H, Yagita H, Holdsworth SR, et al. Endogenous Tim-1 (Kim-1) Promotes T-Cell Responses and Cell-Mediated Injury in Experimental Crescentic Glomerulonephritis. *Kidney Int* (2012) 81(9):844–55. doi: 10.1038/ki.2011.424
93. Moulton VR, Suarez-Fueyo A, Meidan E, Li H, Mizui M, Tsokos GC. Pathogenesis of Human Systemic Lupus Erythematosus: A Cellular Perspective. *Trends Mol Med* (2017) 23(7):615–35. doi: 10.1016/j.molmed.2017.05.006
94. Han G, Chen G, Shen B, Li Y. Tim-3: An Activation Marker and Activation Limiter of Innate Immune Cells. *Front Immunol* (2013) 4:449. doi: 10.3389/fimmu.2013.00449
95. Zhao D, Li C, Yang X, Yan W, Zhang Y. Elevated Soluble Tim-3 Correlates With Disease Activity of Systemic Lupus Erythematosus. *Autoimmunity* (2021) 54(2):97–103. doi: 10.1080/08916934.2021.1891535
96. Krahling S, Callahan MK, Williamson P, Schlegel RA. Exposure of Phosphatidylserine Is a General Feature in the Phagocytosis of Apoptotic Lymphocytes by Macrophages. *Cell Death Differ* (1999) 6(2):183–9. doi: 10.1038/sj.cdd.4400473
97. Fransen JH, Berden JH, Koeter CM, Adema GJ, van der Vlag J, Hilbrands LB. Effect of Administration of Apoptotic Blebs on Disease Development in

Lupus Mice. *Autoimmunity* (2012) 45(4):290–7. doi: 10.3109/08916934.2012.664668
98. Toda S, Hanayama R, Nagata S. Two-Step Engulfment of Apoptotic Cells. *Mol Cell Biol* (2012) 32(1):118–25. doi: 10.1128/MCB.05993-11
99. Miyanishi M, Segawa K, Nagata S. Synergistic Effect of Tim4 and MFG-E8 Null Mutations on the Development of Autoimmunity. *Int Immunol* (2012) 24(9):551–9. doi: 10.1093/intimm/dxs064
100. Bluestone JA, Herold K, Eisenbarth G. Genetics, Pathogenesis and Clinical Interventions in Type 1 Diabetes. *Nature* (2010) 464(7293):1293–300. doi: 10.1038/nature08933
101. Fazeli Farsani S, Brodovicz K, Soleymanlou N, Marquard J, Wissinger E, Maiese BA. Incidence and Prevalence of Diabetic Ketoacidosis (DKA) Among Adults With Type 1 Diabetes Mellitus (T1D): A Systematic Literature Review. *BMJ Open* (2017) 7(7):e016587. doi: 10.1136/bmjopen-2017-016587
102. Marek-Trzonkowska N, Mysliwiec M, Dobyszuk A, Grabowska M, Techmanska I, Juscinska J, et al. Administration of CD4+CD25highCD127-Regulatory T Cells Preserves β-Cell Function in Type 1 Diabetes in Children. *Diabetes Care* (2012) 35(9):1817–20. doi: 10.2337/dc12-0038
103. Millman JR, Xie C, Van Dervort A, Gürtler M, Pagliuca FW, Melton DA. Generation of Stem Cell-Derived β-Cells From Patients With Type 1 Diabetes. *Nat Commun* (2016) 7:11463. doi: 10.1038/ncomms11463
104. van Belle TL, Coppieters KT, von Herrath MG. Type 1 Diabetes: Etiology, Immunology, and Therapeutic Strategies. *Physiol Rev* (2011) 91(1):79–118. doi: 10.1152/physrev.00003.2010
105. Shimokawa C, Kato T, Takeuchi T, Ohshima N, Furuki T, Ohtsu Y, et al. CD8(+) Regulatory T Cells Are Critical in Prevention of Autoimmune-Mediated Diabetes. *Nat Commun* (2020) 11(1):1922. doi: 10.1038/s41467-020-15857-x
106. Sánchez-Fueyo A, Tian J, Picarella D, Domenig C, Zheng XX, Sabatos CA, et al. Tim-3 Inhibits T Helper Type 1-Mediated Auto- and Alloimmune Responses and Promotes Immunological Tolerance. *Nat Immunol* (2003) 4 (11):1093–101. doi: 10.1038/ni987
107. Chou FC, Shieh SJ, Sytwu HK. Attenuation of Th1 Response Through Galectin-9 and T-Cell Ig Mucin 3 Interaction Inhibits Autoimmune Diabetes in NOD Mice. *Eur J Immunol* (2009) 39(9):2403–11. doi: 10.1002/eji.200839177
108. Zhao L, Cheng S, Fan L, Zhang B, Xu S. TIM-3: An Update on Immunotherapy. *Int Immunopharmacol* (2021) 99:107933. doi: 10.1016/j.intimp.2021.107933

Conflict of Interest: The authors declare that the research was conducted in the absence of any commercial or financial relationships that could be construed as a potential conflict of interest.

Publisher's Note: All claims expressed in this article are solely those of the authors and do not necessarily represent those of their affiliated organizations, or those of the publisher, the editors and the reviewers. Any product that may be evaluated in this article, or claim that may be made by its manufacturer, is not guaranteed or endorsed by the publisher.

frontiers in Immunology

ORIGINAL RESEARCH
published: 29 September 2021
doi: 10.3389/fimmu.2021.737990

Apelin Promotes Endothelial Progenitor Cell Angiogenesis in Rheumatoid Arthritis Disease *via* the miR-525-5p/Angiopoietin-1 Pathway

Ting-Kuo Chang[1,2], You-Han Zhong[3], Shan-Chi Liu[4], Chien-Chung Huang[5,6], Chun-Hao Tsai[7,8], Hsiang-Ping Lee[9,10], Shih-Wei Wang[11,12,13], Chin-Jung Hsu[8,9†] and Chih-Hsin Tang[3,5,14,15†]*

[1] Department of Medicine, Mackay Medical College, New Taipei, Taiwan, [2] Division of Spine Surgery, Department of Orthopedic Surgery, MacKay Memorial Hospital, New Taipei, Taiwan, [3] Graduate Institute of Biomedical Science, China Medical University, Taichung, Taiwan, [4] Department of Medical Education and Research, China Medical University Beigang Hospital, Yunlin, Taiwan, [5] School of Medicine, China Medical University, Taichung, Taiwan, [6] Division of Immunology and Rheumatology, Department of Internal Medicine, China Medical University Hospital, Taichung, Taiwan, [7] Department of Sports Medicine, College of Health Care, China Medical University, Taichung, Taiwan, [8] Department of Orthopedic Surgery, China Medical University Hospital, Taichung, Taiwan, [9] School of Chinese Medicine, China Medical University, Taichung, Taiwan, [10] Department of Chinese Medicine, China Medical University Hospital, Taichung, Taiwan, [11] Department of Medicine, MacKay Medical College, New Taipei City, Taiwan, [12] Graduate Institute of Natural Products, College of Pharmacy, Kaohsiung Medical University, Kaohsiung, Taiwan, [13] Institute of Biomedical Sciences, Mackay Medical College, Taipei, Taiwan, [14] Chinese Medicine Research Center, China Medical University, Taichung, Taiwan, [15] Department of Biotechnology, College of Health Science, Asia University, Taichung, Taiwan

Angiogenesis is a critical process in the formation of new capillaries and a key participant in rheumatoid arthritis (RA) pathogenesis. The adipokine apelin (APLN) plays critical roles in several cellular functions, including angiogenesis. We report that APLN treatment of RA synovial fibroblasts (RASFs) increased angiopoietin-1 (Ang1) expression. Ang1 antibody abolished endothelial progenitor cell (EPC) tube formation and migration in conditioned medium from APLN-treated RASFs. We also found significantly higher levels of APLN and Ang1 expression in synovial fluid from RA patients compared with those with osteoarthritis. APLN facilitated Ang1-dependent EPC angiogenesis by inhibiting miR-525-5p synthesis *via* phospholipase C gamma (PLCγ) and protein kinase C alpha (PKCα) signaling. Importantly, infection with APLN shRNA mitigated EPC angiogenesis, articular swelling, and cartilage erosion in ankle joints of mice with collagen-induced arthritis. APLN is therefore a novel therapeutic target for RA.

Keywords: apelin, angiopoietin-1, endothelial progenitor cells (EPC), rheumatoid arthritis, miR-525-5p

OPEN ACCESS

Edited by:
Zhichao Fan,
UCONN Health, United States

Reviewed by:
Salahuddin Ahmed,
Washington State University Health Sciences Spokane, United States
Sadiq Umar,
University of Illinois at Chicago, United States
Wei Lin,
Shandong Academy of Medical Sciences (SDAMS), China

***Correspondence:**
Chih-Hsin Tang
chtang@mail.cmu.edu.tw

†These authors have contributed equally to this work

Specialty section:
This article was submitted to Autoimmune and Autoinflammatory Disorders, a section of the journal Frontiers in Immunology

Received: *08 July 2021*
Accepted: *13 September 2021*
Published: *29 September 2021*

Citation:
Chang T-K, Zhong Y-H, Liu S-C, Huang C-C, Tsai C-H, Lee H-P, Wang S-W, Hsu C-J and Tang C-H (2021) Apelin Promotes Endothelial Progenitor Cell Angiogenesis in Rheumatoid Arthritis Disease via the miR-525-5p/Angiopoietin-1 Pathway. Front. Immunol. 12:737990. doi: 10.3389/fimmu.2021.737990

INTRODUCTION

Rheumatoid arthritis (RA) is one of the most common autoimmune disorders, characterized by the accumulation of inflammatory cytokines in the synovial joint, resulting in pannus formation, cartilage degradation and bone destruction (1). Angiogenesis is a critical driver of RA disease, in which pre-existing blood vessels promote the entry of blood-derived leukocytes into the synovial tissues to facilitate and potentiate inflammation (2).

Endothelial progenitor cells (EPCs) develop from bone marrow-derived endothelial stem cells, which contain the cell surface markers CD133, CD34 and vascular endothelial growth factor receptor 2 (VEGFR2) and are capable of stimulating postnatal vasculogenesis (3) and angiogenic function (4). EPC proliferation and migration facilitate angiogenesis (4), enabling the development of RA (5, 6). EPC-dependent angiogenesis therefore seems to be a worthwhile treatment target in RA. EPC proliferation, migration and angiogenesis is regulated by the balance in activities between proangiogenic factors such as vascular endothelial growth factor (VEGF), platelet-derived growth factor (PDGF) and angiopoietin-1 (Ang1), and antiangiogenic factors including thrombospondin-1 (7, 8). Ang1 plays a critical role in endothelial cell adhesion, migration and production during angiogenesis (9). However, the effects of Ang1 in EPC angiogenesis in RA disease are unclear.

Apelin (APLN) is a member of the adipokine superfamily that is expressed in different human tissues including nervous system, adipose and endothelial tissues (10, 11). APLN has been linked with numerous disorders, including cardiovascular and neurodegenerative diseases (10, 11). Emerging evidence has highlighted the association between APLN and arthritic diseases, including RA and osteoarthritis (OA), for example (12). Treating human chondrocytes with APLN increases the synthesis of matrix metalloproteinases (MMPs) and other catabolic factors (13). APLN also promotes the production of the proinflammatory cytokine interleukin 1 beta (IL-1β) in human OA synovial fibroblasts (OASFs) (14). In RA patients, levels of APLN expression are associated with the expression of the catabolic enzyme MMP-9 (15). These reports suggest that APLN is a novel avenue for treating arthritic diseases.

MiRNAs are single-stranded noncoding RNA molecules that manipulate gene expression at the post-transcriptional level (16). Various miRNA genes expressed in immune, inflammatory and synovial cells from patients with RA (17) can cause synovial hyperplasia and bone damage, or promote inflammation, through positive or negative manipulation (18). Recently, miRNAs have been found to regulate angiogenic activity in the progression of arthritic diseases (19, 20). However, it remains unclear as to how the APLN-miRNA axis regulates angiogenesis in RA disease. Our study has identified higher levels of APLN and Ang1 expression in patients with RA than in those with OA. APLN treatment increased RASF-derived Ang1 production and facilitated EPC angiogenesis by inhibiting miR-525-5p synthesis *via* phospholipase C gamma (PLCγ) and protein kinase C alpha (PKCα) signaling. Inhibition of APLN expression diminished Ang1-dependent angiogenesis and inhibited collagen-induced arthritis (CIA) in mice. APLN is therefore a novel therapeutic target for RA.

MATERIALS AND METHODS

Materials

APN, Ang1, PLCγ and PKCα antibodies were purchased from Santa Cruz Biotechnology (CA, USA). p-PLCγ and p-PKCα antibodies were purchased from Cell Signaling Technology (Danvers, MA, USA). All siRNAs (ON-TARGET*plus*) were obtained from Dharmacon Research (Lafayette, CO, USA). Taqman® one-step PCR Master Mix, qPCR primers and probes were obtained from Applied Biosystems (Foster City, CA, USA). β-Actin antibody and pharmacological inhibitors were obtained from Sigma-Aldrich (St. Louis, MO, USA).

Human Synovial Fluid Samples

Study approval was granted by the Institutional Review Board of China Medical University Hospital (Taichung, Taiwan) and all patients provided written informed consent before participating in the study. Synovial fluid samples were obtained from patients undergoing total knee arthroplasty for OA (n=20) or RA (n=20).

Cell Culture

Human RASFs were purchased from the Riken Cell Bank (Ibaraki, Japan). Primary human EPCs were isolated according to the procedure detailed in our previous reports (21, 22). Mouse osteoblastic cell line MC3T3-E1 were purchased from the American Type Culture Collection (Manassas, VA, USA). RASFs and EPCs were maintained in DMEM while MC3T3-E1 cells were cultured in α-MEM medium. The culture mediums were supplemented with 20 mM HEPES and 10% fetal bovine serum, 2 mM glutamine, penicillin (100 U/ml) and streptomycin (100 μg/ml) at 37°C with 5% CO_2.

Western Blot Analysis

RASF cells (5×10^5 cells) were seeding in 6 well plate. Cell lysates were resolved by SDS-PAGE and transferred to Immobilon® PVDF membranes. Western blot analysis was performed according to the procedures detailed in our previous investigations (23–26).

Quantitative Real-Time PCR (qPCR) Analysis of mRNA and miRNA

Total RNA was extracted from RASFs and paws using TRIzol reagent and then reverse-transcribed into cDNA using oligo(dT) primers. For the miRNA assay, cDNA was synthesized using the TaqMan MicroRNA Reverse Transcription Kit. qPCR analysis was conducted according to an established protocol (27–29).

Preparation of Conditioned Medium (CM)

RASFs were plated in 6-well dishes and grown to confluence. The culture medium was exchanged with serum-free DMEM

medium. CM were collected 1 days after the change of media and stored at -20°C until use. In the series of experiments, cells were pretreated for 30 min with inhibitors, including U73122, GF109203X and Go6976 or transfected with miR-525-5p mimic, PLCγ, PKCα and PKCδ siRNA for 24 h followed by treatment with APLN for 24 h to prevent signaling *via* the APLN pathway.

ELISA Assay

RASFs were treated with pharmacological inhibitors then incubated with APLN for 24 h and the medium was quantified for Ang1 expression using a Ang1 ELISA kit (Peprotech, Rocky Hill, NJ, USA), following the manufacturer's protocol.

EPC Migration and *In Vitro* Tube Formation

EPCs were treated with RASF conditioned medium (CM) for 24 h. EPC migration and *in vitro* tube formation were evaluated by the procedures detailed in our previous publication (30).

The Chick Chorioallantoic Membrane Assay

In vivo angiogenic activity was assessed using the chorioallantoic membrane (CAM) of the chick embryo, as described previously (6, 31). Fertilized chick embryos were incubated in an 80% humidified atmosphere at 37°C. All animal investigations adhered to approved protocols issued by the Institutional Animal Care and Use Committee of China Medical University (Taichung, Taiwan).

In Vivo Matrigel Plug Assay

Four-week-old nude male mice received a single subcutaneous injection of Matrigel containing RASF CM. Mice were subcutaneously injected with 300 μL of Matrigel. On day 7, the Matrigel plugs were harvested, partially fixed with 4% formalin, embedded in paraffin, and subsequently processed for immunohistochemistry staining for CD31, CD34, and CD133. Hemoglobin concentrations were measured, according to previously described methodology (6, 31, 32).

CIA Mouse Model

The CIA mouse model was performed according to the methodology detailed in our previous publications (6, 32, 33). After receiving two immunizations, the mice were given weekly intra-articular injections of ~7.1×10^6 plaque-forming units (PFU) of control or APLN short hairpin RNA (shRNA). Upon sacrifice after 49 days of treatment, phalanges and ankle joints were removed from each mouse then fixed in 4% paraformaldehyde for micro-computed tomography (micro-CT) analysis. Analysis was performed using CTAn 1.18.4 (Bruker micro-CT, Kontich, Belgium). First, we segmented the reaction area which showed less calcium content with porous structure. We then labelled the isolated reaction area with purple color.

Statistical Analysis

All statistical analyses were carried out using GraphPad Prism 5.0 (GraphPad Software) and all values are expressed as the mean ± S.D. Differences between selected pairs from the experimental groups were analyzed for statistical significance using the paired sample *t*-test for *in vitro* analyses and by one-way ANOVA followed by Bonferroni testing for *in vivo* analyses. * $p < 0.05$, ** $p < 0.01$ and *** $p < 0.001$ *versus* the control group; # $p < 0.05$ *versus* the APLN-treated group.

RESULTS

APLN Facilitates Ang1-Dependent EPC Angiogenesis

APLN is associated with the progression of arthritic diseases, including RA (12). Ang1 is an important angiogenetic regulator in endothelial cell angiogenesis (9). First, we examined whether APLN promotes Ang1 synthesis in RASFs. Stimulation of RASFs with APLN dose-dependently increased Ang1 transcription and translation levels (**Figures 1A, B**) and also the secretion of Ang1 protein (**Figure 1C**). EPC tube formation and migration assays examined the effects of APLN-controlled angiogenesis in RASFs (5). CM from APLN-treated RASFs significantly increased the formation and reorganization of capillary-like network structures as well as migratory activity (VEGF-increased vessel formation served as the positive control) (**Figures 1D, E**). Treatment with Ang1 but not VEGF antibody, dramatically reduced the effects of CM from APLN-treated RASFs upon EPC tube formation and migration (**Figures 1D, E**), indicating that Ang1 is more important than VEGF in APLN-promoted EPC angiogenesis. To directly examine whether APLN acts as an angiogenic factor *in vivo*, the CAM assay was used. Matrigel was mixed with CM from APLN-treated RASFs and placed onto the surface of the CAMs. CM from APLN-treated RASFs synthesized new capillaries then control (VEGF-increased vessel formation served as the positive control) (**Figure 1F**), suggesting that APLN promotes Ang1 production in RASFs and enhances tube formation and migration of EPCs.

High Levels of APLN and Ang1 Expression in RA Patients Induce EPC Homing and Angiogenesis

Next, we investigated APLN and Ang1 levels in RA patients. We found markedly higher levels of APLN and Ang1 expression in synovial fluid from RA patients compared with OA synovial fluid samples (**Supplementary Figures 1A, B**). Synovial fluid levels of APLN and Ang1 were positively correlated (**Supplementary Figure 1C**). Next, we examined whether synovial fluid from RA patients promotes EPC homing and angiogenesis. Migratory activity, as well as the formation and reorganization of capillary-like network structures, was significantly greater in EPCs incubated with RA synovial fluid compared with EPCs incubated with OA synovial fluid (**Supplementary Figures 1D, E**). Treatment with Ang1 antibody dramatically diminished the effects of RA synovial fluid upon EPC migration and tube formation (**Supplementary Figures 1D, E**), indicating that high levels of APLN and Ang1 expression in RA patients induce EPC homing and angiogenesis.

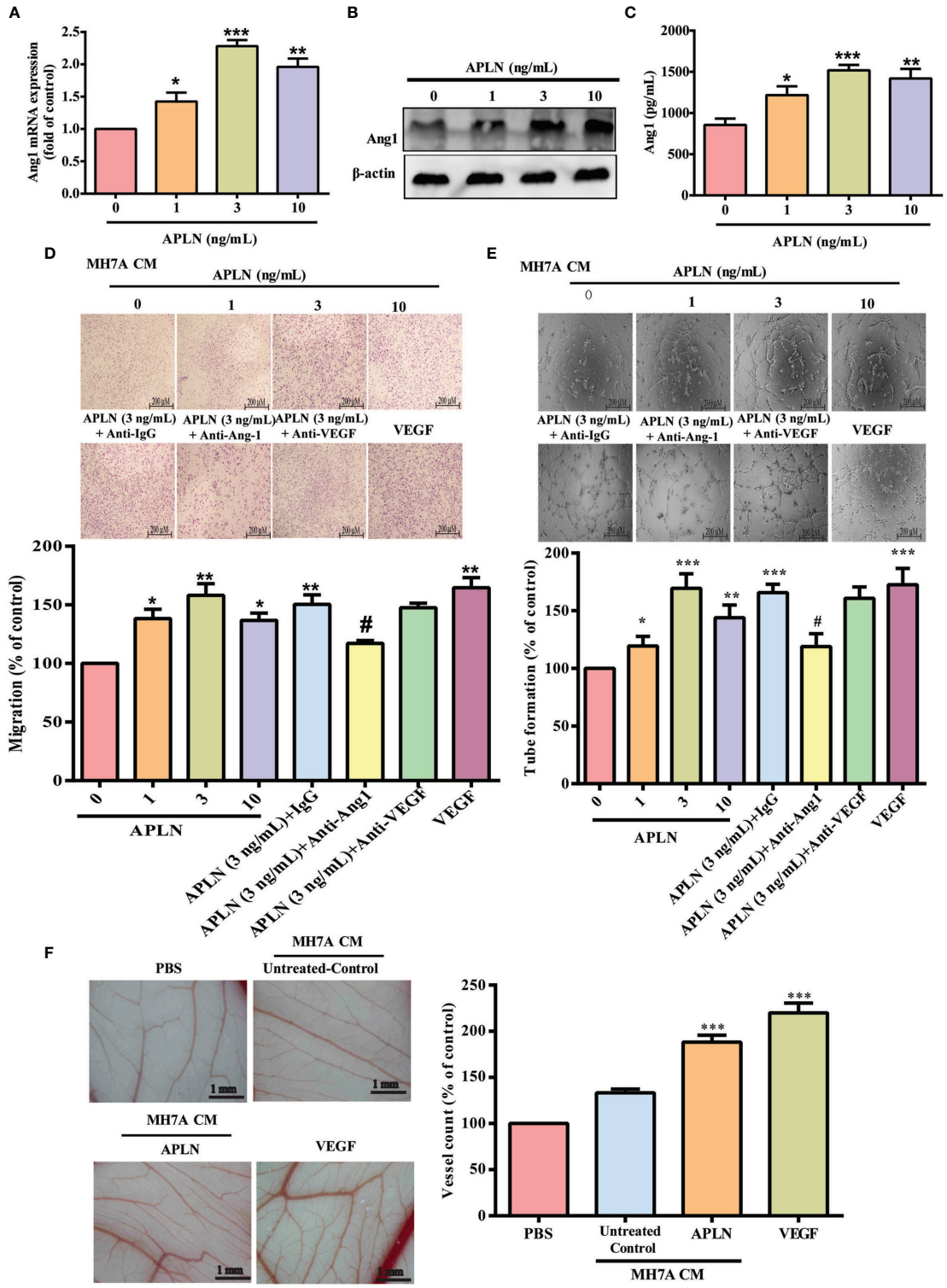

FIGURE 1 | APLN increases Ang1 expression in RASFs and promotes EPCs tube formation and migration. **(A–C)** RASFs were incubated for 24 h with APLN; Ang1 expression was quantified by qPCR, Western blot and ELISA assays. **(D, E)** RASFs cells were treat with APLN does manner for 24 h and collected conditioned medium (CM) was applied to endothelial progenitor cells (EPCs), then EPC migration and angiogenesis was measured. **(F)** Matrigel plugs containing CM from APLN-treated RASFs or VEGF (positive control) were applied to 6-day-old fertilized chick embryos for 4 days. CAMs were examined by microscopy and photographed, and vessels counted. $^{*}p < 0.05$, $^{**}p < 0.01$ and $^{***}p < 0.001$ *versus* the control group; $^{\#}p < 0.05$ *versus* the APLN-treated group.

PLCγ and PKCα Signaling Cascades Regulate APLN-Promoted Ang1 Expression and Angiogenesis in EPCs

PLC and PKC signaling pathways control different cellular functions, including angiogenesis (34). We therefore sought to determine how these pathways affect APLN-induced upregulation of Ang1 synthesis and EPC angiogenesis. Treatment of RASFs with a PLC inhibitor (U73122) or PLCγ siRNA reduced the effects of APLN upon Ang1 expression (**Figures 2A, B**) and inhibited APLN-induced upregulation of EPC migration and tube formation (**Figures 2C, D**). Incubating RASFs with APLN induced PLCγ phosphorylation (**Figures 2E, F**). In addition, the PKCα inhibitors (GF109203X and Go6976) and PKCα siRNA, but not the PKCδ inhibitor (Rottlerin) or PKCδ siRNA, abolished APLN-facilitated Ang1 expression and EPC angiogenesis (**Figures 3A–D**). Stimulation of RASFs with APLN also increased PKCα phosphorylation (**Figure 3E**). Thus, APLN promotes Ang1 expression in RASFs and enhances EPC angiogenesis *via* PLCγ and PKCα signaling.

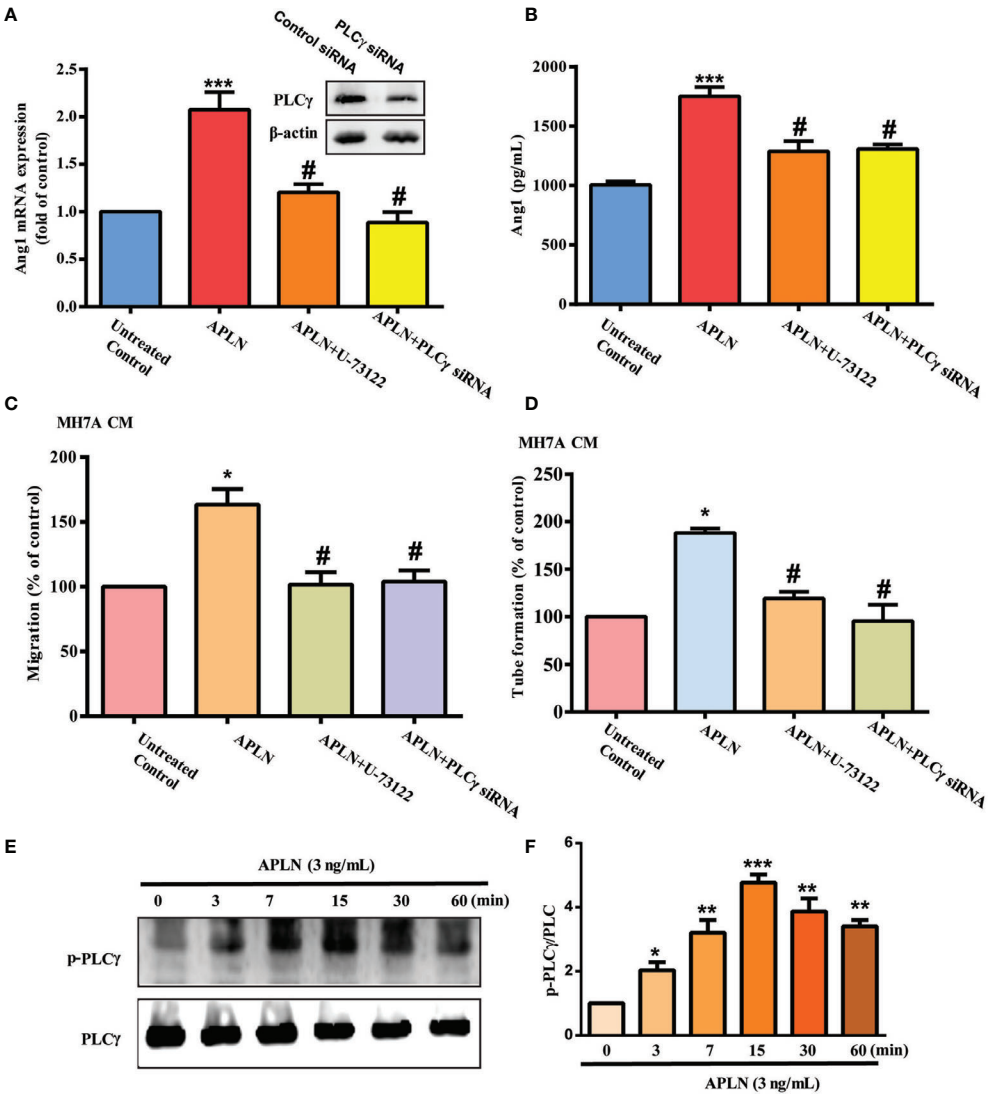

FIGURE 2 | PLCγ signaling regulates APLN-induced effects on Ang1 expression and EPC angiogenesis. **(A, B)** RASFs were left untreated, stimulated with APLN (3 ng/mL) alone for 24 h, or pretreated with U73122 for 30 min, or transfected with PLCγ siRNA for 30 min, prior to 24 h of APLN (3 ng/mL) stimulation. Ang1 expression was examined by qPCR and ELISA assays. **(C, D)** Collected CM was applied to EPCs, and angiogenesis was determined. **(E)** RASFs were treated with APLN for varying amounts of time and Western blot (n=3) determined PLCγ phosphorylation. **(F)** Densitometry analysis of **(E)**. $^{*}p < 0.05$, $^{**}p < 0.01$ and $^{***}p < 0.001$ *versus* the control group; $^{\#}p < 0.05$ *versus* the APLN-treated group.

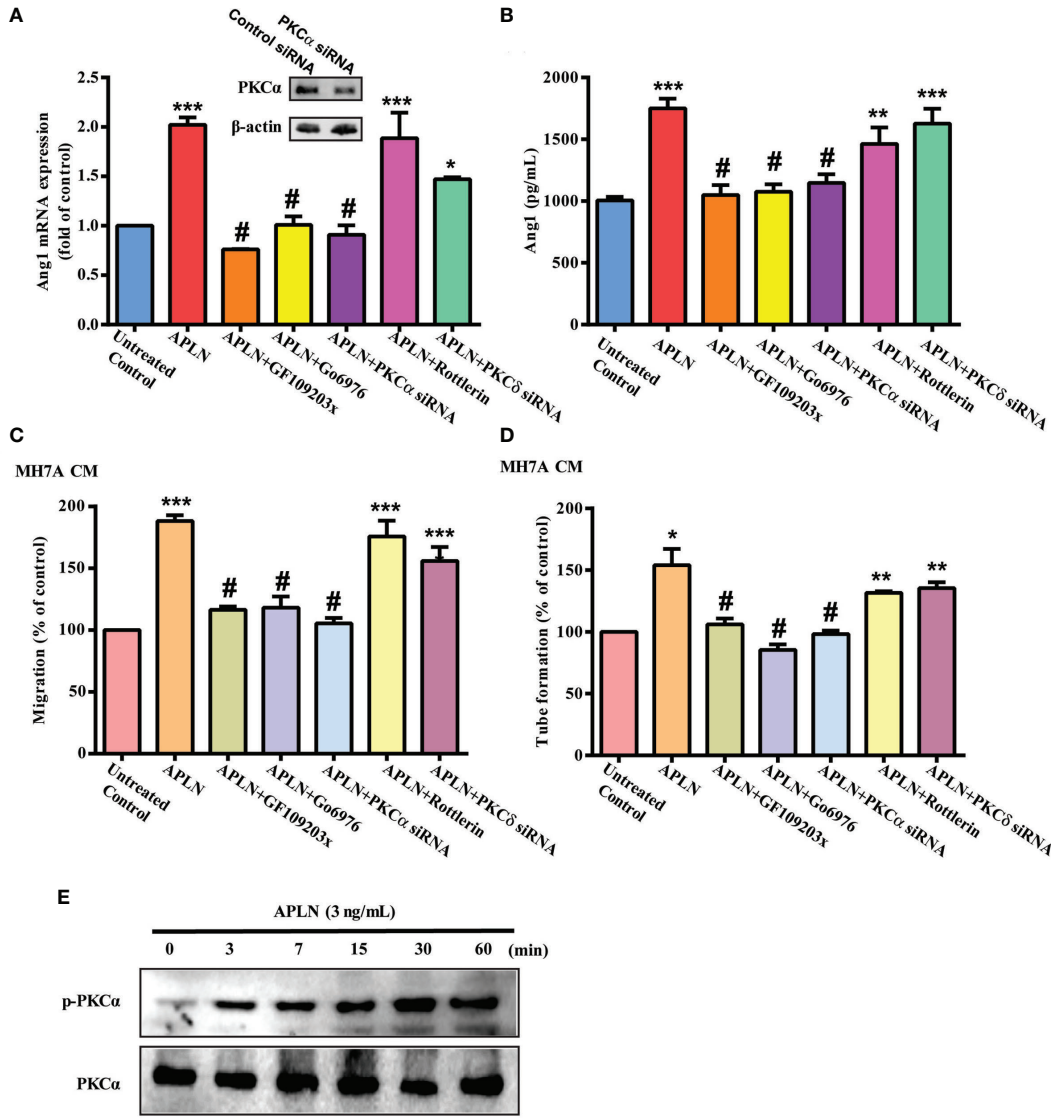

FIGURE 3 | PKCα signaling regulates APLN-induced effects on Ang1 expression and EPC angiogenesis. **(A, B)** RASFs were pretreated with GF109203X and Go6976 for 30 min, or transfected with PKCα and PKCδ siRNAs for 24 h, then stimulated with APLN for 24 h. Ang1 expression was examined by qPCR and ELISA assays. **(C, D)** Collected CM was applied to EPCs, and EPC angiogenesis was determined. **(E)** RASFs were treated with APLN time-manner and Western blot (n=3) determined PKCα phosphorylation. $^{*}p < 0.05$, $^{**}p < 0.01$ and $^{***}p < 0.001$ *versus* the control group; $^{\#}p < 0.05$ *versus* the APLN-treated group.

Inhibition of miR-525-5p Controls APLN-Promoted Ang1 Synthesis and EPC Angiogenesis

The dysregulated expression of miRNAs in patients with RA differs from miRNA expression in healthy individuals (35, 36). Using open-source miRNA software (miRanda, https://bioweb.pasteur.fr/packages/pack@miRanda@3.3a/; Microt4, http://diana.imis.athena-innovation.gr/DianaTools/index.php?r=microtv4/index; and miRWalk, http://mirwalk.umm.uni-heidelberg.de/), we identified 8 candidate miRNAs that could possibly bind to the 3'UTR region of Ang1 mRNA. Among these 8 miRNAs, levels of miR-525-5p expression were suppressed by the greatest extent after APLN administration (**Figure 4A** and **Supplementary Figure S2**). Treating RASFs with APLN concentration-dependently reduced miR-525-5p synthesis (**Figure 4B**). Transfection of RASFs with miR-525-5p mimic antagonized the effects of APLN upon Ang1 production and EPC angiogenesis (**Figures 4C–E**). Similarly, transfection with miR-525-5p mimic downregulated Ang-1 expression in mouse MC3T3-E1 cells (**Supplementary Figure S3**).

To examine whether miR-525-5p regulates *ANG1* gene transcription, we constructed a luciferase reporter vector with the wild-type 3'UTR of *ANG1* mRNA (wt-Ang1-3'UTR) and a mutated vector harboring mismatches in the predicted miR-525-5p binding

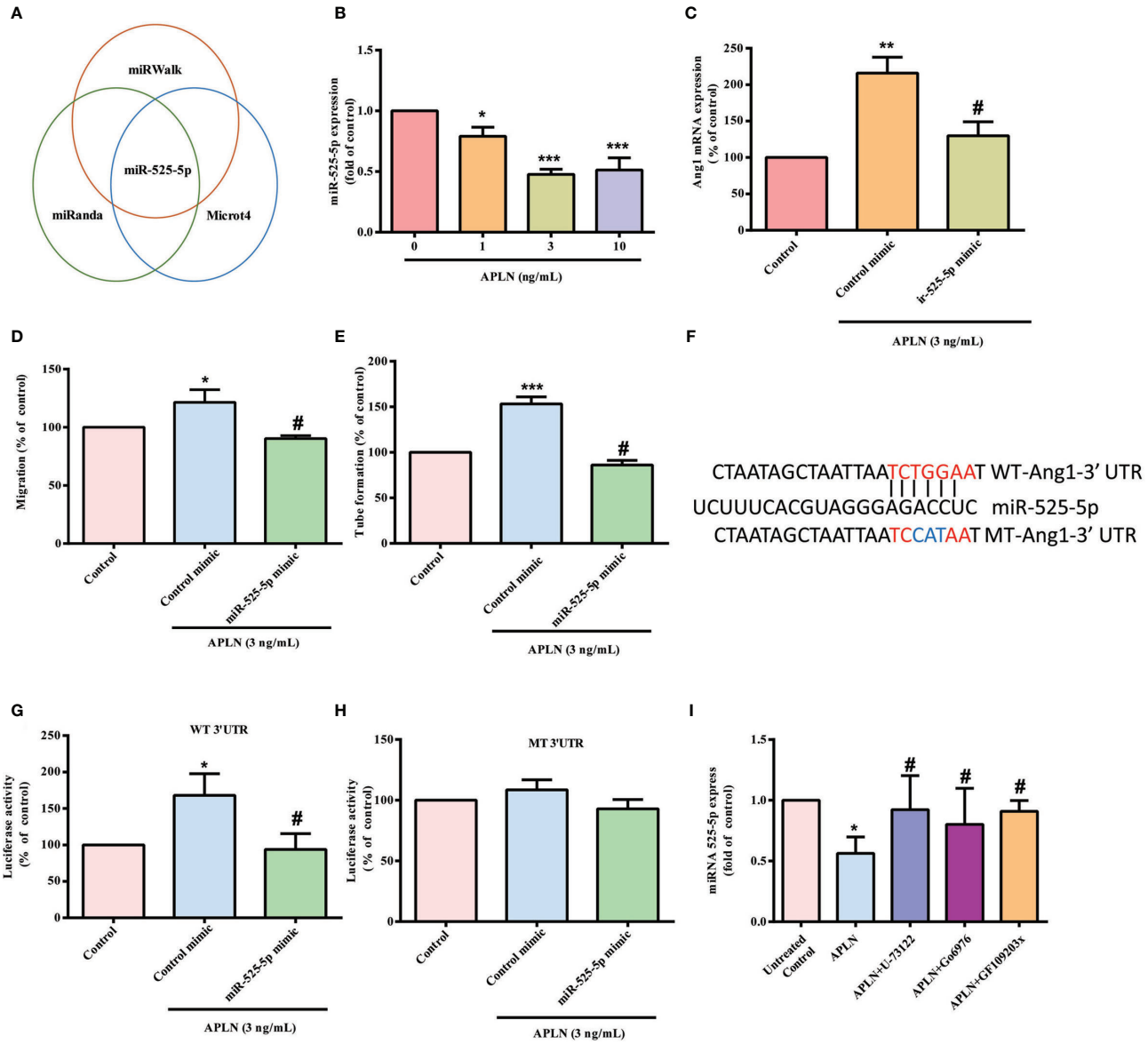

FIGURE 4 | APLN facilitates Ang1 synthesis and EPC angiogenesis by inhibiting miR-525-5p. **(A)** Open-source software enabled identification of miRNAs that possibly interfere with Ang1 transcription. **(B)** RASFs were incubated with APLN for 24 h. miR-525-5p expression was determined by the qPCR assay. **(C)** RASFs were transfected with miR-525-5p mimic for 24 h, then stimulated with APLN for 24 h. Ang1 levels were determined by qPCR. **(D, E)** Collected CM was applied to EPCs, and EPC angiogenesis was quantified. **(F)** Schematic 3′UTR representation of human Ang1 containing the miR-525-5p binding site. **(G, H)** RASFs were transfected with the indicated luciferase plasmid with or without miR-525-5p mimic for 24 h, then stimulated with APLN for 24 h. Relative luciferase activity was determined. **(I)** RASFs were pretreated with U73122, GF109203X and Go6976 for 30 min, then stimulated with APLN for 24 h. miR-525-5p expression was quantified by qPCR. $^{*}p < 0.05$, $^{**}p < 0.01$ and $^{***}p < 0.001$ *versus* the control group; $^{\#}p < 0.05$ *versus* the APLN-treated group.

site (mt-Ang1-3'UTR) (**Figure 4F**). MiR-525-5p mimic reduced APLN-induced luciferase activity in the wt-Ang1-3'UTR plasmid, but not in the mt-Ang1-3'UTR plasmid (**Figures 4G, H**). Moreover, U73122, GF109203X and Go6976 all reversed APLN-induced inhibition of miR-525-5p expression (**Figure 4I**), indicating that PLCγ and PKCα signaling mediate APLN-induced inhibition of miR-525-5p.

Inhibition of APLN Reduces EPC Angiogenesis as Well as Arthritis Severity *In Vivo*

APLN shRNA was used to validate the *in vivo* role of APLN. Infection of RASFs with APLN shRNA reduced APLN and Ang1 levels (**Figures 5A, B**). Compared with RASF CM, APLN shRNA-infected RASF CM reduced EPC migration and tube

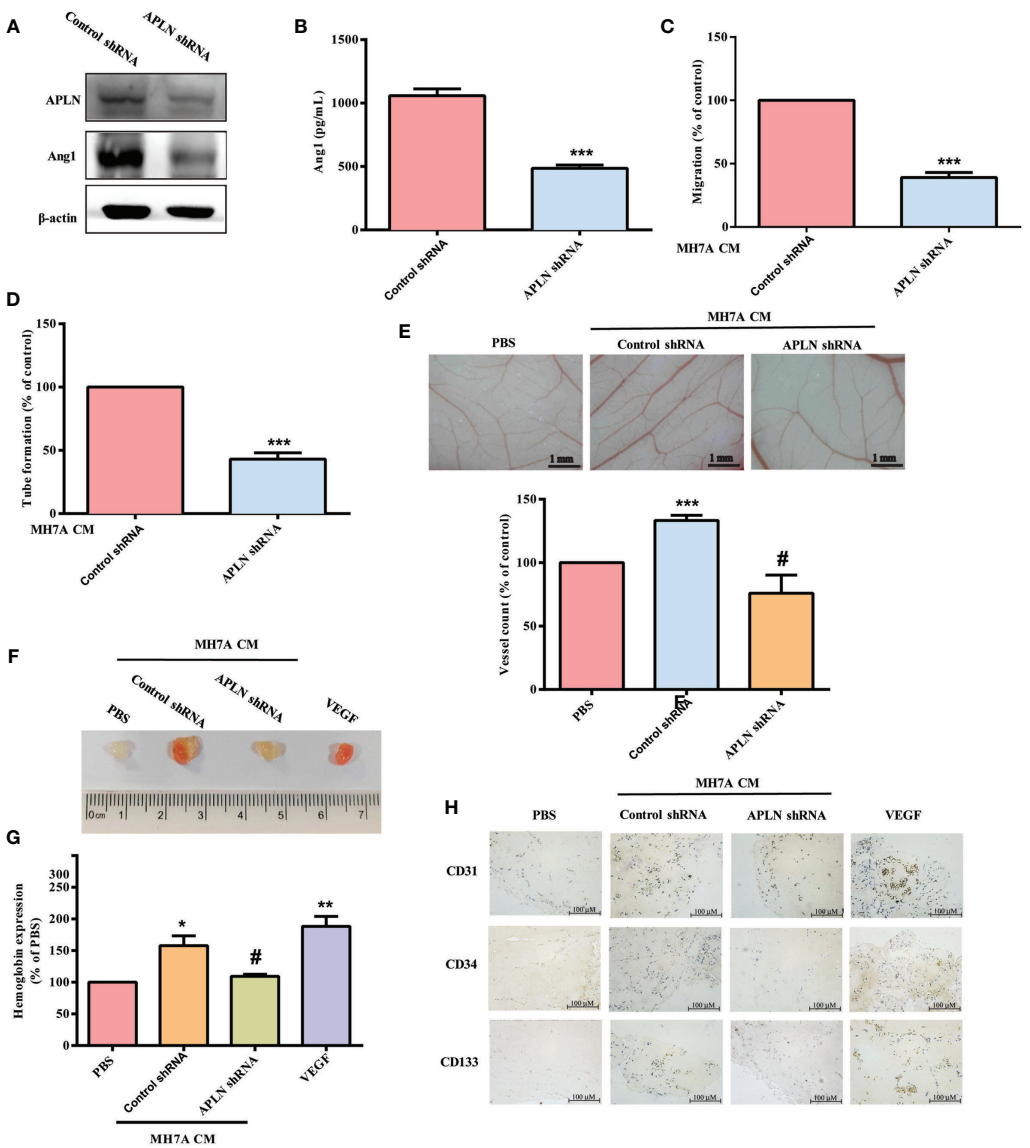

FIGURE 5 | Inhibition of APLN reduces EPC angiogenesis *in vivo*. **(A, B)** RASFs were infected with APLN shRNA for 24 h. APLN and Ang1 expression was examined by Western blot (n=3) and ELISA. **(C, D)** Collected CM was applied to EPCs, and EPC angiogenesis was quantified. **(E)** After subjecting RASFs to the treatment conditions as indicated, the harvested CM was applied to 6-day-old fertilized chick embryos for 4 days. CAMs were examined by microscopy and photographed, and vessels were counted manually. **(F, G)** Matrigel plugs containing the harvested CM were subcutaneously injected into the flanks of nude mice. After 7 days, the plugs were photographed, and hemoglobin levels were quantified. **(H)** Plug specimens were immunostained with CD31, CD34 and CD133 antibodies. $^{*}p < 0.05$, $^{**}p < 0.01$ and $^{***}p < 0.001$ *versus* the control group; $^{\#}p < 0.05$ *versus* the APLN-treated group.

formation (**Figures 5C, D**). CAM and Matrigel investigations demonstrated that CM from RASFs enhanced vessel formation *in vivo* (**Figures 5E, F**), while APLN shRNA reduced RASF CM-promoted induction of vessel formation (**Figures 5E, F**). These results were confirmed by IHC staining of hemoglobin levels and the human-specific vessel marker CD31, as well as EPC markers CD34 and CD133 (**Figures 5G, H**).

Next, we used the CIA mouse model to investigate the therapeutic effect of inhibiting APLN *in vivo*. Compared with controls, CIA mice exhibited significant paw swelling that improved after administration of APLN shRNA (**Figures 6A, B**). Micro-CT images of the hind paws showed that APLN shRNA reversed CIA-induced reductions in bone mineral density ($p<0.01$), bone volume ($p<0.0001$) and trabecular numbers ($p<0.0001$) (**Figures 6C–E**). Moreover, CIA mice exhibited lower cartilage thicknesses, as indicated by H&E and Safranin-O/Fast-green staining (**Figure 6F**). APLN shRNA reversed CIA-induced cartilage degradation (**Figure 6G**). According to IHC staining data, levels of vessel marker (CD31) and EPC markers (CD34 and CD133) were all markedly higher in CIA mice than in controls.

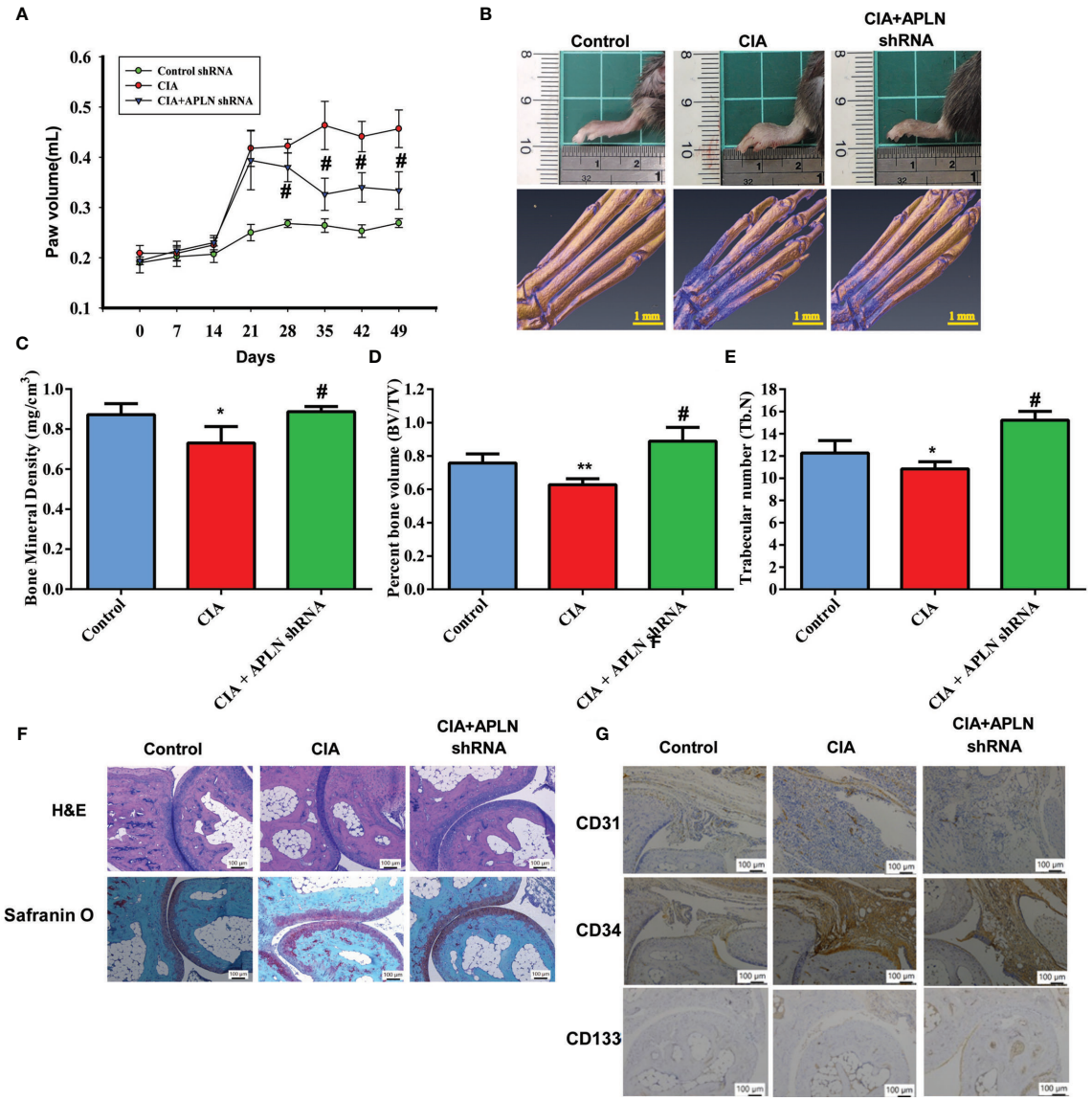

FIGURE 6 | APLN knockdown reduces angiogenesis and the severity of RA *in vivo*. CIA mice received intra-articular injections of 7.1×10^6 PFU APLN shRNA or control shRNA on day 14 and were euthanized on day 49. **(A)** In comparisons of digital plethysmometer values for the amounts of hind paw swelling in the CIA and APLN shRNA groups, the statistical comparisons were not significant on days 14 and 21 (p=0.5 and p=0.3, respectively), but they were significant change on days 14, 21, 28,35,42 and 49 (p=0.001, p<0.0001, p<0.0001, and p<0.0001, respectively). **(B)** Representative micro-CT images of the hind paws taken on day 49. **(C–E)** Micro-CT SkyScan Software quantified bone mineral density, bone volume and trabecular numbers. **(F, G)** Histological sections of ankle joints were stained with H&E or Safranin O and immunostained with CD31, CD34 and CD133. $^*p < 0.05$ versus the control group; $^{\#}p < 0.05$ *versus* the APLN-treated group. $^*p < 0.05$ and $^{**}p < 0.01$ *versus* the control group; $^{\#}p < 0.05$ *versus* the CIA group.

Notably, APLN shRNA treatment antagonized CIA-induced upregulation of CD31, CD34 and CD133 expression (**Figure 6G**). Furthermore, the *in vitro* results were confirmed by qPCR assays, showing lower levels of APLN mRNA in the APLN-shRNA group compared with those in the CIA group, while levels of miR-525-5p were higher in the APLN-shRNA group than in the CIA group (**Supplementary Figure S4**). These results indicate that inhibiting APLN lowers EPC angiogenesis as well as disease activity in CIA-induced arthritis.

DISCUSSION

RA is well recognized for its manifestations of synovial inflammation and joint destruction (1, 37, 38). The development of RA disease relies upon pannus formation and neovascularization (2). Ang1 is a critical modulator during the physiological and pathological progression of angiogenesis (39). APLN reportedly increases IL-1β expression and VEGF-mediated angiogenesis, facilitating OA development (14, 19).

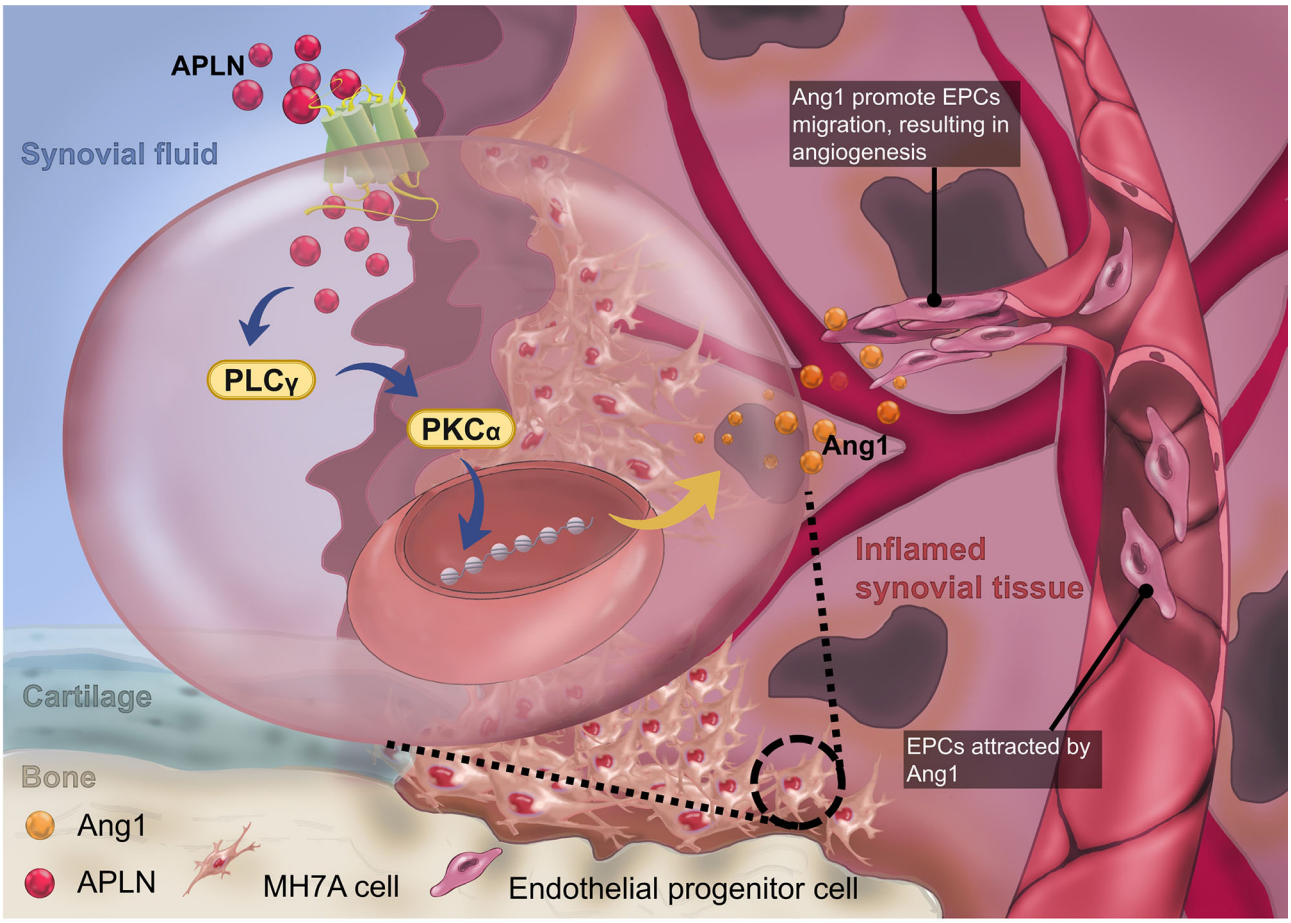

FIGURE 7 | The schematic diagram summarizes the mechanisms of APLN-induced Ang1-dependent EPC angiogenesis during RA pathogenesis. APLN induces Ang1 expression in RASFs by suppressing miR-525-5p expression *via* the PLCγ and PKCα signaling pathways, and promotes EPC angiogenesis in RA.

Here, we report finding higher APLN and Ang1 expression in patients with RA than in those with OA. Moreover, we found that APLN stimulates Ang1 synthesis in RASFs and facilitates EPC angiogenesis by inhibiting miR-525-5p synthesis *via* PLCγ and PKCα signaling. Importantly, inhibiting the expression of APLN reduces EPC angiogenesis, reducing the progression of RA *in vivo*.

EPCs also stimulate new vessel formation (40, 41) and promotion of EPC mobilization by angiogenic factors facilitates tumor development and angiogenesis (42). EPC angiogenesis plays a vital role in RA (5, 43). EPC infiltration into joints has been reported in the CIA-induced RA mouse model (5). Here, we observed that compared with OA synovial fluid, RA synovial fluid facilitates EPC infiltration and angiogenesis, indicating that EPC-dependent angiogenesis is an important step during RA progression. Levels of EPC-specific markers were higher in our CIA mouse model than in controls. APLN shRNA reduced levels of vessel markers and EPC markers and mitigated the severity of RA disease. Thus, inhibition of APLN shows promise as a novel strategy in RA disease, reducing EPC angiogenesis and disease development.

Various proangiogenic factors, including VEGF, fibroblast growth factor, PDGF and Ang, are involved in the angiogenic process of several different diseases, including arthritis (2). Interestingly, we found that Ang1 antibody significantly antagonized increases in EPC angiogenesis induced by RA synovial fluid, suggesting that Ang1 is a vital modulator in EPC-mediated angiogenesis during RA development. Incubation of RASFs with APLN concentration-dependently promotes Ang1 synthesis, resulting in EPC angiogenesis. Importantly, Ang1 antibody, but not VEGF antibody, abolished EPC migration and tube formation in CM from APLN-treated RASFs, indicating that Ang1 is more important than VEGF in APLN-induced angiogenesis during RA disease.

Activation of the PLC/PKC signaling cascade is essential for regulating various cellular functions, including pathogenesis of arthritic diseases (34, 44). The proliferation of synoviocytes from patients with RA has been reported to be suppressed by PLC and PKC inhibitors (44). In our previous research, we found that the PLC/PKC pathway was involved in thrombin-induced interleukin-6 synthesis in rheumatoid synovial cells (45).

However, the impact of these molecules on synovium-induced angiogenesis is not clear. In OA-related research, APLN increased angiogenesis responses, including endothelial cell migration, proliferation, and the capillary tube-like structure formation of endothelial cells (19, 46). Our investigations found that PLC and PKC inhibitors reduced APLN-enhanced Ang1 expression in RASFs and EPC angiogenesis. This was confirmed by findings from genetic siRNA experiments demonstrating that PLCγ and PKCα mediate the angiogenic effects of APLN. Treatment of RASFs with APLN also augmented PLCγ and PKCα phosphorylation. This suggests that PLCγ and PKCα activation are controlled by APLN-dependent Ang1 angiogenesis in EPCs. Recent publications have described how PKCδ activation regulates lymphangiogenesis and angiogenesis in RASFs and LEC cells (31, 47). However, our study showed that neither the PKCδ inhibitor (Rottlerin) nor the genetic siRNA affected APLN-facilitated expression of Ang1 and angiogenesis in EPCs, indicating that the PKCδ pathway is not involved in APLN-regulated angiogenic effects. Thus, PKCα but not PKCδ activation regulates APLN-induced Ang1 expression and EPC angiogenesis.

MiRNAs post-transcriptionally regulate gene expression (48). In RA, aberrant miRNA expression regulates the expression of inflammatory pathways (35, 36). Numerous miRNAs also control angiogenesis during RA progression (49). MiR-525-5p has been implicated in multiple cancers, including for instance glioma (50), cervical cancer (51) and NSCLC (52), but no evidence to date has indicated the involvement of miR-525-5p with RA progression. In this study, stimulation of RASFs with APLN inhibited miR-525-5p expression and transfecting them with miR-525-5p mimic antagonized APLN-promoted upregulation of Ang1 expression and EPC angiogenesis. It has been reported that transcriptional and post-transcriptional regulation play key roles in miRNA activation and inhibition (53). In this study, treating RASFs with PLCγ and PKCα inhibitors reversed APLN-promoted inhibition of miR-525-5p expression, which suggests that APLN may assist with Ang1 production and EPC angiogenesis by inhibiting miR-525-5p synthesis *via* the PLCγ and PKCα signaling cascades. Whether PLCγ/PKCα signaling regulates miR-525-5p expression through transcriptional or post-transcriptional regulation needs further examination.

In conclusion, we have determined that APLN increases Ang1 synthesis and subsequently facilitates EPC angiogenesis by suppressing miR-525-5p synthesis *via* PLCγ and PKCα signaling (**Figure 7**). The evidence supports the targeting of the APLN-dependent miR-525-5p/Ang1 axis in RA treatment regimens.

DATA AVAILABILITY STATEMENT

The original contributions presented in the study are included in the article/**Supplementary Material**. Further inquiries can be directed to the corresponding author.

ETHICS STATEMENT

The studies involving human participants were reviewed and approved by CMUH108-REC3-039. The patients/participants provided their written informed consent to participate in this study. The animal study was reviewed and approved by CMUIACUC-2019-330.

AUTHOR CONTRIBUTIONS

C-HTa, H-PL, and C-JH initiated the research project. Y-HZ, S-CL, C-CH, C-HTs, and S-WW performed the research. C-CH, C-HTs, and S-WW provided the material. C-HTa wrote the paper. All authors contributed to the article and approved the submitted version.

FUNDING

This work was supported by grants from the Ministry of Science and Technology in Taiwan (MOST 110-2320-B-039-022-MY3; MOST 110-2314-B-039-008; MOST 110-2314-B-039-012; MOST 110-2314-B-195-003), China Medical University Beigang Hospital (110CMUBHR-07 and 110CMUBHR-11) and China Medical University Hospital (DMR-110-074).

ACKNOWLEDGMENTS

We would like to thank Iona J. MacDonald from China Medical University for her editing of this manuscript.

SUPPLEMENTARY MATERIAL

The Supplementary Material for this article can be found online at: https://www.frontiersin.org/articles/10.3389/fimmu.2021.737990/full#supplementary-material

REFERENCES

1. Smolen JS, Aletaha D, McInnes IB. Rheumatoid Arthritis. *Lancet* (2016) 388 (10055):2023–38. doi: 10.1016/S0140-6736(16)30173-8
2. MacDonald IJ, Liu SC, Su CM, Wang YH, Tsai CH, Tang CH. Implications of Angiogenesis Involvement in Arthritis. *Int J Mol Sci* (2018) 19(7):2012–30. doi: 10.3390/ijms19072012
3. Asahara T, Masuda H, Takahashi T, Kalka C, Pastore C, Silver M, et al. Bone Marrow Origin of Endothelial Progenitor Cells Responsible for Postnatal Vasculogenesis in Physiological and Pathological Neovascularization. *Circ Res* (1999) 85(3):221–8. doi: 10.1161/01.RES.85.3.221
4. Peplow PV. Influence of Growth Factors and Cytokines on Angiogenic Function of Endothelial Progenitor Cells: A Review of *In Vitro* Human Studies. *Growth Factors* (2014) 32(3-4):83–116. doi: 10.3109/08977194.2014.904300
5. Su CM, Hsu CJ, Tsai CH, Huang CY, Wang SW, Tang CH. Resistin Promotes Angiogenesis in Endothelial Progenitor Cells Through Inhibition of MicroRNA206: Potential Implications for Rheumatoid Arthritis. *Stem Cells* (2015) 33(7):2243–55. doi: 10.1002/stem.2024

6. Chen CY, Su CM, Hsu CJ, Huang CC, Wang SW, Liu SC, et al. CCN1 Promotes VEGF Production in Osteoblasts and Induces Endothelial Progenitor Cell Angiogenesis by Inhibiting miR-126 Expression in Rheumatoid Arthritis. *J Bone Mineral Res* (2017) 32(1):34–45. doi: 10.1002/jbmr.2926
7. Carmeliet P, Jain RK. Molecular Mechanisms and Clinical Applications of Angiogenesis. *Nature* (2011) 473(7347):298–307. doi: 10.1038/nature10144
8. Weis SM, Cheresh DA. Tumor Angiogenesis: Molecular Pathways and Therapeutic Targets. *Nat Med* (2011) 17(11):1359–70. doi: 10.1038/nm.2537
9. Brindle NP, Saharinen P, Alitalo K. Signaling and Functions of Angiopoietin-1 in Vascular Protection. *Circ Res* (2006) 98(8):1014–23. doi: 10.1161/01.RES.0000218275.54089.12
10. Kinjo T, Higashi H, Uno K, Kuramoto N. Apelin/Apelin Receptor System: Molecular Characteristics, Physiological Roles, and Prospects as a Target for Disease Prevention and Pharmacotherapy. *Curr Mol Pharmacol* (2021) 14 (2):210–9. doi: 10.2174/1874467213666200602133032
11. Zhou Q, Cao J, Chen L. Apelin/APJ System: A Novel Therapeutic Target for Oxidative Stress-Related Inflammatory Diseases (Review). *Int J Mol Med* (2016) 37(5):1159–69. doi: 10.3892/ijmm.2016.2544
12. MacDonald IJ, Liu SC, Huang CC, Kuo SJ, Tsai CH, Tang CH. Associations Between Adipokines in Arthritic Disease and Implications for Obesity. *Int J Mol Sci* (2019) 20(6):1505–22. doi: 10.3390/ijms20061505
13. Hu PF, Chen WP, Tang JL, Bao JP, Wu LD. Apelin Plays a Catabolic Role on Articular Cartilage: *In Vivo* and *In Vitro* Studies. *Int J Mol Med* (2010) 26 (3):357–63. doi: 10.3892/ijmm_00000473
14. Chang TK, Wang YH, Kuo SJ, Wang SW, Tsai CH, Fong YC, et al. Apelin Enhances IL-1beta Expression in Human Synovial Fibroblasts by Inhibiting miR-144-3p Through the PI3K and ERK Pathways. *Aging (Albany NY)* (2020) 12(10):9224–39. doi: 10.18632/aging.103195
15. Gunter S, Solomon A, Tsang L, Woodiwiss AJ, Robinson C, Millen AM, et al. Apelin Concentrations Are Associated With Altered Atherosclerotic Plaque Stability Mediator Levels and Atherosclerosis in Rheumatoid Arthritis. *Atherosclerosis* (2017) 256:75–81. doi: 10.1016/j.atherosclerosis.2016.11.024
16. O'Brien J, Hayder H, Zayed Y, Peng C. Overview of MicroRNA Biogenesis, Mechanisms of Actions, and Circulation. *Front Endocrinol* (2018) 9:12. doi: 10.3389/fendo.2018.00402
17. Mousavi MJ, Jamshidi A, Chopra A, Aslani S, Akhlaghi M, Mahmoudi M. Implications of the Noncoding RNAs in Rheumatoid Arthritis Pathogenesis. *J Cell Physiol* (2018) 234(1):335–47. doi: 10.1002/jcp.26911
18. Chen XM, Huang QC, Yang SL, Chu YL, Yan YH, Han L, et al. Role of Micro RNAs in the Pathogenesis of Rheumatoid Arthritis: Novel Perspectives Based on Review of the Literature. *Med (Baltimore)* (2015) 94(31):e1326. doi: 10.1097/MD.0000000000001326
19. Wang YH, Kuo SJ, Liu SC, Wang SW, Tsai CH, Fong YC, et al. Apelin Affects the Progression of Osteoarthritis by Regulating VEGF-Dependent Angiogenesis and miR-150-5p Expression in Human Synovial Fibroblasts. *Cells* (2020) 9(3):594–610. doi: 10.3390/cells9030594
20. Li TM, Liu SC, Huang YH, Huang CC, Hsu CJ, Tsai CH, et al. YKL-40-Induced Inhibition of miR-590-3p Promotes Interleukin-18 Expression and Angiogenesis of Endothelial Progenitor Cells. *Int J Mol Sci* (2017) 18(5):920–34. doi: 10.3390/ijms18050920
21. Lee H-P, Wang S-W, Wu Y-C, Lin L-W, Tsai F-J, Yang J-S, et al. Soya-Cerebroside Inhibits VEGF-Facilitated Angiogenesis in Endothelial Progenitor Cells. *Food Agric Immunol* (2020) 31(1):193–204. doi: 10.1080/09540105.2020.1713055
22. Lee H-P, Wu Y-C, Chen B-C, Liu S-C, Li T-M, Huang W-C, et al. Soya-Cerebroside Reduces Interleukin Production in Human Rheumatoid Arthritis Synovial Fibroblasts by Inhibiting the ERK, NF-κb and AP-1 Signalling Pathways. *Food Agr Immunol* (2020) 31(1):740–50. doi: 10.1080/09540105.2020.1766426
23. Lee HP, Chen PC, Wang SW, Fong YC, Tsai CH, Tsai FJ, et al. Plumbagin Suppresses Endothelial Progenitor Cell-Related Angiogenesis *In Vitro* and *In Vivo*. *J Funct Foods* (2019) 52:537–44. doi: 10.1016/j.jff.2018.11.040
24. Lee HP, Wang SW, Wu YC, Tsai CH, Tsai FJ, Chung JG, et al. Glucocerebroside Reduces Endothelial Progenitor Cell-Induced Angiogenesis. *Food Agr Immunol* (2019) 30(1):1033–45. doi: 10.1080/09540105.2019.1660623
25. Liu JF, Lee CW, Tsai MH, Tang CH, Chen PC, Lin LW, et al. Thrombospondin 2 Promotes Tumor Metastasis by Inducing Matrix Metalloproteinase-13 Production in Lung Cancer Cells. *Biochem Pharmacol* (2018) 155:537–46. doi: 10.1016/j.bcp.2018.07.024
26. Lee H-P, Liu S-C, Wang Y-H, Chen B-C, Chen H-T, Li T-M, et al. Cordycerebroside A Suppresses VCAM-Dependent Monocyte Adhesion in Osteoarthritis Synovial Fibroblasts by Inhibiting MEK/ERK/AP-1 Signaling. *J Funct Foods* (2021) 86:104712–20. doi: 10.1016/j.jff.2021.104712
27. Huang CC, Chiou CH, Liu SC, Hu SL, Su CM, Tsai CH, et al. Melatonin Attenuates TNF-Alpha and IL-1beta Expression in Synovial Fibroblasts and Diminishes Cartilage Degradation: Implications for the Treatment of Rheumatoid Arthritis. *J Pineal Res* (2019) 66(3):e12560. doi: 10.1111/jpi.12560
28. Liu SC, Tsai CH, Wu TY, Tsai CH, Tsai FJ, Chung JG, et al. Soya-Cerebroside Reduces IL-1 Beta-Induced MMP-1 Production in Chondrocytes and Inhibits Cartilage Degradation: Implications for the Treatment of Osteoarthritis. *Food Agr Immunol* (2019) 30(1):620–32. doi: 10.1080/09540105.2019.1611745
29. Wang M, Chao CC, Chen PC, Liu PI, Yang YC, Su CM, et al. Thrombospondin Enhances RANKL-Dependent Osteoclastogenesis and Facilitates Lung Cancer Bone Metastasis. *Biochem Pharmacol* (2019) 166:23–32. doi: 10.1016/j.bcp.2019.05.005
30. Liu SC, Chuang SM, Hsu CJ, Tsai CH, Wang SW, Tang CH. CTGF Increases Vascular Endothelial Growth Factor-Dependent Angiogenesis in Human Synovial Fibroblasts by Increasing miR-210 Expression. *Cell Death Dis* (2014) 5:e1485. doi: 10.1038/cddis.2014.453
31. Wang CQ, Huang YW, Wang SW, Huang YL, Tsai CH, Zhao YM, et al. Amphiregulin Enhances VEGF-A Production in Human Chondrosarcoma Cells and Promotes Angiogenesis by Inhibiting miR-206 *via* FAK/c-Src/PKCdelta Pathway. *Cancer Lett* (2017) 385:261–70. doi: 10.1016/j.canlet.2016.10.010
32. Su CM, Chiang YC, Huang CY, Hsu CJ, Fong YC, Tang CH. Osteopontin Promotes Oncostatin M Production in Human Osteoblasts: Implication of Rheumatoid Arthritis Therapy. *J Immunol* (2015) 195(7):3355–64. doi: 10.4049/jimmunol.1403191
33. Hu SL, Chang AC, Huang CC, Tsai CH, Lin CC, Tang CH. Myostatin Promotes Interleukin-1beta Expression in Rheumatoid Arthritis Synovial Fibroblasts Through Inhibition of miR-21-5p. *Front Immunol* (2017) 8:1747. doi: 10.3389/fimmu.2017.01747
34. Wang LH, Tsai HC, Cheng YC, Lin CY, Huang YL, Tsai CH, et al. CTGF Promotes Osteosarcoma Angiogenesis by Regulating miR-543/Angiopoietin 2 Signaling. *Cancer Lett* (2017) 391:28–37. doi: 10.1016/j.canlet.2017.01.013
35. Zhang L, Wu H, Zhao M, Chang C, Lu Q. Clinical Significance of miRNAs in Autoimmunity. *J Autoimmun* (2020) 109:102438. doi: 10.1016/j.jaut.2020.102438
36. Wang J, Yan S, Yang J, Lu H, Xu D, Wang Z. Non-Coding RNAs in Rheumatoid Arthritis: From Bench to Bedside. *Front Immunol* (2019) 10:3129. doi: 10.3389/fimmu.2019.03129
37. McInnes IB, Schett G. The Pathogenesis of Rheumatoid Arthritis. *N Engl J Med* (2011) 365(23):2205–19. doi: 10.1056/NEJMra1004965
38. Catrina AI, Svensson CI, Malmstrom V, Schett G, Klareskog L. Mechanisms Leading From Systemic Autoimmunity to Joint-Specific Disease in Rheumatoid Arthritis. *Nat Rev Rheumatol* (2017) 13(2):79–86. doi: 10.1038/nrrheum.2016.200
39. Hayashi SI, Rakugi H, Morishita R. Insight Into the Role of Angiopoietins in Ageing-Associated Diseases. *Cells* (2020) 9(12):2636–51. doi: 10.3390/cells9122636
40. Patel J, Donovan P, Khosrotehrani K. Concise Review: Functional Definition of Endothelial Progenitor Cells: A Molecular Perspective. *Stem Cells Trans Med* (2016) 5(10):1302–6. doi: 10.5966/sctm.2016-0066
41. Kiewisz J, Kaczmarek MM, Pawlowska A, Kmiec Z, Stompor T. Endothelial Progenitor Cells Participation in Cardiovascular and Kidney Diseases: A Systematic Review. *Acta Biochim Polonica* (2016) 63(3):475–82. doi: 10.18388/abp.2016_1284
42. Peters BA, Diaz LA, Polyak K, Meszler L, Romans K, Guinan EC, et al. Contribution of Bone Marrow-Derived Endothelial Cells to Human Tumor Vasculature. *Nat Med* (2005) 11(3):261–2. doi: 10.1038/nm1200
43. Chien SY, Huang CY, Tsai CH, Wang SW, Lin YM, Tang CH. Interleukin-1beta Induces Fibroblast Growth Factor 2 Expression and Subsequently Promotes Endothelial Progenitor Cell Angiogenesis in Chondrocytes. *Clin Sci* (2016) 130(9):667–81. doi: 10.1042/CS20150622
44. Furuhashi I, Abe K, Sato T, Inoue H. Thrombin-Stimulated Proliferation of Cultured Human Synovial Fibroblasts Through Proteolytic Activation of

Proteinase-Activated Receptor-1. *J Pharmacol Sci* (2008) 108(1):104–11. doi: 10.1254/jphs.08126FP
45. Chiu YC, Fong YC, Lai CH, Hung CH, Hsu HC, Lee TS, et al. Thrombin-Induced IL-6 Production in Human Synovial Fibroblasts Is Mediated by PAR1, Phospholipase C, Protein Kinase C Alpha, C-Src, NF-Kappa B and P300 Pathway. *Mol Immunol* (2008) 45(6):1587–99. doi: 10.1016/j.molimm.2007.10.004
46. Wen Y, Chen R, Zhu C, Qiao H, Liu Y, Ji H, et al. MiR-503 Suppresses Hypoxia-Induced Proliferation, Migration and Angiogenesis of Endothelial Progenitor Cells by Targeting Apelin. *Peptides* (2018) 105:58–65. doi: 10.1016/j.peptides.2018.05.008
47. Tai HC, Lee TH, Tang CH, Chen LP, Chen WC, Lee MS, et al. Phomaketide A Inhibits Lymphangiogenesis in Human Lymphatic Endothelial Cells. *Marine Drugs* (2019) 17(4):215–30. doi: 10.3390/md17040215
48. Nugent M. MicroRNAs: Exploring New Horizons in Osteoarthritis. *Osteoarthritis Cartilage* (2016) 24(4):573–80. doi: 10.1016/j.joca.2015.10.018
49. Tiwari A, Mukherjee B, Dixit M. MicroRNA Key to Angiogenesis Regulation: MiRNA Biology and Therapy. *Curr Cancer Drug Targets* (2018) 18(3):266–77. doi: 10.2174/1568009617666170630142725
50. Xie P, Han Q, Liu D, Yao D, Lu X, Wang Z, et al. miR-525-5p Modulates Proliferation and Epithelial-Mesenchymal Transition of Glioma by Targeting Stat-1. *Onco Targets Ther* (2020) 13:9957–66. doi: 10.2147/OTT.S257951
51. Chen M, Liu LX. MiR-525-5p Repressed Metastasis and Anoikis Resistance in Cervical Cancer *via* Blocking UBE2C/ZEB1/2 Signal Axis. *Dig Dis Sci* (2020) 65(8):2442–51. doi: 10.1007/s10620-019-05916-9
52. Wu X, Li M, Li Y, Deng Y, Ke S, Li F, et al. Fibroblast Growth Factor 11 (FGF11) Promotes Non-Small Cell Lung Cancer (NSCLC) Progression by Regulating Hypoxia Signaling Pathway. *J Transl Med* (2021) 19(1):353.
53. Ambros V. The Functions of Animal microRNAs. *Nature* (2004) 431 (7006):350–5. doi: 10.1038/nature02871

Conflict of Interest: The authors declare that the research was conducted in the absence of any commercial or financial relationships that could be construed as a potential conflict of interest.

Publisher's Note: All claims expressed in this article are solely those of the authors and do not necessarily represent those of their affiliated organizations, or those of the publisher, the editors and the reviewers. Any product that may be evaluated in this article, or claim that may be made by its manufacturer, is not guaranteed or endorsed by the publisher.

frontiers in Immunology

ORIGINAL RESEARCH
published: 14 October 2021
doi: 10.3389/fimmu.2021.756825

Decreased miR-4512 Levels in Monocytes and Macrophages of Individuals With Systemic Lupus Erythematosus Contribute to Innate Immune Activation and Neutrsophil NETosis by Targeting TLR4 and CXCL2

Binbin Yang[1†], Xinwei Huang[2†], Shuangyan Xu[1,3], Li Li[1,4], Wei Wu[1,5], Yunjia Dai[1,6], Ming-Xia Ge[7,8], Limei Yuan[1], Wenting Cao[1], Meng Yang[1], Yongzhuo Wu[1] and Danqi Deng[1]*

[1] Department of Dermatology, The Second Affiliated Hospital of Kunming Medical University, Kunming, China, [2] Key Laboratory of The Second Affiliated Hospital of Kuming Medical University, Kunming, China, [3] Department of Dermatology, The 6th Affiliated Hospital of Kunming Medical University, The People's Hospital of Yuxi City, Kunming, China, [4] Dai Medicine College, West Yunnan University of Applied Sciences, Xishuangbanna, China, [5] Department of Dermatology, Suining Central Hospital, Suining, China, [6] Department of Dermatology, Panlong District People's Hospital, Kunming, China, [7] State Key Laboratory of Genetic Resources and Evolution/Key Laboratory of Healthy Aging Research of Yunnan Province, Kunming Institute of Zoology, Chinese Academy of Sciences, Kunming, China, [8] Kunming College of Life Science, University of Chinese Academy of Sciences, Beijing, China

Objective: Systemic lupus erythematosus (SLE) is an autoimmune disease with complex etiology that is not yet entirely understood. We aimed to elucidate the mechanisms and therapeutic potential of microRNAs (miRNAs) in SLE in a Tibetan population.

Methods: Peripheral blood mononuclear cells from SLE patients (n = 5) and healthy controls (n = 5) were used for miRNA–mRNA co-sequencing to detect miRNAs related to immune abnormalities associated with SLE. Luciferase reporter assay was used to identify potential targets of candidate miRNA. The target genes were verified in miRNA-agomir/antagomir transfection assays with multiple cells lines and by expression analysis. The effects of candidate miRNA on monocyte and macrophage activation were evaluated by multiple cytokine profiling. Neutrophil extracellular traps (NETs) formation was analyzed *in vitro* by cell stimulation with supernatants of monocytes and macrophages transfected with candidate miRNA. The rodent MRL/lpr lupus model was used to evaluate the therapeutic effect of CXCL2Ab on SLE and the regulation effect of immune disorders.

Results: Integrated miRNA and mRNA expression profiling identified miRNA-4512 as a candidate miRNA involved in the regulation of neutrophil activation and chemokine-related pathways. MiR-4512 expression was significantly reduced in monocytes and macrophages from SLE patients. MiR-4512 suppressed the TLR4 pathway by

OPEN ACCESS

Edited by:
Jianfeng Chen, Shanghai Institute of Biochemistry and Cell Biology (CAS), China

Reviewed by:
Changsheng Du, Tongji University, China
Gang Wang, Fourth Military Medical University, China

***Correspondence:**
Danqi Deng
danqid128@sina.com

†These authors have contributed equally to this work

Specialty section:
This article was submitted to Autoimmune and Autoinflammatory Disorders, a section of the journal Frontiers in Immunology

Received: *11 August 2021*
Accepted: *23 September 2021*
Published: *14 October 2021*

Citation:
Yang B, Huang X, Xu S, Li L, Wu W, Dai Y, Ge M-X, Yuan L, Cao W, Yang M, Wu Y and Deng D (2021) Decreased miR-4512 Levels in Monocytes and Macrophages of Individuals With Systemic Lupus Erythematosus Contribute to Innate Immune Activation and Neutrsophil NETosis by Targeting TLR4 and CXCL2. Front. Immunol. 12:756825. doi: 10.3389/fimmu.2021.756825

targeting *TLR4* and *CXCL2*. Decreased monocyte and macrophage miR-4512 levels led to the expression of multiple proinflammatory cytokines *in vitro*. Supernatants of miR-4512 antagomir-transfected monocytes and macrophages significantly promoted NETs formation ($P < 0.05$). Blocking of CXCL2 alleviated various pathogenic manifestations in MRL/lpr mice, including kidney damage and expression of immunological markers of SLE.

Conclusions: We here demonstrated the role of miR-4512 in innate immunity regulation in SLE. The effect of miR-4512 involves the regulation of monocytes, macrophages, and NETs formation by direct targeting of *TLR4* and *CXCL2*, indicating the miR-4512-TLR4-CXCL2 axis as a potential novel therapeutic target in SLE.

Keywords: systemic lupus erythematosus, miR-4512, CXCl2, neutrophil extracellular trap, innate immune activation

INTRODUCTION

Systemic lupus erythematosus (SLE) is a chronic, incurable autoimmune disease. It is characterized by the induction of abnormal cell death pathways and clearance mechanisms, excessive externalization of modified cells and nuclear debris, loss of tolerance to various self-antigens, and innate and adaptive immune disorders (1). The innate immune system might initiate and promote SLE autoimmunity and organ damage (2). Pro-inflammatory monocytes, macrophages, and neutrophils enter the kidney and other organs during SLE progression (3). Further, abnormal macrophage activation and secretion have been demonstrated in SLE in human and in animal models (4). However, the mechanism by which the innate immune system, especially pro-inflammatory monocytes, macrophages and neutrophils cause organ damage in SLE is not yet fully understood.

MicroRNAs (miRNAs) are small non-coding RNAs that act by regulating gene expression. The roles of miRNAs in regulating immune defense genes remain to be clarified (5). Some information on miRNA activity in SLE is available. For instance, miRNA-30e-5p regulates the innate immune response during viral infection and SLE (6). MiR-146a suppresses nuclear factor-k-gene binding (NF-κB) and cytokine production during SLE development (7). MiR-155 targets the suppressor of cytokine signaling 1 (SOCS1) in macrophages and promotes an inflammatory response and type I interferon (IFN) signaling (8). MiRNA-150 promotes inflammation by suppressing the triggering receptors expressed on myeloid cells 1 (TREM-1), which are positive regulators of the toll-like receptor 4 (TLR-4) signaling pathway (9). MiR-125a regulates autoimmune diseases by stabilizing immune homeostasis mediated by regulatory T cells (10). However, the roles of miRNAs in monocytes and macrophages during autoimmune pathogenesis remain to be elucidated.

We have previously shown that the expression of miR-125b-5p decreases and that of the autophagy gene UVRAG increases, activating cell autophagy after UVB irradiation of the peripheral blood mononuclear cells (PBMCs) of SLE patients of Han ethnicity (11). Tibetans are theoretically more susceptible to systemic lupus than Han Chinese because they live at high altitudes and are exposed to oxygen deprivation and intense ultraviolet radiation. However, the characteristics of gene expression in Tibetan patients with SLE in China have not been reported. In the current study, blood samples from Tibetan patients with SLE in Diqing Shangri-La (Yunnan Province, China) were analyzed by high-throughput sequencing to screen for mRNA and miRNAs differentially expressed between healthy and SLE Tibetan patients. Next, miRNA-mRNA co-sequencing and functional analysis revealed that miRNA-4512 may be involved in immune regulation of SLE. We analyzed the expression of miR-4512 in PBMCs and monocytes of Tibetan and Han SLE patients, and identified the mechanism and direct target of miR-4512 in innate immune regulation. In addition, the therapeutic efficacy of these targets in animal models of SLE was further verified.

MATERIALS AND METHODS

Patients and Controls

Nineteen SLE patients (10 Tibetan, mean age 46.1 ± 16.42 y; nine Han, mean age 35 ± 13.67 y) and 17 healthy controls (nine Tibetan, mean age 39.70 ± 3.76 y; eight Han, mean age 29.78 ± 1.37 y) matched for age, gender, and altitude were recruited (**Supplementary Table S1**). All patients met ≥ 4 of the revised SLE criteria of the American College of Rheumatology (1997) (12). Informed written consent was obtained, and the study design was approved by the Ethics Committee of the Second Affiliated Hospital of Kunming Medical University.

RNA Extraction and Reverse-Transcription Quantitative Polymerase Chain Reaction (RT-qPCR)

Total RNA from freshly isolated PBMCs (section 2.7) or cell cultures was extracted with TRIzol Reagent (Invitrogen, San Diego, CA, USA). The cDNA was synthesized using a SureScript™ First-Strand cDNA Synthesis Kit (GeneCopoeia, Guangzhou, China). The mRNA levels were determined by RT-qPCR with BlazeTaq™ SYBR® Green qPCR Mix 2.0 (GeneCopoeia) and *GAPDH* as the internal control. The primers are listed in **Supplementary Table S2**. Total RNA was reverse-transcribed and quantified with an All-in-One™ miRNA

RT-qPCR Detection kit (QP015, GeneCopoeia). U6 small nuclear RNA was the internal control.

Sample Library Construction and Sequencing

Total RNA was extracted from samples before sequencing using TRIzol reagent (Invitrogen, San Diego, CA, USA). RNA integrity and quantity were evaluated by using a Nanodrop spectrophotometer (Thermo Fisher Scientific, Waltham, MA, USA) and Agilent 2100 Bioanalyzer (Agilent Technologies, Palo Alto, California, USA). The cDNA was synthesized using Superscript II reverse transcriptase (Invitrogen, Carlsbad, CA, USA) and random primers, with enriched and fragmented RNA as template. The cDNA was converted to dsDNA for library construction. The libraries were quantified using an Agilent 2100 Bioanalyzer (Agilent Technologies, Palo Alto, California, USA). Sequencing was performed using Illumina NextSeq6000 platform (Illumina, San Diego, CA, USA). Multiplex Small RNA Library Prep Set for Illumina was used to construct small RNA libraries based on miRNA sequencing, in accordance with the manufacturer's protocol. Fragments (18-35 nt) were extracted from the total RNA, and indices and adaptors were added for PCR amplification. Agilent 2100 Bioanalyzer (Agilent Technologies, Palo Alto, CA, USA) was used for library quantification. The library was sequenced by Shanghai Personal Biotechnology Co. Ltd. (Shanghai, China) using Hiseq platform (Illumina).

Sequencing Data Analysis

The reference genome index was set up using Bowtie2 v. 2.4.1 (http://bowtie-bio.sourceforge.net/bowtie2/index.shtml). HISAT2 v. 2.1.0 (http://www.ccb.jhu.edu/software.shtml) was used to map the filtered reads to the reference genome. Reads for each gene were counted using HTSeq v. 0.11.1 (https://htseq.readthedocs.io/en/master/). Gene expression was standardized using FPKM, and differential expression was analyzed using DESeq v. 1.39.0 (http://bioconductor.org/packages/release/bioc/html/DESeq.html) according to the criteria $|\log2FoldChange| > 1$ and $P < 0.05$. MiRDeep2 v. 2.0.0.8 (https://github.com/Rajewsky-lab/mirdeep2.git) was used to map the clean reads to the reference genome in the miRBase database (http://www.mirbase.org/), to annotate unique reads. Other non-coding RNAs were used for the annotation. Mireap v. 2.0 (https://sourceforge.net/projects/mireap/) was used to analyze the unannotated sequences. MiRNA reads were counted based on the number of sequences conforming with mature miRNA. The most abundant miRNAs were selected for subsequent analysis. DESeq v. 1.30.0 was used to identify differentially expressed miRNAs as those meeting the criteria $|\log2FoldChange| > 1$ and $P < 0.05$.

The mRNA 3′ untranslated region (UTR) was the target sequence. MiRanda v. 3.3a (https://anaconda.org/bioconda/miranda) was used to predict the target genes of the differentially expressed miRNAs. Kyoto Encyclopedia of Genes and Genomes (KEGG, http://www.kegg.jp/) and gene ontology (GO, http://geneontology.org/) were used to analyze the enrichment of target genes associated with differentially expressed mRNA and miRNAs. All genes were mapped to KEGG and GO terms and pathways, and the latter were filtered using corrected $P \leq 0.05$.

Luciferase Reporter Assay

To verify the target genes of miR-4512, putative miR-4512 target sequences located in the 3′-UTR of human C-X-C motif ligand (*CXCL2*, *TLR4*, *CCR1*, *CXCL1*, and *CXCL5* transcripts were synthesized and cloned into pmirGLO vector (Promega, Madison, WI, USA) downstream of the *Luc2* reporter gene. Plasmids harboring mutated sequences were constructed by inserting each target sequence with various base deletions at the putative miR-4512–binding site (The sequences are listed in **Supplementary Figure S1**). Vectors were sequenced and prepared using an Endo-Free Plasmid ezFlow Mini kit (Promega). Then, HEK293T cells were co-transfected with pmirGLO-(CXCL2, TLR4, CCR1, CXCL1 and CXCL5) and pmirGLO-(CXCL2, TLR4, CCR1, CXCL1 and CXCL5)-MUT plasmids using Lipofectamine™ 2000 (Invitrogen, Carlsbad, CA, USA) and miR-4512 agomir or miR-4512 NC. After 48 h, the cells were harvested, and relative luciferase activity was measured using a Dual-Luciferase Reporter Assay System (Promega, Madison WI, USA), according to the manufacturer's instructions. Renilla luciferase normalized firefly luciferase activity.

Enzyme-Linked Immunosorbent Assay (ELISA), Western Blotting

The levels of various cytokines [interleukin (IL)-1β, IL-2, IL-12, tumor necrosis factor (TNF)-α, IFN-γ, IL-4, IL-6, IL-10, and IL-17] in the sera of human patients and experimental mice, supernatants of monocytes or macrophages transfected with NC/miR-4512-agomir/antagomir and mouse renal lysis solution were quantified using ELISA kits (NeoBioscience, Beijing, China), according to the manufacturer's instructions. Mouse serum antinuclear antibody (ANA), anti-dsDNA antibody, and human serum CXCL2 concentrations were measured using appropriate ELISA kits (JL17316-48T, JL12477-48T, and JL25367-96T, respectively; Jianglai Biology, Shanghai, China). Human serum myeloperoxidase (MPO) concentration was measured with an ELISA kit (0-111594; Jonln, Shanghai, China), according to the manufacturer's instructions. Anti-TLR4 monoclonal antibody (1:1000, clone 3G9A4; Proteintech Group, Chicago, IL USA) and Anti-neutrophil elastase (NE) monoclonal antibodies (1:100; 89241S; Cell Signaling Technology, Danvers, MA, USA) were used for western blotting, with β-actin was the internal control.

Cell-Free DNA (cfDNA) Detection

Cell supernatant was treated according to the Picogreen Kit (Invitrogen), and each sample was diluted 1:9 (cell supernatant: TE working solution) with TE working solution; Add 100ul of 10-fold diluted samples to each well, set up two duplicate Wells, and then add 200ul Picogreen reagent in an aqueous working solution chamber to incubate at warm temperature for 10min; Determination: The full-function continuous wavelength

scanning microplate analysis system measured all samples in a 96-well microplate at a final volume of 200ul. The standard curve was established with the concentration of DNA standard as the X axis and the fluorescence at 480nm as the Y axis. The concentration of the corresponding sample was calculated according to the fluorescence value of the sample.

Cell Isolation and Culture

PBMCs were separated from ethylene diamine tetraacetic acid (EDTA) blood by density gradient centrifugation (450 × *g*, 30 min) on Ficoll-Paque Plus (GE Healthcare, Little Chalfont, UK) and resuspended in RPMI 1640 medium supplemented with 100 U/mL penicillin and 100 μg/mL streptomycin (Gibco, Grand Island, NY, USA) and 10% fetal bovine serum (Gibco, Grand Island, NY, USA).

$CD14^+CD16^-$ monocytes were isolated from freshly isolated PBMCs by immunomagnetic negative selection using an EasySep™ Human Monocyte Isolation kit (19669; STEMCELL Technologies, Vancouver, BC, Canada), according to the manufacturer's instructions. Human macrophages were obtained by culturing $CD14^+$ monocytes for 7 d in RPMI 1640 medium containing 50 ng/mL macrophage colony-stimulating factor(M-CSF). The macrophages were identified by F4/80 expression. Neutrophils were isolated by gradient centrifugation (500 × *g*, 30 min) on Hypaque-Ficoll solution (LZS11131; TBD, Tianjin, China). Monocytes, neutrophils, and differentiated macrophages were cultured in complete RPMI 1640 medium.

In Vitro NETs Formation Assay

$CD14^+$ monocytes from healthy donors and macrophages were transfected with NC/miR-4512-agomir/antagomir using EndoFectin™ Max (EF013; Genecopoeia). After 12 h, the conditioned medium was collected. Fresh neutrophils isolated from healthy donors were exposed to the medium for 3 h. Cells treated with 10 μg/mL lipopolysaccharide (LPS) and 50 ng/mL CXCL2 were used as the positive controls. Culture supernatants were collected for ELISA analysis. Stimulated neutrophils were collected for western blotting and NETs staining and quantification.

NETs Staining and Quantification

The neutrophils were inoculated in the confocal dishes at a concentration of 2×10^5/mL, fixed with 4% paraformaldehyde for 15 min, then permeabilized with 0.5% Triton X-100 at room temperature for 10 min. Then the cells were stained with 1 μm Sytox Green (Invitrogen) and Hoechst nucleic acid stain (1:1000; Invitrogen). Random photographs were taken under the condition of scattered light at 520 nm. The obtained images were analyzed by Zen 2012 software (n=4). For quantification of NETs, neutrophils were seeded in 96-well black plates (2×10^5 cells/well) in the presence of 5 μM Sytox Green. After stimulation with different conditioned medium for 3 hours, the florescence intensity was quantified with excitation at 485 nm and emission at 535 nm using Infinite M200 Pro (Tecan).

MLR/lpr Animal Model

Four female MRL/lpr mice (8-wk-old, 19 ± 0.5 g; Hunan Slack Jingda Experimental Animal Co. Ltd., Hunan, China) were intraperitoneally injected with mouse CXCL2 monoclonal antibody (300-39-2; PeproTech, Rocky Hill, NJ, USA), twice weekly (50 μg/50 μL) for 4 wk. The control (n = 4, female MRL/lpr mice, 8-wk-old, 18 ± 0.5 g; Hunan Slack Jingda Experimental Animal Co. Ltd.) received 50 μL of saline per treatment. Sex- and age-matched normal C57BL/6 mice (n = 4, 8-wk-old, 18 ± 0.5 g; Hunan Slack Jingda Experimental Animal Co. Ltd.) were administered saline according to the above schema. Urine was collected twice weekly from each group. Proteinuria was detected by Coomassie Brilliant Blue (CBB) staining (Bayer, Elkhart, IN, USA). Mice were sacrificed by CO_2 asphyxiation at 12 wk. The blood was collected, and serum levels of anti-dsDNA, ANA and multiple cytokines were measured using commercial kits (Jianglaibio, Shanghai, China). The kidneys were excised and dissected for immunocytochemistry (IHC) staining (as described in section 2.10) and cytokine analysis by ELISA.

The mice were randomly assigned to different groups according to their unique code, and all data were collected by technicians blinded to the treatment protocol. The experiment was conducted in a laboratory animal facility of Kunming Medical University and approved by the Animal Research Committee of Kunming Medical University (No. kmmu2021724).

Histopathology and IHC Staining

Mouse kidneys were fixed in 4% (v/v) paraformaldehyde, embedded in paraffin, sectioned (6 μm) using a rotary microtome (Leica Biosystems, Wetzlar, Germany), and stained with hematoxylin and eosin (H&E). Active and chronic renal tubular changes were semi-quantitatively analyzed as previously described (13). The activity index (AI) data included glomerular endocapillary proliferation, intraglomerular leukocyte infiltration, platinum ear-pick and/or hyaline thrombus, fibrinoid necrosis and/or nuclear fragmentation, cellular crescent, and inflammatory cell infiltration in the interstitial space. A score in the range of 0–3 was assigned to each item, and all items were summed to yield a final AI score. The chronic index (CI) parameters included glomerulosclerosis, fibrous crescent, renal tubular atrophy, and renal interstitial fibrosis. A score in the range of 0-3 was assigned to each item, and all items were summed to yield a final CI score. Four items in the renal tubulointerstitial lesion (TIL) category were evaluated: tubular degeneration or necrosis, renal tubular atrophy, renal interstitial fibrous, and renal interstitial inflammatory cell infiltration. A score in the range of 0–3 was assigned to each item, and all items were summed to yield a final TIL score. Tissue sections were examined by an experienced pathologist blinded to the treatments.

For IHC staining, renal paraffin sections were dewaxed, rehydrated, and recovered in antigen recovery solution (ETDA with citric acid) in an autoclave. Endogenous peroxidase activity was blocked with 0.3% (v/v) hydrogen peroxide. The sections were blocked with 10% (v/v) normal goat serum at 37°C for 1 h and incubated with rabbit anti-CXCL2 monoclonal antibody (MAb) (1:200; GTX74085; GeneTex, Irvine, CA, USA), rabbit anti-CD45 MAb (1:1000; 20103-1-AP; Proteintech, Chicago, IL, USA), and rabbit anti-MPO MAb (1:1000; ab188211; Abcam, Cambridge, UK) at 4°C overnight. Tissues were washed with

phosphate-buffered saline, incubated with horseradish peroxidase-conjugated secondary antibody, and analyzed by using a DAB kit. The nuclei were counterstained with hematoxylin. Whole-tissue images were acquired using a Pannoramic 250 flash II scanner (3D HISTECH, Budapest, Hungary) at ×20magnification. According to the intensity of immunohistochemical staining, the glomeruli were divided into four grades. Specifically, deposition <20%, 20% ≤ deposition <50%, 50% ≤ deposition <75%, and deposition ≥ 75 are defined as degrees I, II, III, and IV, respectively. Data are expressed as the percentage of glomeruli in each staining category relative to the total. Three sequential sections per animal were examined, and averages were statistically analyzed.

Statistical Analysis

Data are presented as the mean ± SEM. For normal variance distribution, unpaired Student's *t*-test was used to determine the differences between group pairs. One-way ANOVA and *post hoc* Kruskal–Wallis test were used to compare ≥ 3 groups. GraphPad Prism 5 (GraphPad Software, La Jolla, CA, USA) was used for the calculations. Statistical significance was set at $P < 0.05$.

RESULTS

Integrated miRNA and mRNA Expression Profiling Identifies Putative miRNA-mRNA Regulatory Networks in PBMCs From SLE Patients

We used RNA sequencing to analyze miRNA and mRNA expression profiles of PBMCs from SLE (n = 5) and healthy (n = 5) Tibetans. Overall, 469 mRNAs (DEmRNAs) and 45 miRNAs (DEmiRNAs) were significantly differentially expressed in Tibetan SLE patients. Of these, 356 DEmRNAs and 13 DEmiRNAs were upregulated, while 113 DEmRNAs and 32 DEmiRNAs were downregulated (**Figures 1A, C**).

To identify the functional differences between SLE and healthy patients, we used the 469 DEmRNAs in GO enrichment analysis. We thus obtained top 10 GO terms related to Biological Processes (BP), Molecular Functions (MF), and Cellular Components (CC) at $P < 0.05$ (**Figure 1B**). Most items in the BP category were related to immune and neutrophil activation and degranulation. Chemokine activity and multiple cellular secretion-related components were enriched in the MF and CC categories, respectively. Hence, GO enrichment analysis suggested that neutrophil migration and activation participate in SLE pathogenesis.

To elucidate the regulatory mechanism of DEmRNAs in SLE, we investigated their relationships with DEmiRNAs. We used RT-qPCR to validate four downregulated and four upregulated DEmiRNAs with the largest expression fold changes in PBMCs isolated from five Tibetan SLE patients, and five age- and sex-matched Tibetan controls. MiR-3942-3p, miR-3165 and miR-3614-3p were upregulated, while miR-4482-3p, miR-99a-3p, miR-4728-3p, miR-4512 and miR-4434 were downregulated in PBMCs from Tibetan SLE patients (**Figure 1D**). We predicted the target genes of these candidate miRNAs using TargetScan (http://www.targetscan.org). The analysis revealed 332 target genes of 469 DEmRNAs, miR-4512 was predicted to target the largest number of genes.

According to the KEGG analysis, the DEmRNAs targeted by hsa-miR-4512 were significantly enriched in the chemokine signaling, rheumatoid arthritis-associated, NF-kB signaling, and other immune inflammatory pathways ($P < 0.05$) (**Figure 1E**), while the DEmRNAs targeted by other candidate miRNAs were not enriched in any immune-related pathways (**Supplementary Figure S2**). *CCR1*, *CXCL1*, *CXCL2*, *CXCL5*, and *TLR4* mRNA were negatively correlated with miR-4512 in the immune inflammatory pathways, and we used them to construct regulatory networks (**Figure 1F**). Thus, hsa-miR-4512 might regulate neutrophil activation and chemokine-related pathways.

miR-4512 Inhibited The TLR4 Pathway by Targeting TLR4 and CXCL2

TargetScan and KEGG pathway analysis were used to narrow the range of miR-4512 predicted targets based on differentially expressed mRNAs associated with miR-4512 in immune-inflammatory pathways. The recognized target genes of miR-4512 were used in pathway analysis based on CapitalBio molecular annotation system v.3.0. The prediction results suggested that CCR1, CXCL1, CXCL2, CXCL5, and TLR4 might be the target of miR-4512 (**Figure 1F**). Luciferase reporter plasmid containing mRNA sequences of WT or mutated 3'-UTR target genes was co-transfected into HEK293T cells with NC and miR-4512 agomir. Only TLR4 and CXCL2 were directly targeted by miR-4512 (**Figures 2A, B**). RT-qPCR analysis showed that TLR4 and CXCL2 were also negatively regulated by miR-4512 in BALL-1, Jurkat and K562 cells, as well as in human primary monocytes and macrophages (**Figures 2C–F** and **Supplementary Figure S3**). In addition, miR-4512 inhibited the expression of CXCL2 and TLR4 proteins in human primary monocytes and macrophages (**Figures 2G–I**). The elevated serum CXCL2 level and the high expressed TLR4 in PBMCs of another group of SLE patients indicate that the down-regulation of miR-4512 in SLE promotes the expression of CXCL2 and TLR4 (**Figures 2J–L**).

miR-4512 Downregulation in Monocytes and Macrophages Contributes to The Pro-Inflammatory Condition

Considering the direct regulation of *TLR4* and *CXCL2* by miR-4512, one could speculate that miR-4512 mainly plays a role in cells which express sufficient TLR4, such as monocytes, granulocytes, and macrophages (14). Accordingly, we isolated PBMCs, monocytes, and neutrophils from Tibetan and Han SLE patients and their matched normal controls. RT-qPCR analysis of miR-4512, *CXCL2*, and *TLR4* levels revealed that miR-4512 levels were decreased in monocytes and macrophages, but not neutrophils, from SLE patients (**Figures 3A–C**).

We then analyzed the impact of miR-4512 downregulation on cytokine secretion in monocytes and macrophages. Primary monocytes and macrophages pooled from healthy subjects

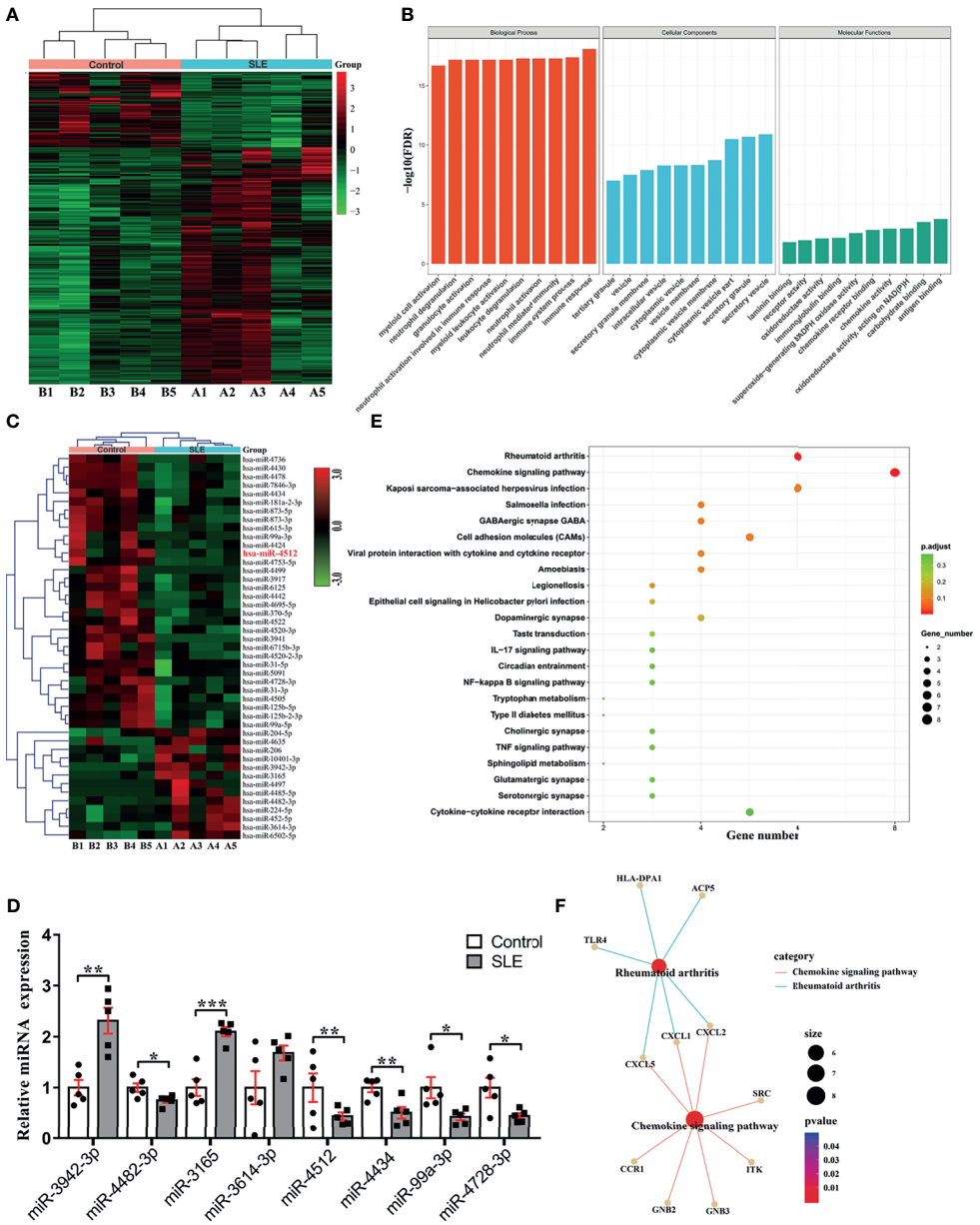

FIGURE 1 | miRNA and mRNA profiling reveals potential regulatory network involved in SLE pathogenesis. **(A)** Heat map representation of differentially expressed genes in SLE patients and control subjects (n = 5). **(B)** Top 10 GO processes determined based on all differentially expressed genes highlight enrichment of neutrophil activation and chemokine activity. **(C)** Hierarchical clustering of 45 differentially expressed miRNAs in SLE patients and control subjects from the same cohort determined by mRNA sequencing (>2-fold change, $P < 0.05$). **(D)** The top four downregulated and upregulated miRNAs were analyzed by RT-qPCR in PBMCs from five SLE patients and five age- and gender-matched healthy controls. PBMC set different from that used in **(C)** was analyzed. Results are presented as the mean ± SEM. $^{***}P < 0.001$; $^{**}P < 0.01$; $^{*}P < 0.05$. **(E)** KEGG analysis of predicted target genes of miR-4512. **(F)** The regulatory networks of miR-4512 target genes and autoimmune disease-related genes.

were transfected with NC/miR-4512-agomir/antagomir, and the cytokines in their cell culture supernatants were quantified. As shown in **Figure 3D**, miR-4512 inhibited the secretion of pro-inflammatory cytokines IL-1β, IL-12, TNF-α, IFN-γ, and IL-17 and promoted the secretion of anti-inflammatory cytokines IL-4 and IL-10. This finding was consistent with the cytokine secretion phenotype of SLE patients (**Figure 3E**). Therefore, miR-4512 downregulation in SLE patient monocytes and macrophages may activate monocytes and macrophages and induce pro-inflammatory cytokine secretion.

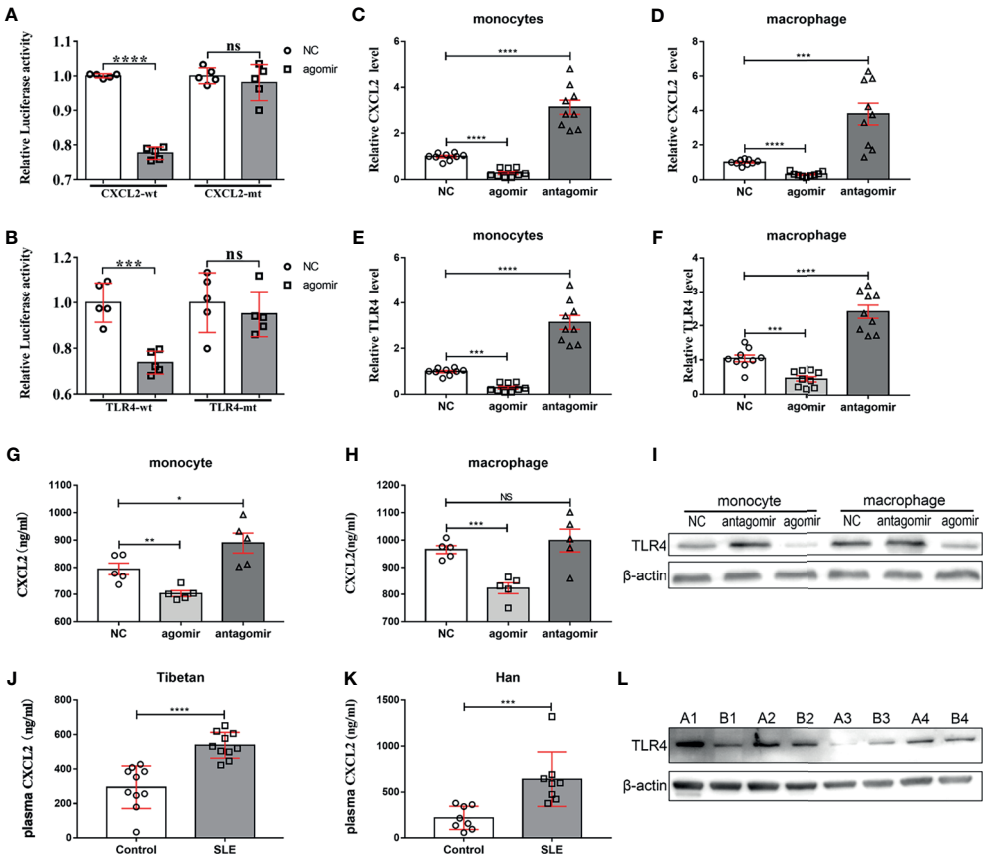

FIGURE 2 | miR-4512 directly targets *TLR4* and *CXCL2*. **(A, B)** Luciferase activity of WT/MUT-CXCL2 and WT/MUT-TLR4 plasmids in HEK293T following transfection with an miR-4512 agomir. Data are presented as the mean ± SEM. ****$P < 0.0001$; ***$P < 0.001$; NS = not significant. **(C–F)** RT-qPCR analysis of *CXCL2* and *TLR4* transcript levels in human primary monocytes and macrophages 48 h after transfection with NC/miR-4512 agomiR/antagomiR. Data are presented as the mean ± SEM. ****$P < 0.0001$; ***$P < 0.001$. **(G, H)** CXCL2 concentration in the supernatants obtained from human primary monocytes **(G)** and macrophages **(H)** 48 h after transfection with NC/miR-4512-agomir/antagomir. Data are presented as the mean ± SEM. ***$P < 0.001$; **$P < 0.01$; *$P < 0.05$; NS, not significant. **(I)** Western blot analysis of TLR4 expression in monocytes and macrophages 72 h after transfection with NC/miR-4512-agomir/antagomir. Results are representative of three independent experiments, with actin used as an internal control. **(J, K)** CXCL2 concentration in the plasma of SLE and control subjects from Tibetan **(J)** and Han **(K)** populations. Data are presented as the mean ± SEM. ****$P < 0.0001$; ***$P < 0.001$. **(L)** Western blot analysis of TLR4 expression in PBMCs isolated from SLE patients (A1–A4) and healthy controls (B1–B4). Results are representative of three independent experiments.

MiR-4512-Transfected Monocytes and Macrophages Inhibit Neutrophil NETosis

Defective apoptotic debris clearance and NETs degradation might lead to the formation of autoantibodies in SLE pathogenesis (15). As miR-4512 downregulation in monocytes and macrophages promotes pro-inflammatory cytokine secretion and CXCL2 expression, miR-4512 may indirectly prime neutrophils for NETosis. As shown in **Figures 4A, B**, the levels of NETs-relevant indicators [MPO and cfDNA] were elevated in SLE patient sera. The levels of NE, the main NETs component, were significantly upregulated in neutrophils isolated from SLE patients (**Figure 4C**). Hence, dysregulation of NETs release and/or defective NETs clearance are involved in the pathogenesis of SLE.

NC/miR-4512-agomir/antagomir was then transfected into primary monocytes and macrophages to determine the role of miR-4512 on the formation of NETs. 12 h after transfection, the supernatants of each group were isolated and used to stimulate neutrophils isolated from the healthy control group. As shown in **Figures 4D, E**, the supernatants of monocytes and macrophages transfected with miR-4512-agomir significantly reduced MPO and cfDNA release by neutrophils. The effect of the supernatant from monocytes and macrophages transfected with miR-4512-antagomir on neutrophil NETosis reached a level comparable to that of the LPS stimulation group. Straining and quantification of extracellular DNA with SYTOX Green (**Figures 4F, G**) and Western-Blot analysis of NE in the neutrophils (**Figure 4H**) also indicated similar results. Remarkably, CXCL2-stimulation also promoted neutrophil NETosis, suggesting that miR-4512 present in monocytes and macrophages may modulate neutrophil NETosis through chemoattraction and activation of neutrophils by secreting CXCL2.

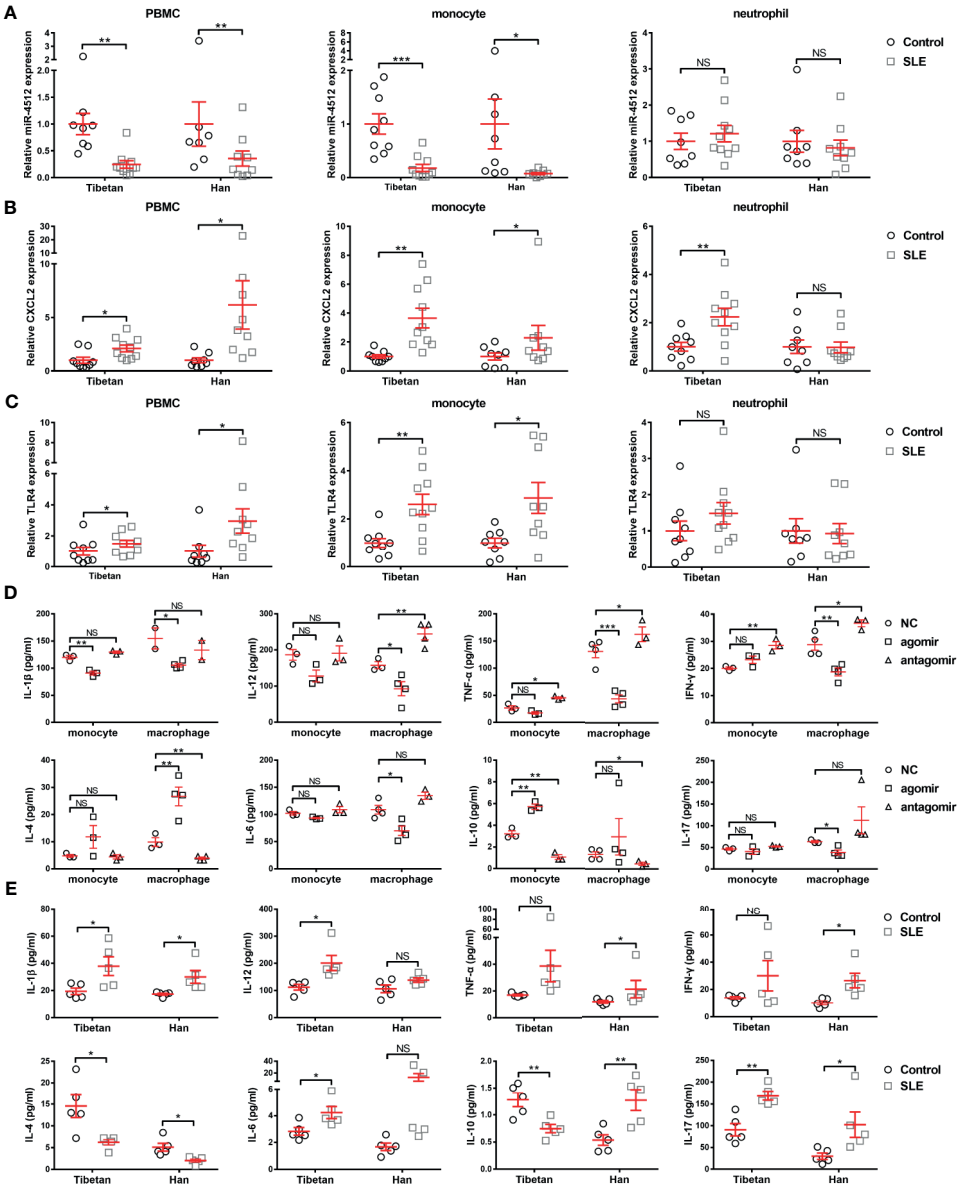

FIGURE 3 | Decreased miR-4512 expression in monocytes and macrophages contributes to a pro-inflammatory state. **(A–C)** Relative expression of miR-4512 **(A)**, *CXCL2* **(B)**, and *TLR4* **(C)** in PBMC, monocytes, and neutrophils isolated from SLE patients and control subjects, as determined by RT-qPCR. Data are presented as the mean ± SEM. ***$P < 0.001$; **$P < 0.01$; *$P < 0.05$; NS, not significant. **(D–E)** Concentrations of Th1 (including IL-1β, IL-12, TNF-α, and IFN-γ), Th2 (including IL-4, IL-6, and IL-10), and Th17 (IL-17) cytokines in the supernatants obtained from monocytes and macrophages transfected with NC/miR-4512-agomir/antagomir **(D)** or in the serum from SLE patients and control subjects **(E)**, as determined by ELISA.

CXCL2 Blocking Alleviates Kidney Damage in MRL/lpr Mouse

In order to verify the function of miR-4512 in SLE pathogenesis, we blocked the target gene CXCL2 with a neutralizing antibody in the MRL/lpr lupus model as the miRNA was not conserved in related species (**Figure 5A**). Compared with normal C57 mice, increasing proteinuria was observed in the anti-CXCL2Ab and untreated groups. However, the proteinuria was significantly reduced in the anti-CXCL2Ab group compared with the untreated group at 11 wk ($P = 0.0044$) (**Figure 5B**). H&E staining (**Figure 5C**) was used to assess the pathological changes in the kidney at the end of the study period. The major features analyzed included inflammatory cell infiltration, membrane proliferation, and arterial wall destruction (**Figures 5D–F**), which were all observed in the untreated group. By contrast, the occurrence of renal lesions was markedly mitigated in the anti-CXCL2Ab group. Therefore, anti-CXCL2Ab might alleviate kidney damage.

ANA is an important element in SLE patient categorization (16). Autoantibody levels are also related to lupus nephritis activity

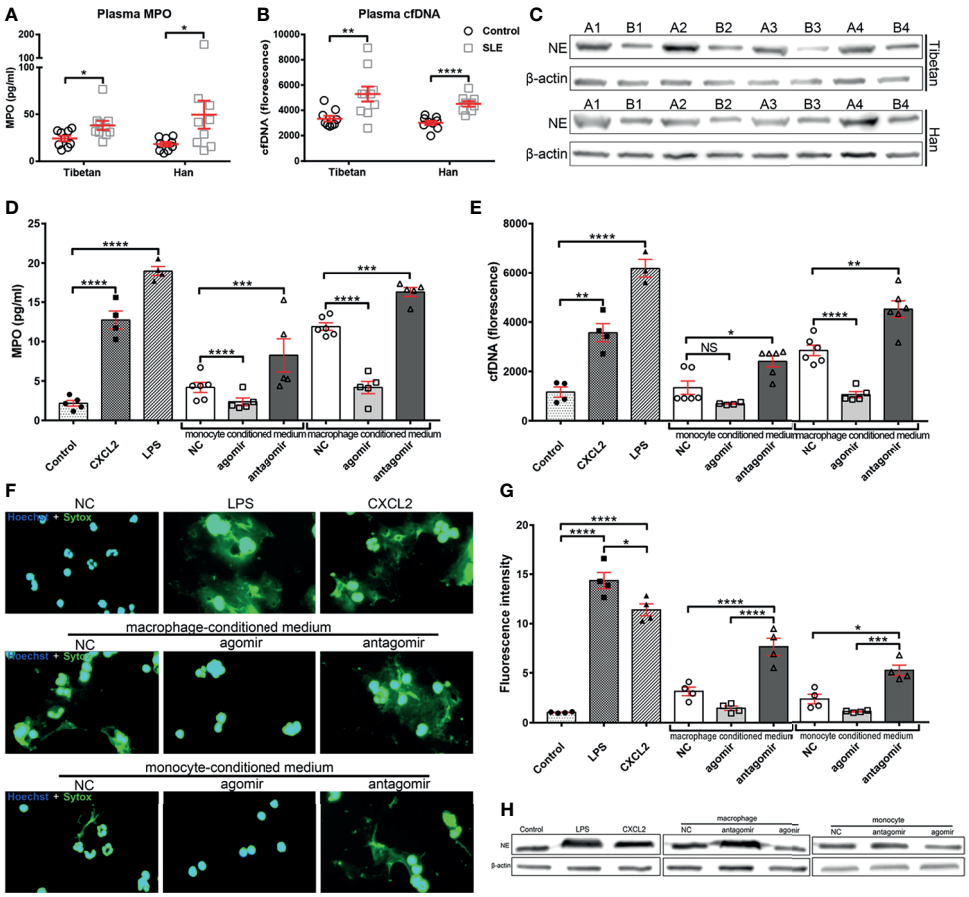

FIGURE 4 | Supernatants of monocytes and macrophages transfected with miR-4512 promote neutrophil extracellular traps formation. **(A, B)** Plasma levels of myeloperoxidase (MPO) **(A)** and cell-free DNA (cfDNA) **(B)** in SLE patients and control subjects from Tibetan and Han populations. Data are presented as the mean ± SEM. ****$P < 0.0001$, **$P < 0.01$, *$P < 0.05$. **(C)** Western blot analysis of neutrophil elastase (NE) expression in neutrophils isolated from SLE patients (A1–A4) and control subjects (B1–B4) from Tibetan and Han populations. Results are representative of three independent experiments, with actin used as an internal control. **(D, E)** MPO **(D)** and cfDNA **(E)** levels in the supernatants of human primary neutrophils culture stimulated with a supernatant of monocytes and macrophages transfected with NC/miR-4512-agomir/antagomir. Neutrophils directly stimulated with LPS or CXCL2 were used as positive controls. Data are presented as the mean ± SEM. ****$P < 0.0001$; ***$P < 0.001$; **$P < 0.01$; *$P < 0.05$; NS, not significant. **(F)** Images of neutrophils stimulated with macrophage and monocyte conditioned medium or with CXCL2 and LPS. Nuclei were stained with Hoechst (blue) and the presence of extracellular DNA were stained with Sytox Green. Images are representatives of three independent experiments. **(G)** Quantification of neutrophils extracellular DNA during NETosis by Sytox Green assays. Data are presented as the mean ± SEM. ****$P < 0.0001$; ***$P < 0.001$; *$P < 0.05$. **(H)** Western blot analysis of elastase expression in neutrophils after stimulation. Images are representatives of three independent experiments.

(17). Serum anti-dsDNA antibody and ANA levels were determined. The anti-dsDNA antibody and ANA levels were significantly lower in the plasma of anti-CXCL2Ab MRL/lpr mice than those in the untreated MRL/lpr mice (**Figures 5G, H**; $P < 0.001$). Hence, anti-CXCL2Ab treatment decreases serum immunological markers of SLE.

Next, immunohistochemistry was used to determine the deposition levels of CXCL2, CD45, and MPO in glomerular sections (**Figures 6A–F**). As we expected, the glomerular CXCL2, CD45, and MPO levels of MRL/lpr mice were significantly higher than those of normal C57 mice (**Figures 6A–E**). The staining levels of CXCL2, CD45 and MPO in the glomeruli of MRL/lpr mice were significantly reduced by CXCL2Ab treatment (**Figures 6B–F**). Specifically, compared with untreated MRL/lpr mice, the percentage of III-degree glomeruli in MRL/lpr mice was significantly decreased, while the percentage of I degree glomeruli was significantly increased by CXCL2Ab, which were confirmed by the quantitative results of CXCL2 and CD45 (**Figures 6A–D**). In the quantitative results of MPO, the percentage of II-degree glomeruli was significantly increased by CXCL2Ab (**Figures 6E, F**). This confirmed that the glomerular damage of MRL/lpr mice was significantly reduced by CXCL2Ab, which was dependent on the decreased monocytes/neutrophils infiltration and activation.

The results of ELISA assay showed that the levels of IL-1β, IL-2, IL-6, IL-12, TNF-α, IFN-γ and IL-17 in the kidney and plasma were significantly down-regulated by CXCL2Ab, while

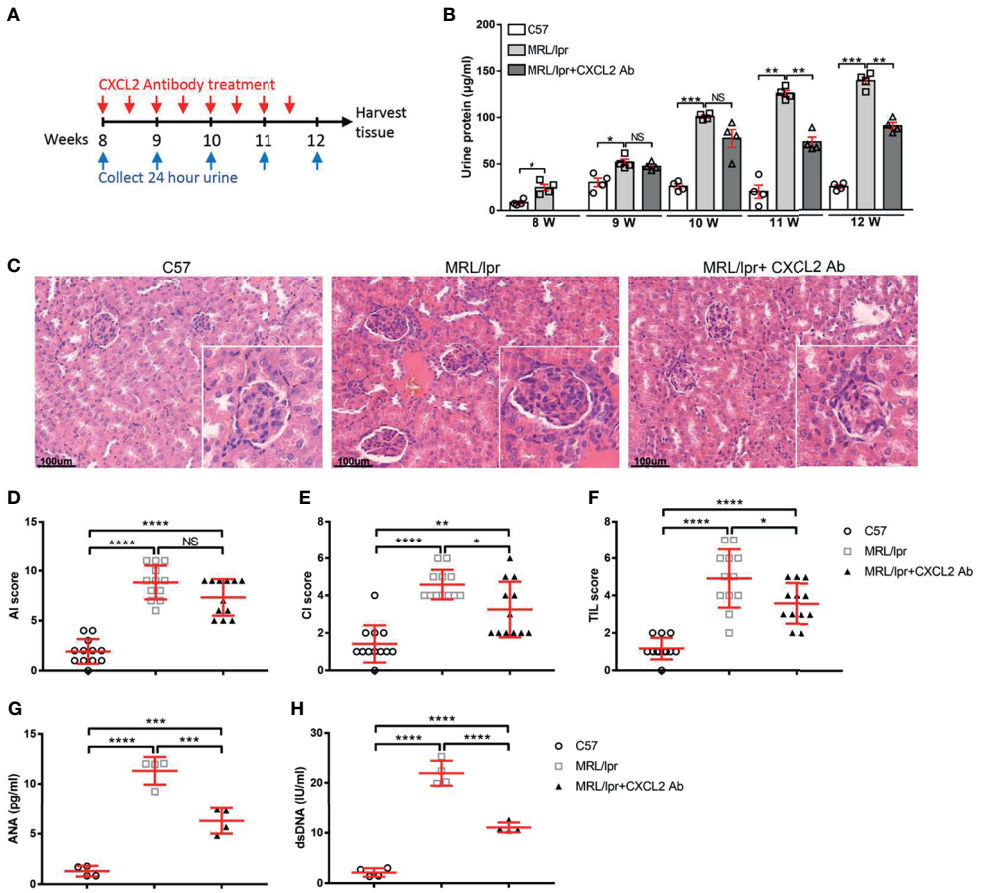

FIGURE 5 | Blocking of CXCL2 alleviates kidney damage in MRL/lpr mice. **(A)** Treatment schema: red arrows indicate days of CXCL2 neutralizing antibody treatment, and the blue arrows indicate time points for detection of 24 urinary proteins. **(B)** Urine of mice from different groups was collected at the indicated time points for the proteinuria assay. ***$P < 0.001$; **$P < 0.01$; *$P < 0.05$; NS, not significant. **(C)** Representative images of H&E straining of kidney sections obtained from mice from different groups. Inserts, details of a typical glomerulus. **(D–F)** Lesion scores of the activity index **(D)**, chronicity index **(E)**, and tubulointerstitial lesions **(F)** of mice in different groups. Data are shown as the mean ± SEM (n = 4 animals/group, 3 sections/animal). ****$P < 0.0001$; ***$P < 0.001$; *$P < 0.05$. **(G, H)** Immunological markers of SLE in the serum of mice from different groups. The antinuclear antibodies (ANA) were determined by immunofluorescence **(G)**, anti-dsDNA levels were measured by ELISA **(H)**. ****$P < 0.0001$; ***$P < 0.001$; **$P < 0.01$.

IL-4 and IL-10 levels were significantly increased (**Figure 6G**). Therefore, CXCL2Ab was confirmed to regulate the secretion of inflammatory cytokines. These results indicate that CXCL2Ab is beneficial to relieve the immune disorder of SLE.

DISCUSSION

In this study, the abnormal expression of miRNAs in PBMCs of Tibetan population and its molecular mechanism involved in the progress of SLE were concerned. Differentially expressed miRNAs and mRNAs in PBMCs of SLE patients were detected by transcriptome sequencing. We detected significantly different miRNAs in Tibetan patients with SLE, including: miR-3942-3p, miR-4482-3p, miR-3165, miR-3164-3p, miR-4512, miR-4434, miR-99a-3p, and miR-4728-3p. Although miRNAs with abnormal expression of SLE have been reported, different studies have not found the same or highly consistent results. In our results, miR-3942-5p was reported as a good candidate diagnostic biomarker for class IV lupus nephritis (LN) (18). miR-3165 was found to be abnormally expressed in the serum of patients with grade IV lupus nephritis (19). The other 7 miRNAs in SLE have not been reported. In our study, miR-4512 was focused on. The results of sample validation and miRNA-mRNA analysis showed that miRNA-4512 was the most critical factor in the abnormal expression of PBMCs transcriptome in SLE patients. Furthermore, miRNA-4512 may be involved in disease progression of SLE by regulating TLR4 and CXCL2.

In vitro mechanism studies revealed that down-regulation of miR-4512 in monocytes and macrophages may promote inflammation and neutrophils NETosis by upregulating CXCL2 expression. Recent studies have shown that NETs formation is a major participant in the pathogenesis of systemic autoimmune diseases (6, 20). This is consistent with

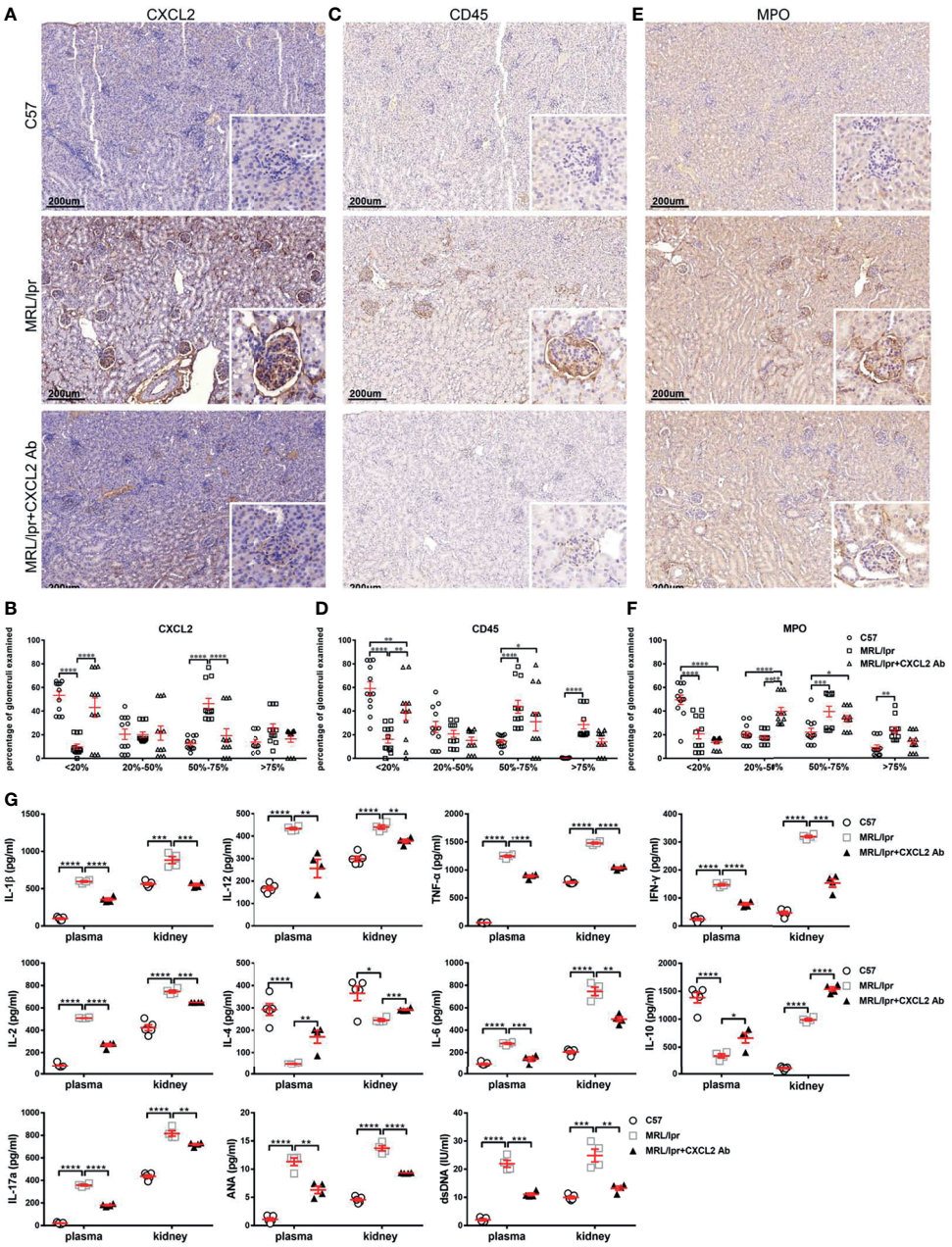

FIGURE 6 | Treatment with CXCL2 antibody inhibits inflammatory cytokine production in the MRL/lpr lupus model. **(A, C, E)** Representative images of CXCL2 **(A)**, CD45 **(C)**, and MPO **(E)** staining of kidney sections of mice from different groups. Inserts, details of a typical staining of the glomerulus. **(B, D, F)** Quantitative analysis of CXCL2 **(B)**, CD45 **(D)**, and MPO **(F)** deposition in the glomeruli in kidney sections. The glomeruli were classified into four categories according to the degree of straining. The glomerulus ratios in each category in different groups are summarized (n = 4 animals/group, 3 sections/animal). Data are presented as the mean ± SEM. $^{****}P < 0.0001$; $^{***}P < 0.001$; $^{**}P < 0.01$; $^{*}P < 0.05$. **(G)** Concentrations of Th1 (including IL-1β, IL-2, IL-12, TNF-α, and IFN-γ), Th2 (including IL-4, IL-6, and IL-10) and Th17 (IL-17) cytokines in the plasma and renal tissue homogenates of mice from different groups, determined by ELISA (n = 4 animals/group). Data are shown as the mean ± SEM. $^{****}P < 0.0001$; $^{***}P < 0.001$; $^{*}P < 0.01$; $^{*}P < 0.05$.

the increased expression of NETs-related proteins that we have observed in both Han and Tibetan SLE patients. The formation of NETs is accompanied by the exposure of a large number of autoantigens, which in turn induce or aggravate autoimmune diseases (21). In fact, NETs-related markers such as cfDNA were significantly upregulated in blood samples of SLE patients (22). Our research has also confirmed that the levels of serum-related indicators (MPO, cfDNA and NE) in SLE patients are abnormally up-regulated. Furthermore, the NETs induced by miR-4512 down-regulation was dependent on CXCL2.

The abnormal expression of chemokines is a major part of the immune disorders of SLE. For instance, CXCL10 and infiltrating CXCR3-positive cells have been implicated in various SLE manifestations (23). CCL21 and IP-10 are blood biomarkers of pulmonary involvement in SLE patients (24). CXCL13 was considerably upregulated in the kidney tissues of LN patients, which might be a therapeutic target in glomerulonephritis and SLE nephritis (25). The CXCR4/CXCL12 axis is a potential therapeutic target for SLE patients undergoing kidney and/or central nervous system pathogenesis (26). These studies suggest that abnormal levels of chemokine ligands are closely related to abnormal levels of inflammation and tissue damage in SLE. However, the mechanism of chemokine ligands in the formation of NETs in SLE patients remains unclear. In the study of chemokine-mediated NETs formation, CXCL1 was reported to rescue alcohol-induced immune disorders in polymicrobial sepsis by promoting the formation of NETs (27). In this study, we found that the NETs induced by miR-4512 down-regulation was dependent on the regulation of TLR4-CXCL2 signaling. It might be a new loop. Specifically, down-regulation of miR-4512 promotes up-regulation of CXCL2 and TLR4, and the CXCL2-TLR4 molecular axis further activates NF-κB-mediated chemokine and inflammatory cytokine expression, including CXCL2, which in turn promotes neutrophils recruitment to inflammatory sites and formation of NETs. The formation of loop may be a special pattern in chemokine-regulated NETosis. The formation of NETs is involved in regulating the recruitment of lung neutrophils to airway tissue, which depends on the TLR4/NF-κB pathway to stimulate airway cells to express CXCL1, CXCL2 and CXCL8 (28). The down-regulated expression of miR-4512 leads to the abnormal expression of CXCL2, which is likely to form a unique loop in the same way. This has been confirmed in studies of other chemokines. For example, the secretion of CXCL10 by $CD4^+$, $CD8^+$, natural killer (NK) and NK-T cells is dependent on IFN-γ, which is itself mediated by the IL-12 cytokine family (29). Under the influence of IFN-γ, CXCL10 is secreted by several cell types including endothelial cells, fibroblasts, keratinocytes, thyrocytes, preadipocytes, etc. Determination of high level of CXCL10 in peripheral fluids is therefore a marker of host immune response, especially T helper (Th)1 orientated T-cells (30). In tissues, recruited Th1 lymphocytes may be responsible for enhanced IFN-γ and tumor necrosis factor-α production, which in turn stimulates CXCL10 secretion from a variety of cells, therefore creating an amplification feedback loop, and perpetuating the autoimmune process (23). This suggests that CXCL2 may form an independent feedback loop in a similar manner.

Based on the immune regulation function of chemokines (including CXCL2) and its feedback loop mechanism, chemokines may be used as targets for the treatment of diseases related to immune disorders. In fact, blocking the interaction of chemokines and chemokine receptors has been proven to be beneficial for the treatment of autoimmune diseases. For example, the lymph node cells (LNC) of MRL/lpr mice was attenuated by CXCL13 blockade (25). Double blockade of CXCL12 and CCL2 shows the same efficacy as high-dose cyclophosphamide administration in murine proliferative LN (31). In this study, since miR-4512 was only expressed in human, and their target site in the 3'UTR of TLR4 and CXCL2 was not conserved in human and mouse, it would be difficult to directly testify the function of miR-4512 in the pathogenesis of SLE. Indeed, it was necessary to inhibit both TLR4 and CXCL2 in the SLE murine model to verify the function of miR-4512 in SLE indirectly. Although the role of TLR4 in SLE pathogenesis was well-defined in C57BL/6(lpr/lpr)-TLR4-deficient SLE model (32), TLR4 antibodies in a phase II clinical trial did not improve disease parameters of rheumatoid arthritis (33). These studies may suggest that antibody or antagonist was not sufficient to block TLR4 signaling as TLR4 are located both on cell surface and endosomal or lysosomal compartments. Moreover, evidences shown that the CXCL2 could be induced by LPS through TLR4 dependent pathway (34, 35), and the CXCL2 alone could induce NETs formation dependent on MAPK signaling pathway (36). Therefore, the CXCL2 would be a superior target in blocking TLR4-mediated inflammatory pathways when neutrophil recruitment and activation was concerned, especially when TLR4 was difficult to be inhibited by neutralizing antibody or small-molecule inhibitor. We thus only evaluate the effect of miR-4512 on MRL/lpr mice by blocking CXCL2 with neutralizing antibodies. Our results showed that proteinuria, ANA and anti-dsDNA antibody levels, pro-inflammatory cytokine secretion, and renal immune complex deposition in MRL/lpr mice were reduced by intraperitoneal administration of anti-CXCL2 neutralizing antibodies. In addition, CXCL2 blockade inhibited the production of MPO and CD45 in neutrophils of MRL/lpr mice. These results confirm that CXCL2 is a potent potential target in the treatment of SLE. It is also worth noting that the development of novel therapies or drugs to promote miR-4512 expression is also a novel strategy for SLE targeting therapy. In subsequent studies, the molecular mechanism of the abnormal expression of DEmiRNA in SLE patients will also provide new targets and insights for the treatment of SLE.

CONCLUSIONS

Here, we detected the differentially expressed miRNAs in the PBMCs of Chinese Tibetan SLE patients. Among them, the abnormal down-regulation of miR-4512 in monocytes and macrophages was confirmed to promote the formation of SLE neutrophil extracellular traps by targeting CXCL2 and TLR4. Moreover, CXCL2 blockade was confirmed to reduce kidney damage in MRL/lpr mice. These data are the first to characterize the mechanism of miRNA in Tibetan SLE patients and provide new insights into the general pathogenesis of SLE patients.

DATA AVAILABILITY STATEMENT

Sequencing data sets have been deposited in the gene expression omnibus (GEO) data repository under the accession numbers GSE175839, GSE175840, GSE175841.

ETHICS STATEMENT

The study design was approved by the Ethics Committee of the Second Affiliated Hospital of Kunming Medical University. The patients/participants provided their written informed consent to participate in this study. The experiment was conducted in a laboratory animal facility of Kunming Medical University and approved by the Animal Research Committee of Kunming Medical University (No. kmmu2021724).

AUTHOR CONTRIBUTIONS

BY was involved in the majority of experiments, data statistics and analysis, and drafting and revision of the manuscript. XH was involved in experiment supervision and management, data analysis, and revision of the manuscript. SX, LL, WW, and YD performed bioinformatics analysis of the RNA sequencing data and differential expression analysis. MG, LY, WC, MY, and YW were involved in the acquisition of human samples, data capture, and analysis of clinical data. DD was involved in the conception and design of the study and interpretation of data. All authors critically revised the manuscript and approved the final version of the manuscript.

FUNDING

This research was supported by National Natural Science Foundation of China (grant no. 81860552, 31860256), Applied Basic Research Programs of Yunnan Province (grant no. 2018FB129).

SUPPLEMENTARY MATERIAL

The Supplementary Material for this article can be found online at: https://www.frontiersin.org/articles/10.3389/fimmu.2021.756825/full#supplementary-material

REFERENCES

1. Dema B, Charles N. Advances in Mechanisms of Systemic Lupus Erythematosus. *Discov Med* (2014) 17:247–55.
2. Herrada AA, Escobedo N, Iruretagoyena M, Valenzuela RA, Burgos PI, Cuitino L, et al. Innate Immune Cells' Contribution to Systemic Lupus Erythematosus. *Front Immunol* (2019) 10:772. doi: 10.3389/fimmu.2019.00772
3. Saferding V, Blüml S. Innate Immunity as the Trigger of Systemic Autoimmune Diseases. *J Autoimmun* (2020) 110:102382. doi: 10.1016/j.jaut.2019.102382
4. Tas SW, Quartier P, Botto M, Fossati-Jimack L. Macrophages From Patients With SLE and Rheumatoid Arthritis Have Defective Adhesion *In Vitro*, While Only SLE Macrophages Have Impaired Uptake of Apoptotic Cells. *Ann Rheum Dis* (2006) 65:216–21. doi: 10.1136/ard.2005.037143
5. Chen JQ, Papp G, Szodoray P, Zeher M. The Role of microRNAs in the Pathogenesis of Autoimmune Diseases. *Autoimmun Rev* (2016) 15:1171–80. doi: 10.1016/j.autrev.2016.09.003
6. Mishra R, Bhattacharya S, Rawat BS, Kumar A, Kumar A, Niraj K, et al. MicroRNA-30e-5p has an Integrated Role in the Regulation of the Innate Immune Response During Virus Infection and Systemic Lupus Erythematosus. *iScience* (2020) 23:101322. doi: 10.1016/j.isci.2020.101322
7. Qu B, Cao J, Zhang F, Cui H, Teng J, Li J, et al. Type I Interferon Inhibition of microRNA-146a Maturation Through Up-Regulation of Monocyte Chemotactic Protein-Induced Protein 1 in Systemic Lupus Erythematosus. *Arthritis Rheumatol* (2015) 67:3209–18. doi: 10.1002/art.39398
8. Wang P, Hou J, Lin L, Wang C, Liu X, Li D, et al. Inducible microRNA-155 Feedback Promotes Type I IFN Signaling in Antiviral Innate Immunity by Targeting Suppressor of Cytokine Signaling 1. *J Immunol* (2010) 185:6226–33. doi: 10.4049/jimmunol.1000491
9. Gao S, Yuan L, Wang Y, Hua C. Enhanced Expression of TREM-1 in Splenic cDCs in Lupus Prone Mice and it was Modulated by miRNA-150. *Mol Immunol* (2017) 81:127–34. doi: 10.1016/j.molimm.2016.12.006
10. Pan W, Zhu S, Dai D, Liu Z, Li D, Li B, et al. MiR-125a Targets Effector Programs to Stabilize Treg-Mediated Immune Homeostasis. *Nat Commun* (2015) 6:7096. doi: 10.1038/ncomms8096
11. Cao W, Qian G, Luo W, Liu X, Pu Y, Hu G, et al. miR-125b is Downregulated in Systemic Lupus Erythematosus Patients and Inhibits Autophagy by Targeting UVRAG. *BioMed Pharmacother* (2018) 99:791–7. doi: 10.1016/j.biopha.2018.01.119
12. Hochberg MC. Updating the American College of Rheumatology Revised Criteria for the Classification of Systemic Lupus Erythematosus. *Arthritis Rheumatol* (1997) 40:1725. doi: 10.1002/art.1780400928
13. Mittal B, Rennke H, Singh AK. The Role of Kidney Biopsy in the Management of Lupus Nephritis. *Curr Opin Nephrol Hypertens* (2005) 14:1–8. doi: 10.1097/00041552-200501000-00002
14. Vaure C, Liu Y. A Comparative Review of Toll-Like Receptor 4 Expression and Functionality in Different Animal Species. *Front Immunol* (2014) 5:316. doi: 10.3389/fimmu.2014.00316
15. Apel F, Zychlinsky A, Kenny EF. The Role of Neutrophil Extracellular Traps in Rheumatic Diseases. *Nat Rev Rheumatol* (2018) 14:467–75. doi: 10.1038/s41584-018-0039-z
16. Pisetsky DS, Bossuyt X, Meroni PL. ANA as an Entry Criterion for the Classification of SLE. *Autoimmun Rev* (2019) 18:102400. doi: 10.1016/j.autrev.2019.102400
17. Alba P, Bento L, Cuadrado MJ, Karim Y, Tungekar MF, Abbs I, et al. Anti-dsDNA, Anti-Sm Antibodies, and the Lupus Anticoagulant: Significant Factors Associated With Lupus Nephritis. *Ann Rheum Dis* (2003) 62:556–60. doi: 10.1136/ard.62.6.556
18. Navarro-Quiroz E, Pacheco-Lugo L, Navarro-Quiroz R, Lorenzi H, Espana-Puccini P, Diaz-Olmos Y, et al. Profiling Analysis of Circulating microRNA in Peripheral Blood of Patients With Class IV Lupus Nephritis. *PloS One* (2017) 12:e0187973. doi: 10.1371/journal.pone.0187973
19. Xiao H, Wei N, Su M, Xiong Z. Down-Regulation of Serum miR-151a-3p is Associated With Renal Tissue Activity in Class IV Lupus Nephritis. *Clin Exp Rheumatol* (2019) 37:67–72.
20. Gupta S, Kaplan MJ. The Role of Neutrophils and NETosis in Autoimmune and Renal Diseases. *Nat Rev Nephrol* (2016) 12:402–13. doi: 10.1038/nrneph.2016.71
21. Lee KH, Kronbichler A, Park DD, Park Y, Moon H, Kim H, et al. Neutrophil Extracellular Traps (NETs) in Autoimmune Diseases: A Comprehensive Review. *Autoimmun Rev* (2017) 16:1160–73. doi: 10.1016/j.autrev.2017.09.012
22. Duvvuri B, Lood C. Cell-Free DNA as a Biomarker in Autoimmune Rheumatic Diseases. *Front Immunol* (2019) 10:502. doi: 10.3389/fimmu.2019.00502
23. Antonelli A, Ferrari SM, Giuggioli D, Ferrannini E, Ferri C, Fallahi P. Chemokine (C-X-C Motif) Ligand (CXCL)10 in Autoimmune Diseases. *Autoimmun Rev* (2014) 13:272–80. doi: 10.1016/j.autrev.2013.10.010
24. Odler B, Bikov A, Streizig J, Balogh C, Kiss E, Vincze K, et al. CCL21 and IP-10 as Blood Biomarkers for Pulmonary Involvement in Systemic Lupus Erythematosus Patients. *Lupus* (2017) 26:572–9. doi: 10.1177/0961203316668418
25. Wu X, Guo J, Ding R, Lv B, Bi L. CXCL13 Blockade Attenuates Lupus Nephritis of MRL/lpr Mice. *Acta Histochem* (2015) 117:732–7. doi: 10.1016/j.acthis.2015.09.001
26. Wang A, Guilpain P, Chong BF, Chouzenoux S, Guillevin L, Du Y, et al. Dysregulated Expression of CXCR4/CXCL12 in Subsets of Patients With

Systemic Lupus Erythematosus. *Arthritis Rheumatol* (2010) 62:3436–46. doi: 10.1002/art.27685
27. Jin L, Batra S, Jeyaseelan S. Diminished Neutrophil Extracellular Trap (NET) Formation is a Novel Innate Immune Deficiency Induced by Acute Ethanol Exposure in Polymicrobial Sepsis, Which can be Rescued by CXCL1. *PloS Pathog* (2017) 13:e1006637. doi: 10.1371/journal.ppat.1006637
28. Wan R, Jiang J, Hu C, Chen X, Chen C, Zhao B, et al. Neutrophil Extracellular Traps Amplify Neutrophil Recruitment and Inflammation in Neutrophilic Asthma by Stimulating the Airway Epithelial Cells to Activate the TLR4/NF-κb Pathway and Secrete Chemokines. *Aging (Albany NY)* (2020) 12:16820–36. doi: 10.18632/aging.103479
29. Engel MA, Neurath MF. Anticancer Properties of the IL-12 Family - Focus on Colorectal Cancer. *Curr Med Chem* (2010) 17:3303–8. doi: 10.2174/092986710793176366
30. Antonelli A, Ferri C, Ferrari SM, Colaci M, Fallahi P. Immunopathogenesis of HCV-Related Endocrine Manifestations in Chronic Hepatitis and Mixed Cryoglobulinemia. *Autoimmun Rev* (2008) 8:18–23. doi: 10.1016/j.autrev.2008.07.017
31. Devarapu SK, Kumar Vr S, Rupanagudi KV, Kulkarni OP, Eulberg D, Klussmann S, et al. Dual Blockade of the Pro-Inflammatory Chemokine CCL2 and the Homeostatic Chemokine CXCL12 is as Effective as High Dose Cyclophosphamide in Murine Proliferative Lupus Nephritis. *Clin Immunol* (2016) 169:139–47. doi: 10.1016/j.clim.2016.07.003
32. Lartigue A, Colliou N, Calbo S, Francois A, Jacquot S, Arnoult C, et al. Critical Role of TLR2 and TLR4 in Autoantibody Production and Glomerulonephritis in Lpr Mutation-Induced Mouse Lupus. *J Immunol* (2009) 183:6207–16. doi: 10.4049/jimmunol.0803219
33. Monnet E, Choy EH, McInnes I, Kobakhidze T, de Graaf K, Jacqmin P, et al. Efficacy and Safety of NI-0101, an Anti-Toll-Like Receptor 4 Monoclonal Antibody, in Patients With Rheumatoid Arthritis After Inadequate Response to Methotrexate: A Phase II Study. *Ann Rheum Dis* (2020) 79:316–23. doi: 10.1136/annrheumdis-2019-216487
34. De Filippo K, Dudeck A, Hasenberg M, Nye E, van Rooijen N, Hartmann K, et al. Mast Cell and Macrophage Chemokines CXCL1/CXCL2 Control the Early Stage of Neutrophil Recruitment During Tissue Inflammation. *Blood* (2013) 121:4930–7. doi: 10.1182/blood-2013-02-486217
35. Hu DN, Zhang R, Yao S, Iacob CE, Yang WE, Rosen R, et al. Cultured Human Uveal Melanocytes Express/Secrete CXCL1 and CXCL2 Constitutively and Increased by Lipopolysaccharide via Activation of Toll-Like Receptor 4. *Curr Eye Res* (2021) 46:1681–94. doi: 10.1080/02713683.2021.1929326
36. Marcos V, Zhou Z, Yildirim AO, Bohla A, Hector A, Vitkov L, et al. CXCR2 Mediates NADPH Oxidase-Independent Neutrophil Extracellular Trap Formation in Cystic Fibrosis Airway Inflammation. *Nat Med* (2010) 16:1018–23. doi: 10.1038/nm.2209

Conflict of Interest: The authors declare that the research was conducted in the absence of any commercial or financial relationships that could be construed as a potential conflict of interest.

Publisher's Note: All claims expressed in this article are solely those of the authors and do not necessarily represent those of their affiliated organizations, or those of the publisher, the editors and the reviewers. Any product that may be evaluated in this article, or claim that may be made by its manufacturer, is not guaranteed or endorsed by the publisher.

frontiers in Immunology

ORIGINAL RESEARCH
published: 17 November 2021
doi: 10.3389/fimmu.2021.770852

Immunological Microenvironment Alterations in Follicles of Patients With Autoimmune Thyroiditis

Ning Huang[1,2,3,4], *Dandan Liu*[1,2,3,4], *Ying Lian*[1,2,3,4], *Hongbin Chi*[1,2,3,4*] *and Jie Qiao*[1,2,3,4*]

[1] Center for Reproductive Medicine, Department of Obstetrics and Gynecology, Peking University Third Hospital, Beijing, China, [2] National Clinical Research Center for Obstetrics and Gynecology, Peking University Third Hospital, Beijing, China, [3] Key Laboratory of Assisted Reproduction (Peking University), Ministry of Education, Beijing, China, [4] Beijing Key Laboratory of Reproductive Endocrinology and Assisted Reproductive Technology, Peking University Third Hospital, Beijing, China

OPEN ACCESS

Edited by:
Jianfeng Chen,
Shanghai Institute of Biochemistry and Cell Biology (CAS), China

Reviewed by:
Bin Li,
Shanghai Jiao Tong University School of Medicine, China
Honglin Wang,
Shanghai Jiao Tong University, China

***Correspondence:**
Hongbin Chi
chihb@163.com
Jie Qiao
jie.qiao@263.net

Specialty section:
This article was submitted to Autoimmune and Autoinflammatory Disorders, a section of the journal Frontiers in Immunology

Received: *05 September 2021*
Accepted: *25 October 2021*
Published: *17 November 2021*

Citation:
Huang N, Liu D, Lian Y, Chi H and Qiao J (2021) Immunological Microenvironment Alterations in Follicles of Patients With Autoimmune Thyroiditis. Front. Immunol. 12:770852. doi: 10.3389/fimmu.2021.770852

Autoimmune thyroiditis (AIT) is the most prevalent autoimmune endocrine disease, with a higher incidence in women than in men. Immunological abnormalities may lead to the impairment of ovarian folliculogenesis; however, whether the presence of AIT affects immunological microenvironment in follicles remains controversial. We performed a cross-sectional study including 122 patients, aged 20–40 years, who underwent IVF/ICSI treatment owing to isolated male or tube factor infertility. Patients were divided into AIT and control groups according to clinical presentation, thyroid function, and thyroid autoantibody measurements. Follicular fluid was collected and the distribution of cytokines/chemokines in follicular fluid was measured by flow cytometry using multiplex bead assays between the two groups. Based on differences in levels of intrafollicular chemokines and cytokines between the AIT and control groups, the relevant inflammatory cascade was further demonstrated. Among the 12 chemokines analyzed, three (CXCL9, CXCL10, and CXCL11) showed significantly elevated levels in the follicular fluid of patients with AIT. Among the 11 cytokines detected, compared with those in the control group, significantly higher levels of IFNγ were observed in patients with AIT. IFNγ dose-dependently stimulated the expression and secretion of CXCL9/10/11 in cultured primary granulosa cells. The percentage of $CXCR3^+$ T lymphocytes was significantly elevated in the follicular microenvironment of patients with AIT. We concluded that the IFNγ-CXCL9/10/11-$CXCR3^+$ T lymphocyte inflammatory cascade is activated in the follicular microenvironment of patients with AIT. These findings indicate that a considerable immune imbalance occurred in the follicular microenvironment of patients with AIT.

Keywords: autoimmune thyroiditis, ovarian microenvironment, follicle development, IFNγ-CXCL9/10/11-$CXCR3^+$ T lymphocyte, follicular fluid

INTRODUCTION

Autoimmune thyroiditis (AIT) is an organ-specific autoimmune disorder characterized by the production of autoimmune thyroid antibodies and the infiltration of self-reactive lymphocytes into the thyroid, resulting in the destruction of thyrocytes and hypothyroidism. T cell-mediated immune disorders play an important role in the pathogenesis of AIT. In patients with AIT, both in the peripheral blood and in the thyroid gland, the balance between Th1 and Th2 cells is skewed toward Th1 cells and cytotoxic T lymphocytes are considerably activated, which triggers a dramatic activation of the immune response. Meanwhile, pro-inflammatory cytokines such as interferon-gamma (IFNγ) and IL-17 were significantly elevated. Pro-inflammatory chemokines CXCL9, CXCL10, and CXCL11 were also activated in patients with AIT, which further promoted the migration of pro-inflammatory Th1 lymphocytes into the thyroid and aggravated the destruction of the thyroid gland (1–4).

Immunological abnormalities may lead to the impairment of ovarian folliculogenesis; however, whether the presence of AIT affects follicular development and ovulation remains controversial and the relevant studies are limited. Our previous large-scale retrospective cohort study found that after adjusting for thyroid function and ovarian reserve markers, the number of oocytes retrieved during *in vitro* fertilization/intracytoplasmic sperm injection (IVF/ICSI) treatment significantly decreased in infertile women with positive thyroid antibodies. This suggests a possible role of AIT in follicular development; however, the mechanism remains unclear (5).

Follicle development and oocyte maturation depend heavily on the follicle fluid, which is derived from blood infiltration and ovarian secretion. An altered follicular microenvironment may directly damage follicle recruitment and growth. A large number of cytokines/chemokines are activated in follicular fluid and interact with each other to form a network that regulates folliculogenesis, oocyte maturation, and luteinization (6). Recent studies have reported an association between abnormal elevation of specific cytokines/chemokines and follicle developmental disorders (7, 8).

This study aimed to investigate the distribution of intrafollicular cytokines/chemokines and the activation of relevant inflammatory pathways in patients with AIT compared to those without AIT.

MATERIALS AND METHODS

Ethical Approval

The study was approved by the Peking University Third Hospital Medical Science Research Ethics Committee.

Patients

The study consisted of 122 patients, aged 20–40 years, who underwent IVF/ICSI treatment owing to isolated male or tube factor infertility. Patients were divided into AIT and control groups according to clinical presentation, thyroid function, and thyroid autoantibody measurements. The reference values for serum thyroid-stimulating hormone (TSH) were 0.55–4.78 uIU/mL, and those for serum-free thyroxin (FT4) were 0.89–1.80 ng/dL. The detection range for thyroglobulin antibody (TGAb) was 15–500 IU/mL, and that for thyroid peroxidase antibody (TPOAb) was 28–1300 IU/mL. A value >60 IU/mL was defined as positive for TGAb or TPOAb. Patients positive for TGAb and/or TPOAb were placed in the AIT group. The levels of TSH and FT4 in all patients were required to be within the normal reference range prior to controlled ovarian stimulation; thus, 14 patients that were thyroid antibody-positive received oral levothyroxine owing to abnormal TSH and FT4 levels. Patients with a history of other reproductive diseases, such as polycystic ovarian syndrome or endometriosis; a history of other thyroid diseases, such as hyperthyroidism or thyroid cancer; abnormal results on parental karyotyping; other endocrinological diseases, such as hyperprolactinemia or diabetes; or positive tests for antinuclear antibodies or lupus anticoagulants were excluded.

IVF/ICSI Procedure and Follicle Fluid Collection

All patients underwent standardized protocols for controlled ovarian stimulation (COS) and oocyte retrieval. The individualized dose of recombinant follicle-stimulating hormones for inducing COS was decided based on the patient's age, body mass index (BMI), antral follicle count, and anti-Mullerian hormone levels. Two hundred and fifty micrograms of recombinant human chorionic gonadotropin (HCG; Eiser, Serono, Germany) was administered to trigger oocyte maturation when at least two follicles reached 18 mm. Oocyte retrieval was performed 34–36 h after HCG administration. Follicular fluid without visible blood contamination was aspirated from the first and largest follicle, collected separately and centrifuged at 800 g for 10 min. Supernatants were collected and stored at −80°C until further analysis.

Cytokine/Chemokine Detection Assay

Concentrations of cytokines/chemokines in the follicle fluid were measured using flow cytometry with multiplex bead assays, and the procedures were performed using the Legendplex Multi-Analyte Flow Assay Kit according to the manufacturer's instructions (BioLegend). Cytokine plexes include IL-2, IL-4, IL-6, IL-9, IL-10, IL13, IL-17A, IL-17F, IL-22, IFNγ, and TNFα. The chemokine plexes included CCL2, CCL3, CCL4, CCL5, CCL11, CCL17, CXCL1, CXCL5, CXCL8, CXCL9, CXCL10, and CXCL11.

Chemokine Secretion Assay

Primary granulosa cells were collected from follicular aspirates and purified *via* centrifugation at 600 g for 30 min using the Ficoll gradient method. For chemokine secretion assays, primary granulosa cells were seeded onto six-well plates in growth medium (Dulbecco's modified Eagle's medium/Ham's F-12

nutrient mixture containing 10% fetal bovine serum). The growth medium containing leukocytes was removed after 24 h, granulosa cells were washed in PBS, and incubated in serum-free growth medium. Cells were incubated for 24 h with different doses of IFNγ (R&D Systems; 500, 1000, 5000, and 10,000 IU/mL). The supernatant was removed after 24 h and stored at −20°C until required for the chemokine assay.

Real-Time Polymerase Chain Reaction (RT-PCR)

Total RNA was extracted from cultured primary granulosa cells using TRIzol reagent (Life Technologies) according to the manufacturer's instructions. RNA was reverse transcribed into first-strand cDNA using a cDNA synthesis kit (Thermo Fisher Scientific). Reverse transcription quantitative RT-PCR was performed on an Applied Biosystems Quant Studio3 Real-Time PCR System in 96 well optical reaction plates. The following primers were used: β-actin F, TGCCCATCTACGAGGGGTAT; β-actin R, CTTAATGTCACGCACGATTTCC; CXCL9 F, CATC ATCTTGCTGGTTCTGATTG; CXCL9 R, GATTGTAGGTGGA TAGTCCCTTG; CXCL10 F, GCTGCCTTATCTTTCTG ACTCT; CXCL10 R, GACCTTGGATTAACAGGTTGATTAC; CXCL11 F, ATGAGTGTGAAGGGCATGG; CXCL11 R, TATGCAAAGACAGCGTCCTC.

Flow Cytometry

The percentage of intrafollicular $CXCR3^+$ T lymphocytes was detected in 14 patients with AIT and in the 12 control patients. The remaining follicle fluid in each patient was collected after the oocytes were removed and centrifugated at 800 g for 10 min. Cells were aspirated and washed with Dulbecco's PBS. The cells were treated with lysis buffer (BD Biosciences) to remove red blood cells. Approximately 2×10^6 cells were filtered through a 70-μm mesh to remove clumps of cells. Cells were incubated with 100 μL PBS containing CD45 microbeads and CD45 antibody. $CD45^+$ cells were isolated using a MACS separator (Miltenyi Biotec). Cells were further phenotyped by staining with CD3, CD4, and CD183 (CXCR3) and counted using a flow cytometer (BD FACSCelesta™).

Statistical Analysis

Statistical analysis was performed using SPSS version 24.0 software (SPSS Inc, Chicago, IL, USA) and GraphPad Prism 6.0 (La Jolla, CA, USA). Comparisons of continuous data among groups were performed using ANOVA or non-parametric tests. A two-tailed P value of <0.05 was defined as statistically significant.

RESULTS

The baseline characteristics of patients with AIT and the control group are shown in **Table 1**. The distributions of age and BMI were similar between the two groups. No significant difference was observed in FT4 and TSH levels in serum or follicular fluid of patients with or without AIT. Significantly higher levels of TGAb and TPOAb in serum and follicular fluid were detected in patients with AIT than in the control group (P <0.001). Thyroid antibodies in serum and follicular fluid were absent in the control group.

We analyzed the distribution of chemokines and cytokines in the follicular fluid between the AIT and control groups (**Figure 1**). Among the 12 chemokines analyzed, only the concentrations of three, CXCL9, CXCL10, and CXCL11, were significantly elevated in the follicular fluid of patients with AIT. There was no significant difference in the levels of other chemokines between the two groups. Among the 11 cytokines analyzed, significantly higher levels of IFNγ were observed in patients with AIT than in the control group (P <0.01). Marginal yet significantly higher levels of IL4, IL-6, and IL-10 were also observed in patients with AIT than in the control group (P <0.05). There was no significant difference in the levels of other cytokines between the two groups.

IFNγ has been evidenced as an effective inducer for the activation of CXCL9/10/11 in thyrocytes, however, the role of

TABLE 1 | Baseline characteristics in patients with and without autoimmune thyroiditis (AIT).

Characteristics	AIT group (n = 66)	Control group (n = 56)	P value
Age	33.1 (3.9)	32.1 (4.2)	0.15
Body mass index	22.3 (3.5)	22.0 (3.1)	0.64
Serum FT4	1.2 (0.1)	1.2 (0.1)	0.19
Serum TSH	2.4 (1.0)	2.3 (0.9)	0.60
Serum TGAb	172.0 (77.1–294.3)	15.0 (15.0–18.8)	<0.001
Serum TGAb positivity (%)	80.3	0	<0.001
Serum TPOAb	289.3 (33.0–1300.0)	28.0 (28.0–30.2)	<0.001
Serum TPOAb positivity (%)	68.2	0	<0.001
FF FT4	1.2 (0.1)	1.2 (0.1)	0.61
FF TSH	2.6 (1.1)	2.5 (1.1)	0.83
FF TGAb	118.2 (44.5–210.2)	15.0 (15.0–15.8)	<0.001
FF TGAb positivity (%)	69.7	0	<0.001
FF TPOAb	198.7 (41.9–1300.0)	36.5 (31.6–42.1)	<0.001
FF TPOAb positivity (%)	71.2	0	<0.001

FT4, free thyroxin; TGAb, thyroglobulin antibody; TPOAb, thyroid peroxidase antibody; TSH, thyroid stimulating hormone; FF, follicular fluid.
Continuous variables were expressed as medians (interquartile range) when the data did not follow a Gaussian distribution, and as means (standard deviation) for normally distributed data.

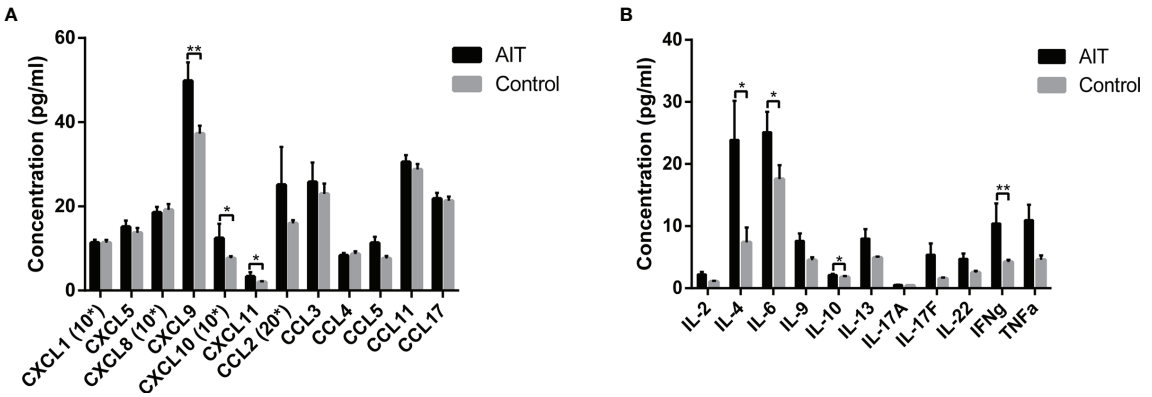

FIGURE 1 | Distribution of cytokines and chemokines in follicle fluid obtained from patients with and without AIT. Among the 12 chemokines analyzed, concentrations of CXCL9, CXCL10, and CXCL11 were significantly higher in patients with AIT than those in the control group **(A)**. Bars represent the mean ± SEM. *P < 0.05 and **P < 0.01 by the Mann-Whitney U test. Among the 11 cytokines analyzed, IL4, IL-6, IL-10, and IFNγ concentrations were significantly higher in patients with AIT than in the control group **(B)**. Bars represent the mean ± SEM. *P < 0.05 and **P < 0.01 by the Mann-Whitney U test. *10, data needed to be multiplied by 10; *20, data needed to be multiplied by 20.

IFNγ in intrafollicular granulosa cells remains unclear. Based on differences in distribution of intrafollicular chemokines and cytokines between the AIT and control groups, elevated CXCL9/10/11 secretion may be induced by increased IFNγ in the follicular microenvironment of patients with AIT. To investigate whether intrafollicular IFNγ stimulates the secretion of CXCL9/10/11 in granulosa cells, primary granulosa cells were cultured *in vitro* and treated with different doses of IFNγ. As shown in **Figure 2**, IFNγ dose-dependently induced the expression and secretion of CXCL9/10/11 in primary granulosa cells.

CXCL9/10/11 shares the common receptor CXCR3 (CD183), which is primarily expressed in T lymphocytes (9, 10). To investigate whether elevated intrafollicular CXCL9/10/11 in

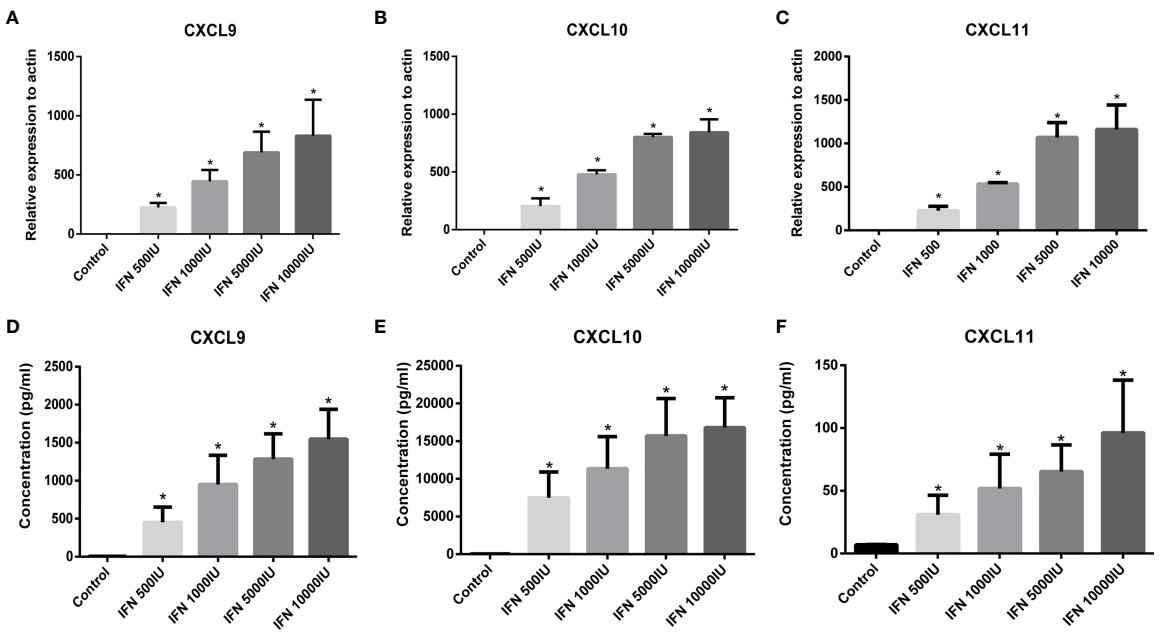

FIGURE 2 | Expression of CXCL9 **(A)**, CXCL10 **(B)**, and CXCL11 **(C)** in primary granulosa cells stimulated by IFNγ (IFN-g) was detected by RT-PCR. Expression of CXCL9/10/11 in granulosa cells was absent under basal conditions (control) and was significantly stimulated by increasing doses of IFNγ (ANOVA, P < 0.05). Bars represent the mean ± SEM. *P < 0.05 vs control by the Bonferroni-Dunn test. Concentration of CXCL9 **(D)**, CXCL10 **(E)**, and CXCL11 **(F)** in the culture supernatant from granulosa cells stimulated by IFNγ. The release of CXCL9/10/11 from granulosa cells was absent under basal conditions (control) and was significantly stimulated by increasing doses of IFNγ (ANOVA, P <0.05). Bars represent the mean ± SEM. *P < 0.05 vs control by the Bonferroni-Dunn test.

patients with AIT promoted the infiltration of T lymphocytes into follicle fluid, we measured the percentage of T lymphocytes expressing CXCR3 in follicular fluid from 14 patients with AIT and compared it with 12 control patients using flow cytometry. As shown in **Figure 3**, of the $CD45^+CD3^+$ T lymphocytes, the proportions of $CD4^+CXCR3^+$ and $CD4^-CXCR3^+$ T lymphocytes in the AIT group were significantly higher than those in the control group.

DISCUSSION

Our study is the first to demonstrate the substantial activation of IFNγ-CXCL9/10/11-$CXCR3^+$ T lymphocytes in the ovarian microenvironment of patients with AIT. This cascade included a classical inflammatory response: IFNγ secreted by T lymphocytes stimulated the release of CXCL9/10/11 from granulosa cells. CXCL9, CXCL10, and CXCL11 belong to the chemokine family and share the common receptor CXCR3, which is particularly expressed in T lymphocytes. Elevation of CXCL9/10/11 in follicle fluid attracts $CXCR3^+$ T lymphocytes to infiltrate the follicle. T lymphocytes that remained in the follicle further increased the secretion of IFNγ, which constitutes an intact response loop in the follicular microenvironment (**Figure 4**).

There is increasing evidence to demonstrate the role of intrafollicular inflammation in the pathogenesis of reproductive diseases. A previous study analyzed the association between follicular pro-inflammatory cytokines/chemokines and infertility related diseases and showed that different types of cytokines/chemokines were activated in patients with different reproductive diseases. For example, higher follicular MIP-1α (CCL3) and CD44 were correlated with polycystic ovary syndrome and IL-23, IFN-γ, and TNF-α correlated with endometriosis (11). An imbalance between pro-inflammatory cytokines such as IFNγ and TNFα and anti-inflammatory cytokines such as IL-10 has also been reported to play a critical role in the pathological mechanism of premature ovarian insufficiency (8). Our study showed a significant difference in the distribution of intrafollicular chemokines and cytokines between the AIT and control groups, suggesting the presence of an activated abnormal immune response in the follicular microenvironment in patients with AIT.

Whether increased levels of intrafollicular CXCL9/10/11 affect follicle development is still unclear; however, CXCL9/10/11 has been reported to inhibit angiogenesis. Several studies have reported that increased levels of CXCL9/10/11 significantly inhibit blood vessel formation and endothelial cell motility (12, 13). In the ovary, angiogenesis is essential for folliculogenesis and ovulation. A rich vascular network surrounding the theca cell layer provides sufficient nutrients and oxygen to support follicle growth, and suppression of normal thecal vasculature leads to considerably reduced thecal thickness, decreased granulosa cell proliferation, prevention of ovulation, and increased rate of follicle atresia (14, 15). Elevated levels of intrafollicular CXCL9/10/11 in patients with AIT may indirectly block follicle development by inhibiting ovarian angiogenesis.

CXCL9/10/11 belongs to a family of chemokines with the capacity to attract circulating leukocytes to inflammatory sites by

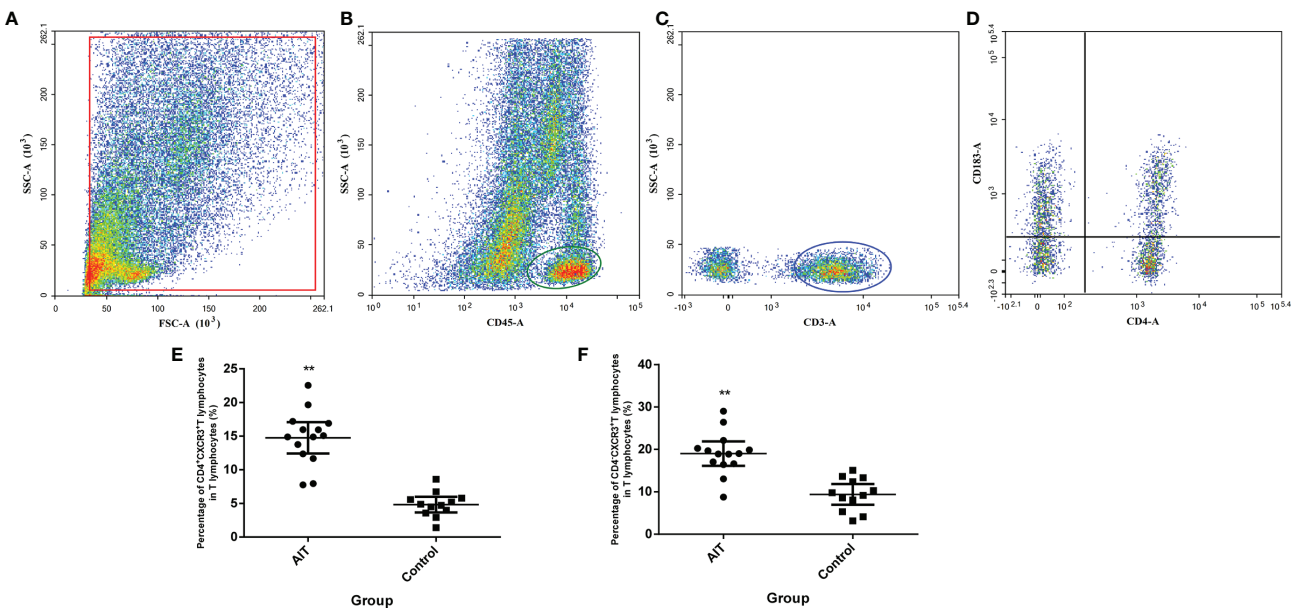

FIGURE 3 | Detection of $CXCR3^+$ T lymphocytes in the follicular microenvironment. Cells were enriched from follicular fluid, and $CD45^+$ cells were positively selected by MACS cell separation. Separated cells were directly incubated with conjugated anti-CD3, CD4, and CXCR3 antibodies and counted by flow cytometry **(A)**. $CD45^+$ cells were gated **(B)** and $CD3^+$ cells were gated from $CD45^+$ cells **(C)**, the expressions of CXCR3 in $CD4^+$ and $CD4^-$T cells were gated from $CD3^+$ cells **(D)**. **(E, F)** The percentage of $CD4^+CXCR3^+$ and $CD4^-$ $CXCR3^+$ T lymphocytes. **P < 0.01 by the Mann-Whitney U test.

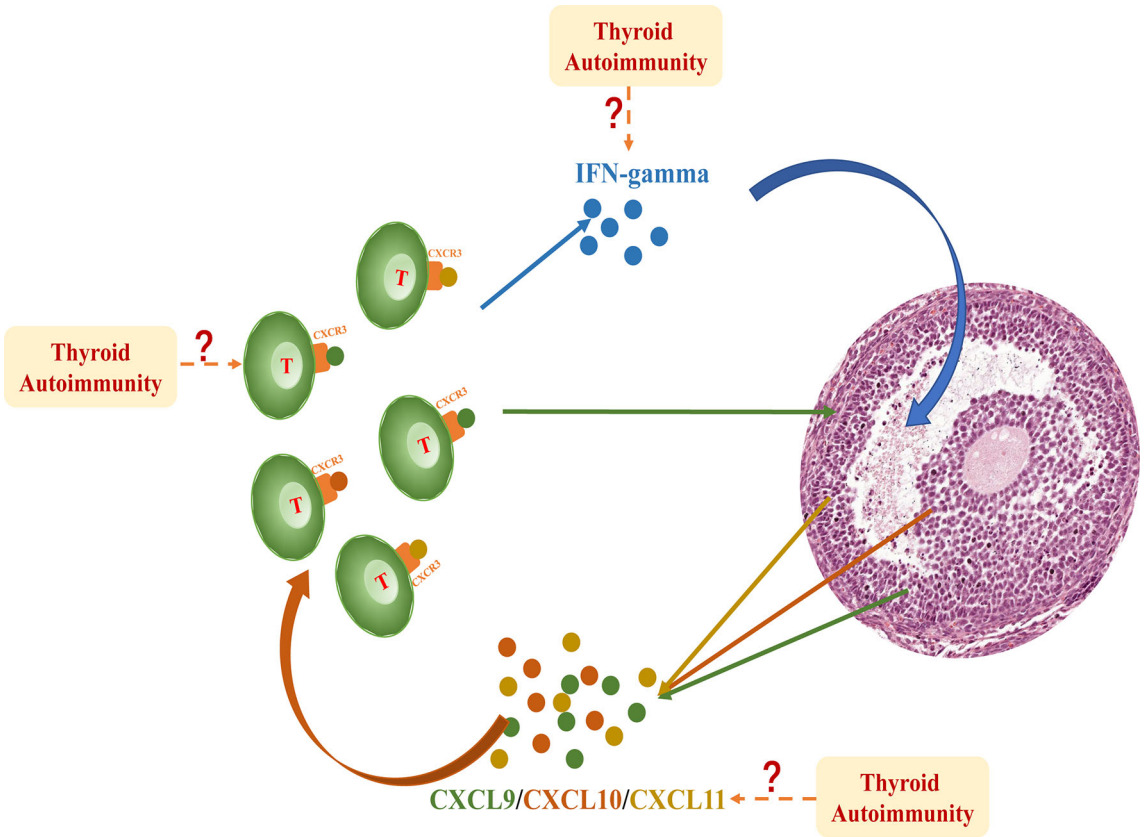

FIGURE 4 | IFNγproduced by T lymphocytes dose-dependently induced the expression and secretion of CXCL9/10/11 in primary granulosa cells. These chemokines bind to their receptor CXCR3 and further promote the migration of T lymphocytes into the follicle, thereby perpetuating an inflammatory cascade in the follicular microenvironment. This intrafollicular response is significantly activated in patients with AIT; however, the initiation of this cascade is still unclear. The excess influx of inflammatory cells and factors into the follicle fluid may be involved in this mechanism.

binding to their specific receptor, CXCR3. Prior to ovulation, only a few resident immune cells were present in vessels around the thecal cells. Upon LH surge or stimulation by HCG, the basal lamina is disrupted and several capillaries form and extend into the granulosa cell compartment, with numerous infiltrating leukocytes and a large number of cytokines are secreted into the follicle fluid (16). The association between the infiltration of leukocytes and ovulation is not completely clear, and the complexity of the inflammatory response and leukocyte types makes it difficult to investigate the role that a specific type of leukocyte plays in follicle fluid. A previous study reported that perfused LH and leukocytes in rat ovaries produced a higher number of ovulations; however, perfused leukocytes alone failed to induce ovulation, suggesting that the influx of leukocytes plays a synergetic, yet not necessary, role in ovulation (17). In our study, elevated CXCL9/10/11 levels enhanced the migration of T lymphocytes *via* CXCR3 and led to a higher proportion of intrafollicular T lymphocytes in patients with AIT, which may aggravate the regional inflammatory response.

In our study, the initiation of the IFNγ-CXCL9/10/11-CXCR3$^+$ T lymphocyte cascade in the follicular microenvironment remains elusive. We provided two possible hypotheses. First, excess infiltration of circulating CXCL9/10/11 or IFNγ from blood in patients with AIT may affect the cascade. Several studies have demonstrated that CXCL9/10/11 is dramatically increased in the development of AIT. Kimura et al. established a transgenic mouse model with features similar to those of human AIT, which aberrantly expresses IFNγ within the thyroid gland. Compared with wild-type littermates, a transgenic mouse model exclusively expressed CXCL9 and CXCL11, and showed increased expression of CXCL10, which verified that IFNγ stimulated the secretion of CXCL9/10/11 from the thyroid gland (3). A study showed that circulating CXCL9 and CXCL10 levels were significantly elevated in patients with AIT compared with normal controls or patients with multinodular goiter (1). Another study found that circulating CXCL9 and CXCL11 levels were significantly elevated in patients with AIT compared with euthyroid controls or patients with multinodular goiter (18). Circulating IFNγ, the upstream stimulator of CXCL9/10/11, also increased in patients with AIT (4).

Second, local activation of the inflammatory response may be another hypothesis for the initiation of this cascade. A previous

study identified thyroid peroxidase using immunocytochemistry in granulosa cells of the human ovarian follicle and provided a hypothesis that the human ovarian follicle may be an independent thyroid-hormone-producing unit (19). Here, thyroid antibodies were detected in the follicular fluid of patients with AIT, with a similar concentration in the serum (**Table 1**). The presence of thyroid peroxidase and thyroid antibodies in follicular fluid may provide a hypothesis for activation of the intrafollicular antibody-mediated immune response.

Although our findings demonstrate an immunological alteration occurred in follicles of patients with AIT, whether the substantial activation of inflammatory cascade affect folliculogenesis requires further study.

In conclusion, our study showed that a considerable immune imbalance occurred in the follicular microenvironment of patients with AIT. Furthermore, to the best of our knowledge, this is the first demonstration of the activation of the intrafollicular IFNγ-CXCL9/10/11-CXCR3$^+$ T lymphocyte cascade in patients with AIT.

DATA AVAILABILITY STATEMENT

The original contributions presented in the study are included in the article/supplementary material. Further inquiries can be directed to the corresponding authors.

ETHICS STATEMENT

The studies involving human participants were reviewed and approved by Peking University Third Hospital Medical Science Research Ethics Committee. The patients/participants provided their written informed consent to participate in this study.

AUTHOR CONTRIBUTIONS

NH, HC, and JQ developed the conception of the study, and all authors contributed to the research discussion. NH, DL, and YL collected the samples. NH and HC performed the experiment and contributed to data analysis. NH wrote the initial draft of the paper, and all authors contributed to manuscript revision. All authors contributed to the article and approved the submitted version.

FUNDING

This work was supported by the National Natural Science Foundation of China (Grant No. 81871212) and The Second Tibetan Plateau Scientific Expedition and Research (Grand No. 2019QZKK0607).

REFERENCES

1. Antonelli A, Ferrari SM, Frascerra S, Galetta F, Franzoni F, Corrado A, et al. Circulating Chemokine (CXC Motif) Ligand (CXCL)9 Is Increased in Aggressive Chronic Autoimmune Thyroiditis, in Association With CXCL10. *Cytokine* (2011) 55(2):288–93. doi: 10.1016/j.cyto.2011.04.022
2. Antonelli A, Ferrari SM, Mancusi C, Mazzi V, Pupilli C, Centanni M, et al. Interferon-α, -β and -γ Induce CXCL11 Secretion in Human Thyrocytes: Modulation by Peroxisome Proliferator-Activated Receptor γ Agonists. *Immunobiology* (2013) 218(5):690–5. doi: 10.1016/j.imbio.2012.08.267
3. Kimura H, Kimura M, Rose NR, Caturegli P. Early Chemokine Expression Induced by Interferon-Gamma in a Murine Model of Hashimoto's Thyroiditis. *Exp Mol Pathol* (2004) 77(3):161–7. doi: 10.1016/j.yexmp.2004.08.004
4. Qin Q, Liu P, Liu L, Wang R, Yan N, Yang J, et al. The Increased But Non-Predominant Expression of Th17- and Th1-Specific Cytokines in Hashimoto's Thyroiditis But Not in Graves' Disease. *Braz J Med Biol Res* (2012) 45(12):1202–8. doi: 10.1590/s0100-879x2012007500168
5. Huang N, Chen L, Lian Y, Wang H, Li R, Qiao J, et al. Impact of Thyroid Autoimmunity on *In Vitro* Fertilization/Intracytoplasmic Sperm Injection Outcomes and Fetal Weight. *Front Endocrinol (Lausanne)* (2021) 12:698579. doi: 10.3389/fendo.2021.698579
6. Field SL, Dasgupta T, Cummings M, Orsi NM. Cytokines in Ovarian Folliculogenesis, Oocyte Maturation and Luteinisation. *Mol Reprod Dev* (2014) 81(4):284–314. doi: 10.1002/mrd.22285
7. Mao XD, Hu CY, Zhu MC, Ou HL, Qian YL. Immunological Microenvironment Alterations in Follicles of Women With Proven Severe Endometriosis Undergoing *In Vitro* Fertilization. *Mol Biol Rep* (2019) 46 (5):4675–84. doi: 10.1007/s11033-019-04753-3
8. Huang Y, Hu C, Ye H, Luo R, Fu X, Li X, et al. Inflamm-Aging: A New Mechanism Affecting Premature Ovarian Insufficiency. *J Immunol Res* (2019) 2019:8069898. doi: 10.1155/2019/8069898
9. Charo IF, Ransohoff RM. The Many Roles of Chemokines and Chemokine Receptors in Inflammation. *N Engl J Med* (2006) 354(6):610–21. doi: 10.1056/NEJMra052723
10. Karin N. CXCR3 Ligands in Cancer and Autoimmunity, Chemoattraction of Effector T Cells, and Beyond. *Front Immunol* (2020) 11:976. doi: 10.3389/fimmu.2020.00976
11. Sarapik A, Velthut A, Haller-Kikkatalo K, Faure GC, Béné MC, de Carvalho Bittencourt M, et al. Follicular Proinflammatory Cytokines and Chemokines as Markers of IVF Success. *Clin Dev Immunol* (2012) 2012:606459. doi: 10.1155/2012/606459
12. Bodnar RJ, Yates CC, Wells A. IP-10 Blocks Vascular Endothelial Growth Factor-Induced Endothelial Cell Motility and Tube Formation *via* Inhibition of Calpain. *Circ Res* (2006) 98(5):617–25. doi: 10.1161/01.Res.0000209968.66606.10
13. Lasagni L, Francalanci M, Annunziato F, Lazzeri E, Giannini S, Cosmi L, et al. An Alternatively Spliced Variant of CXCR3 Mediates the Inhibition of Endothelial Cell Growth Induced by IP-10, Mig, and I-TAC, and Acts as Functional Receptor for Platelet Factor 4. *J Exp Med* (2003) 197(11):1537–49. doi: 10.1084/jem.20021897
14. Wulff C, Wilson H, Wiegand SJ, Rudge JS, Fraser HM. Prevention of Thecal Angiogenesis, Antral Follicular Growth, and Ovulation in the Primate by Treatment With Vascular Endothelial Growth Factor Trap R1r2. *Endocrinology* (2002) 143(7):2797–807. doi: 10.1210/endo.143.7.8886
15. Robinson RS, Woad KJ, Hammond AJ, Laird M, Hunter MG, Mann GE. Angiogenesis and Vascular Function in the Ovary. *Reproduction* (2009) 138 (6):869–81. doi: 10.1530/rep-09-0283
16. Duffy DM, Ko C, Jo M, Brannstrom M, Curry TE. Ovulation: Parallels With Inflammatory Processes. *Endocr Rev* (2019) 40(2):369–416. doi: 10.1210/er.2018-00075
17. Hellberg P, Thomsen P, Janson PO, Brännström M. Leukocyte Supplementation Increases the Luteinizing Hormone-Induced Ovulation Rate in the *In Vitro*-Perfused Rat Ovary. *Biol Reprod* (1991) 44(5):791–7. doi: 10.1095/biolreprod44.5.791
18. Antonelli A, Ferrari SM, Frascerra S, Di Domenicantonio A, Nicolini A, Ferrari P, et al. Increase of Circulating CXCL9 and CXCL11 Associated With Euthyroid or Subclinically Hypothyroid Autoimmune Thyroiditis. *J Clin Endocrinol Metab* (2011) 96(6):1859–63. doi: 10.1210/jc.2010-2905

19. Monteleone P, Faviana P, Artini PG. Thyroid Peroxidase Identified in Human Granulosa Cells: Another Piece to the Thyroid-Ovary Puzzle? *Gynecol Endocrinol* (2017) 33(7):574–6. doi: 10.1080/09513590.2017.1296424

Conflict of Interest: The authors declare that the research was conducted in the absence of any commercial or financial relationships that could be construed as a potential conflict of interest.

Publisher's Note: All claims expressed in this article are solely those of the authors and do not necessarily represent those of their affiliated organizations, or those of the publisher, the editors and the reviewers. Any product that may be evaluated in this article, or claim that may be made by its manufacturer, is not guaranteed or endorsed by the publisher.

frontiers in Immunology

ORIGINAL RESEARCH
published: 07 December 2021
doi: 10.3389/fimmu.2021.758554

Association Between Interleukin 35 Gene Single Nucleotide Polymorphisms and the Uveitis Immune Status in a Chinese Han Population

Meng Feng[1†], Shuping Zhou[1†], Tong Liu[2], Yong Yu[1], Qinghong Su[1], Xiaofan Li[1], Min Zhang[2], Xiao Xie[3,4,5], Tingting Liu[3,4,6] and Wei Lin[1*]*

[1] School of Basic Medicine, Shandong First Medical University & Shandong Academy of Medical Sciences, Jinan, China, [2] Departments of Medicine, Tibet Nationalities University, Xianyang, China, [3] Ophthalmology Department, Eye Hospital of Shandong First Medical University (Shandong Eye Hospital), Jinan, China, [4] State Key Laboratory Cultivation Base, Shandong Provincial Key Laboratory of Ophthalmology, Shandong Eye Institute, Shandong First Medical University & Shandong Academy of Medical Sciences, Qingdao, China, [5] The First Clinical Medical College, Shandong University of Chinese Medicine, Jinan, China, [6] School of Ophthalmology, Shandong First Medical University, Jinan, China

OPEN ACCESS

Edited by:
Zhichao Fan,
UCONN Health, United States

Reviewed by:
Mu Dongzhen,
Weifang Medical University, China
Yi Liao,
Xiamen University, China

***Correspondence:**
Wei Lin
linw1978@163.com;
weilin11@fudan.edu.cn
Tingting Liu
tingtingliu@vip.sina.com

†These authors share first authorship

Specialty section:
This article was submitted to Autoimmune and Autoinflammatory Disorders, a section of the journal Frontiers in Immunology

Received: *14 August 2021*
Accepted: *01 November 2021*
Published: *07 December 2021*

Citation:
Feng M, Zhou S, Liu T, Yu Y, Su Q, Li X, Zhang M, Xie X, Liu T and Lin W (2021) Association Between Interleukin 35 Gene Single Nucleotide Polymorphisms and the Uveitis Immune Status in a Chinese Han Population. Front. Immunol. 12:758554. doi: 10.3389/fimmu.2021.758554

Autoimmune uveitis is characterized by immune disorders of the eyes and the whole body and is often recurrent in young adults, but its pathogenesis is still unclear. IL-35 is an essential regulatory factor in many autoimmune diseases, which is produced by Breg cells and can induce Breg cells to regulate the immune response. The relationship between the expression and gene polymorphism of IL-35 and the immune status of patients with autoimmune uveitis has not been reported. The peripheral blood of the subjects was collected from patients with Behçet's Disease (BD) and those with Vogt–Koyanagi–Harada (VKH) syndrome. The percentage of immune cell subsets including B cells, DC, and T cells, and the expression of IL-35 in serum of these two kinds of disease were analyzed. And then, the associations between seven IL-35 single nucleotide polymorphism (SNP) sites and disease susceptibility, the immune status, the clinical characteristics, and the serum IL-35 levels were analyzed. Our results showed that the percentage of Breg cells was significantly decreased in the blood of patients with VKH syndrome compared to that of healthy controls. The levels of IL-35 in the serum of patients with VKH syndrome or BD patients were not changed significantly, compared to that of healthy controls. Furthermore, the associations between two subunits of IL-35 (IL-12p35 and EBI3) and BD or VKH patients were analyzed. We found that there was an association between the EBI3 rs428253 and the occurrence of BD. There was an association between the IL-12p35 rs2243131 and the low level of Breg cell of VKH patients. In addition, there were associations between the polymorphisms of EBI3 rs4740 and the occurrence of headache and tinnitus of VKH patients, respectively. And the genotype frequency of IL-12p35 rs2243115 was related to the concentration of serum IL-35 in patients with VKH syndrome. Thus, the specific SNP sites change of IL-35 were

correlated to the immune disorders in uveitis. And they may also play a guiding role in the occurrence of clinical symptoms in patients with uveitis, especially for VKH syndrome.

Keywords: interleukin-35, regulatory B cells, interleukin-12p35, EBI3, Behçet's syndrome, Vogt–Koyanagi–Harada syndrome, gene single nucleotide polymorphisms, autoimmune diseases

INTRODUCTION

Uveitis is an autoimmune inflammatory disease that severely impairs visual function (1). Behçet's disease (BD) and Vogt–Koyanagi–Harada (VKH) syndrome are common types of diffuse panuveitis. They usually manifest as chronic and recurrent, which affects multiple organs and systems (2–5). And in the early stage, BD patients often take dental ulcer and ophthalmia as their initial symptoms, while VKH patients are usually accompanied by headache, hearing loss, alopecia, and so on (6, 7). The disorder of the immune system is a key factor for the recurrence of the disease and visual impairment (8–10). However, the cause of the disease is not clear. It had been reported that abnormal autoreactive B cells, activated DC cells, and activated T cells increase in autoimmune uveitis (AIU), and the ratio of T helper type 17 (Th17)/regulatory T cell (Treg) cell was also increased (11, 12). Lacking immunosuppressive molecules or regulatory cells may be the cause of immune over-activation. In experimental autoimmune uveitis (EAU), regulatory B (Breg) cells secreting IL-35 suppress intraocular inflammation by inducing expansion of IL-10-producing and IL-35-producing regulatory B (Breg) and regulatory T (Treg) cells. These indicate that Breg cells orchestrate an immunosuppressive milieu in autoimmune diseases (13, 14). Yet, the statuses of Breg cells in patients with uveitis have not been thoroughly investigated, and the possible factors affecting the Breg cells in uveitis might be an important pathogenic factor for this disease.

Breg cells is a class of B cell subsets with a negative regulatory immune response (15). It had been found that Breg cells can exert their inhibitory effects with different mechanisms in different mice models of autoimmune diseases (16), such as experimental autoimmune encephalomyelitis (EAE), systemic lupus erythematosus (SLE), and uveitis (13, 17, 18). Emerging evidence suggests a potent regulatory function of IL-35 and IL-10 in orchestrating autoreactive Breg cells responses and reveals significantly impaired IL-10/IL-35-producing capacity in Breg cells upon autoimmune disease progression (15, 19). As a member of the IL-12 family, IL-35 comprises two subunits: IL-12p35 and EBI3 (20, 21). IL-12p35 induces Breg cells to secrete IL-10/IL-35, promote Breg cells expansion, stimulate Treg effects, and induce immune tolerance (13, 14). Although IL-35 participates in the proliferation and expansion of Breg cells, it also can effectively alleviate and inhibit the development of autoimmune diseases (22, 23). As previously mentioned, IL-35 induces the expression of IL-10+/IL-35+ Breg, to alleviate EAU (14). However, the status of IL-35 in patients with uveitis is still not clear.

Studying genetic susceptibility is a hot issue to explore the pathogenesis of diseases in recent years (24–26). Some studies have confirmed that there were significant associations between the SNP sites (SNPs) of IL-35 and the occurrence of certain clinical manifestations in patients with autoimmune diseases, for example, IL-35 rs4740 with patients with SLE in the Chinese Han population (24). But it is not clear whether the SNPs of IL-35 are related to the occurrence of BD or VKH.

Therefore, in our study, we separately analyzed the clinical symptoms of patients with BD and those with VKH syndrome in the Chinese Han population and the correlation between IL-35 cytokine levels and these diseases. In addition, we focused on the relationship between the SNPs of IL-35 (including its subunits IL-12p35 and EBI3) and disease susceptibility, immune statuses with BD or VKH patients. Our results shown that there were associations between the polymorphisms of EBI3 rs4740 and the occurrence of headache and tinnitus of VKH patients, respectively. The genotype frequency of IL-12p35 rs2243115 was related to the concentration of serum IL-35 in patients with VKH syndrome. In particular, the polymorphisms of IL-12p35 rs2243131 was related to Breg cells disorder in VKH patients. There was an association between EBI3 rs428253 and the occurrence of BD. Considering these, uveitis may result from the interaction of various factors between the genetic and immune environment, which may provide a new basis for its diagnosis and treatment.

MATERIALS AND METHODS

Subjects

All subjects involved in our study have been recruited from the Shandong Eye Hospital and the Shandong Qilu Hospital Laboratory Department in 2020-2021, including 11 patients with BD, 21 patients with VKH syndrome, and 48 normal healthy people, all of whom were Chinese Han people. All patients with BD met the criteria established by the International Panel on BD (27, 28). All patients with VKH syndrome met the standard set by the international research group (29, 30). All patients were either not treated or stopped taking immunosuppressive drugs at least six months before blood samples were taken. Meanwhile, all healthy controls met the following inclusion criteria: no family history of BD syndrome; no family history of VKH syndrome, no history of autoimmune diseases and severe systemic diseases, no blood relationship with other subjects, and Chinese Han population. The informed consent of all participants was obtained, and the demographic data are consistent with the clinical characteristics. The eyes were analyzed by fundus photography and optical coherence tomography angiography (OCTA) to indicate any eyes lesions, OCTA was performed using AngioVue (Optovue, Fremont, California, USA).

Flow Cytometry

Two milliliters of heparinized venous blood were obtained from patients with uveitis and healthy controls. Human peripheral blood mononuclear cells (PBMCs) were collected at the buffy coat layer using a Human Ficoll-Hypaque (Pharmacia) gradient and then washed twice with phosphate-buffered saline (Genview, cat#: GS3101) to remove red blood cells. Phenotypic analysis of fresh PBMCs was conducted by flow cytometry. Fluorescent antibodies of human CD45 (clone 2D1), human CD3 (clone HIT3a), human CD4 (clone OKT4), human CD8 (clone OKT8), human CD19 (clone HIB19), human CD1d (clone 51.1), human CD5 (clone UCHT2), human CD56 (clone HCD56), human CD14 (clone S18004B), human CD11c (clone Bu15), human HLA-DR (clone L243) were obtained. Furthermore, we used flow cytometry to analyze the expression of immune cells in healthy controls and patients. These cells were tested by BD FACSverse (BD Biosciences, San Diego, CA, USA), including T cells ($CD45^+CD3^+CD19^-$), B cells ($CD45^+CD3^-CD19^+$), Breg cells ($CD45^+CD3^-CD19^+CD1d^+CD5^+$), DC ($CD3^-CD19^-$ $CD56^-CD14^-CD11c^+HLA\text{-}DR^+$). The results were analyzed by Flowjo7.6. In addition, we also analyzed and compared the significant differences of Breg cells and DC between genotypes using the SPSS11.0 software.

SNP Selection and Genotyping

According to previous studies, we selected seven SNPs of IL-35 (including four SNPs of IL-12 p35 and three SNPs of EBI3), including IL-12 p35: rs2243123, rs2227314, rs2243131, rs2243115. EBI3: rs428253, rs9807813, and rs4740. The SNPs of the IL-35 encoding gene were synthesized by the Shanghai Biosune Biotechnology Company. The Hardy-Weinberg equilibrium (HWE) was used to calculate the consistency of all genotype frequencies with all expected control frequencies. Furthermore, information about the SNPs genotypes of IL-12 p35 and EBI3 genes is shown in **Supplementary Table 1** (**Table S1**).

Enzyme-Linked Immunosorbent Assay

Two milliliters of heparinized venous blood were obtained from patients with uveitis and healthy controls, and their serum was collected after centrifugation by Microcentrifuge (M1324R, RWD LifescienceCo., Ltd, China) at 1500 rpm for 5 min. Subsequently, Human-IL-35 (Cusabio, Cat# CSB-E13126h) ELISA kits were used to evaluate the levels of IL-35 in human serum, according to the manufacturer's instructions, and were tested using a microplate reader (Bio Tek, Synergy LX, USA). ELISA Calc and Prism 8.0 were used to analyze the concentration levels of IL-35 in the serum of all statisticians. And the concentration of IL-35 in the serum of all recruited subjects (80 cases in total) was analyzed using the SPSS11.0 software to count the mean ± SD.

Statistical Analysis

We used the Social Science Statistics Package (SPSS) v.11.0 for statistical analysis. The Shapiro–Wilk test was used to test the normality of the data, and the continuous data were described as the mean ± SD of the normally distributed data. The difference of continuous data was evaluated by a *t*-test and a one-way ANOVA test. The difference of categorical data is satisfied by the chi-squared test or Fisher's exact test. The HWE was used to compare the observed genotype with the expected frequency. The case where the two-sided *p*-value is less than 0.05 is considered to be statistically significant.

RESULTS

Characteristics, Clinical Features, and the Immune Status of the Population

The basic demographic characteristics of patients with BD and those with VKH syndrome are presented in **Table S2**. There were no significant differences in gender (BD: $\chi^2 = 0.272$, $p = 0.602$; VKH: $\chi^2 = 0.052$, $p = 0.819$) and age (BD: $t = 0.028$, $p = 0.978$; VKH: $t = -1.358$, $p = 0.185$) between patients with BD or VKH and healthy controls, shown in **Table S2**. The important clinical manifestations of 32 patients are shown: 90.9% of patients with BD had mouth ulcers, 57.14% of patients with VKH syndrome had headache, 47.62% of patients with VKH syndrome had tinnitus, and 47.42% had alopecia or gray hair (**Table S2**). In the acute phase, the ocular involvement of patients with BD is usually characterized by occlusive retinal vasculitis. The color fundus photograph exhibits perivenous white sheathing (**Figure 1A**). OCTA shows a wedge-shaped localized retinal nerve fiber layer micro-thinning in the superior macula and central foveal thinning (**Figure 1B**). Patients with acute VKH are associated with neurological panuveitis. The fundus photograph shows serious inflammatory infiltration and exudation, swollen optic disks, and unclear optic disk boundary (**Figure 1C**). OCTA shows the presence of subretinal fluid, with multifocal serous retinal detachments (SRDs) (**Figure 1D**).

The information about the immune statuses of patients with BD and VKH is provided in **Table S3**. Analysis of the patient's PBMC immune cells showed that the percentage of DC (the reference range: 0.5%–2.5%) was increased in 36.36% of patients with BD and 38.09% of patients with VKH syndrome (**Figure 2A**). There were 18.18% of patients with BD and 14.28% of patients with VKH syndrome showing an increase in the percentage of T cells (the reference range: 60%–85%) (**Figure 2B**). In addition, we found that in 63.64% of patients with BD and 52.38% of patients with VKH syndrome, the percentage of Breg cells (the reference range: 0.8%–2.2%) was decreased (**Figure 2C**). Overall, in patients with BD or VKH, there were different degrees of immune disorders (**Figure 2D**). Notably, in our study, no matter whether they are patients with BD or those with VKH syndrome, the expression of Breg cells decreased, while the expression of the DC increased in PBMC, which may lead to an imbalance of immune response and inflammation in patients.

The Serum Levels IL-35 in Patients With BD and VKH

The concentration of IL-35 in the serum of all recruited subjects was detected using the human ELISA kit. Compared to healthy

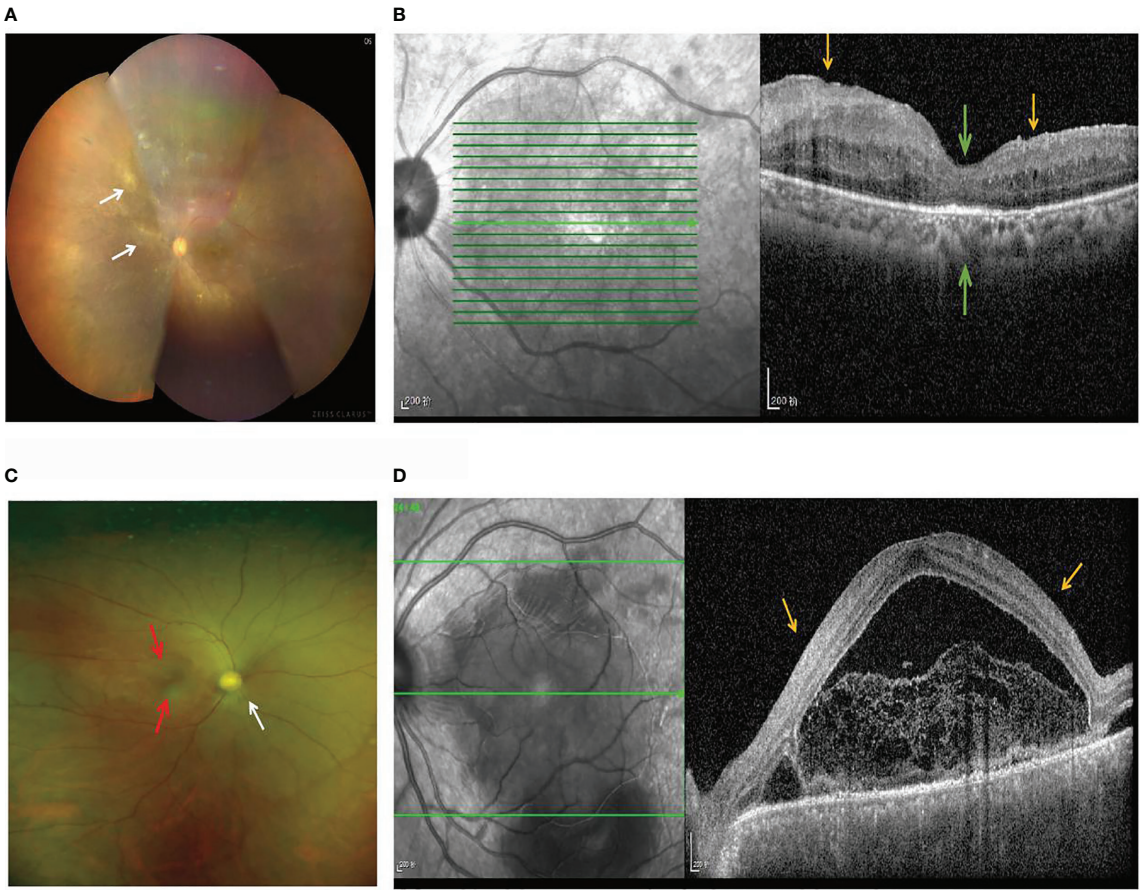

FIGURE 1 | Fundus imaging and OCTA in patients with BD and VKH. **(A)** The color fundus photograph of a patient with BD shows perivenous white sheathing (white arrows). **(B)** OCTA of a patient with BD shows a wedge-shaped localized retinal nerve fiber layer micro-thinning (yellow arrows) in the superior macula and the papillomacular bundle, and the central foveal thinning (green arrows). **(C)** The fundus photograph of a patient with VKH syndrome shows swollen optic disks (white arrows), serous inflammatory infiltration and exudation (red arrows), and an unclear optic disk boundary. **(D)** OCTA of a patient with VKH syndrome shows the presence of subretinal fluid, with multifocal SRDs (yellow arrows).

controls, the serum IL-35 concentration of patients with BD (32.426 ± 85.294 pg/ml *vs.* 54.749 ± 65.583 pg/ml, $p = 0.420$) was not changed (**Figure 3**). And the serum IL-35 concentration of patients with VKH patients was not different from these of healthy controls (52.266 ± 183.383 pg/ml *vs.* 32.426 ± 85.294 pg/ml, $p = 0.540$) (**Figure 3**).

Association of IL-35 Gene Polymorphisms With the Risk of Patients With BD and VKH

The allele and genotype frequencies of four SNPs of IL-12 p35 in patients with BD and those with VKH syndrome and healthy controls are presented in **Tables 1**, **2**. There were no significant differences in allele and genotype frequencies of all genotypes IL-12 p35 SNPs (rs2243123, rs2227314, rs2243131, and rs2243115, $p > 0.05$) between patients with BD or VKH patients and healthy controls. However, we analyzed the allele and genotype frequencies of three SNPs of EBI3 (rs428253, rs9807813, and rs4740) in **Tables 3**, **4**, found that the EBI3 rs428253 genotype CC showed a statistical difference between patients with BD and healthy controls (**Table 3**, $p = 0.021$), and the EBI3 rs428253 allele C/G also showed a statistical difference between patients with BD and healthy controls (**Table 3**, $p = 0.034$). But our results could not demonstrate a significant association between the rs9807813 and rs4740 allele and genotype frequencies between patients with BD or VKH, and healthy controls. Thus, there was a significant association between the polymorphism of rs428253 and susceptibility to BD disease in our study.

Association of IL-35 Gene Polymorphisms With the Immune Status of Patients With BD and VKH

The associations between allele and genotype frequencies of seven SNPs of IL-35 and the immune statuses of BD and VKH patients are detailed in **Tables 5**, **S4–S9**. There was a statistical difference in allele frequency of the IL-12 p35 rs2243131 between VKH patients with the Breg cell attenuated and those without ($\chi^2 = 6.301$, $p =$

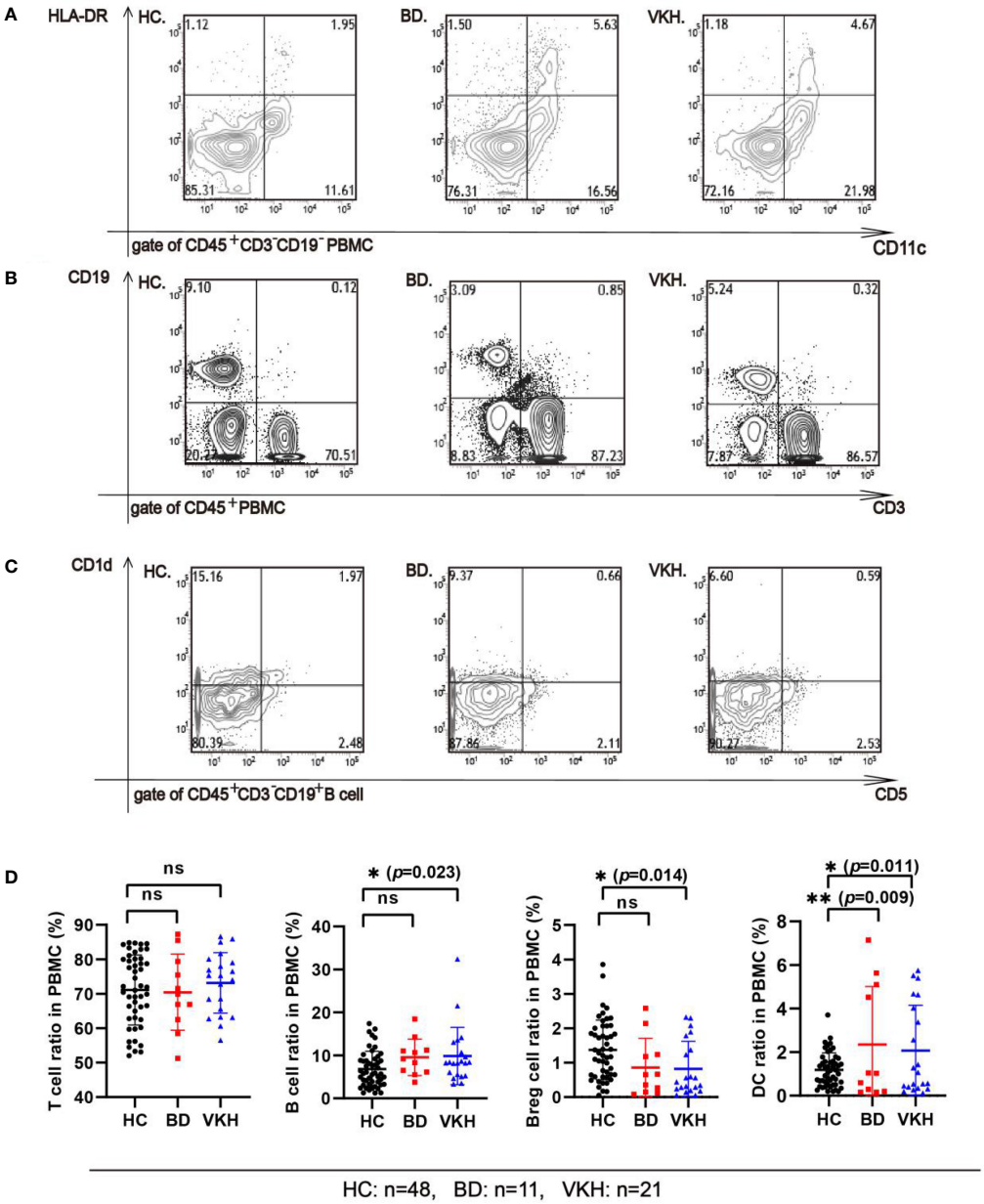

FIGURE 2 | Comparing the subsets of immune cells from the PBMC of the healthy control group and patients. **(A)** The percentage of DC cells in the PBMC of the healthy control group and patients (gate of $CD45^+$ cells). Representative flow cytometry plot shows the percentage of $CD45^+CD3^-CD19^-CD56^-CD14^-CD11c^+HLA\text{-}DR^+$ DC cells in the PBMC of the healthy control group (HC), in BD patient, and in VKH patient. **(B)** The percentage of T and B cells in the PBMC of the healthy control group and patients (gate of $CD45^+$ cells). Representative flow cytometry plot shows the percentage of $CD45^+CD3^+$ T cells, $CD45^+CD3^-CD19^+$B cells in the PBMC of HC, in BD patient, and in VKH patient. **(C)** The percentage of Breg cells ($CD45^+CD3^+CD19^+CD1d^+CD5^+$ B cells) in the PBMC between the healthy control group and patients (gate of $CD45^+CD3^+CD19^+$ B cells). Representative flow cytometry plot shows the percentage of $CD45^+CD3^-CD19^+$ $CD1d^+CD5^+$ Breg cells in the PBMC of HC, BD patient, and in VKH patient. **(D)** The percentage of T cell, B cell, Breg cell and DC in PBMC of healthy control group and patients (*p<0.05; **p<0.01; ns, p>0.05).

0.018, **Table 5**). Although the overall percentage of DC cells in PBMC of BD and VKH patients were higher than the healthy controls. In our study, the SNPs of IL-35 were not related to the expression of DC cells. And there were no significant associations between genotype and allele frequencies of the other SNPs and the immune statuses (including T cell, B cell, the results not shown).

Association of IL-35 Gene Polymorphisms With the Clinical Features of Patients With BD and VKH

The associations between allele and genotype frequencies of seven SNPs of IL-35 with the clinical features of patients with BD and VKH are provided in **Tables 6**, **S10–S15**. There was a statistical

TABLE 1 | IL-12A genotypes and alleles frequencies of genotypes SNPs in BD and healthy controls.

SNPs ID	Genotypes	Patients	Controls	*p* value	*OR*	*95%CI*
rs2243123	TT	9	43	0.473	1.911	0.319-11.450
	CC	0	0	–	–	–
	TC	2	5	0.473	0.523	0.087-3.135
	C	2	5	0.487	0.549	0.099-3.037
	T	20	91	0.487	1.820	0.329-10.060
rs2227314	GG	4	19	0.322	2.293	0.430-12.237
	TT	2	2	0.095	0.196	0.024-1.576
	GT	5	27	0.517	1.543	0.414-5.757
	G	13	65	0.441	1.452	0.561-3.759
	T	9	31	0.441	0.689	0.266-1.784
rs2243131	AA	8	34	0.90	0.911	0.210-3.944
	CC	0	0	–	–	–
	AC	3	14	0.900	1.098	0.254-4.755
	A	19	82	0.909	0.925	0.241-3.543
	C	3	14	0.909	1.081	0.282-4.142
rs2243115	TT	7	36	0.444	1.714	0.426-6.892
	GG	0	0	–	–	–
	TG	4	12	0.444	0.583	0.145-2.345
	G	4	12	0.483	0.643	0.186-2.223
	T	18	84	0.483	1.556	0.450-5.380

Fisher's Exact Test; OR, odds ratio; CI, confidence interval.

difference in allele frequency of the EBI3 rs4740 between VKH patients with headache and without it (χ^2 = 7.291, p = 0.012, **Table 6**). And this allele gene frequency in patients with VKH syndrome was also a statistical difference between the tinnitus and those without (χ^2 = 4.972, p = 0.033, **Table 6**). However, there were no significant associations between all genotype and allele frequencies of SNPs and the clinical features of patients with BD.

Association of Serum IL-35 Levels With IL-35 Genotypes of Patients With BD and VKH

We evaluated the association between serum levels and SNP of IL-35 in patients with BD and VKH (**Tables 7**, **8**). The results revealed that there was an association between the frequency of the IL-12 p35 rs2243115 genotype and the human serum IL-35 levels in patients with VKH syndrome (χ^2 = 7.291, p = 0.012, **Table 8**). The concentration of serum IL-35 in patients with VKH syndrome was no significantly different from that in healthy controls. There was no correlation between other SNPs and serum levels of IL-35.

DISCUSSION

The disorder of immune tolerance has been considered a vital cause for the pathogenesis of autoimmune diseases. Participation

TABLE 2 | IL-12A genotypes and alleles frequencies of genotypes SNPs in VKH and healthy controls.

SNPs ID	Genotypes	Patients	Controls	*p* value	*OR*	*95%CI*
rs2243123	TT	15	43	0.058	3.440	0.915-12.934
	CC	0	0	–	–	–
	TC	6	5	0.058	0.291	0.077-1.093
	C	6	5	0.070	0.330	0.095-1.148
	T	36	91	0.070	3.033	0.871-10.566
rs2227314	GG	6	19	0.381	1.638	0.540-4.968
	TT	3	2	0.136	0.261	0.040-1.693
	GT	12	27	0.945	0.964	0.342-2.716
	G	24	65	0.233	1.573	0.746-3.316
	T	18	31	0.233	0.636	0.302-1.341
rs2243131	AA	15	34	0.960	0.971	0.313-3.016
	CC	2	0	0.090	1.105	0.962-1.270
	AC	4	14	0.378	1.750	0.499-6.135
	A	34	82	0.510	1.378	0.530-3.586
	C	8	14	0.510	0.726	0.279-1.888
rs2243115	TT	16	36	0.916	0.938	0.283-3.106
	GG	1	0	0.128	1.050	0.954-1.155
	TG	4	12	0.590	1.417	0.398-5.045
	G	6	12	0.774	0.857	0.298-2.461
	T	36	84	1.000[#]	1.167	0.406-3.350

Fisher's Exact Test; OR, odds ratio; CI, confidence interval.

TABLE 3 | EBI3 genotypes and alleles frequencies of genotypes SNPs in BD and healthy controls.

SNPs ID	Genotypes	Patients	Controls	*p* value	*OR*	*95%CI*
rs428253	GG	0	4	0.321	0.917	0.842-0.998
	CC	9	20	0.021*	0.159	0.031-0.815
	GC	2	24	0.055	4.500	0.879-23.043
	C	20	64	0.034*	0.200	0.044-0.909
	G	2	32	0.034*	5.000	1.100-22.729
rs9807813	CC	6	35	0.233	2.244	0.584-8.627
	TT	0	1	0.629	0.979	0.940-1.020
	CT	5	12	0.177	0.400	0.103-1.550
	C	17	82	0.349	1.723	0.547-5.424
	T	5	14	0.349	0.580	0.184-1.828
rs4740	GG	1	18	0.069	6.000	0.708-50.847
	AA	4	8	0.143	0.350	0.083-1.483
	GA	6	22	0.602	0.705	0.189-2.628
	A	14	38	0.056	0.374	0.143-0.978
	G	8	58	0.056	2.671	1.023-6.977

Fisher's Exact Test; OR, odds ratio; CI, confidence interval; there is a significant difference (*p<.0.05).*

TABLE 4 | EBI3 genotypes and alleles frequencies of genotypes SNPs in VKH and healthy controls.

SNPs ID	Genotypes	Patients	Controls	*p* value	*OR*	*95%CI*
rs428253	GG	0	4	0.173	0.917	0.842-0.998
	CC	11	20	0.410	0.649	0.232-1.820
	GC	10	24	0.856	1.100	0.394-3.070
	C	32	64	0.263	0.625	0.273-1.429
	G	10	32	0.263	1.600	0.700-3.659
rs9807813	CC	15	35	0.899	1.077	0.344-3.370
	TT	1	1	0.542	0.426	0.025-7.145
	CT	5	12	0.916	1.067	0.322-3.534
	C	35	82	0.754	1.171	0.435-3.152
	T	7	14	0.754	0.854	0.317-2.297
rs4740	GG	8	18	0.963	0.975	0.339-2.806
	AA	5	8	0.485	0.640	0.182-2.254
	GA	8	22	0.551	1.375	0.482-3.921
	A	18	38	0.719	0.874	0.419-1.823
	G	24	58	0.719	1.145	0.549-2.388

Fisher's Exact Test; OR, odds ratio; CI, confidence interval.

in the induction of immune tolerance and the loss of cells with negative immune-regulation functions are essential factors in the occurrence and development of AIU. Breg cells play a negative immune-regulation role in autoimmune diseases, the absence of Breg cells may be an essential reason for the occurrence of some diseases, and they are decreased and/or functionally impaired in these autoimmune diseases, including EAE, rheumatoid arthritis (RA), and SLE (13, 18). However, the status of Breg cells in patients with uveitis is still not known. Our study showed that the percentage of Breg cells is decreased in the blood, suggesting that the lack of negative immune-regulation of Breg cells may be an essential reason for the imbalance of immune response in uveitis. The decrease of Breg cells may contribute to the immune disorders and inflammation in uveitis.

There were no reports about the relationship between the SNPs of IL-35 and the pathogenesis of uveitis (31). We have analyzed the relationship between IL-35 gene SNPs and genetic susceptibility in the Chinese Han population with uveitis (mainly BD and VKH syndrome). Our results suggest that the IL-12 p35 rs2243131 A/C allele was related to the disorder of Breg cells in VKH patients, and IL-35 and its subunit IL-12p35 preferentially induced the expansion of Breg and Treg cells, inhibited the activation of DC, and inhibited the expansion of pathogenic Th17 and Th1 cells (13, 14, 32), to slow down the development of autoimmune diseases. Thus, the IL-12 p35 A/C allele mutation may be the key factor of Breg cells reduction in VKH patients. Additionally, there was no correlation between other immune cells and IL-35 gene polymorphism, but it cannot eliminate these sites associated with the function of immune cells.

VKH patients are usually with extra-ocular manifestations such as headache, hearing loss (7). In our study results, 57.14% of VKH patients had a headache, and 47.62% had tinnitus. And there was associations between the polymorphisms of the EBI3 rs4740 and the occurrence of headache or tinnitus in VKH patients. Previous studies reported that there were associations between EBI3 rs4740 polymorphism and SLE, UC (24, 33). Thus, the polymorphism of the EBI3 rs4740 may be correlated with the occurrence of autoimmune disease.

We also measured the concentration of IL-35 in the serum of all subjects. Compared with the healthy controls group, the

TABLE 5 | Associations of IL-12p35 (rs2243131) with immune states in BD or VKH patients.

Diseases	Immune states	↑/↓	Genotypes			x^2	*p* value	Allele		x^2	*p* value
			AA	AC	CC			A	C		
BD	Breg	↑	2	2	0	1.637	0.491	6	2	1.378	0.527
		↓	6	1	0			13	1		
	DC	↑	2	2	0	1.637	0.491	6	2	1.378	0.527
		↓	6	1	0			13	1		
VKH	Breg	↑	5	3	2	4.630	0.099	13	7	6.301	0.018*
		↓	10	1	0			21	1		
	DC	↑	5	2	1	0.505	0.777	12	4	0.594	0.454
		↓	10	2	1			22	4		

*↑, cell expression increased or in the normal range; ↓, cell expression decreased or in the normal range; Fisher's Exact Test; *There is a statistical difference (*p<0.05).*

TABLE 6 | Associations of EBI3 (rs4740) with clinical manifestations in BD or VKH patients.

Diseases	Manifestations	+/–	Genotypes			x^2	*p* value	Allele		x^2	*p* value
			GG	GA	AA			A	G		
BD	Mouth ulcers	+	1	6	3	2.554	0.455	12	8	1.257	0.515
		–	0	0	1			2	0		
VKH	Headache	+	7	4	1	5.722	0.053	6	18	7.292	0.012*
		–	1	4	4			12	6		
	Tinnitus	+	6	3	1	3.990	0.166	5	15	4.972	0.033*
		–	2	5	4			13	9		
	Alopecia/Grey hair	+	5	3	2	1.218	0.641	7	13	1.123	0.289
		–	3	5	3			16	16		

*+, with symptom; -, without symptom; Fisher's Exact Test; *There is a statistical difference (*p<0.05).*

TABLE 7 | Associations of serum IL-35 levels with IL-35 genotypes in BD patients.

SNP ID	Genotypes	n	IL-35 Level (pg/ml)	*F/t*	*p* value
rs2243123	TT	9	48.719 ± 71.055	-0.627	0.546[@]
	TC	2	81.886 ± 28.642		
	CC	0	–		
rs2227314	GG	4	55.131 ± 36.516	0.330	0.895
	GT	5	75.492 ± 88.477		
	TT	2	2.128 ± 2.868		
rs2243131	AA	8	73.736 ± 66.851	1.836	0.100[@]
	AC	3	1.452 ± 2.342		
	CC	0	–		
rs2243115	GG	0	–	0.010	0.992[@]
	TG	4	54.461 ± 106.035		
	TT	7	54.914 ± 39.328		
rs428253	GG	0	–	0.549	0.596[@]
	GC	2	30.867 ± 43.511		
	CC	9	60.056 ± 70.466		
rs9807813	CC	6	58.916 ± 84.302	-0.220	0.831[@]
	CT	5	49.749 ± 42.566		
	TT	0	–		
rs4740	GG	1	39.841	1.523	0.456
	GA	6	67.459 ± 82.599		
	AA	4	39.411 ± 47.488		

[@]t test; others data analyzed used one-way ANOVA.

concentration of serum IL-35 in patients with BD was not changed, which is different from the previous study about active BD or BD patients with only mucocutaneous involvement (34, 35), but is consistent with the result of BD patients with mucocutaneous manifestations plus ocular involvement. Moreover, the serum IL-35 concentration of VKH patients was not difference from these of healthy controls, which is consistent with the previous study about inactive VKH patients (36). Thus, the disease statuses, and ethnic differences of patients may be important factors for the

TABLE 8 | Associations of serum IL-35 levels with IL-35 genotypes in VKH patients.

SNP ID	Genotypes	n	IL-35 Level (pg/ml)	*F/t*	*p* value
rs2243123	TT	15	15.269 ± 31.241	-0.925	0.397[@]
	TC	6	144.759 ± 342.344		
	CC	0	–		
rs2227314	GG	6	7.769 ± 8.524	1.134	0.423
	GT	12	83.841 ± 241.61		
	TT	3	14.965 ± 22.325		
rs2243131	AA	15	70.311 ± 215.983	0.896	0.567
	AC	2	20.369 ± 28.664		
	CC	4	0.548 ± 0.896		
rs2243115	GG	1	4.157	3.526	0.030*
	TG	4	33.885 ± 58.228		
	TT	16	59.868 ± 209.246		
rs428253	GG	0	–	0.960	0.349[@]
	GC	10	92.617 ± 264.081		
	CC	11	15.584 ± 35.765		
rs9807813	CC	15	14.364 ± 31.795	2.529	0.080
	CT	5	174.684 ± 373.829		
	TT	1	8.708		
rs4740	GG	8	24.306 ± 41.809	0.561	0.812
	GA	8	3.940 ± 5.859		
	AA	5	174.326 ± 374.037		

[@]*t test; others data analyzed used one-way ANOVA; *There is a statistical difference (*p<0.05).*

level of IL-35. Moreover, IL-35 SNPs were associated with RA, type I diabetes, SLE, and other autoimmune diseases (24, 37, 38). Some studies have explored the relationship between IL-35 (including IL-12 p35 and EBI3) gene SNPs and susceptibility to autoimmune diseases. For instance, IL-12 p35 rs2243115 and rs568408 were novel genetic risk factors for Alzheimer's disease in the Han Chinese population (39). IL-12 p35 rs2243115 was significantly related to the high RA disease risk in a Chinese population (37). EBI3 rs428253 had a related effect on Chinese Han patients with allergic rhinitis (40). EBI3 rs4740 had a significant correlation with the clinical manifestations of Chinese Han patients with SLE (24). All of this evidence shows that IL-35 is involved in the occurrence and progression of autoimmune diseases. Unlike previous reports, we have shown that the EBI3 rs428253 CC genotype and C/G allele may be a susceptibility genes for BD patients. Nevertheless, the role of IL-35 SNPs in the pathogenesis of BD or VKH syndrome and the regulation of the immune response still needs further studying. Additionally, large samples would help determine the correlation between SNPs and diseases.

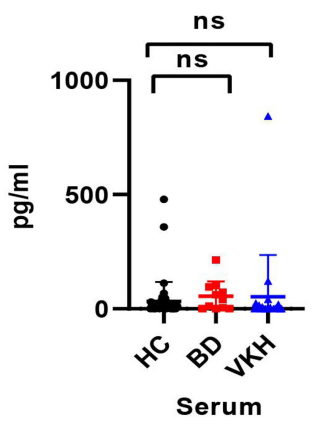

FIGURE 3 | The concentration of IL-35 in serum of the healthy control group and patients with BD or VKH (ns, $p > 0.05$).

In conclusion, our research mainly analyzed the association between IL-35 SNPs and AIU disease susceptibility, immune cells, clinical symptoms, and serum levels. In our study, the polymorphism of EBI3 rs4740, which at the coding region was associated with the occurrence of clinical manifestations in VKH patients. Other SNPs are at the non-coding region. SNPs in the non-coding region not only change gene regulation, but also affect gene expression by affecting gene splicing, binding with transcription factors, degradation of messenger RNA, or other ways. Thus, the polymorphism of IL-35 SNPs are involved in the occurrence of AIU. Above all, uveitis may be affected by genetic and immune factors. Uveitis is resulting from the interaction between genetic and various factors, which may provide a new basis for its diagnosis and treatment.

DATA AVAILABILITY STATEMENT

The original contributions presented in the study are publicly available. This data can be found in dbSNP, batch ID: 1063306.

ETHICS STATEMENT

The studies involving human participants were reviewed and approved by Committee of Shandong Eye Hospital, Shandong Eye Institute, Shandong First Medical University and Shandong

Academy of Medical School (2019-G-012) granted ethical approval for the study. Written informed consent to participate in this study was provided by the participants' legal guardian/next of kin. Written informed consent was obtained from the individual(s) for the publication of any potentially identifiable images or data included in this article.

AUTHOR CONTRIBUTIONS

WL, TTL, MF, and SZ designed research, planned and performed experiments, and drafted and revised the manuscript. TL, YY, QS, XL, MZ, and XX organized the data, generated the figures and tables. TTL provided clinical samples. All authors contributed to the article and approved the submitted version.

FUNDING

This work was supported by grants from the Natural Science Foundation of China (81500710), the Shandong Key Research and Development Project (2019GSF108189), projects of medical and health technology development program in Shandong province (2015WS0194 and 2019WS186), and the Innovation Project of Shandong Academy of Medical Sciences.

SUPPLEMENTARY MATERIAL

The Supplementary Material for this article can be found online at: https://www.frontiersin.org/articles/10.3389/fimmu.2021.758554/full#supplementary-material

REFERENCES

1. Rothova A, Suttorp-van SM, Frits TW, Kijlstra A. Causes and Frequency of Blindness in Patients With Intraocular Inflammatory Disease. *Br J Ophthalmol* (1996) 80:332–6. doi: 10.1136/bjo.80.4.332
2. Yang P, Zhang Z, Zhou H, Li B, Huang X, Gao Y, et al. Clinical Patterns and Characteristics of Uveitis in a Tertiary Center for Uveitis in China. *Curr Eye Res* (2005) 30:943–8. doi: 10.1080/02713680500263606
3. Goto H, Mochizuki M, Yamaki K, Kotake S, Usui M, Ohno S. Epidemiological Survey of Intraocular Inflammation in Japan. *Jpn J Ophthalmol* (2007) 51:41–4. doi: 10.1007/s10384-006-0383-4
4. Ksiaa I, Abroug N, Kechida M, Zina S, Jelliti B, Khochtali S, et al. Eye and Behcet's Disease. *J Fr Ophthalmol* (2019) 42:e133–46. doi: 10.1016/j.jfo.2019.02.002
5. Fang W, Yang P. Vogt-Koyanagi-Harada Syndrome. *Curr Eye Res* (2008) 33:517–23. doi: 10.1080/02713680802233968
6. Alpsoy E. Behcet's Disease: A Comprehensive Review With a Focus on Epidemiology, Etiology and Clinical Features, and Management of Mucocutaneous Lesions. *J Dermatol* (2016) 43:620–32. doi: 10.1111/1346-8138.13381
7. O'Keefe GA, Rao NA. Vogt-Koyanagi-Harada Disease. *Surv Ophthalmol* (2017) 62:1–25. doi: 10.1111/1346-8138.13381
8. Luger D, Caspi RR. New Perspectives on Effector Mechanisms in Uveitis. *Semin Immunopathol* (2008) 30:135–43. doi: 10.1007/s00281-008-0108-5
9. Caspi R. Autoimmunity in the Immune Privileged Eye: Pathogenic and Regulatory T Cells. *Immunol Res* (2008) 42:41–50. doi: 10.1007/s12026-008-8031-3
10. Caspi RR. A Look at Autoimmunity and Inflammation in the Eye. *J Clin Invest* (2010) 120:3073–83. doi: 10.1172/JCI42440
11. Rutitzky LI, Lopes DRJ, Stadecker MJ. Severe CD4 T Cell-Mediated Immunopathology in Murine Schistosomiasis is Dependent on IL-12p40 and Correlates With High Levels of IL-17. *J Immunol* (2005) 175:3920–6. doi: 10.4049/jimmunol.175.6.3920
12. Wang C, Tian Y, Lei B, Xiao X, Ye Z, Li F, et al. Decreased IL-27 Expression in Association With an Increased Th17 Response in Vogt-Koyanagi-Harada Disease. *Invest Ophthalmol Vis Sci* (2012) 53:4668–75. doi: 10.1167/iovs.12-9863
13. Wang RX, Yu CR, Dambuza IM, Mahdi RM, Dolinska MB, Sergeev YV, et al. Interleukin-35 Induces Regulatory B Cells That Suppress Autoimmune Disease. *Nat Med* (2014) 20:633–41. doi: 10.1038/nm.3554
14. Dambuza IM, He C, Choi JK, Yu CR, Wang R, Mattapallil MJ, et al. IL-12p35 Induces Expansion of IL-10 and IL-35-Expressing Regulatory B Cells and Ameliorates Autoimmune Disease. *Nat Commun* (2017) 8:719. doi: 10.1038/s41467-017-00838-4
15. Mizoguchi A, Bhan AK. A Case for Regulatory B Cells. *J Immunol* (2006) 176:705–10. doi: 10.4049/jimmunol
16. Yang M, Rui K, Wang S, Lu L. Regulatory B Cells in Autoimmune Diseases. *Cell Mol Immunol* (2013) 10:122–32. doi: 10.1038/cmi.2012.60
17. Shen P, Roch T, Lampropoulou V, O'Connor RA, Stervbo U, Hilgenberg E, et al. IL-35-Producing B Cells are Critical Regulators of Immunity During Autoimmune and Infectious Diseases. *Nature* (2014) 507:366–70. doi: 10.1038/nature12979
18. Hagn M, Ebel V, Sontheimer K, Schwesinger E, Lunov O, Beyer T, et al. CD5+ B Cells From Individuals With Systemic Lupus Erythematosus Express Granzyme B. *Eur J Immunol* (2010) 40:2060–9. doi: 10.1002/eji.200940113
19. Lin X, Wang X, Xiao F, Ma K, Liu L, Wang X, et al. IL-10-Producing Regulatory B Cells Restrain the T Follicular Helper Cell Response in Primary Sjogren's Syndrome. *Cell Mol Immunol* (2019) 16:921–31. doi: 10.1038/s41423-019-0227-z
20. Vignali DA, Kuchroo VK. IL-12 Family Cytokines: Immunological Playmakers. *Nat Immunol* (2012) 13:722–8. doi: 10.1038/ni.2366
21. Devergne O, Birkenbach M, Kieff E. Epstein-Barr Virus-Induced Gene 3 and the P35 Subunit of Interleukin 12 Form a Novel Heterodimeric Hematopoietin. *Proc Natl Acad Sci USA* (1997) 94:12041–6. doi: 10.1073/pnas.94.22.12041
22. Collison LW, Workman CJ, Kuo TT, Boyd K, Wang Y, Vignali KM, et al. The Inhibitory Cytokine IL-35 Contributes to Regulatory T-Cell Function. *Nature* (2007) 450:566–9. doi: 10.1038/nature06306
23. O'Garra A, Barrat FJ, Castro AG, Vicari A, Hawrylowicz C. Strategies for Use of IL-10 or its Antagonists in Human Disease. *Immunol Rev* (2008) 223:114–31. doi: 10.1111/j.1600-065X.2008.00635.x
24. Guan SY, Liu LN, Mao YM, Zhao CN, Wu Q, Dan YL, et al. Association Between Interleukin 35 Gene Single Nucleotide Polymorphisms and Systemic Lupus Erythematosus in a Chinese Han Population. *Biomolecules* (2019) 9:157. doi: 10.3390/biom9040157
25. Park UC, Kim TW, Yu HG. Immunopathogenesis of Ocular Behcet's Disease. *J Immunol Res* (2014) 2014:653539. doi: 10.1155/2014/653539
26. Horai R, Caspi RR. Cytokines in Autoimmune Uveitis. *J Interferon Cytokine Res* (2011) 31:733–44. doi: 10.1089/jir.2011.0042
27. Davatchi F, Assaad-Khalil S, Calamia K, Crook J, Sadeghi-Abdollahi B, Schirmer M, et al. The International Criteria for Behçet's Disease (ICBD): A Collaborative Study of 27 Countries on the Sensitivity and Specificity of the New Criteria. *J Eur Acad Dermatol* (2014) 28:338–47. doi: 10.1111/jdv.12107
28. Criteria for diagnosis of Behçet's disease. International Study Group for Behçet's Disease. *Lancet (London England)* (1990) 335(8697):1078–80. doi: 10.1016/0140-6736(90)92643-V
29. Rao NA, Sukavatcharin S, Tsai JH. Vogt-Koyanagi-Harada Disease Diagnostic Criteria. *Int Ophthalmol* (2007) 27:195–9. doi: 10.1007/s10792-006-9021-x
30. Read RW, Holland GN, Rao NA, Tabbara KF, Ohno S, Arellanes-Garcia L, et al. Revised Diagnostic Criteria for Vogt-Koyanagi-Harada Disease: Report of an International Committee on Nomenclature. *Am J Ophthalmol* (2001) 131:647–52. doi: 10.1016/s0002-9394(01)00925-4
31. Wang Q, Su G, Tan X, Deng J, Du L, Huang X, et al. UVEOGENE: An SNP Database for Investigations on Genetic Factors Associated With Uveitis and Their Relationship With Other Systemic Autoimmune Diseases. *Hum Mutat* (2019) 40:258–66. doi: 10.1002/humu.23702

32. Jiang H, Li Z, Yu L, Zhang Y, Zhou L, Wu J, et al. Immune Phenotyping of Patients With Acute Vogt-Koyanagi-Harada Syndrome Before and After Glucocorticoids Therapy. *Front Immunol* (2021) 12:659150. doi: 10.3389/fimmu.2021.659150
33. Yamamoto-Furusho JK, Posadas-Sanchez R, Alvarez-Leon E, Vargas-Alarcon G. Protective Role of Interleukin 27 (IL-27) Gene Polymorphisms in Patients With Ulcerative Colitis. *Immunol Lett* (2016) 172:79–83. doi: 10.1016/j.imlet.2016.02.010
34. Sonmez C, Yucel AA, Yesil TH, Kucuk H, Sezgin B, Mercan R, et al. Correlation Between IL-17a/F, IL-23, IL-35 and IL-12/-23 (P40) Levels in Peripheral Blood Lymphocyte Cultures and Disease Activity in Behcet's Patients. *Clin Rheumatol* (2018) 37:2797–804. doi: 10.1007/s10067-018-4049-7
35. Lopalco G, Lucherini OM, Lopalco A, Venerito V, Fabiani C, Frediani B, et al. Cytokine Signatures in Mucocutaneous and Ocular Behcet's Disease. *Front Immunol* (2017) 8:200. doi: 10.3389/fimmu.2017.00200
36. Hu J, Qin Y, Yi S, Wang C, Yang J, Yang L, et al. Decreased Interleukin(IL)-35 Expression is Associated With Active Intraocular Inflammation in Vogt-Koyanagi-Harada (VKH) Disease. *Ocul Immunol Inflammation* (2019) 27:595–601. doi: 10.1080/09273948
37. Shen L, Zhang H, Zhou X, Liu R. Association Between Polymorphisms of Interleukin 12 and Rheumatoid Arthritis Associated Biomarkers in a Chinese Population. *Cytokine* (2015) 76:363–7. doi: 10.1016/j.cyto.2015.09.007
38. Lee YH, Song GG. Genome-Wide Pathway Analysis for Diabetic Nephropathy in Type 1 Diabetes. *Endocr Res* (2016) 41:21–7. doi: 10.3109/07435800.2015.1044011
39. Zhu XC, Tan L, Jiang T, Tan MS, Zhang W, Yu JT. Association of IL-12A and IL-12B Polymorphisms With Alzheimer's Disease Susceptibility in a Han Chinese Population. *J Neuroimmunol* (2014) 274:180–4. doi: 10.1016/j.jneuroim.2014.06.026
40. Zhang Y, Duan S, Wei X, Zhao Y, Zhao L, Zhang L. Association Between Polymorphisms in FOXP3 and EBI3 Genes and the Risk for Development of Allergic Rhinitis in Chinese Subjects. *Hum Immunol* (2012) 73:939–45. doi: 10.1016/j.humimm.2012.07.319

Conflict of Interest: The authors declare that the research was conducted in the absence of any commercial or financial relationships that could be construed as a potential conflict of interest.

Publisher's Note: All claims expressed in this article are solely those of the authors and do not necessarily represent those of their affiliated organizations, or those of the publisher, the editors and the reviewers. Any product that may be evaluated in this article, or claim that may be made by its manufacturer, is not guaranteed or endorsed by the publisher.

frontiers in Immunology

ORIGINAL RESEARCH
published: 02 March 2022
doi: 10.3389/fimmu.2022.831253

Digital Spatial Profiling of Individual Glomeruli From Patients With Anti-Neutrophil Cytoplasmic Autoantibody-Associated Glomerulonephritis

Lin Ye[1†], Yu Liu[1†], Xuejing Zhu[1], Tongyue Duan[1], Chang Wang[1], Xiao Fu[1], Panai Song[1], Shuguang Yuan[1], Hong Liu[1], Lin Sun[1], Fuyou Liu[1], Kyung Lee[2], John Cijiang He[2,3] and Anqun Chen[1]*

[1] Department of Nephrology, Hunan Key Laboratory of Kidney Disease and Blood Purification, Institute of Nephrology, The Second Xiangya Hospital at Central South University, Changsha, China, [2] Division of Nephrology, Department of Medicine, Icahn School of Medicine at Mount Sinai, New York, NY, United States, [3] Renal Program, James J. Peters Veterans Affairs Medical Center at Bronx, New York, NY, United States

We previously showed that the rupture of Bowman's capsule (BC) promotes the progression of crescentic glomerulonephritis by enhancing the entry of $CD8^+$ T cells into the glomeruli. In the present study, we utilized digital spatial profiling to simultaneously profile the altered abundances of the messenger RNA (mRNA) transcripts and proteins in the glomerular and periglomerular areas of four biopsy samples of anti-neutrophil cytoplasmic autoantibody-associated glomerulonephritis (ANCA-GN) and two biopsy specimens of minimal change disease (MCD) controls. The paraffin-embedded biopsy samples were stained with collagen IV, CD45, and SYTO 13 to distinguish the glomeruli with periglomerular infiltration but intact BC, with focal BC rupture, and with extensive rupture of BC and glomeruli without crescent formation and leukocytic infiltration in ANCA-GN. By assessing multiple discrete glomerular areas, we found that the transcript expression levels of the secreted phosphoprotein-1 and its receptor CD44 were upregulated significantly in the glomeruli with more severe ruptures of BC, and their expression levels correlated positively with the fibrotic markers. We also found that both alternative and classic complement pathways were activated in the glomeruli from patients with ANCA-GN. Furthermore, M1 macrophages were involved mostly in the early stage of BC rupture, while M2 macrophages were involved in the late stage and may contribute to the fibrosis process of the crescents. Finally, loss of glomerular cells in ANCA-GN was likely mediated by apoptosis. Our results show that digital spatial profiling allows the comparative analysis of the mRNA and protein profiles in individual glomeruli affected differently by the disease process and the identification of potential novel mechanisms in ANCA-GN.

Keywords: digital spatial profiling (DSP), anti-neutrophil cytoplasmic antibody (ANCA), glomerulonephritis, Bowman's capsule, complement, secreted phosphoprotein 1 (SPP1), CD44, fibrosis

OPEN ACCESS

Edited by:
Frederic Lagarrigue, UMR5089 Institut de Pharmacologie et de Biologie Structurale (IPBS), France

Reviewed by:
Björn Tampe, University Medical Center Göttingen, Germany
Kim Maree O'Sullivan, Monash University, Australia

****Correspondence:***
Anqun Chen
anqunchen@csu.edu.cn

†These authors have contributed equally to this work

Specialty section:
This article was submitted to Autoimmune and Autoinflammatory Disorders, a section of the journal Frontiers in Immunology

Received: *08 December 2021*
Accepted: *31 January 2022*
Published: *02 March 2022*

Citation:
Ye L, Liu Y, Zhu X, Duan T, Wang C, Fu X, Song P, Yuan S, Liu H, Sun L, Liu F, Lee K, He JC and Chen A (2022) Digital Spatial Profiling of Individual Glomeruli From Patients With Anti-Neutrophil Cytoplasmic Autoantibody-Associated Glomerulonephritis. Front. Immunol. 13:831253. doi: 10.3389/fimmu.2022.831253

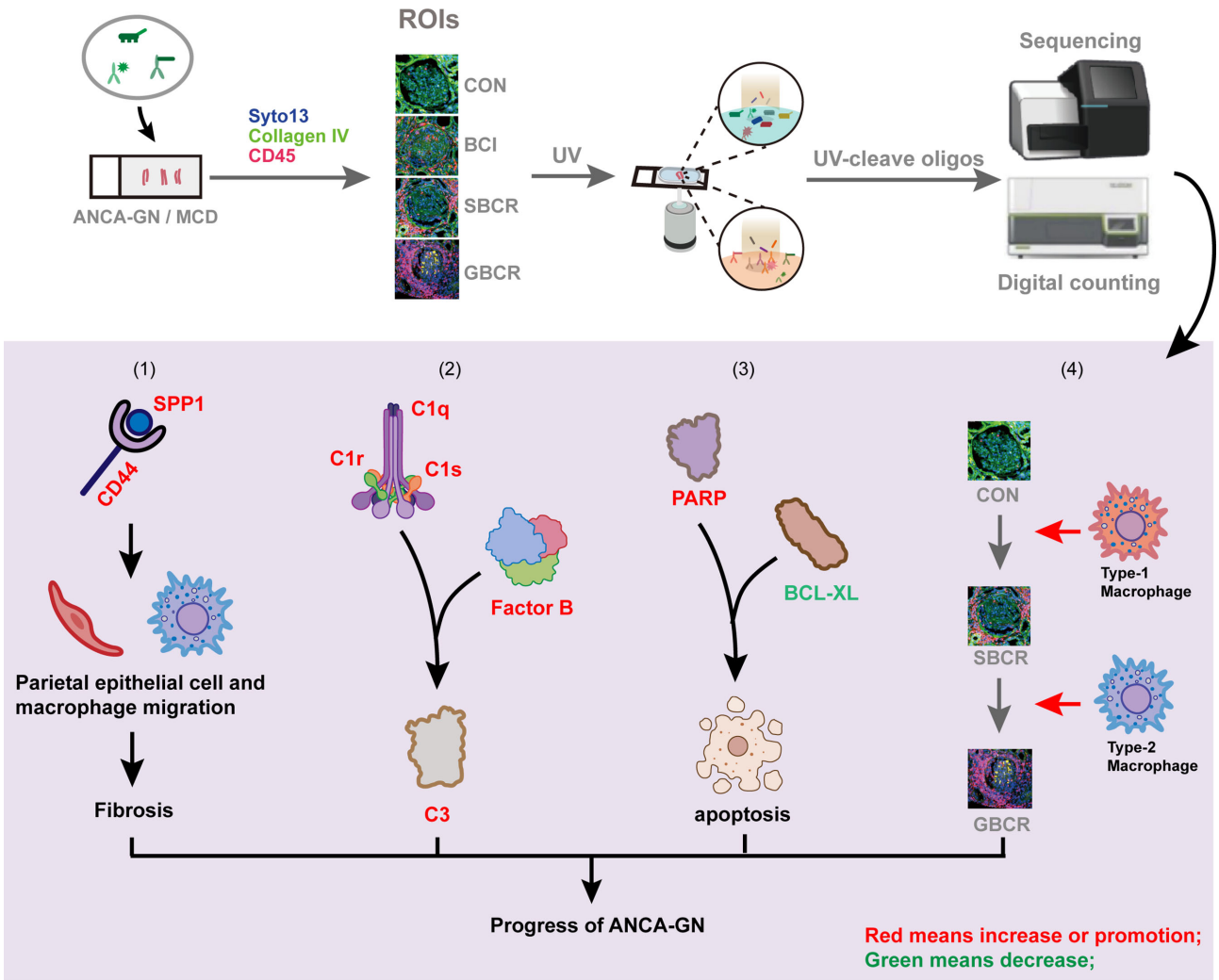

GRAPHICAL ABSTRACT |

INTRODUCTION

Anti-neutrophil cytoplasmic autoantibody-associated glomerulonephritis (ANCA-GN) is defined as a pauci-immune and necrotizing crescentic glomerulonephritis (GN) that is associated with the rapid loss of renal function and proteinuria, frequently progressing to end-stage kidney disease (1). The exact pathogenesis of this disease remains unclear. The glomerular injury in ANCA-GN involves the loss of podocytes, cells critical for maintaining glomerular architecture and function. Podocytes are located in a special environment that is separated from the outside tissues by the Bowman's capsule (BC) and separated from the capillary lumen by the glomerular basement membrane (2).

We have recently shown that the BC provides a protective barrier by preventing the influx of cytotoxic $CD8^+$ T cells into BC under normal physiological conditions (3). Even after the induction of mild nephrotoxic serum-induced nephritis, the $CD8^+$ T cells directed at the podocyte-specific epitope [enhanced green fluorescent protein (EGFP)-specific Jedi T cells] accumulated around the injured glomeruli in mice, with podocyte-specific EGFP expression together with other inflammatory cells, but were not found within the Bowman's space, provided that the BC was intact. However, in more severely damaged glomeruli with BC rupture, a massive influx of $CD8^+$ T cells was observed within the Bowman's space, with concomitant destruction of $EGFP^+$ podocytes and a catastrophic rapidly progressive GN (3). Indeed, recent studies have shown that BC rupture is associated with severe deterioration of kidney function, evidenced by the higher cumulative incidence of renal replacement therapy within 30 days after admission than in those without BC rupture (4). Consistently, BC rupture can be used as a risk marker to improve the outcome prediction for ANCA-GN (5).

Based on these novel findings and previous reports (6), we hypothesized an integrated "two-stage" model of crescentic GN

progression, where the initial insult to the glomerular capillaries in various forms of crescentic GN (first stage) results in podocyte injury through injured glomerular endothelial cell–podocyte crosstalk and/or through infiltrating leukocytes, leading to proteinuria. The release of neoepitopes from damaged podocytes (second stage) results in the activation of dendritic cells and in the subsequent activation and proliferation of $CD4^+$ and $CD8^+$ T cells specific for these epitopes. At the early stage when BC is intact, $CD8^+$ T cells and other immune cells, activated by cytokines and chemokines released by the injured glomeruli, migrate and accumulate near and around the glomerulus. As the disease progresses, activated parietal epithelial cells and infiltrated periglomerular immune cells may secrete proteases causing BC rupture, allowing the entry of inflammatory immune cells, including $CD8^+$ T cells, into the Bowman's space to destroy the neoepitope-carrying podocytes and further damage the glomeruli (7).

To assess the difference between glomeruli with or without BC rupture, we used digital spatial profiling (DSP), a novel technology capable of medium- to high-plex spatial profiling of proteins and RNAs in formalin-fixed paraffin-embedded (FFPE) section samples (8). One of the advantages of DSP compared to other spatial transcriptome technologies is its ability to sectionalize specific regions of interest (ROIs) with high magnification, defined by the researchers, using multiple fluorescence labeling, thereby enabling the analysis of multiple proteins and RNAs (9). Using this novel method, we performed a "pilot study" with kidney sections from four patients with ANCA-GN and two minimal change disease (MCD) controls. We especially selected the areas with or without BC rupture accompanied by periglomerular infiltration in the kidneys of ANCA-GN patients in order to profile the expressions of the RNAs and proteins specifically in these areas.

A comparison of the expression profiles of the glomeruli affected differently by the disease process provided new insights into the mechanisms of ANCA-GN progression.

RESULTS

Digital Spatial Profiling of Peri-Glomerular and Intra-Glomerular Areas of Renal Biopsy Samples With ANCA-GN

To explore the mechanisms of BC rupture on the progression of ANCA-GN, the GeoMx® Digital Spatial Profiler was used to quantitate the expressions of specific panels of genes and proteins in the spatially defined regions. Together with the fluorescent-labeled antibodies, ultraviolet (UV)-photocleavable oligos (DSP barcodes) linked with target complementary sequences (RNA) or target antibodies (protein) were co-incubated. After the ROIs were selected, the specific regions were lit up with UV. Subsequently, the DSP barcodes were collected and amplified for further Illumina sequencing (RNA) or linked with a fluorescent label reporter for further counting with the NanoString counter machine (protein) (**Figure 1A** and **Supplementary Figure S1**).

The continuity of collagen IV-positive staining represented the integrity of the BC, CD45-positive staining showed the infiltration of immune cells, while SYTO 13 staining was used to label the cell nuclei. The glomeruli were selected evenly from two renal biopsies with MCD (n = 12). The following groups were included for transcription profiling: four ANCA-GN renal biopsies with normal appearance [control (CON), n = 4], periglomerular infiltration but with intact BC (BCI, n = 7), segmental BC rupture (SBCR, n = 11), and global BC rupture (GBCR, n = 13) (**Figure 1B**). For the protein assay, because the panel of proteins mainly focused on immune-related cells and the two renal samples from patients with MCD were patched with a renal sample from the fourth patient with ANCA, we only selected the renal samples from three other ANCA patients for protein analysis owing to cost considerations. Glomeruli with the characteristics of CON (n = 6), BCI (n = 7), SBCR (n = 5), and GBCR (n = 7) were selected from three ANCA-GN renal biopsies and were included in the protein assay after passing quality control (**Figure 1B**).

For some analyses, the CON and BCI groups were combined into WBCR (without BC rupture) and the SBCR and GBCR groups combined into BCR (BC rupture). Representative pictures are shown in **Figure 1C**. The demographic and clinical features of each patient are displayed in **Supplementary Table S1**, and detailed information on the histopathology scoring of the ANCA-GN patients is shown in **Supplementary Table S2**.

For the RNA DSP assay, the probes specific for 1,833 genes are listed in detail in **Supplementary Table S2**. The geometric mean of the housekeeping genes was calculated logarithmically (log2), and the histogram of the mean per ROI is displayed in **Supplementary Figure S2A**. The surface area and nuclei counts of all ROIs passed quality control (**Supplementary Figure S2B**). The housekeeping gene *TMUB2* correlated well with the other housekeeping genes such as *ARMH3* and *TLK2* (**Supplementary Figure S2C**). Normalization with a housekeeper and the Q3 method matched very well (**Supplementary Figure S2D**); therefore, the Q3 method was used for normalization, as recommended. The count distributions of the genes and negative controls after normalization from each ROI are displayed in **Figure 1D**.

For the protein DSP assay, the probes targeting 45 proteins are provided in detail in **Supplementary Table S3**. The geometric mean of the housekeeping proteins was calculated logarithmically (log2), and the histogram of the mean per ROI is displayed in **Supplementary Figure S3A**. The surface area and nuclei counts of all ROIs passed quality control (**Supplementary Figure S3B**). The ratio of the count value of each target in each ROI to the count value of immunoglobulin G (IgG) was calculated logarithmically (log2), and the proteins with log values <0 (labeled blue), including CD80, FOXP3, CD66b, PD-L1, PD-L2, and CD95/Fas, were excluded from further analysis (**Supplementary Figure S3C**). Housekeeping proteins were used to normalize the raw protein counts (**Supplementary Figure S3D**). The count distribution of the proteins after normalization from each ROI are shown in **Figure 1E**.

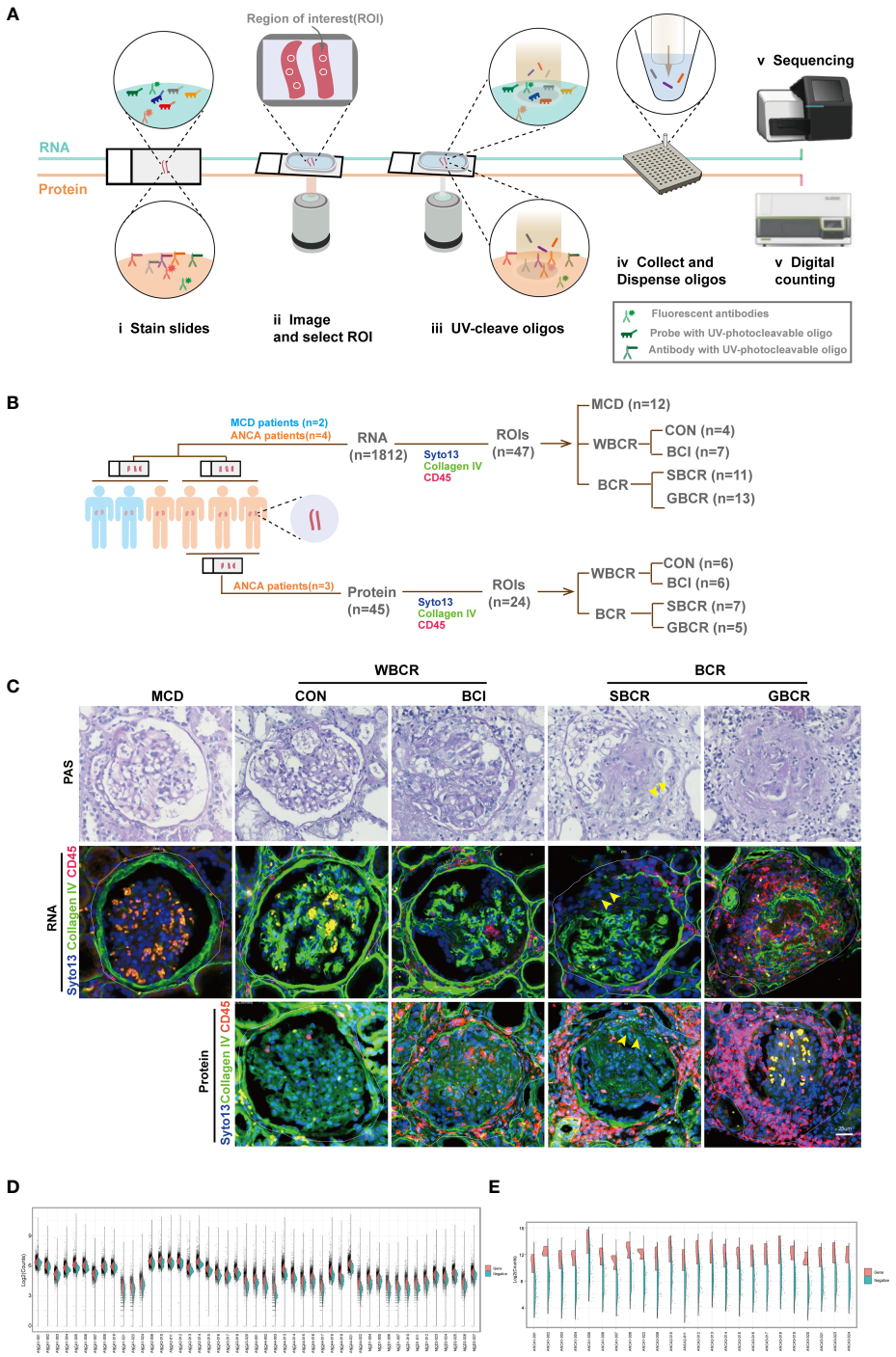

FIGURE 1 | Digital spatial profiling of renal biopsies from patients with ANCA-GN and MCD. **(A)** Schematic overview of the DSP workflow. **(B)** Information on the glomeruli included in this analysis. Four patients with ANCA-GN and two patients with MCD were enrolled. The region of interest (ROI) was selected evenly from patients according to the immunofluorescence staining with collagen IV, CD45, and SYTO 13. For the RNA profiles, the glomeruli from MCD (n = 12), from ANCA-GN with crescent formation but intact BC (BCI, n = 7), with segmental BC rupture (SBCR, n = 11), with global BC rupture (GBCR, n = 13), and without crescent formation and leukocyte infiltration (CON, n = 4) were included for analysis. For the protein profiles, glomeruli with the characteristics of CON (n = 6), BCI (n = 7), SBCR (n = 5), and BCR (n = 7) were included for further analysis. **(C)** Representative images from each group. *Scale bar*, 25 μm. **(D)** Split violin plot of the RNA counts by ROIs. Gene counts are shown on the *left* (*orange*) and the negative probe counts are displayed on the *right* (*green*). **(E)** Split violin plot of the protein counts by ROIs. *ANCA-GN*, anti-neutrophil cytoplasmic autoantibody-associated glomerulonephritis; *MCD*, minimal change disease; *DSP*, digital spatial profiling; *WBCR*, without Bowman's capsule rupture; *BCR*, Bowman's capsule rupture; *BC*, Bowman's capsule.

Involvement of the Classic Complement Pathway in the Pathogenesis of ANCA-GN

The heatmap of the normalized counts of each ROI is displayed in **Figure 2A**. The genes of cluster 6 were highlighted in the red box, the pathway enrichment analysis of which is provided in **Figure 2B**. The neutrophil degranulation and complement-related pathways, including initial triggering of complement, regulation of complement cascade, and complement cascade, were significantly enriched (**Figure 2B**). The genes related to neutrophil degranulation and complement-related pathways are listed separately in **Figure 2C**, with the majority of genes involved in neutrophil degranulation found to be upregulated. The genes involved in the complement pathway are displayed separately in **Figures 2D–F**. There was no significant difference with regard to the genes involved in the lectin pathway, including mannose-binding lectin 2 (*MBL2*), MBL-associated serine protease 1 (*MASP1*), and MBL-associated serine protease 2 (*MASP2*) (**Figure 2D**). Complement factor B (CFB) increased significantly with the rupture of BC, but the other genes involved in the alternative complement pathway, including complement factor D (*CFD*), complement factor properdin (*CFP*), and granzyme M (*GZMM*), showed no difference (**Figure 2E**). Notably, most of the genes involved in the classic complement pathway were remarkably elevated in the group with BC rupture compared with the MCD group. These genes included complement C1q A chain (*C1QA*), complement C1q B chain (*C1QB*), complement C1r (*C1R*), complement C1s (*C1S*), complement C4b (*C4B*), and complement C3 (**Figure 2F**). Especially, the expression levels of *C1R* and *C1S* markedly increased in the glomeruli from ANCA-GN patients even without rupture of the BC compared with the MCD group. These results showed that the classic complement pathway is likely activated in ANCA-GN.

SPP1 Signaling Contributes to the Fibrosis Pathway in ANCA-GN

Among the 1,812 genes detected, secreted phosphoprotein 1 (*SPP1*), also named osteopontin (OPN), was remarkably increased in the WBCR and BCR groups compared to the MCD group. Its transcription level notably increased in the BCR group compared to that in the WBCR group, indicating its pathologic role in the progression of ANCA-GN (**Figure 3A**). CD44 functioned as the receptor of SPP1 (10), which showed a similar expression pattern to *SPP1* (**Figure 3B**), and their expressions showed a strong positive correlation (r = 0.7875, p < 0.0001) (**Figure 3C**). *SPP1* is considered a major driver for renal fibrosis (11), the secretion of which is stimulated by inflammatory cytokines (12) and the suppression of which could alleviate kidney fibrosis (13). In our study, the expressions of fibronectin and Col1A1 were gradually elevated in the WBCR and BCR groups compared to those in MCD (**Figures 3E, F**). Their expressions were strongly positively correlated with SPP1 (r = 0.85, p < 0.0001; r = 0.7517, p < 0.0001, respectively) (**Figures 3G, H**). Consistently, SPP1 was also moderately positively correlated with TGF-b1, a master regulator of fibrosis (r = 0.5556, p < 0.0001) (**Figure 3D**).

The above results highlighted the critical role of *SPP1* in glomerulosclerosis and possibly in fibrous crescent formation. Moreover, *SPP1* is known to mediate M2-type macrophage polarization (14), which also plays a role in fibrosis (15, 16). Our data showed that the expression of CD163 gradually increased with worsening of the glomerular injury (**Figure 3I**), and SPP1, together with its receptor CD44, strongly correlated with CD163 (an M2-type macrophage marker; r = 0.8328, p < 0.0001; r = 0.7231, p < 0.0001, respectively) (**Figures 3J, L**), but not with CD86 expression (an M1-type macrophage marker; r = 0.1856, p = 0.2121) (**Figure 3K**).

Protein Profiling Reveals That Apoptosis Is the Main Pathway Responsible for Glomerular Cell Injury in ANCA-GN

To confirm the finding in the DSP RNA profile, the immune-related proteins were detected in ANCA-GN applying DSP protein analysis. Forty-five proteins, including three housekeeping proteins, were detected together with three negative controls. Their expression heatmap is displayed in **Figure 4A**. Genes such as *CD44*, *CD68*, *CD11C*, *CD34*, and *FAP* exhibited strong correlations at the RNA and protein levels, whereas *BAD*, *FOXP3*, *BCLXL*, and *B2M* exhibited weak correlations (**Figure 4B**). CD34, an endothelial cell marker, was remarkably decreased in the BCI, SBCR, and GBCR groups compared with the CON group. Their expression levels also showed a gradual decrease with more severe rupture of the BC and worsening of the glomerular injury (**Figure 4C**). Furthermore, the CD34 protein level was strongly negatively correlated with CD45 (r = −0.7840, p < 0.0001), suggesting a close relationship between leukocyte infiltration and endothelium injury in ANCA-GN (**Figure 4D**). Consistently, vascular endothelial growth factor A (VEGFA), produced by podocytes, also decreased progressively with worsening of glomerular injury (**Figure 4E**). In addition, the expression of BCL-XL, an anti-apoptotic protein, was decreased significantly in the BCI, SBCR, and GBCR groups compared with that in the CON group (**Figure 4F**). The expression of PARP, a protein involved in programmed cell death, was significantly increased in the BCI, SBCR, and GBCR groups compared with that in the CON group (**Figure 4F**). CD34 is a cell surface transmembrane protein that is often shed from endothelial cells when they are injured. To determine whether apoptosis contributes to the injury of endothelial cells, we performed immunofluorescence co-staining of caspase-3 and CD34. As shown in **Figure 4G**, caspase-3 staining was co-localized with CD34. These results imply that apoptosis might be responsible for glomerular cell injury in ANCA-GN.

DSP Identified That the Types of Immune Cell Infiltration Were Different During BC Rupture

We investigated what cell types might be responsible for BC rupture. The 16 categories of immune cells generated from the

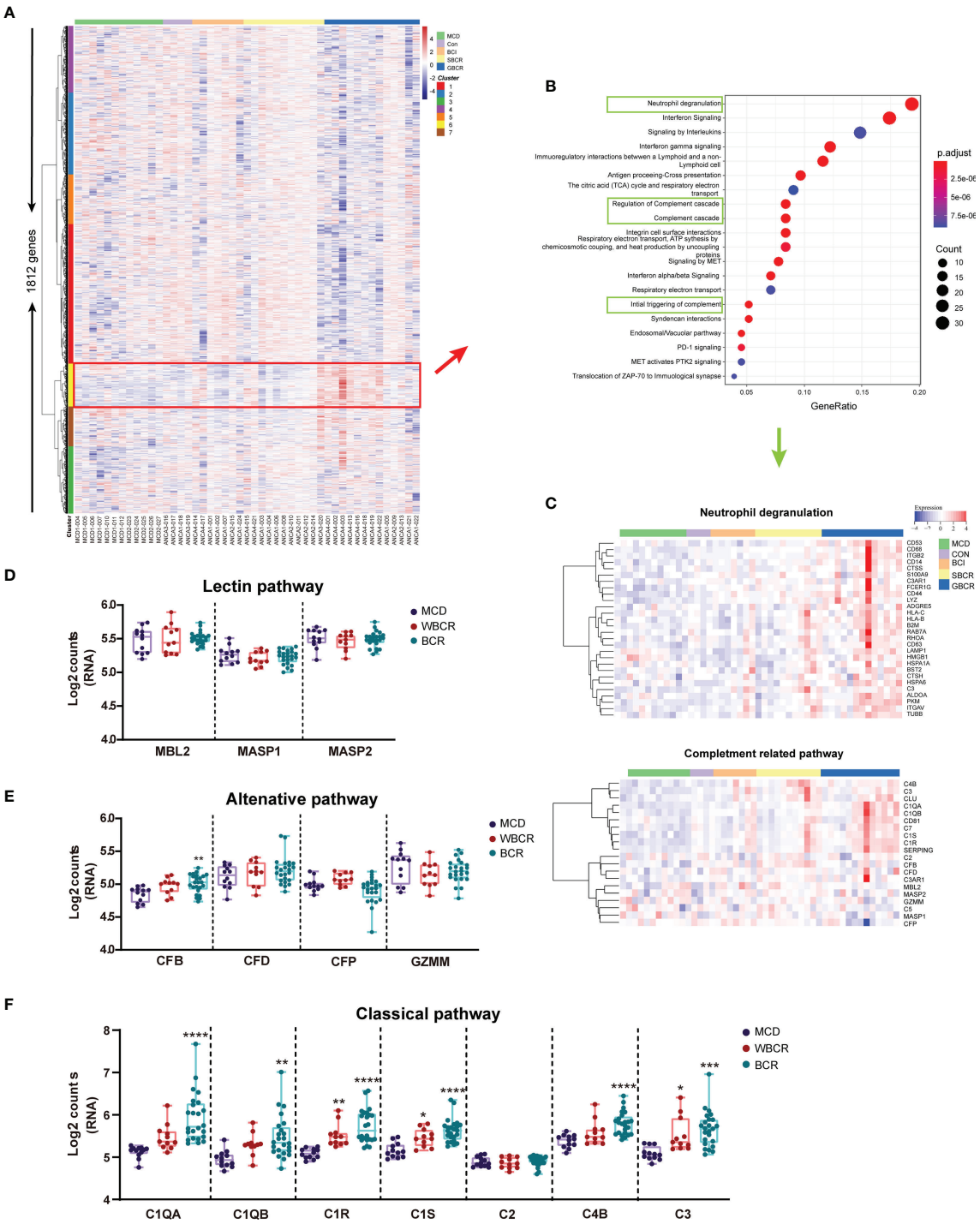

FIGURE 2 | The classic complement pathway is involved in the pathogenesis of anti-neutrophil cytoplasmic autoantibody-associated glomerulonephritis (ANCA-GN). **(A)** Heatmap of the 1,813 detected genes. Cluster analysis indicated seven main clusters marked in *different colors* (*left*). **(B)** Pathway enrichment analysis of cluster 6 [*red box* in **(A)**]. **(C)** Neutrophil degranulation and complement-related pathways are highlighted in *green box*, and the heatmap of related genes is displayed separately. **(D)** RNA expression of the complement pathway of lectin-related genes. **(E)** RNA expression of the alternative complement pathway-related genes. **(F)** RNA expression of the classic complement pathway-related genes. All data were analyzed by one-way analysis of variance (ANOVA). Compared with the minimal change disease (MCD) group: $^{*}p < 0.05$, $^{**}p < 0.01$, $^{***}p < 0.001$, and $^{****}p < 0.0001$.

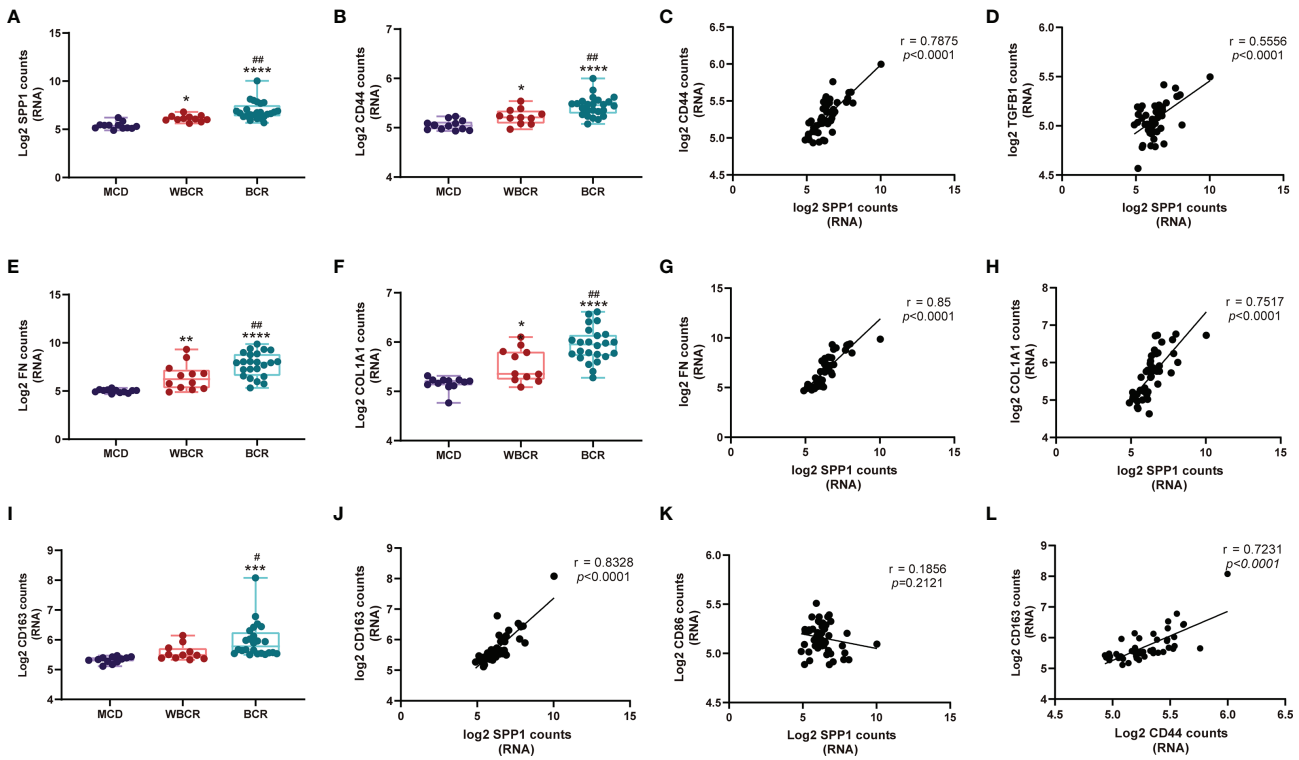

FIGURE 3 | SPP1 signaling contributes to the fibrosis pathway in anti-neutrophil cytoplasmic autoantibody-associated glomerulonephritis (ANCA-GN). **(A, B, E, F, I)** RNA expression of *SPP1*, *CD44*, *COL1A1*, *FN*, and *CD163* with worsening of glomerular injury. **(C, D, G, H, J, K)** Correlation of the RNA expressions between *SPP1* and *CD44*, *TGF-β1*, *COL1A1*, *FN*, *CD163*, and *CD86*. **(L)** Correlation of the RNA expressions between *CD44* and *CD163*. All data were analyzed by one-way analysis of variance (ANOVA). Compared with the MCD (minimal change disease) group: $^{*}p < 0.05$, $^{**}p < 0.01$, $^{***}p < 0.001$, and $^{****}p < 0.0001$. Compared with the WBCR (without Bowman's capsule rupture) group: $^{\#}p < 0.05$ and $^{\#\#}p < 0.01$. *SPP1*, secreted phosphoprotein 1; *COL1A1*, collagen type I alpha 1 chain; *FN*, fibronectin 1.

transcription profiles of ROIs selected from ANCA-GN renal samples are displayed in **Figure 5A**, which showed more immune cell infiltration in the groups with BC rupture. The highest number of immune cells was observed in the GBCR group. When the data were rearranged into a bar chart, we found that the infiltration of memory $CD4^+$ T cells, naive $CD8^+$ T cells, memory $CD8^+$ T cells, naive B cells, memory B cells, and macrophages increased, whereas the infiltration of naive $CD4^+$ T cells decreased with more BC rupture and worse glomerular injury (**Figure 5B**). The protein profiles further confirmed the findings in the RNA analysis, which showed that CD8 and CD68 might be involved in the early development of BC rupture, whereas CD20 and CD4 might be involved in the late stage of progression (**Figure 5C**). When we classified CD68 macrophages into subgroups of M1 macrophages (CD11c) and M2 macrophages (CD163), the protein profiles indicated that M1 macrophages were involved mostly in the early stage of BC rupture, while M2 macrophages were involved in the late stage (**Figure 5C**). These findings were further confirmed by immunofluorescence staining with inducible nitric oxide synthase (iNOS) (another M1 macrophage marker) and CD206 (another M2 macrophage marker) (**Figure 5D**).

DISCUSSION

The renal damage secondary to ANCA-associated vasculitis appeared heterogeneous, and individual glomeruli showed different extents of injury, including crescent formation, infiltration of immune cells, and rupture of BC. In the same kidney, some glomeruli appeared quite normal, some glomeruli showed crescent formation but with intact BC, some glomeruli had focal BC rupture, and some glomeruli had extensive BC rupture with massive infiltration of immune cells. As we previously demonstrated, the BC can protect podocytes from damage, and its rupture promotes more infiltration of immune cells into the glomeruli, leading to more podocyte loss and rapid progression of GN (3). To understand the mechanisms of injury in these individual glomeruli with different degrees of injury, we profiled the transcriptomics and proteomics in different areas of ANCA-GN kidney by selecting those individual glomeruli with different degrees of BC rupture in FFPE samples using the DSP method. This study helped us to identify the underlying pathogenesis mediating the progression of ANCA-GN.

Although ANCA-GN was previously considered a pauci-immune necrotizing crescentic GN, accumulating evidence has

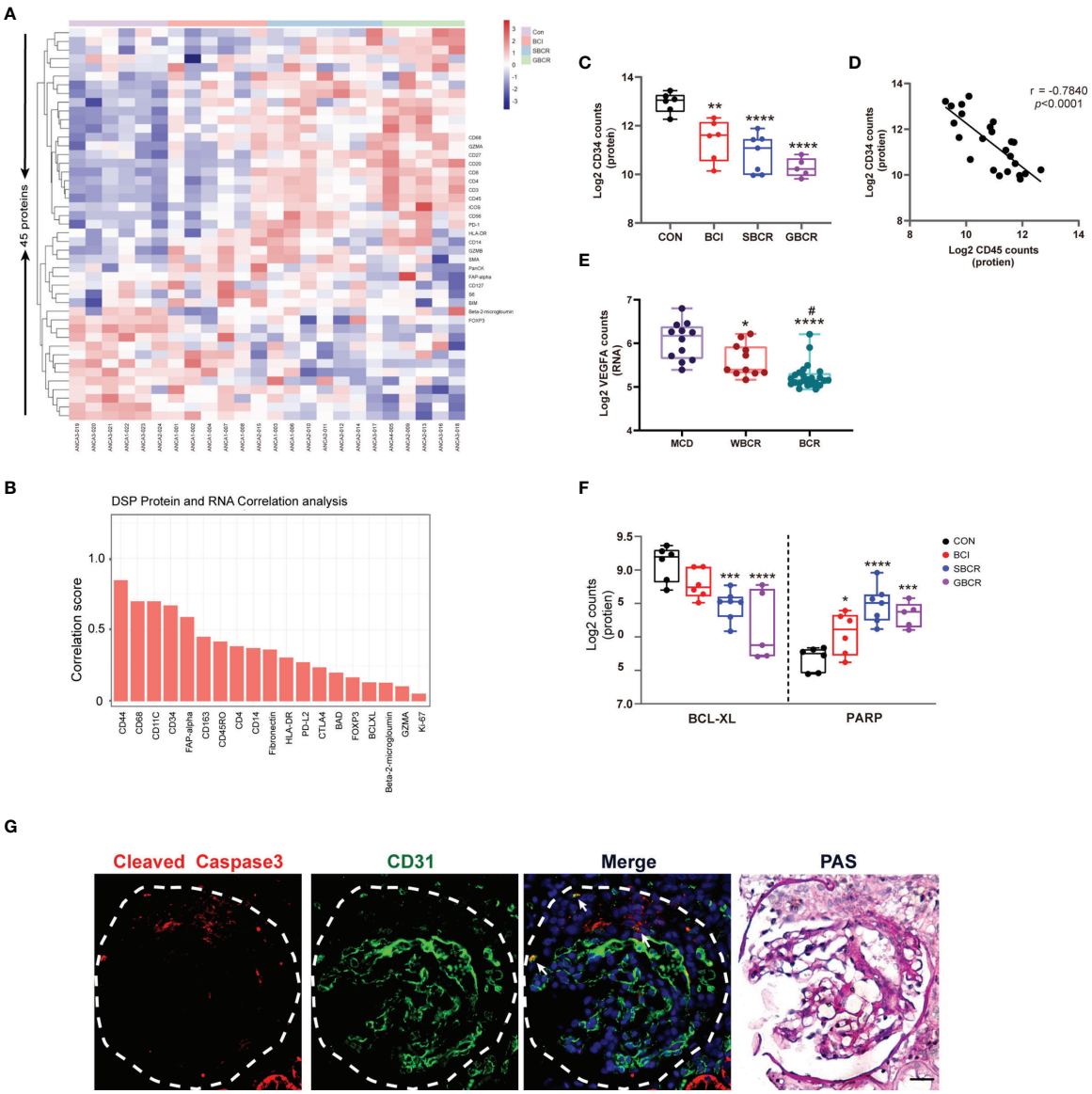

FIGURE 4 | Protein profiles indicating that apoptosis might be the main pathway responsible for the glomerular cell injury in anti-neutrophil cytoplasmic autoantibody-associated glomerulonephritis (ANCA-GN). **(A)** Heatmap of 45 detected proteins. **(B)** Correlation analysis of common proteins and RNAs of individual targets generated from digital spatial profiling (DSP) based on all regions of interest (ROIs). **(C)** Protein expression of CD34 with worsening of the glomerular injury. **(D)** Protein expression correlation of CD34 and CD45. **(E)** Transcription expression of VEGFA with worsening of the glomerular injury. **(F)** Protein expressions of BCL-XL and PARP. **(G)** Immunofluorescence co-staining of caspase-3 and CD31 in serial renal biopsy specimens of patients with ANCA-GN. *Scale bar*, 25 μm. The image of collagen IV staining was from the serial kidney section for protein DSP. PAS staining was performed on the same slide after co-staining with caspase-3 and CD31. Compared with the CON (control) group: $^{*}p < 0.05$, $^{**}p < 0.01$, $^{***}p < 0.001$, and $^{****}p < 0.0001$. Compared with the WBCR (without Bowman's capsule rupture) group: $^{\#}p < 0.05$. *VEGFA*, vascular endothelial growth factor A; *BCL-XL*, B-cell lymphoma—extra large; *PARP*: poly(ADP-ribose) polymerase; *PAS*, periodic acid–Schiff.

shown that immune complex and complement deposition were present in the glomeruli of patients with ANCA-GN, which was associated with more severe proteinuria, higher percentages of crescents, and poorer renal function (1). Local complement dysregulation was identified as an essential component of crescent formation and disease progression (17). A recent study has shown that the C5a receptor inhibitor had renal protective effects in these patients (18). Consistent with this, our study suggests that multiple complement-related pathways, such as initial triggering of complement, regulation of complement cascade, and complement cascade, were enriched in the glomeruli from ANCA-GN.

Previous data reported that a greater degree of neutrophil degranulation could result in a more abundant local complement

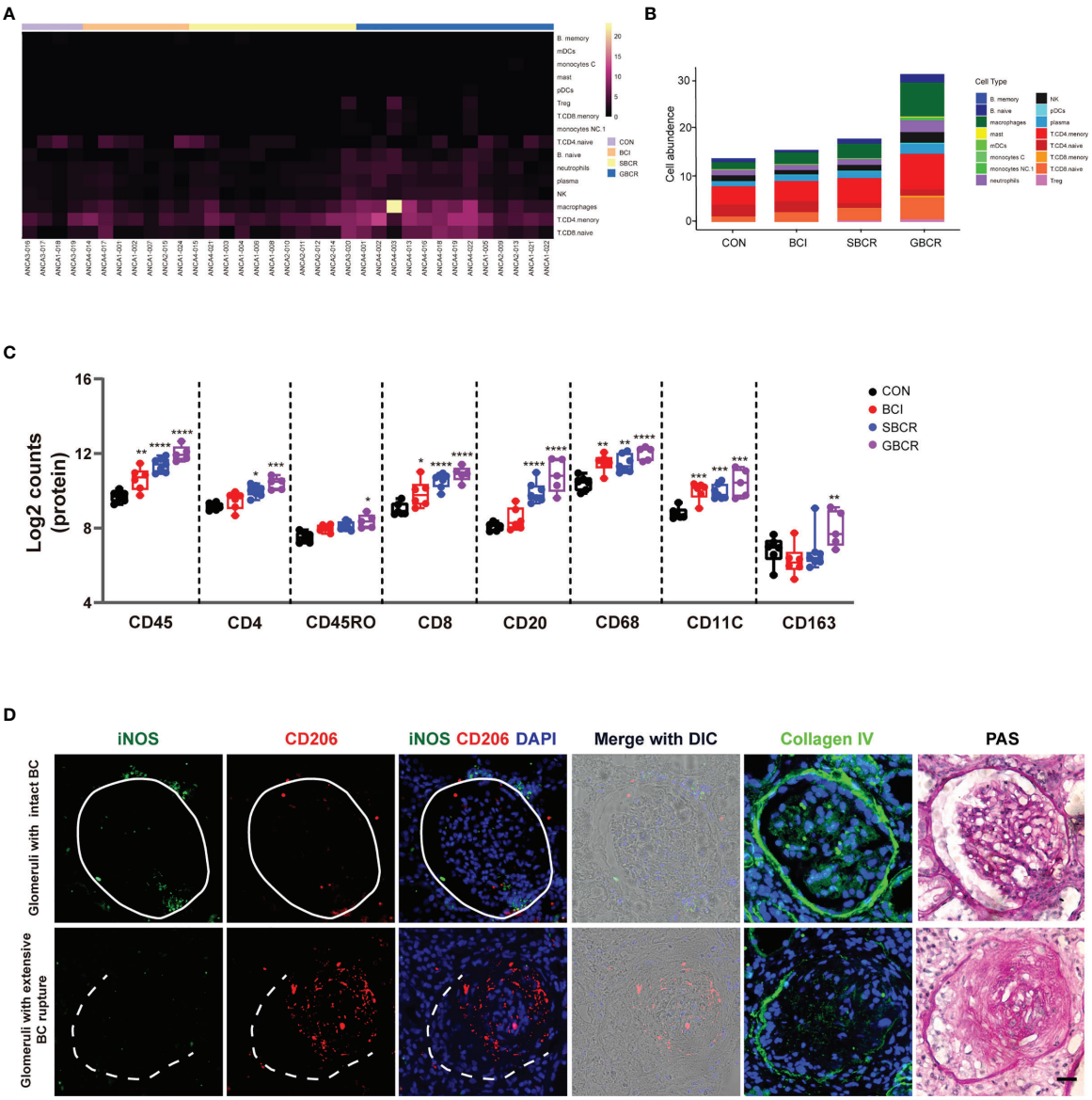

FIGURE 5 | Different types of immune cell infiltration during rupture of the Bowman's capsule. **(A)** Heatmap of the cell abundance of immune cell infiltration based on the regions of interest (ROIs) selected from anti-neutrophil cytoplasmic autoantibody-associated glomerulonephritis (ANCA-GN) patients. **(B)** Average cell abundance of each category of immune cells in different groups. **(C)** Protein expressions of immune cell markers, including CD45, CD4, CD45RO, CD8, CD20, CD68, CD11C, and CD163. **(D)** Immunofluorescence co-staining of iNOS and CD206 in serial renal biopsy specimens of patients with ANCA-GN. *Scale bar*, 25 μm. Intact Bowman's capsule is indicated by *solid circle*, while extensive Bowman's capsule rupture is indicated by the *dotted line*. The image of collagen IV staining from the serial section for protein digital spatial profiling (DSP) indicated the integrity of the Bowman's capsule. Periodic acid–Schiff (PAS) staining was performed on the same slide after co-staining with iNOS and CD206. Compared with the CON (control) group: $^{*}p < 0.05$, $^{**}p < 0.01$, $^{***}p < 0.001$, and $^{****}p < 0.0001$.

activation and account for the more severe renal damage in patients with ANCA-GN (19). Consistent with this, our study showed that, with worsening of the glomerular injury, the neutrophil degranulation pathway was significantly upregulated together with complement activation. The alternative complement pathway was thought to be critical in the pathogenesis of ANCA-GN for several reasons: 1) depletion of factor B, critical for the alternative complement pathway, could protect mice from this disease (20); 2) the membrane attack complex (MAC), C3d, factor B, and factor P were detected in renal biopsy samples with pauci-immune myeloperoxidase (MPO)-ANCA-GN (21); and 3) both the renal staining and

the urinary and plasma levels of the proteins involved in the alternative complement pathway were significantly upregulated in ANCA-GN (20).

The common path of the classical and alternative complement pathways is the conversion of C3 to its active forms, C3a and C3b, the latter forming C5 convertase and subsequently converting C5 to C5a and C5b (1). C5a could recruit inflammatory cells such as neutrophils, monocytes, and T cells to the activation site, whereas C5b forms the MAC (1). In our experiment, we found that the RNA expression levels of C3 and CFB, together with C1QA, C1QB, and C1R, increased progressively with worsening of glomerular injury and more severe rupture of the BC, indicating that the classic complement pathway is also involved in the progression of glomerular injury in ANCA-GN. This was supported by the previous observation from others showing that C4d was found positive in the kidney in 70.8% of 187 renal biopsies in patients with ANCA-associated vasculitis (22). Previous studies suggested that activation of the complement was different between ANCA-positive and ANCA-negative GN (19). The study showed larger proportions of C3, C9, complement factor H-related protein 1, C4, C5, and immunoglobulins in ANCA-negative GN than in ANCA-positive GN. Previous studies were mostly obtained from immunofluorescence staining or mass spectrometry analysis of whole kidney biopsies, not considering the heterogeneous lesion of the individual glomeruli, which could mask the contribution of the classical complement pathway in disease progression. The reason for the activation of the classical complement pathway without visible electron-dense deposition might be the rapid degradation of local immune complexes in ANCA-GN (22).

SPP1, also named OPN, is a secreted protein mainly expressed in bone and epithelial tissues (10). It is present in healthy kidneys and other cell types, including activated T cells and macrophages, among others, and its expression is upregulated in the diseased condition (10). In crescentric GN, the mRNA and protein expressions of SPP1 were markedly upregulated (10). CD44 functions as the receptor of SPP1 (23), which is expressed on activated parietal epithelial cells (PECs) (24). The RNA expression level of SPP1 showed a strong positive correlation with that of CD44, and CD44 was identified to be regulated by phosphorylated extracellular signal-related kinase (pERK). CD44 upregulation was accompanied by a notably increased expression of collagen IV and the migration of parietal epithelial cells (25). Additionally, SPP1 is considered an epithelial–mesenchymal transition hallmark marker (15). Consistent with this, our data showed that the expression of SPP1 increased progressively with worsening of glomerular injury and was correlated with the expressions of fibronectin and collagen. Collectively, these findings suggest that SPP1 may promote the development of fibrous crescent by binding to CD44, thereby playing a pivotal role in the progression of ANCA-GN. Therefore, treatment specifically targeting the SPP1–CD44 axis can be considered for patients with ANCA-GN.

Our previous study showed that, with the rupture of BC, large proportions of CD8 and CD68 infiltrate the capillary loop (3). In this study, we found that CD8 and CD68 might be involved in the early development of BC rupture, whereas CD20 and CD4 might be involved during the late stage of progression. CD68 is widely accepted as a pan-macrophage marker, CD86 is known as a specific marker for M1 macrophages, and CD163 is considered as a marker for M2 macrophages (26). These data indicate that M1 macrophages might play a role in BC rupture, whereas M2 macrophages increase at the late stage of the disease, which might contribute to fibrosis. In addition, we found that the RNA and protein expression levels of CD163 increased significantly when the BC ruptured, together with the increased expression of SPP1, which was reported to be significantly correlated with macrophage infiltration and M2 polarization (15). It was previously reported that both the high expression of SPP1 and that of its receptor CD44 correlated with an increased macrophagic infiltration (27). Together, our data suggest that early M1 macrophage infiltration may be involved in the rupture of BC and that SPP1-mediated M2 macrophage polarization may contribute to glomerulosclerosis and crescent fibrosis.

Our previous data showed that, upon BC rupture, a greater number of podocytes were lost (3). Our present study shows that with the progression of the disease, the apoptotic marker PARP was markedly increased, whereas the anti-apoptosis protein BCL-XL decreased significantly, which may be due to the increased podocyte apoptosis. In addition, the expression of VEGFA notably decreased with the progression of individual glomeruli, consistent with podocyte loss. CD34, a marker of endothelial cells, decreased drastically with worsening of the glomerular lesion, indicating the loss or injury of the glomerular endothelial cells in ANCA-GN. Interestingly, the protein expression level of CD34 showed a negative correlation with that of CD45, a marker of leukocytes, indicating that endothelial cell injury is tightly associated with the infiltration of immune cells in the glomeruli. Taken together, these data imply that apoptosis might be one of the mechanisms responsible for the loss of podocytes and glomerular endothelial cells in ANCA-GN, which is consistent with a previous study indicating that apoptotic regulation is important in the development of pathologic glomerular sclerosis in crescentic GN (3, 28).

This study had some limitations. Firstly, the sample size was not large enough due to cost limitations and therefore may not detect all the variations in patients with ANCA-GN. Secondly, the RNA target panel included only 1,833 genes and the protein analysis included only 45 proteins. Wider and deeper gene/protein panels will provide more comprehensive information. Thirdly, the preliminary results needed to be validated by other methods. Therefore, the mechanism underlying the results needs to be investigated further.

In conclusion, our study applied novel special transcriptomic and proteomic technology to profile the gene and protein expressions in individual glomeruli with different degrees of BC rupture. Our study demonstrated that both classic and alternative complement pathways are involved in the progression of ANCA-GN, that the SPP1–CD44 axis plays a dominant role in the development of fibrous crescent, and that apoptosis might be the important mechanism leading to the loss of glomerular cells in ANCA-GN.

MATERIALS AND METHODS

Study Population and Ethical Approval

FFPE tissues were obtained from patients who underwent renal biopsy and were diagnosed with ANCA-GN (n = 4) and MCD (n = 2) from July 2020 to July 2021. Patients' clinical information is provided in **Supplementary Table S1**. This study was approved by the Ethics Committee of the Second Xiangya Hospital of Central South University (approval no. 2021-072). Written informed consent for tissue use in research was obtained at the Second Xiangya Hospital of Central South University. The renal biopsy sections measuring 5 μm in thickness from three patients with ANCA-GN were patched into one DSP slide, and those from other patients with ANCA-GN together with those from two patients with MCD were patched into another DSP slide. The histopathology scores generated specifically from the serial kidney sections for the DSP profiles were evaluated independently by two pathologists according to previous literature (29). Differences in the scoring between the two pathologists were resolved by reviewing the biopsies to reach a consensus.

General Description of DSP

DSP was performed according to the literature (8, 9, 30). Briefly, DSP barcodes containing UV-photocleavable oligos comprising collagen IV (a marker for BC integrity), CD45 (a marker for immune cells), and SYTO 13 (nuclei) to allow for the morphological outline of interesting areas were used synchronously. The DSP slides were stained with immunofluorescent antibodies to identify the glomerulus and the BC, followed by high-resolution scanning (×20 objective lens) using the DSP instrument to allow ultimate precise selection for ROIs. Different shapes of regions, such as geometric, segment, contour, gridded, and any polygon shapes, were accepted for ROI selection. The DSP barcodes of RNAs linked with UV-photocleavable oligos targeted the complementary sequences of specific mRNAs. Similarly, the DSP barcodes of proteins linked with UV-photocleavable oligos targeted specific proteins (antigens). The barcodes were released by UV light shed on the selected ROIs in the micro-sized programmable digital micromirror device (DMD; NanoString Technologies, Inc. Seattle, WA, USA), which were collected subsequently into a 96-well plate. Each barcode had its own unique sequence to distinguish from one another. The DSP barcodes collected from the RNA assay procedure were amplified by PCR, and subsequent sequencing was performed using the Illumina sequencing platform. Concurrently, the DSP barcodes generated from the protein probes were collected and hybridized with fluorescent label reporters for further fluorescence counting (proteins).

DSP of RNA

Sections were deparaffinized in sequential xylene and rehydrated in graded ethanol. Target retrieval was performed in a water bath with 1 M Tris-EDTA buffer (pH 9.0) for 15 min. The FFPE samples were stained with a primary mouse CD45 antibody (13917; Cell Signaling Technology, Danvers, MA, USA) and subsequently with the Alexa Fluor 594 secondary mouse antibody (A-11012; Thermo Scientific, Waltham, MA, USA), Alexa Fluor 555-labeled collagen IV antibody, and the DNA stain SYTO 13 (GMX-PRO-MORPH-HST-12; NanoString Technologies Inc.) to identify the tissue morphology. The Alexa Fluor 555-labeled collagen IV antibody was covalently labeled using the collagen IV antibody (ab6586; Abcam, Cambridge, UK) with Alexa Fluor 555 Conjugation Kit—Lightning-Link (ab269820; Abcam) according to the protocol, and the resulting final concentration was 0.5 mg/ml. The slides were incubated with the aforementioned fluorescent antibodies in addition to the RNA probe sets (1,833 genes with 8,659 pairs of probes, provided with detail in **Supplementary Table S2**), which is similar to conventional immunofluorescence or immunohistochemistry (IHC). Stained slides were scanned with the GeoMx™ Digital Spatial Profiler (NanoString Technologies, Inc.). The ROIs were selected according to the integrity of the BC outlined by collagen IV staining, the leukocyte infiltration marked by CD45 staining, and crescent formation indicated by the large numbers of nuclei labeled by SYTO 13. Glomeruli with crescent formation but intact BC (BCI; n = 7 ROIs), with segmental or focal BC rupture (SBCR; n = 11 ROIs), with global or extensive BC rupture (GBCR; n = 13 ROIs), and glomeruli without crescent formation and leukocyte infiltration (control, CON; n = 4 ROIs) selected from four renal biopsy specimens from ANCA-GN patients and from two renal biopsy specimens from MCD patients (n = 12 ROIs) were included for further study. The selection of ROIs was performed by two professional pathologists to estimate the crescent formation, infiltration of leukocytes, and the degree of BC rupture.

DSP of Protein

After deparaffinization and rehydration, antigen retrieved from renal slides was soaked in 1× citrate buffer, pH 6.0 (C9999; Sigma, St. Louis, MO, USA), in a preheated pressure cooker for 15 min. Then, the slides were stained with a Texas red-labeled CD45 antibody (GMX-PRO-MORPH-HST-12; NanoString Technologies, Inc.), Alexa Fluor 555-labeled collagen IV, and SYTO 13, together with the DSP antibody barcodes including immune cell core profiling, the immune activation status module, immune cell typing module, and cell death module, which are provided in detail in **Supplementary Table S3**. The corresponding ROIs from the RNA slides were selected for protein detection, whenever possible. The photocleaved oligos from all of the ROIs were collected using a similar method to the RNA profiling, then reacted directly with NanoString's probe R and probe U (GMX-PRO-MORPH-HST-12 and GMX-PRO-HYB-96; NanoString Technologies, Inc.), which carried the fluorescence reporters and can be used for fluorescence counting with the nCounter® MAX Analysis System (NanoString Technologies, Inc.).

Library Preparation and RNA Sequencing

The UV-cleaved oligos from each ROI were collected, followed by PCR amplification using a pair of primers with the following sequences: forward: CAAGCAGAAGAC GGCATACG AGATXXXXXXXXXXGTGACTGGAGTTCAGACGT

GTGCTCTTCCGATCT; reverse: AATGATACGGC GACCACCGAGATCTACAC XXXXXXXXACACTCTT TCCCTACACGACGCTCTTCCGATCT (GeoMx Seq Code Pack, GMX-NGS-SEQ-AB; NanoString Technologies, Inc.). ROI identity was preserved in the custom Illumina i5/i7 unique dual indexing sequences of the primer pairs (marked as X). The PCR products were amalgamated, mixed with AMPure XP beads (A63881; Beckman Coulter, Brea, CA, USA) twice for purification, and then sequenced. A high-sensitivity DNA Bioanalyzer chip (C105102-S1; BiOptic, New Taipei City, Taiwan) was used to measure the concentration and purity of the library. The Illumina NovaSeq instrument (Illumina, Inc., San Diego, CA, USA) was applied for sequencing paired ends (2 × 27-bp reads).

Data Processing and Analysis

Reads were aligned to reveal the unique identities of the probe after sequencing. PCR duplicate reads were removed according to the unique identifier regions, followed by converting reads to digital counts. RNA sequencing saturation was set at 50%, as recommended by NanoString. The final count value of each gene was the arithmetic average of the rest of the individual probe counts after eliminating the outlier probes. The limit of quantitation (LOQ) was calculated based on the distributions of the negative control probes and was intended to approximate the quantifiable limits of gene expression per segment. The formula used to calculate the LOQ in an *i*-th segment was LOQ_i = geomean (NegProbei) × geoSD (NegProbei)*n*. Two geometric standard deviations above the geometric means were typically used as the LOQ. Of the 1,833 detected genes, 660 (36%) were above the LOQ in at least one ROI, and all the genes, except the 21 negative genes, were included for further analysis. With regard to normalization, the methods used included Q3 (top 25%), based on the genes whose expression levels were in the top 25%, housekeeping, and negative probe. If the correlations among the three methods are good, either of them can be chosen; otherwise, the Q3 method is recommended. In our experiment, the Q3 method was used for normalization.

For protein analysis, six proteins (CD80, FOXP3, CD66b, PD-L1, PD-L2, and CD95/Fas) were excluded owing to failure to reaching the detection threshold in all ROIs. A signal-to-noise ratio (SNR) was obtained by dividing the counts of each antibody by the three IgG-negative control antibodies. Protein counts were normalized using housekeeping proteins (histone H3 and ribosomal protein S6). Based on 1,000 accelerated bootstrap repetitions, uncertainty was calculated by bias correction and 95% confidence intervals. All analyses were performed with version 3.6.3 and RStudio 1.4.1103 by R.

Immune-Infiltrating Cell Analyses

Immune-infiltrating cell analyses were performed using NanoString's SpatialDecon tool to classify immune-infiltrating cells from the gene expression dataset of each ROI. Different from other variance-stable least squares deconvolution tools, SpatialDecon uses the constrained log-normal regression algorithm, which is more consistent with the long tail of the gene expression data. SafeTME, a predefined robust immune-infiltrating cell expression matrix, was used to analyze immune infiltration.

Immunofluorescence Staining

Serial paraffin-embedded renal sections of patients with ANCA-GN were analyzed by immunofluorescence staining as previously reported (31). Briefly, sections were deparaffinized and antigen retrieval was performed in microwave-heated Tris-EDTA buffer, pH 9.0 (AWI0152a; Abiowell, China), for 20 min, followed by blocking with 10% goat serum in phosphate-buffered saline (PBS), and were then incubated overnight at 4°C with the following primary antibodies: CD206 (18704; Proteintech, Rosemont, IL, USA), iNOS (MAB9502; R&D System, Minneapolis, MN, USA), CD31 (BBA7; R&D System), and cleaved caspase-3 (9661; Cell Signaling Technology). Secondary antibodies conjugated with Alexa Fluor dye were obtained from Abcam. DAPI (P36941; Invitrogen, Carlsbad, CA, USA) was used as a nuclear counterstain. Images were obtained using Zeiss Axio Scope.A1 (Carl Zeiss Canada Ltd., Toronto, Canada).

Periodic Acid–Schiff Staining

Mounted kidney sections after immunofluorescence staining were rinsed in 1× PBS to remove cover glass. Subsequently, periodic acid–Schiff (PAS) staining was performed according to the instructions in the PAS stain kit (G1008; Servicebio, Wuhan, China). Images were obtained using Zeiss Axio Scope.A1 (Carl Zeiss Canada Ltd.).

Statistical Analysis

Data were presented as the mean ± SD. One-way ANOVA followed by Bonferroni correction was applied to the comparison of more than two groups. Correlation was determined with Pearson's correlation analysis. Statistical analysis was performed as shown in the figure legends using GraphPad Prism v9 (GraphPad software, San Diego, CA, USA).

DATA AVAILABILITY STATEMENT

'The datasets presented in this study can be found in online repositories. The names of the repository/repositories and accession number(s) can be found below: Gene Expression Omnibus, accession number: GSE192996, available at https://www.ncbi.nlm.nih.gov/geo/query/acc.cgi?acc=GSE192996.

ETHICS STATEMENT

The studies involving human participants were reviewed and approved by the Clinical Research Ethics Committee of the Second Xiangya Hospital of Central South University. The patients/participants provided written informed consent to participate in this study.

AUTHOR CONTRIBUTIONS

LY, YL, TD, PS, HL, LS, FL, and AC designed and conducted the experiments and acquired and analyzed data. CW and XF conducted the renal biopsy and collected the clinical data of patients. XZ and SY evaluated the renal pathology. LY, YL, FL, KL, JH, and AC wrote the manuscript. All authors contributed to the article and approved the submitted version.

FUNDING

AC was supported by grants from the National Natural Science Foundation of China (no. 81800637) and Hunan Natural Science Outstanding Youth Fund Projects (no. 2021JJ10075). YL was supported by the National Natural Science Foundation of China (no. 81570622). PS was supported by grants from the National Natural Science Foundation of China (no. 81800649).

SUPPLEMENTARY MATERIAL

The Supplementary Material for this article can be found online at: https://www.frontiersin.org/articles/10.3389/fimmu.2022.831253/full#supplementary-material

Supplementary Table S1 | The demographic and clinical features of patients.

Supplementary Table S2 | The histopathological features of the patients with ANCA-associated glomerulonephritis.

Supplementary Table S3 | DSP probes list for mRNA.

Supplementary Table S4 | DSP probes list for proteins.

Supplementary Figure S1 | The principle of DSP transcription and protein profiles. Oligo-labeled probes with photocleavable linker target complimentary sequences for RNA assay **(A)**, while Oligo-labeled antibodies target specific antigens for protein assay **(B)**, which were incubated with samples. After selection of region of interests (ROIs), UV light was applied to specifically cleave the photocleavable linker, which released the DSP barcodes in each individual ROI **(C)**. Then the DSP barcodes were collected individually into 96-plate-well from each ROI **(D)**. For RNA assay, the DSP barcodes which are responsible for specific recognition of each mRNA (26bp label with blue and rose red) were incubated with primer pairs to amplify the products by PCR and then were sequenced **(F)**. For protein assay, the DSP barcodes were reacted with NanoString's probe R and probe U **(G, H)**.

Supplementary Figure S2 | Quality control of ROIs for the RNA assay. **(A)** Counts distribution of ROIs' housekeeping genes (HKs). The geometric means of housekeeping genes were calculated logarithmic (log2) and presented in the figure. **(B)** ROIs' nuclei counts and surface area assessment. The GeoMxTM DSP requires certain nuclei counts and surface area of each ROI. The nuclei counts and surface areas of all the ROIs have met the limit. **(C)** Correlation among housekeeping Genes. There were 32 HK genes in this experiment, and 3 of HK genes were randomly selected to show the correlations. The results showed a high correlation among TMUB2, ARMH3 and TLK2. **(D)** Selection of normalization method. Normalization methods include Top 25%, which uses the top 25% genes as the benchmark for normalization, as well as HKs and Neg Probe methods. The relation between HK and Top 25% shows a highly strong correlation. In this study, Top 25% method was used for normalization.

Supplementary Figure S3 | Quality control of ROIs for the protein assay. **(A)** Counts distribution of ROIs' housekeeping proteins (HKs). The geometric means of housekeeping proteins were calculated logarithmic (log2) and presented in the figure. **(B)** ROIs' nuclei counts and surface areas assessment. The nuclei counts and surface areas of this study were qualified for further analysis. **(C)** The quality control of the expression of each target protein relative to negative control. The targets whose calculated value were always lower than or close to the background value were excluded in the further analysis (highlighted in blue color). **(D)** The expression correlations among housekeeping proteins. The results showed a high expression correlation between Histone H3 and S6.

REFERENCES

1. Chen M, Jayne DRW, Zhao M-H. Complement in ANCA-Associated Vasculitis: Mechanisms and Implications for Management. *Nat Rev Nephrol* (2017) 13(6):359–67. doi: 10.1038/nrneph.2017.37
2. Benzing T, Salant D. Insights Into Glomerular Filtration and Albuminuria. *N Engl J Med* (2021) 384(15):1437–46. doi: 10.1056/NEJMra1808786
3. Chen A, Lee K, D'Agati VD, Wei C, Fu J, Guan TJ, et al. Bowman's Capsule Provides a Protective Niche for Podocytes From Cytotoxic CD8+ T Cells. *J Clin Invest* (2018) 128(8):3413–24. doi: 10.1172/JCI97879
4. Hakroush S, Tampe D, Korsten P, Strobel P, Tampe B. Bowman's Capsule Rupture Links Glomerular Damage to Tubulointerstitial Inflammation in ANCA-Associated Glomerulonephritis. *Clin Exp Rheumatol* (2021) 39 Suppl 129(2):27–31.
5. L'Imperio V, Vischini G, Pagni F, Ferraro PM. Bowman's Capsule Rupture on Renal Biopsy Improves the Outcome Prediction of ANCA-Associated Glomerulonephritis Classifications. *Ann Rheum Dis* (2020). doi: 10.1136/annrheumdis-2020-217979
6. Heymann F, Meyer-Schwesinger C, Hamilton-Williams EE, Hammerich L, Panzer U, Kaden S, et al. Kidney Dendritic Cell Activation is Required for Progression of Renal Disease in a Mouse Model of Glomerular Injury. *J Clin Invest* (2009) 119(5):1286–97. doi: 10.1172/JCI38399
7. Chen A, Lee K, Guan T, He JC, Schlondorff D. Role of CD8+ T Cells in Crescentic Glomerulonephritis. *Nephrol Dial Transplant* (2020) 35(4):564–72. doi: 10.1093/ndt/gfz043
8. Merritt CR, Ong GT, Church SE, Barker K, Danaher P, Geiss G, et al. Multiplex Digital Spatial Profiling of Proteins and RNA in Fixed Tissue. *Nat Biotechnol* (2020) 38(5):586–99. doi: 10.1038/s41587-020-0472-9
9. Beechem JM. High-Plex Spatially Resolved RNA and Protein Detection Using Digital Spatial Profiling: A Technology Designed for Immuno-Oncology Biomarker Discovery and Translational Research. *Methods Mol Biol* (2020) 2055:563–83. doi: 10.1007/978-1-4939-9773-2_25
10. Xie Y, Sakatsume M, Nishi S, Narita I, Arakawa M, Gejyo F. Expression, Roles, Receptors, and Regulation of Osteopontin in the Kidney. *Kidney Int* (2001) 60 (5):1645–57. doi: 10.1046/j.1523-1755.2001.00032.x
11. Kumar A, Elko E, Bruno SR, Mark ZF, Chamberlain N, Mihavics BK, et al. Inhibition of PDIA3 in Club Cells Attenuates Osteopontin Production and Lung Fibrosis. *Thorax* (2021). doi: 10.1136/thoraxjnl-2021-216882
12. Morse C, Tabib T, Sembrat J, Buschur KL, Bittar HT, Valenzi E, et al. Proliferating SPP1/MERTK-Expressing Macrophages in Idiopathic Pulmonary Fibrosis. *Eur Respir J* (2019) 54(2):1802441. doi: 10.1183/13993003.02441-2018
13. Popovics P, Jain A, Skalitzky KO, Schroeder E, Ruetten H, Cadena M, et al. Osteopontin Deficiency Ameliorates Prostatic Fibrosis and Inflammation. *Int J Mol Sci* (2021) 22(22):12461. doi: 10.3390/ijms222212461
14. Zhu X, Cheng YQ, Du L, Li Y, Zhang F, Guo H, et al. Mangiferin Attenuates Renal Fibrosis Through Down-Regulation of Osteopontin in Diabetic Rats. *Phytother Res* (2015) 29(2):295–302. doi: 10.1002/ptr.5254
15. Dong B, Wu C, Huang L, Qi Y. Macrophage-Related SPP1 as a Potential Biomarker for Early Lymph Node Metastasis in Lung Adenocarcinoma. *Front Cell Dev Biol* (2021) 9:739358. doi: 10.3389/fcell.2021.739358
16. Tang PM, Nikolic-Paterson DJ, Lan HY. Macrophages: Versatile Players in Renal Inflammation and Fibrosis. *Nat Rev Nephrol* (2019) 15(3):144–58. doi: 10.1038/s41581-019-0110-2
17. Anguiano L, Kain R, Anders HJ. The Glomerular Crescent: Triggers, Evolution, Resolution, and Implications for Therapy. *Curr Opin Nephrol Hypertens* (2020) 29(3):302–9. doi: 10.1097/MNH.0000000000000596

18. Jayne DRW, Merkel PA, Schall TJ, Bekker P, Group AS. Avacopan for the Treatment of ANCA-Associated Vasculitis. *N Engl J Med* (2021) 384(7):599–609. doi: 10.1056/NEJMoa2023386
19. Sethi S, Zand L, De Vriese AS, Specks U, Vrana JA, Kanwar S, et al. Complement Activation in Pauci-Immune Necrotizing and Crescentic Glomerulonephritis: Results of a Proteomic Analysis. *Nephrol Dial Transpl* (2017) 32(suppl_1):i139–i45. doi: 10.1093/ndt/gfw299
20. Xiao H, Schreiber A, Heeringa P, Falk RJ, Jennette JC. Alternative Complement Pathway in the Pathogenesis of Disease Mediated by Anti-Neutrophil Cytoplasmic Autoantibodies. *Am J Pathol* (2007) 170(1):52–64. doi: 10.2353/ajpath.2007.060573
21. Xing GQ, Chen M, Liu G, Heeringa P, Zhang JJ, Zheng X, et al. Complement Activation is Involved in Renal Damage in Human Antineutrophil Cytoplasmic Autoantibody Associated Pauci-Immune Vasculitis. *J Clin Immunol* (2009) 29(3):282–91. doi: 10.1007/s10875-008-9268-2
22. Hilhorst M, van Paassen P, van Rie H, Bijnens N, Heerings-Rewinkel P, van Breda Vriesman P, et al. Complement in ANCA-Associated Glomerulonephritis. *Nephrol Dial Transplant* (2017) 32(8):1302–13. doi: 10.1093/ndt/gfv288
23. Nallasamy P, Nimmakayala RK, Karmakar S, Leon F, Seshacharyulu P, Lakshmanan I, et al. Pancreatic Tumor Microenvironment Factor Promotes Cancer Stemness *via* SPP1-CD44 Axis. *Gastroenterology* (2021) 161(6):1998–2013 e7. doi: 10.1053/j.gastro.2021.08.023
24. Eymael J, Sharma S, Loeven MA, Wetzels JF, Mooren F, Florquin S, et al. CD44 Is Required for the Pathogenesis of Experimental Crescentic Glomerulonephritis and Collapsing Focal Segmental Glomerulosclerosis. *Kidney Int* (2018) 93(3):626–42. doi: 10.1016/j.kint.2017.09.020
25. Roeder SS, Barnes TJ, Lee JS, Kato I, Eng DG, Kaverina NV, et al. Activated ERK1/2 Increases CD44 in Glomerular Parietal Epithelial Cells Leading to Matrix Expansion. *Kidney Int* (2017) 91(4):896–913. doi: 10.1016/j.kint.2016.10.015
26. Satoh T, Kidoya H, Naito H, Yamamoto M, Takemura N, Nakagawa K, et al. Critical Role of Trib1 in Differentiation of Tissue-Resident M2-Like Macrophages. *Nature* (2013) 495(7442):524–8. doi: 10.1038/nature11930
27. He C, Sheng L, Pan D, Jiang S, Ding L, Ma X, et al. Single-Cell Transcriptomic Analysis Revealed a Critical Role of SPP1/CD44-Mediated Crosstalk Between Macrophages and Cancer Cells in Glioma. *Front Cell Dev Biol* (2021) 9:779319. doi: 10.3389/fcell.2021.779319
28. Shimizu A, Masuda Y, Kitamura H, Ishizaki M, Sugisaki Y, Yamanaka N. Apoptosis in Progressive Crescentic Glomerulonephritis. *Lab Invest* (1996) 74 (5):941–51.
29. Berden AE, Ferrario F, Hagen EC, Jayne DR, Jennette JC, Joh K, et al. Histopathologic Classification of ANCA-Associated Glomerulonephritis. *J Am Soc Nephrol* (2010) 21(10):1628–36. doi: 10.1681/ASN.2010050477
30. Brady L, Kriner M, Coleman I, Morrissey C, Roudier M, True LD, et al. Inter- and Intra-Tumor Heterogeneity of Metastatic Prostate Cancer Determined by Digital Spatial Gene Expression Profiling. *Nat Commun* (2021) 12(1):1426. doi: 10.1038/s41467-021-21615-4
31. Chen A, Feng Y, Lai H, Ju W, Li Z, Li Y, et al. Soluble RARRES1 Induces Podocyte Apoptosis to Promote Glomerular Disease Progression. *J Clin Invest* (2020) 130(10):5523–35. doi: 10.1172/JCI140155

Conflict of Interest: The authors declare that the research was conducted in the absence of any commercial or financial relationships that could be construed as a potential conflict of interest.

frontiers | Frontiers in Immunology

ORIGINAL RESEARCH
published: 14 April 2022
doi: 10.3389/fimmu.2022.857813

Clinical and Renal Histology Findings and Different Responses to Induction Treatment Affecting the Long-Term Renal Outcomes of Children With ANCA-Associated Vasculitis: a Single-Center Cohort Analysis

*Jing Yang[1], Yuan Yang[1], Yongli Xu[1], Lanqi Zhou[1], Luowen Zhou[2], Xiaoling Yin[1], Jinyun Pu[1], Fengjie Yang[1], Yaping Liu[1], Yonghua He[1], Yaxian Chen[1], Huiqing Yuan[1], Liru Qiu[1], Yu Zhang[1], Yu Chen[1], Tonglin Liu[1], Jinhui Tang[1] and Jianhua Zhou[1]**

[1] Department of Pediatrics, Tongji Hospital, Tongji Medical College, Huazhong University of Science and Technology, Wuhan, China, [2] Department of Neurosurgery, Tongji Hospital, Tongji Medical College, Huazhong University of Science and Technology, Wuhan, China

Introduction: Antineutrophil cytoplasmic antibody (ANCA)-associated vasculitis (AAV) is relatively rare in children. This article aimed to analyze clinical and renal histology findings and different responses to induction treatment associated with the long-term renal outcomes in children with AAV in a single center.

Methods: All pediatric patients with AAV admitted to Tongji Hospital from January 2002 to January 2021 were included in the study. The demographic, clinical, pathological, laboratory, and treatment data and outcomes were collected and analyzed to identify predictors associated with response to induction treatment and progression to end-stage renal disease (ESRD).

Results: In total, 48 children with AAV were included in this cohort; 81.25% of them were women, and 91.7% were microscopic polyangiitis (MPA). Kidney involvement was found in 45 patients (93.75%). The most common histopathological subtype was crescentic form in this cohort according to Berden's classification. In total, 34 patients (70.8%) showed eGFR <60 ml/min/1.73 m^2 at the time of diagnosis. Complete and partial remission was achieved in 8 patients (16.7%) and 19 patients (39.6%), respectively, following 6-month induction treatment. Half of the patients eventually progressed to ESRD at a mean time of (13.04 ± 15.83) months after diagnosis. The independent predictors of nonremission following induction treatment and progression to ESRD were baseline eGFR <60 ml/min/1.73 m^2 and hypertension at diagnosis. Renal survival significantly decreased over time in patients with renal sclerotic subtypes or those with nonremission following induction treatment by Kaplan–Meier curve estimation.

OPEN ACCESS

Edited by:
Hao Sun,
University of California, San Diego, United States

Reviewed by:
Kerstin Westman,
Lund University, Sweden
Lingli He,
Harvard University, United States

***Correspondence:**
Jianhua Zhou
jhzhou99@qq.com

Specialty section:
This article was submitted to Autoimmune and Autoinflammatory Disorders, a section of the journal Frontiers in Immunology

Received: *19 January 2022*
Accepted: *11 March 2022*
Published: *14 April 2022*

Citation:
Yang J, Yang Y, Xu Y, Zhou L, Zhou L, Yin X, Pu J, Yang F, Liu Y, He Y, Chen Y, Yuan H, Qiu L, Zhang Y, Chen Y, Liu T, Tang J and Zhou J (2022) Clinical and Renal Histology Findings and Different Responses to Induction Treatment Affecting the Long-Term Renal Outcomes of Children With ANCA-Associated Vasculitis: a Single-Center Cohort Analysis. Front. Immunol. 13:857813. doi: 10.3389/fimmu.2022.857813

Conclusions: Our study demonstrates that women, MPA, and crescentic subtypes are predominant in pediatric AAV in China. Initial renal failure (eGFR <60 ml/min/1.73 m^2), hypertension, sclerotic pathological subtype, and nonremission following induction treatment are predictive of long-term renal outcomes.

Keywords: ANCA-associated vasculitis, children, remission-induction treatment, ESRD, progression, renal survival

INTRODUCTION

Antineutrophil cytoplasmic antibody (ANCA)-associated vasculitis (AAV) is a multisystemic autoimmune disease characterized by a necrotizing inflammation in the small to medium vessels. According to the 2012 Chapel Hill International Consensus Conference nomenclature of vasculitis (CHCC) (1), AAV includes microscopic polyangiitis (MPA), granulomatosis with polyangiitis (GPA, formerly known as Wegener's granulomatosis), and eosinophilic granulomatosis with polyangiitis (EGPA, also known as Churg–Strauss syndrome). MPA is a kind of necrotizing vasculitis predominantly affecting the kidney. GPA is a necrotizing granulomatous vasculitis with more sinus and pulmonary involvement, but necrotizing glomerulonephritis is also common. EGPA is an eosinophil-rich and necrotizing granulomatous vasculitis affecting the respiratory tract. In addition, nervous system, skin, mucous, ocular, and cardiovascular involvement can occur in all kinds of AAV.

AAV is associated with the occurrence of circulating autoantibodies against myeloperoxidase (MPO), proteinase 3 (PR3), and other uncommon antigens. MPO-ANCA is common in patients with MPA and usually occurs as perinuclear immunofluorescence patterns (P-ANCA), while PR3-ANCA is commonly associated with GPA and presents as cytoplasmic immunofluorescence patterns (C-ANCA) (2). AAV mainly occurs in adults with an annual incidence of 13–20 cases/million in Europe. However, they are very rare in children with an estimated incidence of 1–6 cases per million (3). A combination of immunosuppression and glucocorticoids remains the mainstream treatment and has saved the lives of a lot of patients with AAV. Despite strong immunotherapy, many AAV patients still died of ESRD, infectious or cardiovascular complications, etc. According to previous reports (4–10), 20% to 45% of children with AAV eventually progressed to ESRD. A recent multicenter study of 85 children with AAV in Italy and Canada (9) has not found any independent prognostic factors of renal outcome in multivariable Cox regression analysis. In a French national study of 66 children with AAV (11), low baseline eGFR levels, non-Caucasian ethnicity, and sclerotic or mixed histopathological patterns were associated with the occurrence of ESRD. Since AAV in children is rare, risk factors of renal long-term outcomes have not been extensively studied. So far, there have been a few reports on the risk factors for renal prognosis in Chinese children with AAV, and there has been no study on the effect of induction therapy on renal long-term outcomes. Hence, the present study is intended to provide such information through analyzing the demographic, clinical, pathological, laboratory, and follow-up data in children with AAV in a single pediatric center.

MATERIALS AND METHODS

Patients

This cohort included all AAV patients hospitalized from January 2002 to January 2021 at the Pediatric Department of Tongji Hospital and younger than 18 years old at diagnosis. The diagnosis of AAV was established according to the Pediatric Rheumatology European Society (PRES) criteria for childhood vasculitis and the 2012 revised Chapel Hill consensus conference nomenclature of vasculitis. Some patients were included in the study due to typical pauci-immune necrotizing glomerulonephritis in renal pathology, although the ANCA tested negative (IF or ELISA for MPO, PR3). AAV secondary to drugs and other autoimmune diseases such as systemic lupus erythematosus (SLE), IgA-associated vasculitis, and rheumatoid arthritis, and primary kidney diseases such as membranous nephropathy and IgA nephropathy were all excluded in this study.

The study was approved by the Ethics Committee of Tongji Hospital and conducted in accordance with the Declaration of Helsinki.

Data Collection, Treatment, and Definition in Evaluation

The demographic, clinical, pathological, and laboratory treatment data and renal outcomes were collected for analysis. Baseline data included sex, age, height, time from onset to diagnosis, baseline serum creatinine, 24 h urinary protein amount, ESR, PVAS score, ANCA types (immunofluorescence detection), MPO and PR3 titers, remission-induction treatment approaches, and stages of CKD.

The remission-induction treatment was conducted with glucocorticoids and monthly intravenous cyclophosphamides (CYC) at a dosage of 0.5–0.75g/m^2 for up to 6 months (12). For those presented with eGFR <60 ml/min/1.73 m^2, plasma exchange (three to five times within 2 weeks) and/or rituximab (at a dosage of 375 mg/m^2 for 2–4 times) were considered in addition to glucocorticoids and monthly intravenous cyclophosphamides (CYC). Normally, response to induction treatment was assessed after 6 months. After remission-induction therapy, patients were on maintenance treatment with glucocorticoids and mycophenolate mofetil (MMF) or AZA in most cases, only a few patients were on intravenous CYC every 3 months. All patients were evaluated monthly during remission-induction treatment and thereafter every 2 to 4 months during maintenance treatment.

Data were collected and analyzed at the time of diagnosis, after 6-month remission-induction treatment, and at the observation endpoint or the final follow-up.

Definition

Renal symptoms or parameters at presentation were defined as follows: nephrotic-ranged proteinuria was defined as the 24-h urine protein excretion of more than 40 mg/h/m^2 or urine protein/Cr ≥2.0 (mg/mg). eGFR was calculated by using the modified Schwartz formula; CKD was defined and classified according to the KDOQI standards; the observation endpoint was defined as arrival of CKD stage V or the last follow-up for those who had not progressed to CKD stage V; kidney survival time was defined as the time from diagnosis to CKD stage V or the last follow-up; disease activity was assessed by the Pediatric Vasculitis Activity Score (PVAS) (13). Renal complete remission (CR) was defined as negative for proteinuria amount of less than 150 mg/24 h, urine red blood cells were less than 10/HPF, and serum creatinine level was stable; renal partial remission (PR) was defined as a 50% decrease in the daily amount of proteinuria, a decrease in urine red blood cells, and a stable serum creatinine level; nonremission was defined as those that did not meet the above criteria.

Kidney pathologies were classified into focal, crescentic, sclerotic, and mixed subtypes according to Berden's classification (14). Briefly, samples with ≥50% normal glomeruli were classified as focal; those with ≥50% cellular crescentic glomeruli as crescentic; those with ≥50% sclerotic glomeruli as sclerotic; and those with a combination of normal, crescentic, and sclerotic glomeruli, and all occurring in <50% of glomeruli as mixed.

Statistical Analysis

Continuous variables with normally distributed measurement were expressed as mean ± standard deviation (SD), evaluated by the Student's *t*-test. Continuous variables with nonnormal distributed measurement were expressed as median [interquartile range (IQR)], evaluated by the Mann–Whiney *U* test or Wilcoxon rank-sum test. Categorical variables were expressed as percentages and were tested by the Person Chi-square test or Fisher's exact test. Logistic regression analysis was applied to the multivariate analysis of renal remission, and Cox regression analysis was used to study the risk factors of progressing to ESRD. Kaplan–Meier survival curves and the Log-rank test were applied to compare renal survival among four renal pathological classification and three renal remission-induction responses. All differences were considered statistically significant at $p < 0.05$.

RESULTS

Main Characteristics at the Time of Diagnosis of the 48 Patients With MPA and GPA

The baseline data of 48 patients with childhood-onset ANCA-associated vasculitis were summarized in **Table 1**. Most patients were women (81.25%), the mean age at diagnosis was 10.62 ± 3.53 years, and the median time from onset to diagnosis was 1 month. MPA was predominant (91.7%) with just 4 patients with GPA in this cohort; 70.8% of patients showed eGFR <60 ml/min/1.73 m^2 at diagnosis. Renal involvement was found in 93.75% of patients, as manifested with proteinuria, hematuria, hypertension, and renal insufficiency. The respiratory system was involved in 23% of patients, including 2% with pulmonary nodules and 21% with pulmonary hemorrhage, which was significantly higher in GPA than in MPA ($p = 0.025$). ESR was much faster in MPA than in GPA ($p = 0.007$).

Main Characteristics at the Time of Diagnosis of the 33 Patients Based on Kidney Pathology

The crescentic subtype was the most frequent (66.7%) form among 33 patients who received kidney biopsies. As shown in **Table 2**, the main characteristics were not significantly different at the time of diagnosis among the four pathological subtypes.

Different Responses to Induction Treatment and Predictive Factors Analysis of Baseline Data

After up to 6-month induction treatment, complete remission was achieved in 8 patients (16.7%), partial remission in 19 patients (39.6%), and nonremission in 21 patients (43.7%). The baseline data were compared among the three groups; significant differences were found in levels of serum creatinine and C3, hypertension, eGFR grades, and PVAS score (**Table 3**). eGFR <60 ml/min/1.73 m^2 ($p = 0.001$) and hypertension ($p = 0.002$) were independent predictors for no response to induction treatment by multivariate analysis (**Table 4**).

Renal Outcomes and Risk Factors Associated With Progression to ESRD

The median time of follow-up was 24.5 months (0–228 months). A total of 24 patients (50%) progressed to ESRD. The mean time they progressed to ESRD was (13.04 ± 15.83) months, and the median time was 7.5 months (0–58 months). A total of 8 patients reached ESRD at the time of diagnosis, and 4 patients progressed to ESRD in the first 6 months after diagnosis. The other 12 patients progressed to ESRD thereafter; among them, 4 patients showed partial remission postinduction treatment, and 8 patients showed nonremission.

The baseline data of 48 patients were applied to Cox regression analysis to identify the risk factors of ESRD. As shown in **Table 5**, hypertension, eGFR <60 ml/min/1.73 m^2, PVAS >11, and nephrotic proteinuria at diagnosis were significantly associated with ESRD in univariate analysis, but only hypertension ($p = 0.001$) and eGFR <60 ml/min/1.73 m^2 ($p = 0.013$) were proved to be independent risk predictors of ESRD in multivariate Cox regression analysis.

Renal biopsies were performed in 33 patients, including 9 patients of crescentic subtype, 6 of sclerotic subtype, and 2 of mixed subtype. The renal survival curves of different pathological subtypes are shown in **Figure 1A**; a significant difference was found among four renal pathological subtypes ($p = 0.031$). The sclerotic subtype showed the worst and the focal showed the best outcomes. The renal outcomes at final evaluation in patients with different pathological subtypes are shown in **Supplementary Figure S1**.

All patients of focal subtype remained under normal renal function, but all patients of sclerotic and mixed subtypes

TABLE 1 | Main characteristics at the time of diagnosis of the 48 patients.

	MPA (*n* = 44)	GPA (*n* = 4)	*p*-value
Women (*n* (%))	34 (77)	3 (75)	0.661
Age at diagnosis (years)	11 (0.8–18)	12 (4.8–17)	0.614
Time from onset to diagnosis (median (months))	1 (0.1–72)	0.875 (0.25–1)	0.586
Renal features			
Serum creatinine (μmol/L)	317.29 ± 290.11	145.50 ± 131.51	0.25
24 h urine protein (mg/24 h)	1,610.97 ± 1,437.23	2,125.90 ± 3,438.13	0.589
Nephrotic-range proteinuria (*n* (%))			
Hypertension (*n* (%))	24 (55)	1 (25)	0.338
eGFR level (*n* (%))			0.802
eGFR >90 (ml/min/1.73 m^2)	9 (20)	2 (50)	
eGFR = 60–90 (ml/min/1.73 m^2)	3 (7)	0 (0)	
eGFR = 30–60 (ml/min/1.73 m^2)	14 (32)	0 (0)	
eGFR = 15–30 (ml/min/1.73 m^2)	11 (25)	1 (25)	
eGFR <15 (ml/min/1.73 m^2)	7 (16)	1 (25)	
Respiratory system (*n* (%))			
Pulmonary hemorrhage	7 (16)	3 (75)	0.025
Pulmonary nodules	0 (0)	1 (25)	0.085
Eye involvement (*n* (%))	1 (2)	0 (0)	1.000
ENT involvement (*n* (%))	0 (0)	1 (25)	0.083
Neural involvement (*n* (%))	1 (2)	0 (0)	1.000
PVAS scores	12.61 ± 4.45	12.50 ± 6.40	0.962
C3 (g/L)	0.91 ± 0.27	0.85 ± 0.20	0.703
C4 (g/L)	0.22 ± 0.08	0.18 ± 0.04	0.399
ESR (mm/h)	65 ± 41	14 ± 11	0.007
ANCA (IF) (*n* (%))			0.039
Negative	7 (16)	1 (25)	
C-ANCA	4 (9)	2 (50)	
P-ANCA	33 (75)	1(25)	
ANCA (ELISA) (*n* (%))			0.068
Negative	10 (23)	1(25)	
MPO-ANCA	30 (68)	1 (25)	
PR3-MPO	4 (9)	2 (50)	
Kidney histopathology (*n* (%)) (Total calculated as the patients with renal biopsy)			1.000
Focal	3 (10)	0 (0)	
Crescentic	20 (65)	2 (100)	
Sclerotic	6 (19)	0 (0)	
Mixed	2 (6)	0 (0)	
Treatment (*n* (%))			0.031
Glucocorticoids	9 (21)	2 (50)	
Glucocorticoids+CYC	20 (45)	0 (0)	
Glucocorticoids+CYC+PE	10 (23)	0 (0)	
Glucocorticoids+CYC+PE+RTX	5 (11)	2 (50)	

PVAS, Pediatric Vasculitis Activity Score; IF, immunofluorescence; CYC, cyclophosphamides; PE, plasma exchange; RTX, rituximab.

progressed to ESRD. Since the patients of the crescentic subtype showed variable outcomes, we compared their baseline data between those who remained under normal renal function (eGFR >90 ml/min/1.73 m^2) and those who progressed to ESRD (eGFR <15 ml/min/1.73 m^2) and found significant differences in age, serum creatinine level, eGFR level, and response to remission-induction treatment (**Table 6**).

To evaluate the effect of different responses to induction treatment on renal survival, Kaplan–Meier survival curves were used to assess the time to ESRD in 48 patients. Those patients with complete remission showed the best renal outcome and those with nonremission showed the worst (**Figure 1B**).

About 7 patients were treated with rituximab (RTX); 3 cases with crescentic subtype obtained improvement of eGFR from 19 to 47 ml/min/1.73 m^2, 27 to 79 ml/min/1.73 m^2, and 59 to 67 ml/min/1.73 m^2, respectively. Two cases with crescentic subtype and 2 cases with sclerotic subtype still showed eGFR deterioration (**Supplementary Figure S2**).

DISCUSSION

AAV is a severe autoimmune disorder mainly affecting the kidney, lung, nose, paranasal sinus, skin, etc. (15). It mainly occurs in adults and rarely in children. So far, a few large cohorts are focusing on the long-term outcome of pediatric patients with AAV. Our study summarized the clinicopathological features, their relationship with response to induction treatment, and renal long-term outcome of pediatric AAV in a single center. The results showed that MPA accounted for the overwhelming majority (91.7%) of AAV in Chinese children, and female patients also made up the majority (81.25%) of AAV. The

TABLE 2 | Clinical features at the time of diagnosis of patients with different histopathological subtypes.

	Focal (*N* = 3)	Crescentic (*N* = 22)	Sclerotic (*N* = 6)	Mixed (*N* = 2)	*p*-value
Women (*n* (%))	2 (67)	16 (73)	6 (100)	0 (0)	0.055
Age at onset (years)	11.67 ±1.15	9.99 ±3.31	10.78 ±1.65	10.15 ±4.03	0.799
Time from onset to biopsy	0.5 (0.1–6)	1 (0.1–6)	0.5 (0.1–3)	36.1 (0.25–72)	0.701
Clinical type					1.000
MPA (*n* (%))	3 (100)	20 (91)	6 (100)	2	
GPA (*n* (%))	0 (0)	2 (9)	0 (0)	0	
ANCA (IF) (*n* (%))					0.128
Negative	1 (33)	4 (18)	0 (0)	2	
C-ANCA	0 (0)	3 (14)	0 (0)	0	
P-ANCA	2 (67)	15 (68)	6 (100)	0	
ANCA (ELISA) (*n* (%))					0.162
Negative	1 (33)	6 (27)	0 (0)	2	
MPO	2 (67)	13 (59)	6 (100)	0	
PR3	0 (0)	3 (14)	0 (0)	0	
eGFR level (*n* (%))					0.022
eGFR >90	2 (67)	3 (14)	0 (0)	1 (50)	
eGFR = 60–90	1 (33)	1 (5)	1 (17)	0 (0)	
eGFR =30–60	0 (0)	6 (27)	3 (50)	1 (50)	
eGFR = 15–30	0 (0)	10 (45)	0 (0)	0 (0)	
eGFR <15	0 (0)	2 (9)	2 (33)	0 (0)	
Serum creatinine (μmol/L)	55 ± 32.5	327.5 ± 266.6	396.2 ± 389.5	132 ± 152.7	0.406
24h urine protein (mg/24h)	1,040 ± 650.5	1,642.3 ± 1,870.7	2,502.1 ± 1,158.9	3,384.9 ± 3,014	0.412
ESR (mm/H)	74.5 ± 41.7	67.6 ± 49.8	75.5 ± 41.6	68 ± 69.3	0.986
C3 (g/L)	0.93 ± 0.46	0.93 ± 0.28	0.95 ± 0.18	0.57 ± 0.13	0.395
C4 (g/L)	0.23 ± 0.11	0.21 ± 0.76	0.33 ± 0.14	0.11 ± 0.02	0.068
PVAS	11 ± 1.4	13.0 ± 3.9	13.5 ± 3.2	13 ± 4.2	0.876
Treatment (*n* (%))					0.217
Glucocorticoids	1 (33)	1 (5)	0 (0)	1 (50)	
Glucocorticoids+CTX	2 (67)	12 (55)	2 (33)	0 (0)	
Glucocorticoids+CTX+PE	0 (0)	4 (18)	2 (33)	1 (50)	
Glucocorticoids+CTX+PE+RTX	0 (0)	5 (23)	2 (33)	0 (0)	

PVAS, Pediatric Vasculitis Activity Score; IF, immunofluorescence; CYC, cyclophosphamides; PE, plasma exchange; RTX, rituximab.

demographic and AAV-type distribution characteristics were consistent with other previous studies on Chinese and other East Asian children (10, 11, 16, 17). These were different from adult patients, suggesting a somewhat male predominance (18). It is interesting to note that an MPA majority not only existed in studies comprising Chinese pediatric (97.1%) (10) and adult patients (83.64%) (19) but also in Korean (59.4%) (20) and Japanese patients with AAV (21). It was different from AAV in Europe and North America where a GPA majority was more common (21). Renal involvement is much higher than pulmonary involvement in MPA patients. Similarly, our study showed renal and pulmonary involvement in 93.75% and 23% of patients, respectively.

As shown in the present paper, the effect of induction therapy significantly affected renal survival in patients with AAV. Currently, glucocorticoids combined with cyclophosphamide remain the "gold standard" treatment for induction therapy. Mycophenolate mofetil and azathioprine are the main immunosuppressants for maintenance therapy. In recent years, rituximab, immunoadsorption, and plasma exchange have also been successfully used in the treatment of AAV (3). Other biologics like anti-TNF-α and anti-BLyS monoclonal antibodies have been tried in the treatment of AAV. The overall remission rate was 56.3% after 6-month induction treatment in our patients, which was significantly lower than that in previously reported AAV cohorts (9, 10, 22). As shown in our study, baseline eGFR <60 ml/min/1.73 m^2 was an independent predictor of nonremission and found in a percentage as high as 71% of patients. Therefore, the reason for the lower remission rate of induction treatment was probably due to the higher proportion of eGFR <60 ml/min/1.73 m^2 at diagnosis.

Around 50% of patients progressed to ESRD, higher than in other reports showing only between 20% and 45% (4–10). Through multivariate Cox regression analysis, we identified eGFR <60 ml/min/1.73 m^2 and hypertension at the time of diagnosis as independent risk predictors for progression to ESRD. Our results confirmed the poor prognostic value of decreased eGFR at diagnosis, which was consistent with previous studies (4, 8–10, 23). Additionally, this study revealed a new finding that hypertension at diagnosis was also an independent risk predictor for progression to ESRD in childhood-onset AAV. Moreover, this study also identified nephrotic-range proteinuria and PVAS >11 at the time of diagnosis as risk factors for ESRD in univariate analysis. PVAS was established in 2012 when redefining the Birmingham Vasculitis Activity Score (BVAS) components and adding eight pediatric items (13). The present study also confirmed high PVAS as a risk factor of renal long-term outcome in pediatric AAV patients (24–26). A total of eight patients reached ESRD at the time of diagnosis, and four patients progressed to ESRD in the periods of remission-induction treatment. Considering that immunosuppressants were not necessarily needed in these cases, they received a shorter period of induction therapy to avoid adverse effects, and this might have an impact on renal outcomes.

TABLE 3 | The baseline data at diagnosis and treatments in patients with different renal responses to induction treatment.

	Complete remission (*N* = 8)	Partial remission (*N* = 19)	Nonremission (*N* = 21)	*p*-value
Women (*n* (%))	7 (87.5)	14 (73.7)	16 (76.2)	0.816
Age at diagnosis (years)	12 (2.3–17)	11 (2.5–18)	11 (8–16)	0.222
Time from onset to diagnosis (median (months))	0.875 (0.1–2)	1 (0.25–72)	1 (0.1–36)	0.592
Renal features				
Serum creatinine (μmol/L)	102.20 ± 147.59	184.87 ± 221.49	486.32 ± 269.27	<0.001
24 h urine protein (mg/24 h)	717.113 ± 990.41	1,579.61 ± 1,584.66	2,077.94 ± 1,764.77	0.129
Nephrotic-range proteinuria (*n* (%))	0 (0)	3 (16.7)	6 (27.3)	0.263
Hypertension (*n* (%))	0 (0)	9 (50)	15 (68.2)	0.003
eGFR level (*n* (%))				<0.001
eGFR >90 (ml/min/1.73 m^2)	6 (75)	5 (26.3)	0 (0)	
eGFR = 60–90 (ml/min/1.73 m^2)	1 (12.5)	2 (10.5)	0 (0)	
eGFR = 30–60 (ml/min/1.73 m^2)	0 (0)	9 (47.4)	5(23.8)	
eGFR = 15–30 (ml/min/1.73 m^2)	1 (12.5)	3 (15.8)	8 (38.1)	
eGFR <15 (ml/min/1.73 m^2)	0 (0)	0 (0)	8 (38.1)	
C3 (g/L)	1.04 ± 0.32	0.97 ± 0.21	0.77 ± 0.24	0.027
C4 (g/L)	0.21 ± 0.06	0.19 ± 0.07	0.23 ± 0.10	0.54
ESR (mm/h)	35 ± 46.88	62.69 ± 38.63	67.25 ± 40.87	0.22
PVAS scores	9 (1–15)	12 (3–20)	12 (10–27)	0.002
ANCA (IF) (*n* (%))				0.379
Negative	2 (25)	2 (11.1)	4 (18.2)	
C-ANCA	2 (25)	3 (16.7)	1 (4.5)	
P-ANCA	4 (50)	14 (72.2)	16 (77.3)	
ANCA (ELISA) (*n* (%))				0.288
Negative	3 (37.5)	3 (16.7)	5 (22.7)	
MPO-ANCA	3 (37.5)	13 (66.7)	15 (72.7)	
PR3-MPO	2 (25)	3 (16.7)	1 (4.5)	
Kidney histopathology (*n* (%))		(Total calculated as the patients with renal biopsy)		0.156
Focal	2 (66.7)	2 (12.5)	0 (0)	
Crescentic	1 (33.3)	11 (68.75)	9 (64.29)	
Sclerotic	0 (0)	2 (12.5)	4 (28.57)	
Mixed	0 (0)	1 (6.25)	1 (7.14)	
Treatment (*n* (%))				0.183
Glucocorticoids	4 (50)	3 (15.8)	4 (19.0)	
Glucocorticoids+CYC	4 (50)	10 (52.6)	6 (28.6)	
Glucocorticoids+CYC+PE	0 (0)	3 (15.8)	7 (33.3)	
Glucocorticoids+CYC+PE+RTX	0 (0)	3 (15.8)	4 (19.0)	

PVAS, Pediatric Vasculitis Activity Score; IF, immunofluorescence; CYC, cyclophosphamides; PE, plasma exchange; RTX, rituximab.

TABLE 4 | Multivariate analysis of risk factors associated with nonremission in 48 patients after remission-induction therapies.

Factors	*p*-value	OR value	95% CI
Women	0.544	1.737	0.292–10.325
Hypertension	0.002	19.574	3.036–126.219
Nephrotic-range proteinuria	0.658	1.598	0.200–12.751
eGFR <60 ml/min/1.73 m^2	0.001	28.020	3.786–207.364
PVAS scores	0.562	0.544	0.069–4.261
Age >11	0.833	0.847	0.181–3.958

PVAS, Pediatric Vasculitis Activity Score.

TABLE 5 | Analysis of risk predictors at diagnosis associated with progression to ESRD in follow-up.

Factors	Univariate analysis			Multivariate analysis		
	p-value	OR	95% CI	*p*-value	OR	95% CI
Women	0.767	0.869	0.344–2.196	0.879	1.094	0.344–3.484
Age >11	0.367	0.690	0.309–1.544	0.568	1.344	0.487–3.711
Hypertension	<0.001	9.675	3.208–29.18	0.001	13.12	2.995–57.45
Nephrotic proteinuria	0.028	2.596	1.107–6.086	1.000	1.000	0.350–2.856
eGFR <60 ml/min/1.73 m^2	0.012	6.374	1.493–27.21	0.013	9.597	1.625–56.67
PVAS score >11	0.004	8.593	1.999–36.93	0.598	1.640	0.261–10.33
PE	0.772	0.884	0.383–2.040	0.910	0.974	0.373–2.409

PVAS, Pediatric Vasculitis Activity Score; PE, plasma exchange; RTX, rituximab.

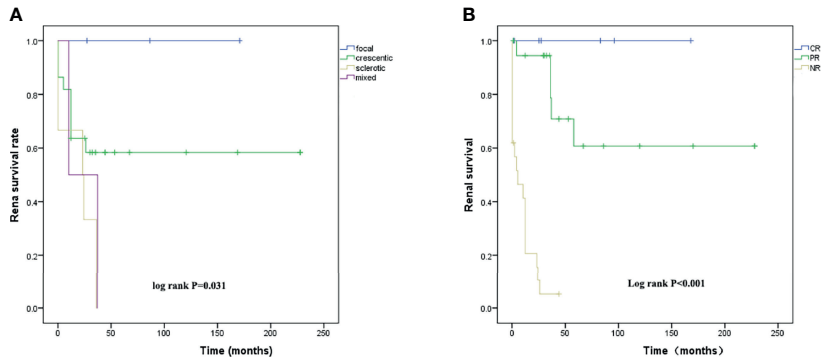

FIGURE 1 | **(A)** Renal survival analysis K-M curves of the time from diagnosis to ESRD or last follow-up in patients with different renal pathological subtypes and **(B)** in patients with different induction remission responses after 6-month treatment.

TABLE 6 | The clinical data at diagnosis and response to induction treatment in patients of a crescentic subtype with different renal outcomes at the endpoint.

	eGFR >90 ml/min/1.73 m^2	eGFR <15 ml/min/1.73 m^2	*p*-value
Women (*n*, %)	6 (75)	7 (78)	1.000
Age >11	12±2.8	8.6±2.7	0.022
Serum creatinine (μmol/L)	159.2±140.4	552.2±257.1	0.002
24 h urine protein (mg/24 h)	1,370.2±1,706	2,332.7;±2,335.1	0.353
PVAS score	11.5±4.8	13.1 ± 4.2	0.159
Hypertension (*n*, %)	4 (50%)	5 (56)	0.614
eGFR level (*n*, %)			0.001
eGFR >90 (ml/min/1.73 m^2)	3 (37.5%)	0 (0)	
eGFR = 60–90 (ml/min/1.73 m^2)	1 (12.5)	0 (0)	
eGFR = 30–60 (ml/min/1.73 m^2)	3 (37.5)	0 (0)	
eGFR = 15–30 (ml/min/1.73 m^2)	1 (12.5)	7 (78)	
eGFR <15 (ml/min/1.73 m^2)	0 (0)	2 (22)	
Treatment (*n*, %)			0.424
Glucocorticoids+CTX	7 (87.5)	5 (55.6)	
Glucocorticoids+CTX+PE	1 (12.5)	3 (33.3)	
Glucocorticoids+CTX+RTX	0 (0)	1 (11.1)	
Remission at 6-month (*n*, %)			<0.001
Complete remission	2 (25)	0 (0)	
Partial remission	6 (75)	1 (11.1)	
Nonremission	0 (0)	8 (88.9)	

PVAS, Pediatric Vasculitis Activity Score; CYC, cyclophosphamides; PE, plasma exchange; RTX, rituximab.

Our results also demonstrated that renal pathological patterns were significantly associated with long-term renal outcomes, as shown in adult AAV patients. There were studies even showing that renal pathological patterns affected the outcome more than baseline eGFR (27, 28). As in adults, those with a sclerotic subtype rapidly progressed to ESRD. Sclerotic lesions were thought to result not only from vasculitis but also from other factors, such as aging, atherosclerosis, dyslipidemia, and hypertension (9, 29). Patients with focal subtype showed a favorable renal outcome. Interestingly, the outcome of those with crescentic subtype turned out to see many variations, and whether they restored to normal eGFR levels or progressed to ESRD (CKD stage V) was significantly associated with baseline eGFR levels and with response to induction treatment. There were three patients with eGFR levels between 30 and 60 ml/min/1.73 m^2 and one patient with an eGFR level between 15 and 30 ml/min/1.73 m^2; they all finally returned to normal eGFR levels following a 6-month remission-induction treatment. These results demonstrated the importance of treatment responsiveness in affecting the outcome. Of course, the active lesions were more likely to be reversible if treated in a timely and effective manner (30). In addition to glucocorticoid and CYC, RTX was also proven to be as effective as CYC in remission-induction and relapse treatment of AAV (31, 32). Among seven serious AAV patients treated with RTX, three patients obtained a significant improvement in eGFR and proteinuria, which demonstrated the promising prospects of RTX in the treatment of pediatric patients with AAV.

The advantages of this study were based on the fact that it represented the largest pediatric cohort of AAV in Chinese children and provided actual clinicopathological features different from adults and children in the EU and North America. Secondly, our study demonstrated that eGFR <60 ml/

min/1.73 m^2 and hypertension at diagnosis were independent predictors for progression to ESRD. Moreover, the study particularly pointed out the importance of induction treatment responsiveness in affecting the outcome of AAV. Through multivariate logistic regression analysis, hypertension and eGFR <60 ml/min/1.73 m^2 at diagnosis were also considered risk factors associated with failure of induction therapies. Thus, these risk factors might affect the long-term renal outcomes by influencing the response to induction treatment. However, the limitations of this study lie mainly in its retrospective nature, and the total number of included cases is not large enough to allow further statistical analysis. In addition, since we included only hospitalized patients, a selection bias may exist in that some patients with mild AAV in the outpatient were omitted.

In conclusion, our study demonstrates that women, MPA, and crescentic subtypes are predominant in pediatric AAV in China. Initial renal failure (eGFR <60 ml/min/1.73 m^2), hypertension, sclerotic pathological pattern at diagnosis, and nonremission to induction treatment are predictors of poor long-term renal outcome. Apparently, AAV remains a rough challenge to the pediatric community.

DATA AVAILABILITY STATEMENT

The original contributions presented in the study are included in the article/**Supplementary Material**, further inquiries can be directed to the corresponding author/s.

ETHICS STATEMENT

The studies involving human participants were reviewed and approved by the Human Ethics Committee of Tongji Hospital, Tongji Medical College, Huazhong University of Science and Technology. Written informed consent to participate in this study was provided by the participants' legal guardian/next of kin.

AUTHOR CONTRIBUTIONS

All authors contributed to the intellectual content of this manuscript and approved the final manuscript as submitted. JY collected data, performed the statistical analysis, and drafted the manuscript with the help of YX, YY, LQZ, LWZ, XY, FY, YH, JP, YL, YXC, and JZ. HY, LQ, YZ, YC, TL, and JT were responsible for the renal pathological interpretation and patients' care. JZ interpreted the data and revised the article for important intellectual content. All authors have critically read and approved the manuscript.

FUNDING

This work was supported by a grant (No. 81873596) from the National Natural Science Foundation of China to JZ.

ACKNOWLEDGMENTS

We thank all patients and their families for participation in this study.

SUPPLEMENTARY MATERIAL

The Supplementary Material for this article can be found online at: https://www.frontiersin.org/articles/10.3389/fimmu.2022.857813/full#supplementary-material

REFERENCES

1. Jennette JC, Falk RJ, Bacon PA, Basu N, Cid MC, Ferrario F, et al. Revised International Chapel Hill Consensus Conference Nomenclature of Vasculitides. *Arthritis Rheum* (2013) 65(1):1–11. doi: 10.1002/art.37715
2. Calatroni M, Oliva E, Gianfreda D, Gregorini G, Allinovi M, Ramirez GA, et al. ANCA-Associated Vasculitis in Childhood: Recent Advances. *Ital J Pediatr* (2017) 43(1):46. doi: 10.1186/s13052-017-0364-x
3. Geetha D, Jefferson JA. ANCA-Associated Vasculitis: Core Curriculum 2020. *Am J Kidney Dis* (2020) 75(1):124–37. doi: 10.1053/j.ajkd.2019.04.031
4. Noone DG, Twilt M, Hayes WN, Thorner PS, Benseler S, Laxer RM, et al. The New Histopathologic Classification of ANCA-Associated GN and its Association With Renal Outcomes in Childhood. *Clin J Am Soc Nephrol* (2014) 9(10):1684–91. doi: 10.2215/CJN.01210214
5. Basu B, Mahapatra TKS, Mondal N. Favourable Renal Survival in Paediatric Microscopic Polyangiitis: Efficacy of a Novel Treatment Algorithm. *Nephrol Dialysis Transplant* (2015) 30(suppl 1):i113–8. doi: 10.1093/ndt/gfv016
6. Khalighi MA, Wang S, Henriksen KJ, Bock M, Keswani M, Chang A, et al. Pauci-Immune Glomerulonephritis in Children: A Clinicopathologic Study of 21 Patients. *Pediatr Nephrol* (2015) 30(6):953–9. doi: 10.1007/s00467-014-2970-9
7. Kouri AM, Andreoli SP. Clinical Presentation and Outcome of Pediatric ANCA-Associated Glomerulonephritis. *Pediatr Nephrol* (2017) 32(3):449–55. doi: 10.1007/s00467-016-3490-6
8. Ozcelik G, Sonmez HE, Sahin S, Ozagari A, Bayram MT, Cicek RY, et al. Clinical and Histopathological Prognostic Factors Affecting the Renal Outcomes in Childhood ANCA-Associated Vasculitis. *Pediatr Nephrol* (2019) 34(5):847–54. doi: 10.1007/s00467-018-4162-5
9. Calatroni M, Consonni F, Allinovi M, Bettiol A, Jawa N, Fiasella S, et al. Prognostic Factors and Long-Term Outcome With ANCA-Associated Kidney Vasculitis in Childhood. *Clin J Am Soc Nephrol* (2021) 16(7):1043–51. doi: 10.2215/CJN.19181220
10. Wu J, Pei Y, Rong L, Zhuang H, Zeng S, Chen L, et al. Clinicopathological Analysis of 34 Cases of Primary Antineutrophil Cytoplasmic Antibody-Associated Vasculitis in Chinese Children. *Front Pediatr* (2021) 9:656307. doi: 10.3389/fped.2021.656307
11. Sacri AS, Chambaraud T, Ranchin B, Florkin B, See H, Decramer S, et al. Clinical Characteristics and Outcomes of Childhood-Onset ANCA-Associated Vasculitis: A French Nationwide Study. *Nephrol Dial Transplant* (2015) 30 Suppl 1:i104–12. doi: 10.1093/ndt/gfv011
12. Mukhtyar C, Guillevin L, Cid MC, Dasgupta B, Groot K, Gross W, et al. EULAR-Recommendations-Fpr-The-Management-Of-Primary-Small-And-Medium-Vessel-Vasculitis. *Ann Rheum Dis* (2009) 68:310–7. doi: 10.1136/ard.2008.088096
13. Dolezalova P, Price-Kuehne FE, Ozen S, Benseler SM, Cabral DA, Anton J, et al. Disease Activity Assessment in Childhood Vasculitis: Development and Preliminary Validation of the Paediatric Vasculitis Activity Score (PVAS). *Ann Rheum Dis* (2013) 72(10):1628–33. doi: 10.1136/annrheumdis-2012-202111

14. Berden AE, Ferrario F, Hagen EC, Jayne DR, Jennette JC, Joh K, et al. Histopathologic Classification of ANCA-Associated Glomerulonephritis. *J Am Soc Nephrol* (2010) 21(10):1628–36. doi: 10.1681/ASN.2010050477
15. Kronbichler A, Shin JI, Lee KH, Nakagomi D, Quintana LF, Busch M, et al. Clinical Associations of Renal Involvement in ANCA-Associated Vasculitis. *Autoimmun Rev* (2020) 19(4):102495. doi: 10.1016/j.autrev.2020.102495
16. Morishita KA, Moorthy LN, Lubieniecka JM, Twilt M, Yeung RSM, Toth MB, et al. Early Outcomes in Children With Antineutrophil Cytoplasmic Antibody-Associated Vasculitis. *Arthritis Rheumatol* (2017) 69(7):1470–9. doi: 10.1002/art.40112
17. Cabral DA, Canter DL, Muscal E, Nanda K, Wahezi DM, Spalding SJ, et al. Comparing Presenting Clinical Features in 48 Children With Microscopic Polyangiitis to 183 Children Who Have Granulomatosis With Polyangiitis (Wegener's): An ARChiVe Cohort Study. *Arthritis Rheumatol* (2016) 68 (10):2514–26. doi: 10.1002/art.39729
18. Binda V, Moroni G, Messa P. ANCA-Associated Vasculitis With Renal Involvement. *J Nephrol* (2018) 31(2):197–208. doi: 10.1007/s40620-017-0412-z
19. Wu T, Zhong Y, Zhou Y, Chen J, Yang Y, Tang R, et al. Clinical Characteristics and Prognosis in 269 Patients With Antineutrophil Cytoplasimc Antibody Associated Vasculitis. *Zhong Nan Da Xue Xue Bao Yi Xue Ban* (2020) 45(8):916–22. doi: 10.11817/j.issn.1672-7347.2020.190436
20. Yoo J, Kim J, Ahn S, Jung M, Song J, Park Y, et al. Clinical and Prognostic Features of Korean Patients With MPO-ANCA, PR3-ANCA, and ANCA-Negative Vascylitis. *Clin Exp Rheumatol* (2017) 35:S111–8.
21. Fujimoto S, Watts RA, Kobayashi S, Suzuki K, Jayne DR, Scott DG, et al. Comparison of the Epidemiology of Anti-Neutrophil Cytoplasmic Antibody-Associated Vasculitis Between Japan and the U.K. *Rheumatol (Oxf)* (2011) 50 (10):1916–20. doi: 10.1093/rheumatology/ker205
22. Flossmann O, Berden A, de Groot K, Hagen C, Harper L, Heijl C, et al. Long-Term Patient Survival in ANCA-Associated Vasculitis. *Ann Rheum Dis* (2011) 70(3):488–94. doi: 10.1136/ard.2010.137778
23. Ford SL, Polkinghorne KR, Longano A, Dowling J, Dayan S, Kerr PG, et al. Histopathologic and Clinical Predictors of Kidney Outcomes in ANCA-Associated Vasculitis. *Am J Kidney Dis* (2014) 63(2):227–35. doi: 10.1053/j.ajkd.2013.08.025
24. Bai YH, Li ZY, Chang DY, Chen M, Kallenberg CG, Zhao MH. The BVAS is an Independent Predictor of Cardiovascular Events and Cardiovascular Disease-Related Mortality in Patients With ANCA-Associated Vasculitis: A Study of 504 Cases in a Single Chinese Center. *Semin Arthritis Rheum* (2018) 47(4):524–9. doi: 10.1016/j.semarthrit.2017.07.004
25. Yoo J, Ahn SS, Jung SM, Song JJ, Park YB, Lee SW. Delta Neutrophil Index Is Associated With Vasculitis Activity and Risk of Relapse in ANCA-Associated Vasculitis. *Yonsei Med J* (2018) 59(3):397–405. doi: 10.3349/ymj.2018.59.3.397
26. Zhang Z, Liu S, Guo L, Wang L, Wu Q, Zheng W, et al. Clinical Characteristics of Peripheral Neuropathy in Eosinophilic Granulomatosis With Polyangiitis: A Retrospective Single-Center Study in China. *J Immunol Res 2020* (2020) 1–10. doi: 10.1155/2020/3530768
27. de Lind van Wijngaarden RA, Hauer HA, Wolterbeek R, Jayne DR, Gaskin G, Rasmussen N, et al. Clinical and Histologic Determinants of Renal Outcome in ANCA-Associated Vasculitis: A Prospective Analysis of 100 Patients With Severe Renal Involvement. *J Am Soc Nephrol* (2006) 17(8):2264–74. doi: 10.1681/ASN.2005080870
28. Chen YX, Xu J, Pan XX, Shen PY, Li X, Ren H, et al. Histopathological Classification and Renal Outcome in Patients With Antineutrophil Cytoplasmic Antibodies-Associated Renal Vasculitis: A Study of 186 Patients and Metaanalysis. *J Rheumatol* (2017) 44(3):304–13. doi: 10.3899/jrheum.160866
29. Menez S, Hruskova Z, Scott J, Cormican S, Chen M, Salama AD, et al. Predictors of Renal Outcomes in Sclerotic Class Anti-Neutrophil Cytoplasmic Antibody Glomerulonephritis. *Am J Nephrol* (2018) 48(6):465–71. doi: 10.1159/000494840
30. Hauer HA, Bajema IM, van Houwelingen HC, Ferrario F, Noël LH, Waldherr R, et al. Determinants of Outcome in ANCA-Associated Glomerulonephritis: A Prospective Clinico-Histopathological Analysis of 96 Patients. *Kidney Int* (2002) 62:1732–42. doi: 10.1046/j.1523-1755.2002.00605.x
31. Jones RB, Tervaert JW, Hauser T, Seo P. Rituximab Versus Cyclophosphamide for ANCA-Associated Vasculitis. *N Engl J* (2010) 363:221–32. doi: 10.1056/NEJMoa0909169
32. Jones RB, Luqmani R, Savage C, van Paassen P, Westman K. Rituximab Versus Cyclophosphamide in ANCA-Associated Renal Vasculitis. *N Engl J Med* (2010) 363:211–20. doi: 10.1056/NEJMoa0909169

Conflict of Interest: The authors declare that the research was conducted in the absence of any commercial or financial relationships that could be construed as a potential conflict of interest.

frontiers | Frontiers in Immunology

REVIEW
published: 22 April 2022
doi: 10.3389/fimmu.2022.809590

β2-Integrins – Regulatory and Executive Bridges in the Signaling Network Controlling Leukocyte Trafficking and Migration

Carla Guenther[1,2,3]*

[1] Department of Veterinary Biosciences, University of Helsinki, Helsinki, Finland, [2] Department of Molecular Immunology, Research Institute for Microbial Diseases, Osaka University, Osaka, Japan, [3] Laboratory of Molecular Immunology, Immunology Frontier Research Center, Osaka University, Osaka, Japan

Leukocyte trafficking is an essential process of immunity, occurring as leukocytes travel within the bloodstream and as leukocyte migration within tissues. While it is now established that leukocytes can utilize the mesenchymal migration mode or amoeboid migration mode, differences in the migratory behavior of leukocyte subclasses and how these are realized on a molecular level in each subclass is not fully understood. To outline these differences, first migration modes and their dependence on parameters of the extracellular environments will be explained, as well as the intracellular molecular machinery that powers migration in general. Extracellular parameters are detected by adhesion receptors such as integrins. β2-integrins are surface receptors exclusively expressed on leukocytes and are essential for leukocytes exiting the bloodstream, as well as in mesenchymal migration modes, however, integrins are dispensable for the amoeboid migration mode. Additionally, the balance of different RhoGTPases – which are downstream of surface receptor signaling, including integrins – mediate formation of membrane structures as well as actin dynamics. Individual leukocyte subpopulations have been shown to express distinct RhoGTPase profiles along with their differences in migration behavior, which will be outlined. Emerging aspects of leukocyte migration include signal transduction from integrins *via* actin to the nucleus that regulates DNA status, gene expression profiles and ultimately leukocyte migratory phenotypes, as well as altered leukocyte migration in tumors, which will be touched upon.

Keywords: leukocyte migration, β2-integrins, RhoGTPases, epigenetics, actin tread milling, amoeboid migration, LFA-1

OPEN ACCESS

Edited by:
Hao Sun,
University of California, San Diego, United States

Reviewed by:
Ralph Böttcher,
Max Planck Institute of Biochemistry, Germany
Myriam Chimen,
University of Birmingham, United Kingdom

***Correspondence:**
Carla Guenther
carla.guenther@arcor.de

Specialty section:
This article was submitted to Autoimmune and Autoinflammatory Disorders, a section of the journal Frontiers in Immunology

Received: *05 November 2021*
Accepted: *11 March 2022*
Published: *22 April 2022*

Citation:
Guenther C (2022) β2-Integrins – Regulatory and Executive Bridges in the Signaling Network Controlling Leukocyte Trafficking and Migration. Front. Immunol. 13:809590. doi: 10.3389/fimmu.2022.809590

INTRODUCTION

Leukocyte trafficking is a multifaceted process that not only encompasses the cell adhesion cascade, transmigration and migration through tissues, but also gains further depth by the fact that leukocytes can use the mesenchymal migration mode as well as a unique amoeboid migration mode that sets them apart from other cell types. Additionally, our understanding of leukocyte

migration is rapidly evolving to the extent that not differentiating between these aspects – be it transmigration, crawling on 2D or migration through 3D environments – and instead refering to them in equal fashion as 'leukocyte migration' hinders us from appreciating the true complexity of these processes. The importance of this is heightened by the fact that leukocyte subpopulations show distinct migratory behavior across all these aspects. Additionally, while it is now appreciated that environmental parameters dictate which migration mode is possible for all leukocytes and these parameters are integrated into the cell by adhesion receptors such as β2-integrins, it is becoming clear that how the appropriate migration modes are executed is down to a distinct combination of β2-integrin downstream components which are, in turn, acting uniquely and are expressed in different leukocyte populations. It is clear that our collective understanding of leukocyte migration is just scratching the surface and this is due to several factors. One hindering factor is that not all aspects of leukocyte migration are researched to the same degree. Transwell migration assays represent the vast majority of assays used to study leukocyte migration; this means we have much more data on transmigration than on migration in tissues. Additionally, the 2D or 3D migration assays which are carried out often rely on single-protein coatings or matrices, respectively, and this fails to represent the complexity of living endothelium and tissues. Furthermore, the structural organization of proteins in bundles or fibers is neglected, just as is their stiffness and elasticity. Finally, leukocyte subpopulations such as neutrophils, macrophages and T-cells have been studied most, while eosinophils and basophils have been almost entirely ignored. This review seeks to outline some of the field's complexity and why the aforementioned aspects of the environment are important, in the context of β2-integrins, which are essential for the leukocyte adhesion cascade.

THE LEUKOCYTE ADHESION CASCADE

The majority of leukocyte trafficking occurs in the bloodstream, in which leukocytes – typically T- and B-cells, neutrophils, monocytes, eosinophils and basophils – are passively carried by the bloodstream close to sites of infections. In response to infections, the endothelium lining the blood vessels closest to the site of infection expresses chemokines and adhesion receptor ligands which initiate and mediate the cell adhesion cascade. This cascade is the process through which leukocytes leave the bloodstream and extravasate into the tissue. In this multistep process, leukocytes first tether on the endothelium, followed by fast and slow rolling along the vessel wall until the leukocyte is arrested on the endothelium (1, 2). Leukocytes then typically begin to spread and crawl across the endothelium (3). The distinctive steps in the adhesion cascade are: step 1 – tethering and fast rolling, step 2 – slow rolling and arrest, step 3 – spreading and crawling, step 4 – transmigration. The adhesion cascade step of crawling across the endothelium has been termed locomotion (3). This process is depicted in **Figure 1** and has been reviewed multiple times in detail [for example (4)]. Selectins are the first adhesion receptors mediating tethering and fast rolling during which their activity typically overlaps with β2-integrins (4). β2-integrins are especially crucial for the fast and slow rolling, cell arrest, and spreading and crawling steps (4). They have been identified as mechanoreceptors (5) and therefore likely play a role in probing the endothelium for points of exit as well. Further detail in regards to involvement of each adhesion receptor at each step and their typical ligands are depicted and described in **Figure 1**.

β2-integrins are a group of essential adhesion receptors, consisting of CD11a/CD18 (LFA-1, αLβ2), CD11b/CD18 (MAC1, αMβ2), CD11c/CD18 (αXβ2), and CD11d/CD18 (αDβ2) (6). Leukocytes express several different types of integrins (7) (**Table 1** and **Figure 2**), and they express β2- and β7-integrins as the only cells [β2-integrins are also expressed on platelets (28)]. Furthermore, in most circulating leukocytes β2-integrins are the integrin class expressed in the highest amounts (13). β2-integrins are differently expressed on different leukocytes and they differ in terms of ligand binding. CD11a and CD11d bind limited ligands (CD11a/ICAMs, CD11d/ICAM-3, VCAM-1), while CD11c and CD11b form diverse receptor–ligand interactions with more than 40 identified ligands. β2-integrins have been shown to be essential for pro- as well as anti-inflammatory processes (19, 29–31).

Integrins can signal from the inside to the outside, which is especially important during the cell adhesion cascade. A central aspect of such signaling is typically conformational changes of integrins, which in turn regulate the individual bond strength between individual integrin heterodimers and ligands (30, 32). Integrins can only bind ligands if they are in an active – meaning open, extended (high affinity) conformation (33) (depicted in **Figure 3**). A 'bent', inactive integrin conformation (33) predominates when leukocytes travel through the bloodstream to prevent cell aggregation (19). For example, a 9:1 ratio between inactive and active conformations was established for a mutant form of CD11b in the absence of ligands (34, 35). When leukocytes bump into endothelial cells producing chemokines and expressing selectin ligands, chemokine-receptor and selectin engagement initiates the binding of talin and kindlin to integrin cytoplasmic tails (36, 37). This leads to integrin switching from the bent into the extended conformation, akin to a switch blade, and is an example of integrin inside-out signaling. This conformational switch reveals ligand binding sites in the extracellular domain in parts that were facing the cell membrane in the bent conformation (38). At the same time, the conformational switch leads to integrin cytoplasmic tail separation which enables the binding of further interaction partners like tensin and vinculin (39).

LEUKOCYTE MIGRATION

Transmigration

During crawling and spreading, leukocytes probe the endothelium for suitable sites of exit, through which they transmigrate. Such sites of exit can be cell–cell junctions, but they also travel through endothelial cell bodies (1, 4, 40, 41). Monocytes have been shown to typically choose gap-junctions to transmigrate. If crawling/

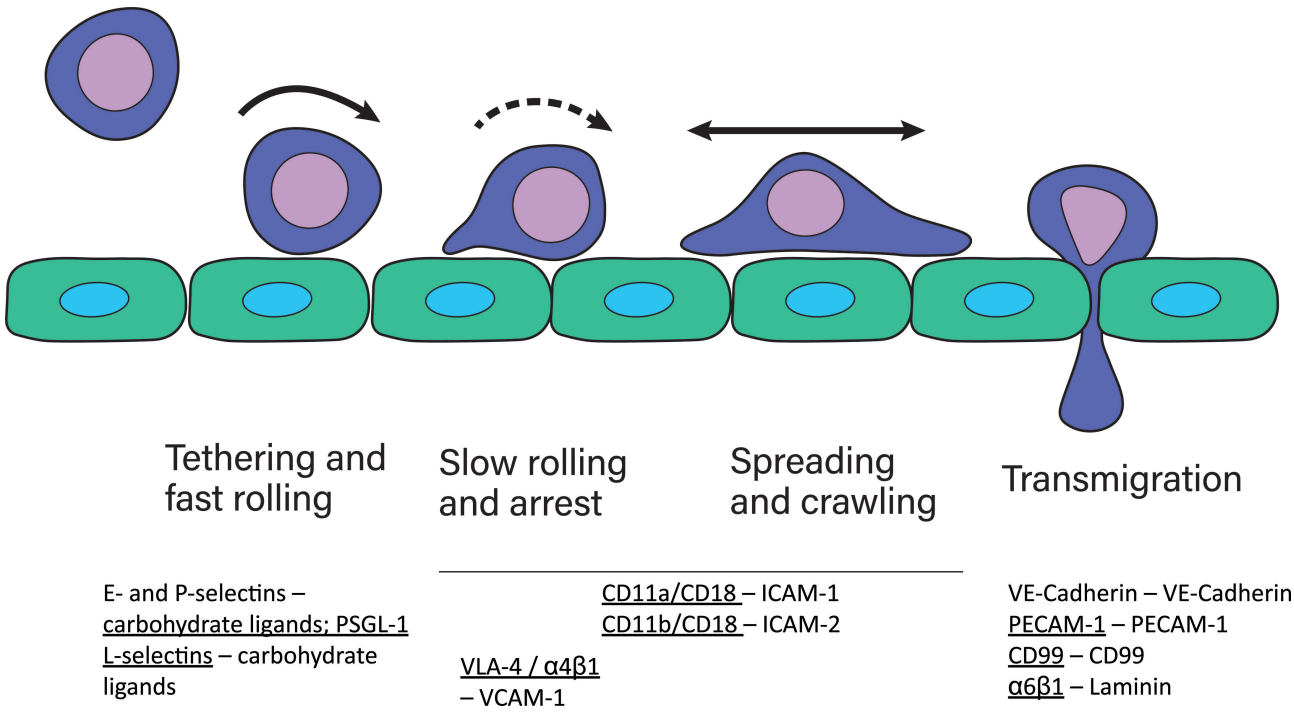

FIGURE 1 | The cell adhesion cascade. During adhesion to and extravasation through the endothelium, leukocytes undergo several steps, namely fast rolling and tethering, slow rolling and arrest, spreading and crawling and lastly transmigration. These steps are mediated by several different adhesion receptors expressed by leukocytes, indicated by underscore, and the endothelium (2). P-selectins and E-selectins expressed by the endothelium bind to their carbohydrate ligands on leukocytes during fast rolling. Leukocytes express L-selectins, which bind to ligands on the endothelium during fast rolling. The most well known selectin ligand is P-selectin glycoprotein ligand-1 (PSGL-1). Selectin-ligand binding results in integrin activation in leukocytes, which then mediates slow rolling, arrest, spreading and crawling. During transmigration, several homophilic adhesion receptors, including VE-cadherins important for tight junctions between endothelial cells, and CD99 and PECAM-1 are expressed by endothelial cells and leukocytes. Additionally, leukocytes express α6β1 integrins that bind to laminin.

locomotion is disabled, for example due to CD11b/CD18 knockdown, neutrophils transmigrate transcellularly, meaning through endothelial cells (3). During transmigration, leukocytes change their integrin expression profiles, for example α6β1-integrin is upregulated, which mediates transmigration (4). Transmigration is the migration process modeled best in transwell/Boyden chamber assays (42). This assay consists of two champers, one filled with normal media and one with media including chemokines. These chambers are separated by a porous membrane, which creates a chemokine gradient (43). However, these assays fail to present leukocyte–endothelial cell interactions as well as gap junctions. Based on the number of papers tagged with 'transwell leukocyte migration' vs '2D leukocyte migration' or '3D leukocyte migration' in Pubmed to date, transwell assays are the most used assay to investigate leukocyte migration, however, data generated with this model is often referred to as 'migration' or 'chemotaxis' instead of 'transmigration'.

Leukocytes Navigate Different Microenvironments During Migration

After transmigrating, leukocytes proceed to actively migrate through tissues towards the site of infection, guided by chemokines. This means all migrating leukocytes navigate numerous tissues that present different microenvironments and necessitate different migration modes. This is especially true for leukocytes that migrate long distances. Leukocytes, that have transmigrated from the bloodstream, however typically migrate relatively short distances. For example, the typical maximum distance of (tissue) cells to their nearest blood vessel is 100 µm and rarely exceeds 200 µm (44), and leukocytes likely don't migrate into other tissues or microenvironments. Leukocytes that actively migrate long distances across several microenvironments are typically antigen–presenting cells, such as dendritic cells, neutrophils and macrophages (45, 46), which migrate through the tissues towards and transmigrate into the lymph system. The lymph system is closely related to and connected to the blood system, however, lymph flow rates are much lower. For example, in mice the blood flow rate in microvessels (45.8 µm diameter) in the retina can be up to 1.55 µl/min (47), while in the lymph system a flow rate of 0.3 µl/h has been measured (48). The slow flow rates necessitate the active migration of leukocytes to the nearest draining lymph node to present antigens. Besides antigen presenting cells, high numbers of T-cells and low numbers of monocytes, all types of granulocytes, and B-cells have also been found in afferent

TABLE 1 | Leukocyte Integrins And Their Ligands, Expanded On From (8).

Leukocyte	Integrin name	Ligands (most important)
eosinophils	CD11a/CD18 (αLβ2)	ICAM-1, -2, -3, -5
	CD11b/CD18 (αMβ2) (9)	iC3b (11), fibrinogen, heparin, many others (40+)
	CD11d/CD18 (αDβ2)	ICAM-3, VCAM-1
	α4β1 (VLA-4)	VCAM-1, fibronectin
	α6β1 (10)	Laminin
	α4β7 (10)	MAdCAM-1, fibronectin
basophils	CD11a/CD18 (αLβ2)	ICAM-1, -2, -3, -5
	CD11b/CD18 (αMβ2) (9)	iC3b (11), fibrinogen, heparin, many others (40+)
	CD11d/CD18 (αDβ2)	ICAM-3, VCAM-1
	β1 (12)	
	α4β1 (12)	VCAM-1, fibronectin
	α5β1 (12)	Fibronectin
	β3 (12)	
	β4 (12)	
neutrophils	CD11a/CD18 (αLβ2)	ICAM-1, -2, -3, -5
	CD11b/CD18 (αMβ2)	iC3b (11), fibrinogen, heparin, many others (40+)
	CD11d/CD18 (αDβ2)	ICAM-3, VCAM-1
	α2β1 (induced expression) (13)	Collagen, laminin (13)
	α3β1 (induced expression) (13)	Collagen, laminin, fibronectin, tenascin (13)/RGD
	α4β1 (induced expression) (13)	VCAM-1, fibronectin, expression decreases during maturation (14)
	α5β1 (induced expression) (13)	Fibronectin
	α6β1 (induced expression) (13)	Laminin
	α9β1 (induced expression) (13)	VCAM-1, tenascin
	αVβ3 (13)	Arg-Gly-Asp (RGD) (15)
monocytes	CD11a/CD18 (αLβ2)	ICAM-1, -2, -3, -5
	CD11b/CD18 (αMβ2)	iC3b (11), fibrinogen, heparin, many others (40+)
	CD11c/CD18 (αXβ2)	iC3b (11), fibrinogen, heparin, many others
	CD11d/CD18 (αDβ2)	ICAM-3, VCAM-1 (16)
	α4β1	VCAM-1, fibronectin
	α4β7	MAdCAM-1, fibronectin
	α1β1	Collagen
	α2β1	Collagen
	α5β1	Fibronectin
	α6β1	Laminin
macrophages	CD11a/CD18 (αLβ2)	ICAM-1, -2, -3, -5
	CD11b/CD18 (αMβ2)	iC3b (11), fibrinogen, heparin, many others (40+)
	CD11c/CD18 (αXβ2)	iC3b (11), fibrinogen, heparin, many others
	CD11d/CD18 (αDβ2)	ICAM-3, VCAM-1 (16)
	αVβ3 (7)	RGD (15)
dendritic cells	CD11a/CD18 (αLβ2)	ICAM-1, -2, -3, -5
	CD11b/CD18 (αMβ2)	iC3b (11), fibrinogen, heparin, many others (40+)
	CD11c/CD18 (αXβ2)	iC3b (11), fibrinogen, heparin, many others
	CD11d/CD18 (αDβ2) (17)	ICAM-3, VCAM-1 (16)
	α4β1 (18) *	VCAM-1, fibronectin
	α5β1 (18) *	Fibronectin
	αVβ1 (18) *	Vitronectin (15)
	αVβ3 (18) *	RGD (15)
	α4β7 (18) *	MAdCAM-1, fibronectin
	*subunit expression *via* FC	
lymphocytes (general)	CD11a/CD18 (αLβ2)	ICAM-1, -2, -3, -5
	α4β1	VCAM-1, fibronectin
	α4β7	MAdCAM-1, fibronectin
natural killer cells	CD11a/CD18 (αLβ2)	ICAM-1, -2, -3, -5
	CD11b/CD18 (αMβ2)	iC3b (11), fibrinogen, heparin, many others (40+)
	CD11c/CD18 (αXβ2)	iC3b (11), fibrinogen, heparin, many others
	α4β7	MAdCAM-1, fibronectin
	α4β1	VCAM-1, fibronectin

(Continued)

TABLE 1 | Continued

Leukocyte	Integrin name	Ligands (most important)
B-cells	CD11a/CD18 (αLβ2)	ICAM-1, -2, -3, -5
	α4β1	VCAM-1, fibronectin
	α4β7	MAdCAM-1, fibronectin
	α1β1	Collagen
	α2β1	Collagen
T-cells	CD11a/CD18 (αLβ2)	ICAM-1, -2, -3, -5
	α4β1	VCAM-1, fibronectin
	α4β7	MAdCAM-1, fibronectin
	α5β1	Fibronectin
	α6β1	Laminin
small fraction circulating T-cells	CD11a/CD18 (αLβ2)	ICAM-1, -2, -3, -5
	CD11d/CD18 (αDβ2)	ICAM-3, VCAM-1 (16)
	α4β1	VCAM-1, fibronectin
	α4β7	MAdCAM-1, fibronectin
	α5β1	Fibronectin
	α6β1	Laminin
intra-epithelial T-cells	CD11a/CD18 (αLβ2)	ICAM-1, -2, -3, -5
	α4β1	VCAM-1, fibronectin
	α4β7	MAdCAM-1, fibronectin
	αEβ7	E-cadherin
long-term activated T-cells	CD11a/CD18 (αLβ2)	ICAM-1, -2, -3, -5
	α4β1	VCAM-1, fibronectin
	α4β7	MAdCAM-1, fibronectin
	α1β1	Collagen
	α2β1	Collagen
mast cells	CD11a/CD18 (αLβ2)	ICAM-1, -2, -3, -5
	CD11b/CD18 (αMβ2) (19)	iC3b (11), fibrinogen, heparin, many others (40+)
	α4β1 (20)	VCAM-1, fibronectin
	α4β7 (21)	MAdCAM-1, fibronectin
	αVβ6 (22)	tenascin, fibronectin (23)
	α2β3 (24)	fibrinogen
microglia	CD11a/CD18 (αLβ2)	ICAM-1, -2, -3, -5
	CD11b/CD18 (αMβ2) (25)	iC3b (11), fibrinogen, heparin, many others (40+)
	CD11c * (26)	iC3b (11), fibrinogen, heparin, many others
	CD11d * (26)	ICAM-3, VCAM-1 (273)
	α1 subunit * (26)	
	α2 subunit * (26)	
	α2b subunit * (26)	
	α3 subunit * (26)	
	α5 subunit * (26)	
	α6 subunit * (26)	
	α7 subunit * (26)	
	α8 subunit * (26)	
	α9 subunit * (26)	
	α11 subunit * (26)	
	β1 subunit * (26)	
	β3 subunit * (26)	
	β4 subunit * (26)	
	β5 subunit * (26)	
	β7 subunit * (26)	
	β8 subunit * (26)	
	*subunit expression *via* RNA-sequencing, positive glia-brain_log fold change	

Integrins expressed by leukocytes and their ligands sorted by leukocyte type.

lymph vessels (49–53), however, it is unclear how much active migration is involved in the presence of these leukocytes. Additionally, mast cells migrate from the skin to lymph nodes after UV exposure (54).

The most obvious and most acknowledged difference in the microenvironments that leukocytes migrate through is dimensionality. Crawling on the endothelium of blood- or lymph vessels happens in 2D environments (4, 55) and

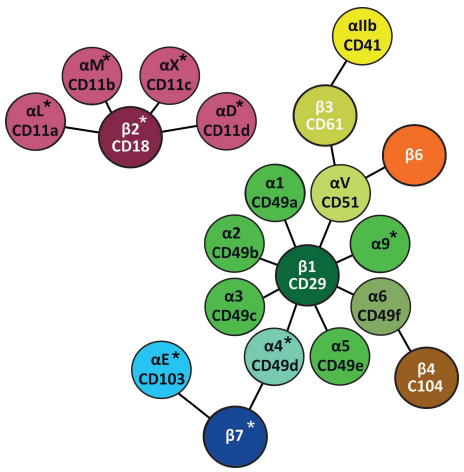

FIGURE 2 | Leukocyte integrins. Leukocyte integrins arranged around their β chains. α and β chains marked with * are specific for leukocytes (27), while platelets also express β2-integrins (28).

migration through tissues happens in 3D environments (56). While direct *in vivo* microscopy has shed much light on migratory processes (57, 58), the molecular mechanisms are often investigated using *in vitro* models. 2D migration is often modeled in assays using Zigmond or Dunn chambers, which involves two or three tissue plastic chambers, one or two of which are filled with media containing chemokines and one without chemokines to establish a chemokine gradient (59). Since 2D migration *in vivo* typically happens during crawling on the endothelium (4, 55), leukocyte–endothelial cell interactions are neglected in these models as are shear forces from the bloodstream.

3D migration is typically investigated using collagen or matrigel matrices in which cells are embedded (60). These matrices can be sandwiched between chambers of media with different initial chemokine concentrations, establishing a chemokine gradient. One example of a commercially-available setup is 'μ-Slides Chemotaxis' by ibidi (59). Additionally gel matrices can be set atop transwells to first model 3D migration and then transmigration (61), however, direct observation of 3D migration would be difficult. The downside of collagen and matrigel matrices is that they fail to replicate the complexity of tissues, be it in structure or in the variety of components. Cancer spheroids are used to model leukocyte invasion into tumors (62). These are often limited to cancer cells and fail to account for the stroma that support cancer progression. *Ex vivo* models are also used, in which mice ears are utilized that allow direct observation by microscopy of fluorescently labeled leukocytes (63). Mice ears offer few specific tissue environments for leukocytes to migrate in and would not be comparable to other tissues and organs.

Leukocyte Migration Modes

On 2D surfaces such as the endothelium of blood and lymph vessels (55), leukocytes use the mesenchymal migration mode, which is heavily dependent on integrins. Monocyte crawling on the endothelium of blood vessels is particularly dependent on CD11b/CD18 and ligand ICAM-1 (3, 64).

The molecular mechanism of the mesenchymal migration mode is the following: Integrins establish adhesion sites at the edge of the cell in the direction the cell is migrating. At this leading edge, lamellipodia are formed, that contain adhesion receptors, which bind ligands and transduce pulling forces (65). The cell then pulls its body towards this adhesion site. Meanwhile, at the cell rear the adhesion sites are broken and recycled to the front. The force required for the cell's movement is generated by the actin filament treadmill. This treadmill consists of actin polymerization at the leading cell edge and actin depolymerization at the cell rear (66–68). Actin polymerization ultimately generates power by pushing against elastic proteins that mediate the force by unbending at the cell front (69). The actin network as a whole presses against the cell's leading edge and the membrane that forms the lamellipodia containing the adhesion receptors (65).

Leukocytes migrate differently in 3D. In particular, dendritic cells (during homeostasis) (18, 53) and neutrophils (70) have been shown to use an amoeboid migration mode independent of integrins. So instead of the actin treadmill, this mode is facilitated by actin polymerization and squeezing and pushing (18). In a groundbreaking study, Lämmermann et al. knocked down all integrins in dendritic cells and proved that this migration mode is independent of integrin-mediated adhesion (18). Instead of lamellipodia, such migrating cells form blebs that do not strongly adhere or pull on the substrate (18, 71–73).

Mechanistically, this migration mode is powered by myosin II filaments sliding along actin filaments and thereby generating contractile forces (65). These contractile forces are present in the cell's rear and push the cytoplasmic fluid (74), as well as move the cell body (71) forward. At a molecular level, actin and myosin II form the actomyosin complex. In this complex, myosin is bound and travels along actin filaments in an ATP-dependent manner. Myosin travels by binding to consecutive actin binding sites further along the actin filament and in this manner generates force (75, 76). Consecutive binding and detachment in turn is dependent on conformational changes that induce rotation of myosin's motor protein structures that lead to the 'power stroke'. The power stroke signifies myosin changing from one actin binding site to another (75). Both migration modes are depicted in **Figure 4**.

The regulation of the two different cell migration modes occurs by a combination of both intracellular mechanisms and sensed extracellular parameters. Intracellularly, cell migration modes are regulated by cell shape and adhesiveness. These processes in turn are regulated by the balance of Ras homologous A (RhoA), Ras-related C3 botulinum toxin substrate (Rac) proteins and cell division cycle 42 (Cdc42), which are small GTPases central to actin remodeling dynamics and are characterized further below.

Extracellular parameters are sensed by integrins. In order to function properly, integrins are typically located at the edges of filopodia and lamellipodia, which are organized membrane structures that T-cells have been shown to use to navigate the extracellular matrix (ECM) (78), a mechanism most likely shared

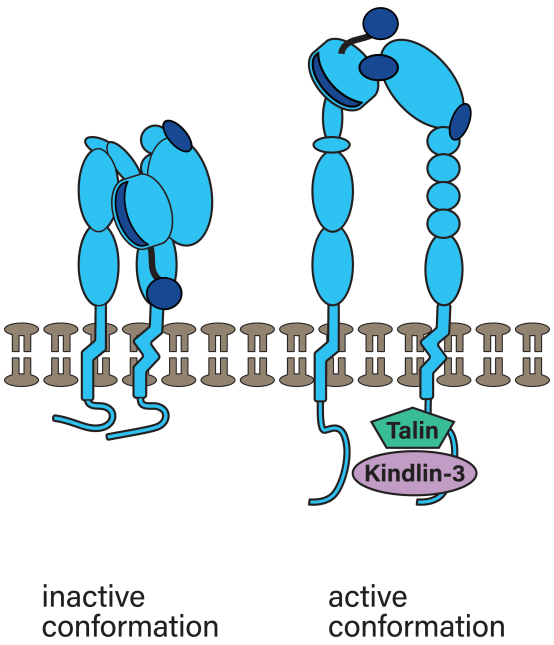

FIGURE 3 | Integrin conformation. In leukocytes traveling through the bloodstream, in absence of ligands, 90% of integrins are in the bent inactive conformation, depicted on the left. Inside-out signaling as a result of chemokine receptor/ligand and selectin/ligand binding during fast rolling results in talin and kindlin-3 binding to β chains which results in unbending and changing to the active conformation (right). The unbending results in ligand binding sites being revealed.

by all leukocytes (depicted in **Figure 5**). Filopodia are highly dynamic, finger-like protrusions containing parallel bundles of filamentous actin (F-actin) (79). The lamellipodia is a flat membrane protrusion at the leading cell edge, mainly consisting of F-actin, and the persistence of the lamellipodia is important for directionality during cell migration (80). Lamellipodia formation is associated with the mesenchymal migration mode (81). The area directly behind the lamellipodia is termed the lamella and is also relatively flat but contains myosin II (82–84). The lamellipodia has been proposed to be dispensable for cell migration, while the lamella is essential in epithelial cell migration (84). The cell rear of migrating cells is called the uropod. Migrating leukocytes form pseudopodial protrusions (membrane structures that facilitate material uptake) at the leading edge during amoeboid migration (85). Macrophages, dendritic cells and neutrophils form podosomes, which are actin-rich membrane protrusions used to degrade the ECM (86). Additionally, leukocytes form membrane blebs during amoeboid migration modes through which they push into the ECM and generate anchoring stresses, as well as shear stress at bleb protrusions (81). Amoeboid migrating neutrophils in a zebrafish model have been found to form knobs, as the beginning of long trailing extensions that undergo dynamic retractions at the cell rear (87). However, it is not clear what kind of proteins are present in these trailing extensions and what function they serve.

Extracellular matrix parameters that regulate migratory modes include ligand availability (for adhesion receptors), density, stiffness, elasticity and pore size. Of these parameters, pore size is a critical factor. Pores that are many times larger than cells render matrices into essentially 2D surfaces and thereby prevent leukocytes from utilizing the 3D migration mode. Pores that are many times smaller than cells block cell migration (71, 88). The nucleus is a major obstacle in leukocyte migration because it is the stiffest and largest organelle (89, 90), and if a cell is unable to move its nucleus through a pore, it has to find a way around (91–93). In order to efficiently navigate ECM environments, leukocytes use their nuclei as mechanical force sensors to scan their environment for adequate pore sizes (94). Leukocytes can further use their nuclei to push ECM components such as collagen apart, and test ECM qualities like stiffness and elasticity, which sets them apart from other migrating cells, that typically drag their nuclei behind (71, 88, 95, 96). Stiffness has been shown to guide cell migration towards stiffer matrices and this process is called durotaxis (71, 88, 95). Elasticity is closely linked to stiffness. Adhesion receptor availability dictates which migration mode can be used. Integrin ligand availability is critical for the mesenchymal migration mode, which is powered by pushing filaments, causing the membrane to protrude (97). This can only happen if there is actin retrograde flow and this in turn is dependent on a counter force such as integrin engagement (77, 97). Dependent on integrin or adhesion receptor ligand availability, dendritic cells switch from adhesion-dependent to independent modes (97). This is probably some of the most direct evidence regarding how integrins regulate migration modes as engagement of the integrin–actin clutch translates to protrusion, whereas disengagement of this clutch leads to fast actin retrograde flow and slippage (amoeboid migration mode) (77, 97). Basically, ECM parameters dictate which migration modes are possible for leukocytes, while RhoA, Rac and Cdc42 mediate migration modes intracellularly.

β2-INTEGRIN SIGNALING

Integrins function as regulatory and executive bridges between these two components since they bind ECM components and are upstream of RhoA and Rac. The function as executive bridges is based on the characteristic integrin signaling in which they 'integrate' extracellular information into the inside of the cell. This type of signaling is called 'outside-in' signaling. The ability of integrins to mediate 'outside-in' signaling is due to their structure as well as binding of a multitude of cytoplasmic interaction partners. Integrins are transmembrane proteins and are linked to the intracellular cytoskeleton *via* interaction partners such as talin and kindlin (98, 99). Extracellular information is further transmitted *via* the actin cytoskeleton directly to the nucleus (100, 101) or is translated into chemical information in a multitude of signaling pathways downstream of integrins. Many such pathways contain focal adhesion kinase (FAK), Src kinase family members, adaptor molecules bearing immunoreceptor tyrosine-based activation motifs (ITAMs, e.g.

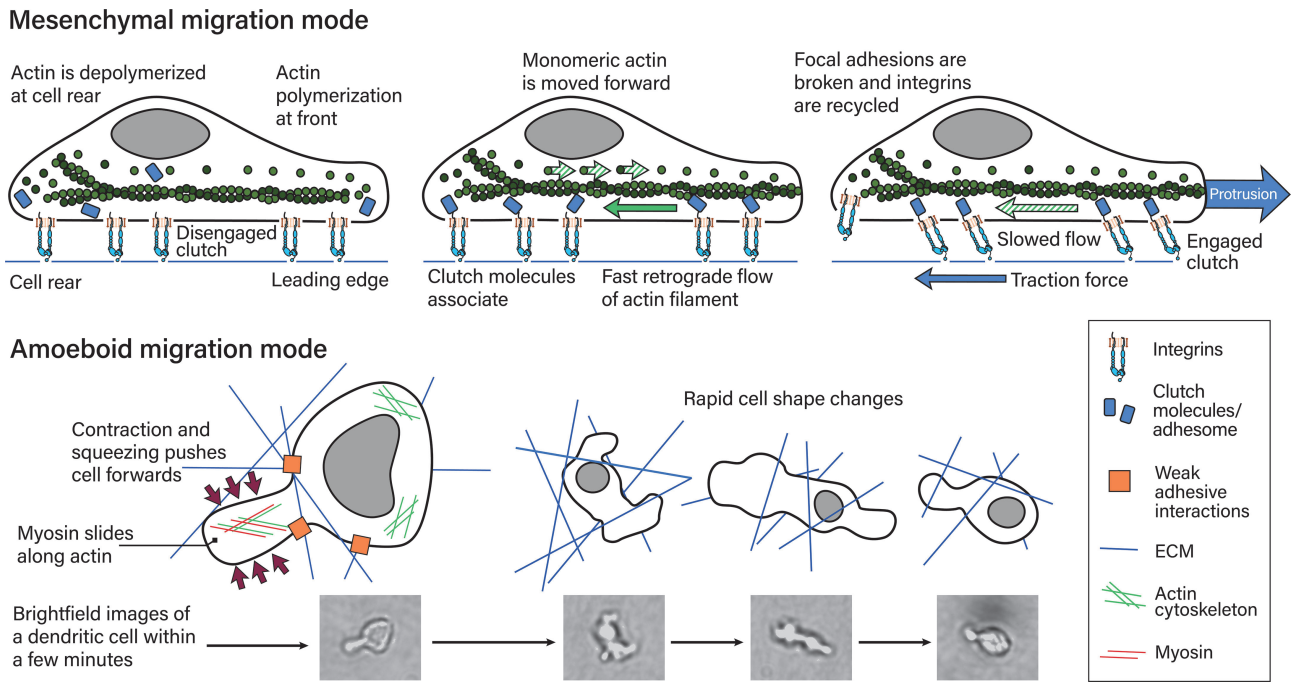

FIGURE 4 | Mesenchymal and amoeboid migration modes. The mesenchymal migration mode, depicted on top, is mediated by strong focal adhesions including integrin–ligand bonds to the substrate. Actin polymerization at the cell's leading edge and actin retrograde flow powers this migration mode, which requires the counterforce of the adhesion sites. In more detail (77): (left) Actin is polymerized at the leading edge while it is depolymerized at the rear. In this depiction adhesome/ clutch proteins have not bound integrin cytoplasmic tails and are instead distributed in the cytoplasm. This means the integrin-actin clutch is disengaged. (middle) Actin polymerization at the front necessitates actin monomers being moved to the front. The growing actin polymer at the front pushes against the elastic fibers at the cell membrane and generates an actin retrograde flow relative to actin's position in the cell. If the integrin-actin clutch is not engaged this flow is fast. Integrin–ligand bonds are reinforced by adhesome protein binding, which results in focal adhesions, along with the metaphorical clutch, being formed. The clutch is still disengaged if the clutch does not bind actin. (right) The adhesome proteins within the clutch mediate binding to polymerized actin moving towards the rear. This results in slowing of the retrograde actin flow, traction force generation and ultimately protrusion. At the cell rear, focal adhesions are broken and proteins, including integrins recycled. During amoeboid migration (bottom), leukocytes exert weak adhesive forces on the extracellular matrix. This mode is powered by myosin II sliding along actin filaments at the cell's rear, which translates into contraction and squeezing forces that push the cytoplasm and cell body forwards. Leukocytes find their paths through complex 3D environments and navigating these involves rapid cell shape changes within minutes and shorter, as depicted on the right. The reference pictures were taken during a timelapse 3D dendritic cell migration experiment through a collagen matrix and are of a single dendritic cell, with most cell shapes not being depicted.

Fc receptor γ-chain IIa), Syk and Rho GTPases that regulate actin polymerization (98, 102–104). For example, β1-integrins (105, 106) and β2-integrins (17) regulate actin dynamics *via* RhoA. Whether β2-integrin signaling stimulates or inhibits Rac seems to be cell type–dependent. In neutrophils, β2-integrin–mediated adhesion has been shown to downregulate Rac and stimulate Cdc42 (107). In human T-cells, CD11a/CD18 has been shown to activate Rac-1 and Cdc42, which mediates cell adhesion (108).

Inside-out and outside-in signaling can happen seamlessly during adhesion processes. An example is, again, adhesion in the bloodstream. In order to withstand the shear forces leukocytes are subjected to, adhesion sites are strengthened under force. Single adhesion points consisting of individual or a few integrin-ligand bonds can be reinforced by recruiting other integrins to form multiprotein clusters (focal adhesion points). This reinforcement is a result of outside-in signaling followed by inside-out signaling (109).

As indicated throughout, both ways of integrin signaling are mediated by cytoplasmic interaction partners. Cytoplasmic interaction partners and proteins that are recruited to integrin adhesion sites are collectively termed the integrin adhesome. Hundreds to thousands (110) of integrin adhesome proteins have been identified (111, 112); 60 integrin adhesome proteins are shared between integrin classes such as α-actinin, talin, tensin and filamin (113). Talin, kindlin(-2) and filamin crosslink integrins to the actin cytoskeleton (114, 115) and recruit other proteins to mediate downstream signaling *via* Src kinases (Lck, Lyn, Fyn) and Syk (116).

β2-INTEGRIN INTERACTION PARTNERS THAT LINK β2-INTEGRINS AND RHOGTPASES

In the following sections β2-integrin downstream signaling components will be characterized to outline rough pathways before the components' involvement in migration of individual leukocyte subpopulations is explored.

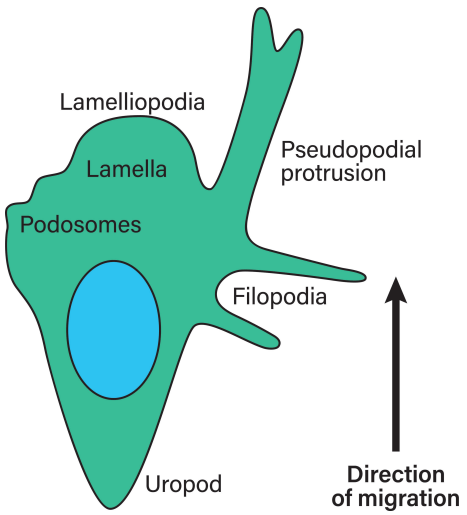

FIGURE 5 | Membrane structures in migrating leukocytes. Actively migrating leukocytes on 2D surfaces form distinct membrane structures. Depicted is the lamellipodia, the actin-rich leading cell edge, the lamella behind it (containing myosin II), as well as the uropod or the cell rear of migrating leukocytes, which are membrane structures that need to be formed during polarization to achieve directional migration. Pseudopodial protrusions are thick, arm-like membrane protrusions in the direction of migration that mediate material uptake. Podosomes are small membrane protrusions which are associated with ECM degradation using proteases. Finally, filopodia are thin finger-like membrane protrusions used to probe the surrounding environment. During amoeboid migration in 3D, leukocytes form small membrane blebs to enact low adhesive forces on the ECM.

Talin

Talin is an important integrin cofactor in general, and its binding to integrin cytoplasmic tails is involved in activation of β3-integrins during inside-out signaling (117). Talin is mechanosensitive and unfolds under applied forces of 5–25 pN (118, 119). In neurons, talin signaling initiates RhoA/ROCK activation *via* Src (120). Talin binds DLC1 (121), which activates RhoA, RhoB, RhoC and Cdc42 and is a negative regulator of RhoA in non-small cell lung carcinoma cells (122).

Kindlin-3

Kindlin-3 is important for integrin inside-out signaling mediating the active integrin conformation and is essential for proper function of multiple integrin classes (β1, β2 and β3 at least) (123–125). In fact, this signaling is so important that mutations affecting the kindlin-3 gene result in leukocyte adhesion deficiency III (LAD III; mutations mainly affecting CD18 lead to LAD I). LAD III is prevented by the expression of only 5% of the typical kindlin-3 level during homeostasis, however, higher amounts are needed for leukocytes to function properly (126). Kindlin-3 is mainly expressed in the haematopoietic system, so it is important for leukocytes and platelets (123, 127). Kindlin-3 is essential for CD11a/CD18 inside-out signaling (125).

Filamin A

Filamin A is an integrin cytoplasmic cofactor interacting with β-1, β-2, β-3 and β-7 integrins (128–134), mechanosensitive (135) and an actin crosslinking protein (136). Filamin A-actin crosslinking establishes leading-edge actin networks which distribute forces over the entire cytoskeleton (137). This force distribution is especially important during adhesion to and crawling across the endothelium since it allows cells to withstand shear forces (138).

Stretching Filamin A/actin crosslinks under forces of 2–5 pN (135) leads to Filamin A unfolding and dissociates the FilaminA-binding GTPase-activating protein (FilGAP) from filamin. Instead, Filamin A binding to integrins is increased (139). FilGAP inactivates Rac1 in a Rho-associated kinase (ROCK)-dependent manner, and it inactivates Cdc42 to a lesser extent. The forced expression of Filamin A together with FilGAP decreases active Rac1 amounts, and since FilGAP is localized at lamellae, it inhibits lamellae formation and integrin-mediated cell spreading, which could be important for amoeboid migration (140). Filamin A itself is an important regulator of leukocyte adhesion, migration and homing.

RhoGTPases

Actin is indispensable for both migration modes. In accordance with the importance of the actin network, RhoGTPases – integral to actin remodeling – have been shown to be involved in many migrating leukocytes. RhoGTPases include 20 members and are excellently reviewed in (141). Of these 20 members, RhoA, Rac proteins and Cdc42 will be characterized below and their downstream effectors are depicted in **Figure 6**.

RhoA

RhoA has been linked to cell migration in general. It has been shown to be essential for, for example, colon cancer (142), stellate cell (143) and mature osteoclast migration (144). In leukocytes, RhoA is important for actin contractility; this enables retraction of the cell rear during monocyte transmigration (145) and pushes cell migration in several cell types (68, 71, 73, 146), which is characteristic of amoeboid migration and its associated round cell shapes and weak adhesion (18, 71). However, RhoA plays a role in both active migration modes. RhoA induces ROCK, which regulates actin *via* LIMK and cofilin (141). This has been shown to be essential for leukocyte migration, especially in 2D conditions in which RhoA/ROCK is essential for establishing one leading membrane lamella and thereby directionality (147). RhoA also enhances the activity of mammalian Diaphanous-related formins (mDia)2, which is important for actin polymerization (148, 149).

RhoA also regulates leukocyte arrest on the endothelium, by mediating CD11a/CD18 conformational change into the active conformation as part of an inside-out signaling pathway (4, 150, 151) downstream of RAP1 (in thymocytes) (152). It is important to note that (β2)-integrins are not the only adhesion receptors upstream of RhoA. For example, $P2Y_1$, a platelet purinergic receptor, has been shown to be upstream of RhoA activation, and both were essential for platelet-dependent leukocyte chemotaxis *in vitro* and leukocyte recruitment in thrombocytopenic mice (153).

Rac Proteins

Rac, or Rac proteins (Rac1, Rac2, Rac3 and RhoG), is another group of GTPases that can activate RhoA in fibroblasts (154,

155). Rac proteins are critical for generating actin rich, stimulated lamellipodia formation and membrane ruffling, and are important for establishing adhesion sites to the extracellular matrix together with Cdc42 in macrophages (156). While Rac1 is ubiquitously (141) and RhoG widely expressed (157), Rac2 is mostly only expressed in cells of the hematopoietic lineage (158, 159), and Rac3 is mostly found in the brain (141, 160, 161). Rac, along with increased adhesion, is associated with increased spreading and the slower mesenchymal migration mode (68, 71, 73, 146). Rac in leukocytes is critically dependent on DOCK2, a haematopoietic cell-specific CDM family protein downstream of chemokine receptors (162). T-lymphocytes and B-lymphocytes deficient in DOCK2 exhibit homing and migratory defects *in vivo*, however, these migratory defects where not present in monocytes (162). Rac signals *via* several different downstream proteins to initiate lamellipodia formation. Actin polymerization is initiated by Rac *via* the WAVE complex, which activates actin-related protein (Arp) 2/3 that activates actin polymerization in a branched network (163), or Rac initiates mDia2 which mediates actin polymerization directly. Similarly to Cdc42, Rac initiates actin turnover *via* active P-21–activated kinases (PAK), LIM kinase (LIMK) and Cofilin (141).

Cdc42

Cdc42 in turn can activate Rac1 (154, 155, 164). Not only does Cdc42 regulate the actin cytoskeleton, it also has an important function in regulating cell polarity, which is well conserved in many eukaryotic organisms (141). Cdc42 controls actin polymerization *via* WASp and IRSp53, which activate ARP2/3 and mDia2 – which initiates actin polymerization directly – and PAK, which inhibits actin turnover *via* LIMK and Cofilin (141).

RhoGTPase Expression Profiles Differ Across Leukocytes

RhoGTPases are clearly involved in regulating adhesion and migration of many different leukocytes. However, expression levels differ across leukocyte subpopulations and even within monocytes. A study by van Helden et al. (165) investigated mRNA levels of RhoGTPases in neutrophils, differentiating dendritic cells and macrophages. They found that neutrophils expressed high levels of Cdc42, RhoQ, Rac1, Rac2, RhoA and RhoC and low and specific expression of RhoG, RhoB, RhoF and RhoV. While this GTPase expression profile was similar between different cell types, differences emerged during differentiation. During dendritic cell differentiation, Rac1 was up- and Rac2 downregulated and the dendritic cell populations expressed very low levels of RhoV, which was also present at low levels in macrophages and at higher levels in CD34+ progenitors. Macrophage GTPase expression profiles looked similar to those of dendritic cells, however, M-CSF–differentiated macrophages also expressed low levels of RhoBTB1. Apart from these minuscule differences, neutrophils, dendritic cells and macrophages differed regarding whether RhoA, Rac1, Rac2 or CdC42 was most expressed. The individual percentages were also dependent on which growth factor had been used to differentiate the cells. For example, GM-CSF–differentiated macrophages expressed high Rac2 levels while M-CSF–differentiated macrophages expressed high levels of RhoA.

Furthermore, RhoH is a GTPase only expressed in the haematopoietic linage (166). While myeloid cells and lymphocytes have both been shown to express RhoH, lymphocytes express high levels of this GTPase (167, 168). Thymocyte development and T-cell receptor signaling is critically dependent on RhoH (169, 170). B-cell receptor signaling is intact in RhoH-deficient cells, however B-cell chronic lymphocytic leukemia is dependent on RhoH (171). RhoH has been described as an inhibitor of other RhoGTPase activity, because it negatively regulates RhoA-induced NfKB and p38 signaling in Jurkat cells (172), however, its active contribution to T-cell receptor signaling does not involve Rac inhibition (170). Knockdown of RhoH in T-cells leads to the activation of CD11a/CD18, but does not affect the heterodimer's ability to bind ligands and mediate adhesion (170). It is important to note that RhoH is regulated on a transcriptional level (172).

These results might explain some of the discrepancies between cell types and even studies. RhoGTPase expression profiles are clearly closely linked to individual cell identity, based on which stimuli the cell had experienced. Additionally, leukocyte migration mechanisms should be more closely investigated based on cell types and even sub-populations.

β2-INTEGRINS REGULATE NUCLEAR ELEMENTS AND GENE EXPRESSION IN LEUKOCYTES

Integrins are mechanosensors and they transmit mechanical forces directly, *via* the actin cytoskeleton, to the nucleus (173) and the nuclear lamina, consisting of lamin. Lamin A/C has been shown to be force-sensitive and scales in response to higher extracellular stiffness in order to maintain the cell's tensional integrity (174, 175). Lamin A/C is responsible for nuclear stiffness (176) and high lamin A/C levels hinder 3D leukocyte migration through porous environments (92). If the β2-integrin/kindlin-3 binding is abolished by mutating the β2-cytoplasmic tail, lamin A/C levels are downregulated. Furthermore, this leads to an increase in H3K4me3 levels, a methylation mark associated with active transcription, changes in open chromatin formation and activation of an IKAROS network, which includes RelA. Compared to WT dendritic cells, dendritic cells that had an abolished β2-integrin/kindlin-3 interaction have been shown to migrate faster in a 3D collagen matrix, express higher levels of maturation surface receptors and induce superior tumor rejection responses in a B16.Ova and B16.F10 melanoma model. Directly targeting H3K4 methylation and disrupting the adhesion in WT dendritic cells was shown to be enough to replicate this phenotype (177). Confinement of Jurkat cells in a 3D collagen I matrix resulted in H3K4me3 upregulation *via* WD repeat domain 5 (178). Furthermore, in Jurkat cells or primary

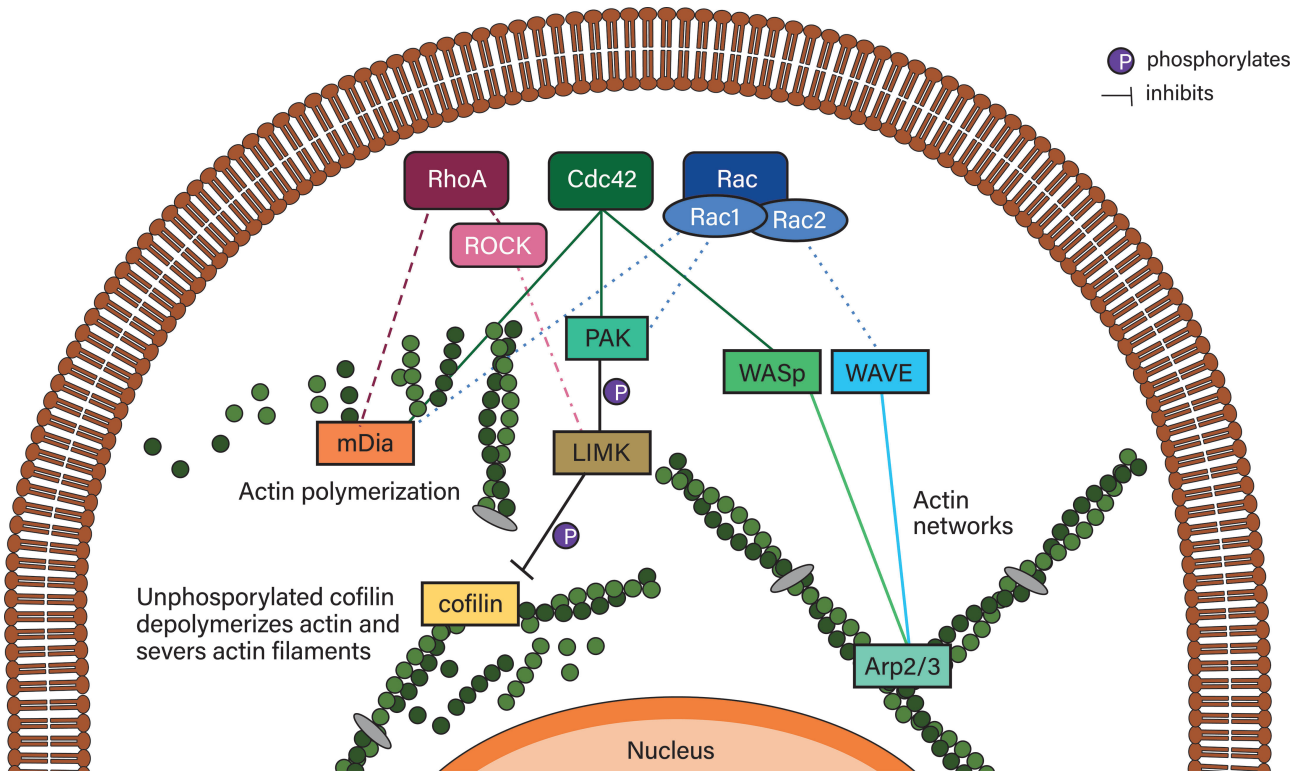

FIGURE 6 | Simplified RhoGTPase signaling to their downstream effectors. RhoA signals to mDia2 and, *via* ROCK, can inhibit actin depolymerization *via* LIMK/cofilin. Cdc42 can activate Rac proteins, which activates PAK proteins that phosphorylate LIMK family proteins, which phosphorylate and thereby deactivate cofilin. Deactivated phosphorylated cofilin is reactivated by dephosphorylation mediated by slingshot proteins such as SSHL1 (not shown). Cdc42 also initiates actin polymerization *via* mDia2 and actin network formation (typically in lamellipodia/lamella) *via* WASp, which activates Arp2/3. Arp2/3 is also activated by the WAVE complex of which hem1 is an associated protein. WAVE is activated by Rac proteins such as Rac1 and Rac2. Rac proteins also activate mDia2 as well as the PAK/LIMK/cofilin axis.

CD4+ T-cells VCAM1 adhesion mediated by α1β1-integrin leads to triple methylation of another lysine, H3K9me2/3. This involves interaction of methyltransferase G9a with lamin B1 and mediates nuclear stiffness and viscoelasticity and ultimately regulates T-cell migration in 2D and 3D as G9a depletion blocks T-cell migration (179). Finally, histone deacetylation has been shown to be essential for CD4+ T-cell extravasation as histone deacetylase 1 deficiency resulted in reduced transwell transmigration, aberrant migration on ICAM-1 surfaces *in vitro* and decreased migration into the intestinal epithelium and lamina propria *in vivo*. Additionally, during the cell adhesion cascade fewer histone deacetylase 1 deficient T-cells were found to probe the surface for places to transmigrate. Abolished histone deacetylation further resulted in downregulation of CD11a, CD18 and β7 chain as well as selectins on a transcriptional level, however, deficient T-cells spread more on ICAM-1 and formed more F-actin, while their random cell migration speed was increased by 10% (180). It is clear, that as with RhoGTPases, the mechanism of how epigenetic marks regulate leukocyte migration is complex and context dependent and much effort is required to unravel this mechanism fully.

CHARACTERISTICS OF DIFFERENT LEUKOCYTE MIGRATION

Leukocyte migration and specific migratory elements such as chemotaxis, transmigration, membrane architecture and adhesion are regulated differently by varying RhoGTPases and their downstream effectors across leukocyte cell types. In accordance with this, migratory behavior also differs between leukocyte cell types, however, some leukocytes have been much more extensively studied, while leukocytes such as basophils and eosinophils have not been studied much regarding migration and trafficking.

Monocytes

Blood-derived monocytes enter tissues from the bloodstream *via* the cell adhesion cascade, which involves utilizing the 2D mesenchymal migration mode. Additionally, they are able to use the amoeboid migration mode in fibrous, porous collagen I matrices, however, they are unable to infiltrate dense matrigel matrices or to form podosomes (181). Successful invasion of such matrices is dependent on proteolytic degradation (see section on macrophages). Monocyte migration seems to be

intracellularly governed by RhoA and ROCK, while Filamin A merely restricts monocyte transmigration *in vitro* (182). RhoA and ROCK control β2-integrin localization (145) and leading edge formation during transmigration (147). Furthermore, RhoA/ROCK promote monocyte adhesion, migration and transendothelial transmigration (183). RhoA, as well as Cdc42, regulate filopodia formation (184, 185), and Cdc42 also regulates monocyte migration across endothelial cells (185).

Dendritic Cells

Dendritic cell migration is dependent on their maturity, with immature dendritic cells being relatively immobile, while sampling antigens and intrinsically activated or extrinsically stimulated maturation leads to CCR7 upregulation, which initiates haptotaxis (directed migration along an immobilized chemokine gradient) (186). Dendritic cells use different migration modes when migrating to lymph nodes. To exit constrained porous environments, such as in ear tissues and the skin, dendritic cells use the amoeboid migration mode (18, 187, 188). Like macrophages, dendritic cells can use a protease-dependent, ROCK-independent migration mode in dense 3D environments like matrigel. In such dense 3D environments, podosome formation, rather than maturation status, has been shown to be essential for 3D migration. Dendritic cells migrate through heterogenous environments such as tumor spheroids using both mesenchymal and amoeboid migration modes (188). Once dendritic cells are inside the lymph vessels, they form lamellipodia to crawl along the endothelium (55). CCL-21/CCR7 activation initiates chemotaxis/haptotaxis (189, 190) and arrests dendritic cells on the endothelium. In addition to the chemokine cue, dendritic cells also sense the lymph flow which directs them to proceed downstream (55). Dendritic cells can enter lymph nodes by transmigrating through the subcapsular sinus on the afferent side and then prepare the entry of T-cells into these sites. During intranodal migration, dendritic cells have been shown to exhibit extensive polarization, which established leading edges and a long uropod, which was necessary to translocate to the paracortex. Dendritic cell polarization is dependent on CCR7 (191). Motile dendritic cells are also found in the gut, the lamina propria, Peyer's patches and solitary intestinal lymphoid tissues from where dendritic cells migrate to gut-draining lymph nodes. During gut infections accompanied by rupture of afferent lymph vessels, dendritic cell migration is prevented (186). Dendritic cell migration from the lung tissue to draining lymph nodes has been shown to be dependent on CCR7, but CCR8 was also implicated (186, 192). Intracellularly, β2-integrin/kindlin-3 signaling restricts the mature, migratory phenotype of dendritic cells, and abolishing the β2-integrin/kindlin-3 interaction leads to increased expression of maturity markers, increased migration speed in 3D towards CCL19, increased IL-12a production and induction of superior anti-tumor responses in B16.OVA and B16.F10 melanoma models *in vivo* (177, 193). Furthermore, in dendritic cells the β2-integrin/kindlin-3 signaling is upstream of RhoA in a ROCK-independent pathway that regulates adhesion but not 3D migration (17).

Macrophages

Macrophages use mesenchymal migration modes, as well as amoeboid migration modes in 3D environments, and this depends on the specific environment/matrix architecture. For example, the amoeboid migration mode is utilized in porous fibrillar collagen I, and mesenchymal migration mode in dense matrigel (194). During mesenchymal migration modes, macrophages form podosomes that can lyse collagen, however, this migration mode is not dependent on matrix metalloproteinase (MMPs) and might be mediated by other proteolytic systems (194). If collagen I is in the form of a gel, macrophages also utilize mesenchymal migration modes and this could be due to the increased stiffness and viscosity of this form of collagen I (194) or the matrix structure, such as the availability of pores. Macrophages use a migration mode dependent on ROCK and MMPs to infiltrate tumor cell spheroids encapsulated in matrigel (195). These spheroids would present a heterogeneous matrix architecture similar to another collagen I matrix polymerized at 3.6 mg/ml. The 3.6 mg/ml collagen I matrix has been found to contain fibrillar collagen structures, be porous and have intermediate stiffness (G' is around 30 Pa, though this is quite soft) and viscosity (G" is around 8–9 Pa) (195). Macrophages used a combination of amoeboid migration mode and MMP-dependent mesenchymal migration mode in this collagen I matrix, which resembled spheroid infiltration. In a follow-up study, Filamin A was shown to be essential for a macrophage mesenchymal migration mode utilizing proteolytic podosomes. Filamin A is, however, dispensable for amoeboid migration modes (196), and restricts macrophage transmigration *in vitro* (197). Macrophage migration mode seems to be additionally dependent on macrophage status and β2-integrin expression levels (198). CD11d/CD18 is upregulated on M1 proinflammatory macrophages, while CD11b/CD18 is highly expressed on resident macrophages. High expression levels of these integrins inhibit migration and promote adhesion, while intermediate integrin expression promotes amoeboid and mesenchymal migration modes. Knocking out these heterodimers has also been shown to result in reduced migration (198). Finally, individual levels of RhoGTPases seem to be critical for macrophage migration: RhoA mediates actin cable formation, macrophage rounding up and contractility (156) and has to be precisely concentrated in order to facilitate macrophage migration (199). Rac1 and Rac2 are important GTPases in macrophages (200), with Rac1 being the most abundant Rac isoform (201, 202) and being essential for lamellipodia formation and macrophage migration (199). Rac1 is also important for macrophage invasion through matrigel (203), which would have likely utilized the mesenchymal migration mode (194). Rac2 mediates transmigration; additionally, its role in macrophage migration is somewhat substratum-dependent, since it mediates migration across laminin and fibronectin (203).

Microglia

Microglia are a type of leukocyte found in the brain. They express CD11b (a β2-integrin alpha chain) (204, 205) and are phenotypically similar to macrophages. While a study with β2-

integrin knockout mice has shown that β2-integrins are not necessary for microglia migration (206), similar to dendritic cells, this experiment reduced β2-integrins to just 2–16 % of CD18 expression (206), therefore not precluding their involvement to a small degree. Microglia *in vitro* were shown to migrate with similar speeds (ca. 60 μm/min) to leukocytes. During migration, microglia were shown to use thin transparent lamellipodia as 'sails' to glide forward (207). In murine brain slices, microglia migrated at an average of 5.02 ± 0.06 μm/min, with spurts of 10 μm/min speeds and migrated individually and not highly directionally (208). In another study using murine brain slices, CD11a was knocked down in a microglia cell line and this inhibited microglia migration. Although CD11a-deficient microglia were able to migrate up to 50 μm into the slices, WT microglia were able to migrate down to 80 μm (209).

Neutrophils

Neutrophils are capable of using the mesenchymal migration mode, as well as the amoeboid migration mode (18). In matrices such as fibrillar, porous collagen I matrices, neutrophils use the amoeboid migration mode, however, they are unable to invade dense matrigel matrices or to form podosomes (181). It is important to note that neutrophils express adhesion receptors dynamically (210); for example, α4β1-integrin expression is downregulated during neutrophil maturation (14). Neutrophils have been observed to swarm into tissues and form clusters as a response to sterile inflammation or infections with bacteria, fungi and parasites. Neutrophil swarming behavior can be categorized into two patterns, transient swarms and persistent swarms. Transient swarms are formed by neutrophils migrating towards a chemoattractant, forming a cluster for a few minutes and migrating out again to join nearby clusters. Persistent swarms are formed by sustained neutrophil migration into clusters that can last for hours. There seems to be tissue-specific parameters dictating which kind of swarming behavior occurs, although in some tissues swarming behaviors can also co-occur. Transient swarms occur in lungs, lymph nodes and intestine, while persistent swarms occur in skin, liver, spleen and cornea. Further parameters that have been shown to influence which swarming behavior occurs are the extent of initial and secondary tissue damage, presence of pathogens and number of recruited neutrophils (211). CD11a/CD18 and CD11b/CD18 were both shown to be essential for the final stages of accumulation in collagen-free zones (212).

The role of β2-integrin cofactors in neutrophil trafficking is dependent on the dimensionality of the environment: in 2D talin mediates adhesion, spreading, polarization and migration, while in 3D it plays a role in chemotactic velocity (213, 214). Furthermore, talin is important for activating integrins to mediate neutrophil entry into sites of infections, to arrest in venules and to emigrate out of venules (214). Kindlin-3 mediates directionality in neutrophils crawling on 2D surfaces (213). Filamin A seems to be an important regulator of neutrophil migration. Not only does it enable fast migration speed in 2D and 3D (215), it also mediates RhoA activation and localization in uropods. Furthermore, Filamin A regulates myosin II–mediated uropod contractility *via* RhoA, and Filamin A mediates spreading on β1- and β2-integrin ligands (216, 217).

Different RhoGTPases regulate different aspects of neutrophil migration: Rac1 is important for directed neutrophil migration (218), while Rac2 mediates chemokinesis (random movement), spreading as well as proper F-actin generation, which regulates polarization and directed movement (219, 220). Conversely, Cdc42 restricts neutrophil migration speed, but is important for proper directed migration and steering *in vitro* (221, 222). Cdc42 regulates directed neutrophil migration by controlling polarity *via* its effector Wiskott-Aldrich Syndrome Protein (WASp), whose activation and localization in uropods is controlled by Cdc42. WASp in turn controls CD11b localization in uropods, and the integrin heterodimer then recruits and stabilizes tubulin (223).

Eosinophils and Basophils

Eosinophil transmigration has been mainly shown to be mediated by CD11a/CD18 and CD11b/CD18 when the cells were stimulated by IL-1. IL-4–mediated transmigration, however, seems to be dependent on α4β1 (VLA-4). Inhibiting CD11b/CD18 and α4β1 has been shown to impair eosinophil accumulation in the airways in *in vivo* models (10). Similarly, inhibiting CD18 with antibodies inhibited basophil transendothelial transmigration in transwell assays (224).

Mast Cells

Mast cell progenitors traffic from the bone marrow into tissues where they mature, and their homing to different (healthy and inflamed mucosal) tissues is dependent on different integrins (225, 226). Homing to the intestine is dependent on integrin α4β7 (the α4 chain, which can also pair with β1, but especially the β7 chain in this case) (21, 225), while homing to the lungs is dependent on α4β7 as well as α4β1 (20, 225). Mast cell homing to the peritoneum is dependent on CD11b/CD18 and αIIbβ3 (23, 227). Migrating mast cells form pericentral actin clusters that prevent cell flattening and localize secretory granules at the cell center, and this actin organization is mDia(1) dependent. mDia1 knockdown was shown to impair mast cell transmigration in a transwell model, however, mDia1 knockout mice have normal mast cell distribution in tissues (228). Mast cells migrate in response to UV exposure from the skin to draining lymph nodes, and this is important for immune suppression. The extent of such migrating mast cells is dependent on the degree of UV exposure, and mast cells primarily migrate to B-cell areas in lymph nodes guided by CXCL12 secreted by B-cells (receptor CXCR4) (54). Additionally, mast cells accumulate at sites of angiogenesis (i.e. blood vessel formation), and are guided by angiogenic factors, such as VEGF, PDGF-AB and bFGF (229). Interestingly, mast cells can secrete heparin, a polysaccharide, and use it to induce endothelial cell migration *in vitro* (230).

NK Cells

Similarly to T-cells and B-cells, NK cells exit the bone marrow to enter secondary lymphoid organs in a β2-integrin–dependent mode (231). In lymph nodes, NK cells are activated by dendritic

cells during infections, however, *in vivo* they have been shown to barely form stable dendritic cell interactions, instead forming short-lived contacts with dendritic cells. During this process, NK cells are highly motile in order to establish multiple interactions with dendritic cells and migrate with a less straight trajectory than T-cells (232). Conversely, in superficial lymph node regions, NK cells have been shown to exhibit low motility and long interactions with dendritic cells (233). On stroma, human NK cell subsets have different migratory profiles, with CD56 ^{bright} NK cells migrating in short, multidirectional tracks, CD56 ^{dim} NK cells migrating in linear and rapid fashion and CD56 ^{neg} NK cells ($CD56^{low}$ $CD3^{-}$ $CD16^{+}$ $CD57^{+}$ KIR^{+}) migrating to a minimal extent. NK cell migration is dependent on CD56 expression, and more mature NK cells exhibit the most motility (234). Furthermore, NK cell migration on 2D surfaces *in vitro* can consist of a series of short, constrained motions mixed with highly directed motions or migration in a straight line for the entirety of migration, the latter being observed in few NK cells (235). NK cells are proposed to be capable of transmigration and invasion in response to chemokine and cytokine stimulation and without being activated by dendritic cells. NK cell invasion into cancer spheroids was further proposed to be β2-integrin–dependent and, unlike T-cells, NK cells do not recirculate (236).

T-Cells

T-cells in the afferent lymph system are transported by lymph flow into the medullary sinus system. These T-cells then cross the endothelium and enter lymph nodes by directly transmigrating into medullary cords (191). Intranodal migration of T-cells has been shown to be dependent on CCR7, with the chemokine receptor stimulating migration in T-cell areas but not in subcapsular regions *in vivo* (237). T-cells exit the lymph nodes and travel to sites of infections, which involves adhesion to the endothelium under shear conditions. As mentioned, this adhesion is dependent on the CD18/Kindlin-3 interaction (238). Arrested T-cells that crawl on endothelial cells and ICAM-1–coated surfaces form lamellipodia, which contain low amounts of CD11a/CD18, and uropods, which contain high amounts of CD11a/CD18. Additionally, T-cells that crawl on ICAM-1, incorporated in lipid bilayers, form a specific zone in the middle of their bodies. This zone contains high affinity CD11a/CD18 and mediates adhesion to and migration on ICAM-1, and its stability is dependent on talin (239). In tissues as well as fibrillar, porous collagen I matrixes, T-cells – like monocytes and neutrophils – can use the amoeboid migration mode (181). However T-cells are unable to form podosomes or to invade dense matrigel matrices (181). Intracellularly, T-cell homing and trafficking is critically dependent on Kindlin-3, which mediates CD11a/CD18 inside-out signaling (125, 238). The involvement of further β2-integrin signaling components for T-cell trafficking is context dependent. T-cell transmigration is dependent on RhoA (240), while the tight binding of Filamin A to integrin tails inhibits transmigration (134). Rac1 signaling mediates T-cell adhesion (241) and can, together with Cdc42, compensate for loss of β2-integrin/14-3-3 signaling to mediate T-cell spreading (108).

B-Cells

B-cells are capable of using the amoeboid migration mode (242, 243), however, their 2D migration seems somewhat atypical. During migration on CXCL13-coated surfaces, the leading membrane edge has been shown to undergo dilation and shrinking events, and the balance of these events was predictive of turning versus directional persistence. During this migration, an imbalance of dilation versus shrinking events was associated with changes in direction (244). This phenomenon might involve β2-integrins, since CXCL13/CXCR5 mediates CD11a/CD18 adhesion in B-cells (243). In large B-cell lymphoma, the amoeboid migration mode is mediated by an IL-10-JAK-STAT-3-RhoH pathway that was shown to increase RhoA activity and suppress tubulin acetylation (245).

Leukocyte Migration in Tumors

Leukocyte migration also has a huge implication in cancer therapy, as therapeutic antibodies targeting immune checkpoints have revolutionized cancer treatment in recent years. However, for 70-80% of patients their tumors do not respond to this treatment (246). This poor response has been linked to the presence or absence of T-cells in the tumor environments (247). T-cell tumor invasion is hindered by the prolonged interaction of T-cells with tumor-associated macrophages (TAMs), and depletion of TAMs can restore T-cell migration and invasion (248). In order to mount an anti-tumor immune response, antigen-presenting cells have to present antigens to and fully activate T-cells first. However, this mechanism is warped in order to support tumor growth by dendritic cell–like cells in the tumor periphery that engage CD8+ T-cells in long interactions without fully activating the T-cells (249, 250). This results in 'immune excluded' tumors with leukocytes stuck in the periphery. Macrophages and dendritic cells have, in turn, been found to be regulated by myeloid-derived suppressor cells (MDSCs) in glioma (251). MDSCs arise as monocytes from the bone marrow and then effectuate homing to secondary lymphatic organs before being recruited into the tumor, where they are retained. This process is thought to be a result of crosstalk between the bone marrow and the tumor, involving growth factors and chemokines produced in the tumor microenvironment. MDSC homing culminates in their retention in the tumor microenvironment, however, less is known about this process then about T-cell retention (252). Our understanding of leukocyte migration is limited in general and is even more elusive in regards to how it is impaired on a molecular level specifically in tumors.

CONCLUSION

It is now established in the literature that leukocytes use a distinct migration mode – the amoeboid migration mode – which sets them apart from other migrating cells. However, there are distinct differences between migration profiles of leukocyte populations, and especially the individual molecular mechanisms that mediate these, which were broadly outlined

in this review. Future research will hopefully flesh out these differences and should address exactly how the molecular balance between RhoGTPases is regulated. The focus of this review was on β2-integrins – some of the most studied adhesion receptors. However, there are many other adhesion and surface receptors that signal *via* RhoGTPases and have been shown to play a role in leukocyte migration, such as NOTCH (253–255) and cadherins (256–258). Incorporating other ECM ligands for these receptors could reveal more RhoGTPase profiles and even new migration modes or unique leukocyte migration behavior. Furthermore, individual surface receptors might be key regulators or could strengthen and perpetuate signaling. The ultimate goal would be to establish exactly how collective surface receptor signaling mediates distinct RhoGTPase profiles and how this translates to exact migratory behavior. This should also include unraveling how leukocyte migration is regulated by histone methylation and acetylation downstream of integrin and adhesion receptor signaling. Thus far, deacetylation, H3K4me3, as well as H3K9me2/3, have been implicated in dendritic cell and T-cell migration, respectively. It would be important to see if other methylation marks are associated with the migration of distinct leukocyte subpopulations. Moreover, histone methylation and acetylation have received the most attention thus far but are only a small portion of the many types of histone modifications: it is possible that the others also play a role in regulating leukocyte migration.

Progress in cancer therapy has focused on combination treatments. Combining immune checkpoint inhibitors as well as combination therapy using radiotherapy first and then immune checkpoint inhibitors can improve objective response rates as well as progression free survival (259, 260). Ultimately similar improvements could be possible by mapping out the intracellular signaling that governs leukocyte migration. This could empower us to reestablish migratory behavior in effector T-cells stuck in the periphery of immune-excluded tumors, which could further increase patient survival rates after immune checkpoint inhibitor combination treatment, as well as control leukocyte migration in other diseases.

AUTHOR CONTRIBUTIONS

The author confirms being the sole contributor of this work and has approved it for publication.

FUNDING

IFReC Kishimoto Foundation for supporting the study with a fellowship.

ACKNOWLEDGMENTS

My biggest gratitude for improving the manuscript goes to James Alexander Geraets and Mercedes Said. I would also like to very much thank my editor Alyce M Whipp. I thank the University of Helsinki Library for covering the article publishing costs and I thank Susanna Fagerholm for helpful discussion.

REFERENCES

1. McEver RP, Zu C. Rolling Cell Adhesion. *Annu Rev Cell Dev Biol* (2010) 26:363–96. doi: 10.1146/annurev.cellbio.042308.113238
2. Muller WA. Getting Leukocytes to the Site of Inflammation. *Vet Pathol* (2013) 50(1):7–22. doi: 10.1177/0300985812469883
3. Schenkel AR, Mamdouh Z, Muller WA. Locomotion of Monocytes on Endothelium is a Critical Step During Extravasation. *Nat Immunol* (2004) 5:393–400. doi: 10.1038/ni1051
4. Klaus Ley CL, Cybulsky MI, Nourshargh S. Getting to the Site of Inflammation: The Leukocyte Adhesion Cascade Updated. *Nat Rev Immunol* (2007) 7(9):678–89. doi: 10.1038/nri2156
5. Baker EL, Zaman MH. The Biomechanical Integrin. *J Biomech* (2010) 43 (1):38–44. doi: 10.1016/j.jbiomech.2009.09.007
6. Evans R, Patzak I, Svensson L, De Filippo K, Jones K, McDowall A, et al. Integrins in Immunity. *J Cell Sci* (2009) 122:215–25. doi: 10.1242/jcs.019117
7. Harris ES, McIntyre TM, Prescott SM, Zimmerman GA. The Leukocyte Integrins. *J Cell Biol* (2000) 275(31):23409–12. doi: 10.1074/jbc.R000004200
8. Luo B-H, Carman CV, Springer TA. Structural Basis of Integrin Regulation and Signaling. *Annu Rev Immunol* (2007) 25:619–47. doi: 10.1146/annurev.immunol.25.022106.141618
9. Lima CSP, Franco-Penteado C, Canalli AA, Conran N, Lorand-Metze I, Costa F, et al. Expressions of the VLA-4, LFA-1 and Mac-1 Integrins in Eosinophil Migration in a Case of Chronic Eosinophilic Leukaemia. *Leukemia Res* (2007) 31(5):695–7. doi: 10.1016/j.leukres.2006.07.025
10. Wardlaw AJ, Walsh GM, Symon FA. Mechanisms of Eosinophil and Basophil Migration. *Allergy* (1994) 49:797–807. doi: 10.1111/j.1398-9995.1994.tb00778.x
11. Moser M, Bauer M, Schmid S, Ruppert R, Schmidt S, Sixt M, et al. Kindlin-3 is Required for Beta2 Integrin-Mediated Leukocyte Adhesion to Endothelial Cells. *Nat Med* (2009) 15(3):300–5. doi: 10.1038/nm.1921
12. Füreder W, Agis H, Sperr WR, Lechner K, Valent P. The Surface Membrane Antigen Phenotype of Human Blood Basophils. *Allergy* (1994) 49(10):861–5. doi: 10.1111/j.1398-9995.1994.tb00788.x
13. Lindbom L, Werr J. Integrin-Dependent Neutrophil Migration in Extravascular Tissue. *Immunology* (2002) 14:115–21. doi: 10.1006/smim.2001.0348
14. Petty JM, Lenox CC, Weiss DJ, Poynter ME, Suratt BT. Crosstalk Between CXCR4/Stromal Derived Factor-1 and VLA-4/VCAM-1 Pathways Regulates Neutrophil Retention in the Bone Marrow. *J Immunol* (2009) 182:604–12. doi: 10.4049/jimmunol.182.1.604
15. Plow EF, Haas TA, Zhang L, Loftusi J, Smith JW. Ligand Binding to Integrins. *J Biol Chem* (2000) 275(29):21785–8. doi: 10.1074/jbc.R000003200
16. Van der Vieren M, Crowe DT, Hoekstra D, Vazeux R, Hoffman PA, Grayson MH, et al. The Leukocyte Integrin αdβ2 Binds VCAM-1: Evidence for a Binding Interface Between I Domain and VCAM-1. *J Immunol* (1999) 163 (4):1984–90.
17. Guenther C, Faisal I, Uotila LM, Asens ML, Harjunpää H, Savinko T, et al. A β2-Integrin/MRTF-A/SRF Pathway Regulates Dendritic Cell Gene Expression, Adhesion, and Traction Force Generation. *Front Immunol* (2019) 10. doi: 10.3389/fimmu.2019.01138
18. Lämmermann T, Bader BL, Monkley SJ, Worbs T, Wedlich-Söldner R, Hirsch K, et al. Rapid Leukocyte Migration by Integrin-Independent Flowing and Squeezing. *Nature* (2008) 453(7191):51–5. doi: 10.1038/nature06887
19. Arnaout MA. Biology and Structure of Leukocyte β Integrins and Their Role in Inflammation. *F1000 Res* (2016) 5(2433):13. doi: 10.12688/f1000research.9415.1
20. Abonia JP, Hallgren J, Jones T, Shi T, Xu Y, Koni P, et al. Alpha-4 Integrins and VCAM-1, But Not MAdCAM-1, are Essential for Recruitment of Mast Cell Progenitors to the Inflamed Lung. *Blood* (2006) 108:1588–94. doi: 10.1182/blood-2005-12-012781

21. Abonia JP, Austen KF, Rollins BJ, Joshi SK, Flavell RA, Kuziel WA, et al. Constitutive Homing of Mast Cell Progenitors to the Intestine Depends on Autologous Expression of the Chemokine Receptor CXCR2. *Blood* (2005) 105:4308–13. doi: 10.1182/blood-2004-09-3578
22. Knight PA, Wright SH, Brown JK, Huang X, Sheppard D, Mille HRP. Enteric Expression of the Integrin alphaV Beta6 Is Essential for Nematode-Induced Mucosal Mast Cell Hyperplasia and Expression of the Granule Chymase, Mouse Mast Cell Protease-1. *Am J Pathol* (2002) 161(3):771–9. doi: 10.1016/S0002-9440(10)64236-8
23. Berlanga O, Emambokus N, Frampton J. GPIIb (CD41) Integrin is Expressed on Mast Cells and Influences Their Adhesion Properties. *Exp Hematol* (2005) 33:403–12. doi: 10.1016/j.exphem.2005.01.011
24. Weinacker A, Ferrando R, Elliott M, Hogg J, Balmes J, Sheppard D. Distribution of Integrins Alpha V Beta 6 and Alpha 9 Beta 1 and Their Known Ligands, Fibronectin and Tenascin, in Human Airways. *Am J Respir Cell Mol Biol* (1995) 12(5):547–57. doi: 10.1165/ajrcmb.12.5.7537970
25. Li Q, Barres BA. Microglia and Macrophages in Brain Homeostasis and Disease. *Nat Rev Immunol* (2018) 18:225–41. doi: 10.1038/nri.2017.125
26. Galatro TF, Holtman IR, Lerario AM, Vainchtein ID, Brouwer N, Sola PR, et al. Transcriptomic Analysis of Purified Human Cortical Microglia Reveals Age-Associated Changes. *Nat Neurosci* (2017) 20:1162–71. doi: 10.1038/nn.4597
27. Goswami S. Importance of Integrin Receptors in the Field of Pharmaceutical & Medical Science. *Adv Biol Chem* (2013) 3:224–52. doi: 10.4236/abc.2013.32028
28. Philippeaux M, Vesin C, Tacchini-Cottier F, Piguet PF. Activated Human Platelets Express Beta2 Integrin. *Eur J Haematol* (1996) 56(3):130–7. doi: 10.1111/j.1600-0609.1996.tb01331.x
29. Fagerholm SC, Guenther C, Asens ML, Savinko T, Uotila LM. Beta2-Integrins and Interacting Proteins in Leukocyte Trafficking, Immune Suppression, and Immunodeficiency Disease. *Front Immunol* (2019) 10 (254). doi: 10.3389/fimmu.2019.00254
30. Mitroulis I, Alexaki VI, Kourtzelis I, Ziogas A, Hajishengallis G, Chavakis T. Leukocyte Integrins: Role in Leukocyte Recruitment and as Therapeutic Targets in Inflammatory Disease. *Pharmacol Ther* (2015), 123–35. doi: 10.1016/j.pharmthera.2014.11.008
31. Schittenhelm L, Hilkens CM, Morrison VL. β2 Integrins As Regulators of Dendritic Cell, Monocyte, and Macrophage Function. *Front Immunol* (2017) 8(1866). doi: 10.3389/fimmu.2017.01866
32. Carman CV, Springer TA. Integrin Avidity Regulation: Are Changes in Affinity and Conformation Underemphasized? *Curr Opin Cell Biol* (2003) 15:547–56. doi: 10.1016/j.ceb.2003.08.003
33. Askari JA, Buckley PA, Mould AP, Humphries MJ. Linking Integrin Conformation to Function. *J Cell Sci* (2009) 122(2):165–70. doi: 10.1242/jcs.018556
34. Li R, Rieu P, Griffith DL, Scott D, Arnaout MA. Two Functional States of the CD11b A-Domain: Correlations With Key Features of Two Mn2 +-Complexed Crystal Structures. *J Cell Biol* (1998) 218(9):1523–34. doi: 10.1083/jcb.143.6.1523
35. McCleverty CJ, Liddington RC. Engineered Allosteric Mutants of the Integrin Alphambeta2 I Domain: Structural and Functional Studies. *Biochem J* (2003) 372(1):121–7. doi: 10.1042/bj20021273
36. Zarbock A, Abram CL, Hundt M, Altman A, Lowell CA, Ley K. PSGL-1 Engagement by E-Selectin Signals Through Src Kinase Fgr and ITAM Adapters DAP12 and Fcrγ to Induce Slow Leukocyte Rolling. *J Exp Med* (2008) 205(10):2339–47. doi: 10.1084/jem.20072660
37. Tadayuki Yago NZ, Zhao L, Abrams CS, McEver RP. Selectins and Chemokines Use Shared and Distinct Signals to Activate β2 Integrins in Neutrophils. *Blood Adv* (2018) 2(7):731–44. doi: 10.1182/bloodadvances.2017015602
38. Takagi J, Petre BM, Walz T, Springer TA. Global Conformational Rearrangements in Integrin Extracellular Domains in Outside-In and Inside-Out Signaling. *Cell* (2002) 110(5):599–611. doi: 10.1016/S0092-8674(02)00935-2
39. Wegener KL, Partridge AW, Han J, Pickford AR, Liddington RC, Ginsberg MH, et al. Structural Basis of Integrin Activation by Talin. *Cell* (2007) 128 (1):171–82. doi: 10.1016/j.cell.2006.10.048
40. Choi EY, Santoso S, Chavakis T. Mechanisms of Neutrophil Transendothelial Migration. *Front Biosci (Landmark edition)* (2009) 14:1596–605. doi: 10.2741/3327
41. Nourshargh S, Hordijk PL, Sixt M. Breaching Multiple Barriers: Leukocyte Motility Through Venular Walls and the Interstitium. *Nat Rev Moclec Cell Biol* (2010) 11:366–78. doi: 10.1038/nrm2889
42. Partsch G, Schwarzer C. An Indirect Bioluminescence Method for the Quantitative Measurement of Polymorphonuclear Cell Chemotaxis. *J Biolumin Chemilumin* (1991) 6(3):159–67. doi: 10.1002/bio.1170060305
43. Kramer N, Walzl A, Unger C, Rosner M, Krupitza G, Hengstschläger M, et al. In Vitro Cell Migration and Invasion Assays. *Mutat Res/Rev Mutat Res* (2013) 752(1):10–24. doi: 10.1016/j.mrrev.2012.08.001
44. Place TL, Domann FE, Case AJ. Limitations of Oxygen Delivery to Cells in Culture: An Underappreciated Problem in Basic and Translational Research. *Free Radical Biol Med* (2017) 113:311–22. doi: 10.1016/j.freeradbiomed.2017.10.003
45. Trombetta ES, Mellman I. Cell Biology of Antigen Processing In Vitro and In Vivo. *Annu Rev Immunol* (2005) 23:975–1028. doi: 10.1146/annurev.immunol.22.012703.104538
46. Culshaw S, Millington OR, Brewer JM, McInnes IB. Murine Neutrophils Present Class II Restricted Antigen. *Immunol Lett* (2008) 118:49–54. doi: 10.1016/j.imlet.2008.02.008
47. Joseph A, Guevara-Torres A, Schallek J. Imaging Single-Cell Blood Flow in the Smallest to Largest Vessels in the Living Retina. *eLIFE* (2019) 8:1–36: e45077. doi: 10.7554/eLife.45077
48. Blatter C, Meijer EFJ, Nam AS, Jones D, Bouma BE, Padera TP, et al. In Vivo Label-Free Measurement of Lymph Flow Velocity and Volumetric Flow Rates Using Doppler Optical Coherence Tomography. *Sci Rep* (2016) 6:10. doi: 10.1038/srep29035
49. Hall JG, Morris B. The Output of Cells IN Lymph From THE Popliteal Node Of Sheep. *Exp Physiol Cognate Med Sci* (1962) 47(4):360–9. doi: 10.1113/expphysiol.1962.sp001620
50. Smith JB, McIntosh GH, Morris B. The Traffic of Cells Through Tissues: A Study of Peripheral Lymph in Sheep. *J Anat* (1970) 107(1):87–100. doi: 10.1002/path.1711000104
51. Sokolowski J, Jakobsen E, Johannessen JV. Cells in Peripheral Leg Lymph of Normal Men, Lymphology. *Lymphology* (1978) 11(4):202–7.
52. Olszewski WL, Grzelak I, Ziolkowska A, Engeset A. Immune Cell Traffic From Blood Through the Normal Human Skin to Lymphatics. *Clinics Dermatol* (1995) 13(5):473–83. doi: 10.1016/0738-081X(95)00087-V
53. Schineis P, Runge P, Halin C. Cellular Traffic Through Afferent Lymphatic Vessels. *Vasc Pharmacol* (2019) 112:31–41. doi: 10.1016/j.vph.2018.08.001
54. Byrne SN, Limo´n-Flores AY, Ullrich SE. Mast Cell Migration From the Skin to the Draining Lymph Nodes Upon Ultraviolet Irradiation Represents a Key Step in the Induction of Immune Suppression. *J Immunol* (2008) 180:4648–55. doi: 10.4049/jimmunol.180.7.4648
55. Tal O, Lim HY, Gurevich I, Milo I, Shipony Z, Ng LG, et al. DC Mobilization From the Skin Requires Docking to Immobilized CCL21 on Lymphatic Endothelium and Intralymphatic Crawling. *J Exp Med* (2011) 208(10):2141–53. doi: 10.1084/jem.20102392
56. Friedl P, Bröcker E-B. Reconstructing Leukocyte Migration in 3D Extracellular Matrix by Time-Lapse Videomicroscopy and Computer-Assisted Tracking. *Cell Migration Inflammation Immunity Methods Mol Biol* (2004) 239:77–90. doi: 10.1385/1-59259-435-2:77
57. Mempel TR, Scimone ML, Mora JR, von Andrian UH. In Vivo Imaging of Leukocyte Trafficking in Blood Vessels and Tissues. *Curr Opin Immunol* (2004) 16(4):406–17. doi: 10.1016/j.coi.2004.05.018
58. Torcellan T, Stolp J, Chtanova T. In Vivo Imaging Sheds Light on Immune Cell Migration and Function in Cancer. *Front Immunol* (2017) 8:309. doi: 10.3389/fimmu.2017.00309
59. Rumianek AN, Greaves DR. How Have Leukocyte In Vitro Chemotaxis Assays Shaped Our Ideas About Macrophage Migration? *Biology* (2020) 9 (439):1–13. doi: 10.3390/biology9120439
60. Friedl P, Zänker KS, Bröcker E-B. Cell Migration Strategies in 3-D Extracellular Matrix: Differences in Morphology, Cell Matrix Interactions, and Integrin Function. *Microscopy Res Technique* (1998) 43(5):369–78. doi: 10.1002/(SICI)1097-0029(19981201)43:5<369::AID-JEMT3>3.0.CO;2-6
61. Repesh LA. A New In Vitro Assay for Quantitating Tumor Cell Invasion. *Invasion Metastasis* (1989) 9(3):192–208.
62. Giannattasio A, Weil S, Kloess S, Ansari N, Stelzer EHK, Cerwenka A, et al. Cytotoxicity and Infiltration of Human NK Cells in In Vivo-Like Tumor Spheroids. *BMC Cancer* (2015) 15(351):13. doi: 10.1186/s12885-015-1321-y

63. Weber M, Sixt M. Live Cell Imaging of Chemotactic Dendritic Cell Migration in Explanted Mouse Ear Preparations. *Chemokines Methods Mol Biol (Methods Protocols)* (2013) 1013:1013. doi: 10.1007/978-1-62703-426-5_14
64. Phillipson M, Heit B, Colarusso P, Liu L, Ballantyne CM, Kubes P. Intraluminal Crawling of Neutrophils to Emigration Sites: A Molecularly Distinct Process From Adhesion in the Recruitment Cascade. *J Exp Med* (2006) 203(12):2569–75. doi: 10.1084/jem.20060925
65. Blanchoin L, Boujemaa-Paterski R, Sykes C, Plastino J. Actin Dynamics, Architecture, and Mechanics in Cell Motility. *Physiol Rev* (2014) 94(1):235–63. doi: 10.1152/physrev.00018.2013
66. Gardel ML, Schneider IC, Aratyn-Schaus Y, Waterman CM. Mechanical Integration of Actin and Adhesion Dynamics in Cell Migration. *Annu Rev Cell Dev Biol* (2010) 26:315–33. doi: 10.1146/annurev.cellbio.011209.122036
67. Huse M. Mechanical Forces in the Immune System. *Nat Rev Immunol* (2017) 17(11):679–90. doi: 10.1038/nri.2017.74
68. Ridley AJ, Schwartz MA, Burridge K, Firtel RA, Ginsberg MH, Borisy G, et al. Cell Migration: Integrating Signals From Front to Back. *Science* (2003) 302(5651):1704–9. doi: 10.1126/science.1092053
69. Pollard TD, Borisy GG. Cellular Motility Driven by Assembly and Disassembly of Actin Filaments. *Cell* (2003) 112(4):453–65. doi: 10.1016/S0092-8674(03)00120-X
70. Smith LA, Aranda-Espinoza H, Haun JB, Dembo M, Hammer DA. Neutrophil Traction Stresses are Concentrated in the Uropod During Migration. *Biophys J* (2007) 92(7):L58–60. doi: 10.1529/biophysj.106.102822
71. Friedl P, Wolf K. Plasticity of Cell Migration: A Multiscale Tuning Model. *J Cell Biol* (2009) 188(1):11–9. doi: 10.1083/jcb.200909003
72. Fackler OT, Grosse R. Cell Motility Through Plasma Membrane Blebbing. *J Cell Biol* (2008) 181(6):879–84. doi: 10.1083/jcb.200802081
73. Sanz-Moreno, Marshall CJ. Rho-GTPase Signaling Drives Melanoma Cell Plasticity. *Cell Cycle* (2009) 8(10):1484–7. doi: 10.4161/cc.8.10.8490
74. Janson LW, Taylor DL. In Vitro Models of Tail Contraction and Cytoplasmic Streaming in Amoeboid Cells. *J Cell Biol* (1993) 123(2):345–56. doi: 10.1083/jcb.123.2.345
75. Houdusse A, Sweeney HL. How Myosin Generates Force on Actin Filaments. *Trends Biochem Sci* (2016) 41(12):989–97. doi: 10.1016/j.tibs.2016.09.006
76. Kato Y, Miyakawa T, Tanokura M. Overview of the Mechanism of Cytoskeletal Motors Based on Structure. *Biophys Rev* (2018) 10:571–81. doi: 10.1007/s12551-017-0368-1
77. Case LB, Waterman CM. Integration of Actin Dynamics and Cell Adhesion by a Three-Dimensional, Mechanosensitive Molecular Clutch. *Nat Cell Biol* (2015) 17:955–63. doi: 10.1038/ncb3191
78. Song KH, Kwon KW, Choi J-C, Jung J, Park Y, Suhb K-Y, et al. T Cells Sense Biophysical Cues Using Lamellipodia and Filopodia to Optimize Intraluminal Path Finding. *Integr Biol* (2014) 6:450–9. doi: 10.1039/c4ib00021h
79. Gupton SL, Gertler FB. Filopodia: The Fingers That Do the Walking. *Sci Signaling* (2007) 2007(400):re5. doi: 10.1126/stke.4002007re5
80. Krause M, Gautreau A. Steering Cell Migration: Lamellipodium Dynamics and the Regulation of Directional Persistence. *Nat Rev Mol Cell Biol* (2014) 15:577–90. doi: 10.1038/nrm3861
81. Yip AK, Chiam K-H, Matsudaira P. Traction Stress Analysis and Modeling Reveal That Amoeboid Migration in Confined Spaces is Accompanied by Expansive Forces and Requires the Structural Integrity of the Membrane–Cortex Interactions. *Integr Biol* (2015) 7(1196):16. doi: 10.1039/C4IB00245H
82. Vallotton P, Small JV. Shifting Views on the Leading Role of the Lamellipodium in Cell Migration: Speckle Tracking Revisited. *J Cell Sci* (2009) 122(12):1955–8. doi: 10.1242/jcs.042036
83. Heath JP, Holifield BF. Cell Locomotion: New Research Tests Old Ideas on Membrane and Cytoskeletal Flow. *Cell Motil Cytoskeleton* (1991) 18:245–57. doi: 10.1002/cm.970180402
84. Gupton SL, Anderson KL, Kole TP, Fischer RS, Ponti A, Hitchcock-DeGregori SE, et al. Cell Migration Without a Lamellipodium: Translation of Actin Dynamics Into Cell Movement Mediated by Tropomyosin. *J Cell Biol* (2005) 168:619–31. doi: 10.1083/jcb.200406063
85. Hiromi M, Tsubota K, Hoyano T, Adachi T, Liu H. Three-Dimensional Modulation of Cortical Plasticity During Pseudopodial Protrusion of Mouse Leukocytes. *Biochem Biophys Res Commun* (2013) 438:594–9. doi: 10.1016/j.bbrc.2013.08.010
86. Murphy DA, Courtneidge SA. The 'Ins' and 'Outs' of Podosomes and Invadopodia: Characteristics, Formation and Function. *Nat Rev Moclec Cell Biol* (2011) 12:413–26. doi: 10.1038/nrm3141
87. Manley HR, Potter DL, Heddleston JM, Chew T-L, Keightley MC, Lieschke GJ. Frontline Science: Dynamic Cellular and Subcellular Features of Migrating Leukocytes Revealed by In Vivo Lattice Lightsheet Microscopy. *J Leukocyte Biol* (2020) 108:455–68. doi: 10.1002/JLB.3HI0120-589R
88. Doyle AD, Petrie RJ, Kutys ML, Yamada KM. Dimensions in Cell Migration. *Curr Opin Cell Biol* (2013) 25:642–9. doi: 10.1016/j.ceb.2013.06.004
89. Caille N, Thoumine O, Tardy Y, Meister J-J. Contribution of the Nucleus to the Mechanical Properties of Endothelial Cells. *J Biomech* (2002) 35(2):177–87. doi: 10.1016/S0021-9290(01)00201-9
90. Lammerding J. Mechanics of the Nucleus. *Compr Physiol* (2011) 1(2):783–807. doi: 10.1002/cphy.c100038
91. Kameritsch P, Renkawitz J. Principles of Leukocyte Migration Strategies. *Trends Cell Biol* (2020) 30(10):818–32. doi: 10.1016/j.tcb.2020.06.007
92. Harada T, Swift J, Irianto J, Shin J-W, Spinler KR, Athirasala A, et al. Nuclear Lamin Stiffness is a Barrier to 3D Migration, But Softness can Limit Survival. *J Cell Biol* (2014) 204(5):669–82. doi: 10.1083/jcb.201308029
93. Wolf K, te Lindert M, Krause M, Alexander S, te Riet J, Willis AL, et al. Physical Limits of Cell Migration: Control by ECM Space and Nuclear Deformation and Tuning by Proteolysis and Traction Force. *J Cell Biol* (2013) 201(7):1069–84. doi: 10.1083/jcb.201210152
94. Renkawitz J, Kopf A, Stopp J, de Vries I, Driscoll MK, Merrin J, et al. Nuclear Positioning Facilitates Amoeboid Migration Along the Path of Least Resistance. *Nature* (2019) 568:546–50. doi: 10.1038/s41586-019-1087-5
95. Lo C-M, Wang H-B, Dembo M, Wang Y-l. Cell Movement Is Guided by the Rigidity of the Substrate. *Biophys J* (2000) 79:144–52. doi: 10.1016/S0006-3495(00)76279-5
96. Calero-Cuenca FJ, Janota CS, Gomes ER. Dealing With the Nucleus During Cell Migration. *Curr Opin Cell Biol* (2018) 50:35–41. doi: 10.1016/j.ceb.2018.01.014
97. Renkawitz J, Schumann K, Weber M, Lämmermann T, Pflicke H, Piel M, et al. Adaptive Force Transmission in Amoeboid Cell Migration. *Nat Cell Biol* (2009) 11(12):1438–43. doi: 10.1038/ncb1992
98. Harburger DS, Calderwood DA. Integrin Signalling at a Glance. *J Cell Sci* (2009) 122:159–63. doi: 10.1242/jcs.018093
99. Legate KR, Wickström SA, Fässler R. Genetic and Cell Biological Analysis of Integrin Outside-in Signaling. *Genes Dev* (2009) 23(4):397–418. doi: 10.1101/gad.1758709
100. Maniotis AJ, Chen CS, Ingber DE. Demonstration of Mechanical Connections Between Integrins, Cytoskeletal Filaments, and Nucleoplasm That Stabilize Nuclear Structure. *PNAS* (1997) 94:849–54. doi: 10.1073/pnas.94.3.849
101. Madrazo E, Conde AC, Redondo-Muñoz J. Inside the Cell: Integrins as New Governors of Nuclear Alterations? *Cancers* (2017) 9(82):1–17. doi: 10.3390/cancers9070082
102. Hogg N, Patzak I, Willenbrock F. The Insider's Guide to Leukocyte Integrin Signalling and Function. *Nat Rev Immunol* (2011) 11:416–26. doi: 10.1038/nri2986
103. Huveneers S, Danen EHJ. Adhesion Signaling – Crosstalk Between Integrins, Src and Rho. *Oncogene* (2009) 122:1059–69. doi: 10.1242/jcs.039446
104. Zhi H, Rauova L, Hayes V, Gao C, Boylan B, Newman DK, et al. Cooperative Integrin/ITAM Signaling in Platelets Enhances Thrombus Formation In Vitro and In Vivo. *Blood* (2013) 121(10):1858–67. doi: 10.1182/blood-2012-07-443325
105. Kalappurakkal JM, Anilkumar AA, Patra C, van Zanten TS, Sheetz MP, Mayor S. Integrin Mechano-Chemical Signaling Generates Plasma Membrane Nanodomains That Promote Cell Spreading. *Cell* (2019) 177(7):1738–56. doi: 10.1016/j.cell.2019.04.037
106. Chronopoulos A, Thorpe SD, Cortes E, Lachowski D, Rice AJ, Mykuliak VV, et al. Syndecan-4 Tunes Cell Mechanics by Activating the Kindlin-Integrin-RhoA Pathway. *Nat Mater* (2020) 19:669–78. doi: 10.1038/s41563-019-0567-1
107. Dib K, Melander F, Axelsson L, Dagher M-C, Aspenstrom P, Andersson T. Down-Regulation of Rac Activity During Beta2 Integrin-Mediated Adhesion of Human Neutrophils. *J Biol Chem* (2003) 278(26):24181–8. doi: 10.1074/jbc.M302300200

108. Nurmi SM, Autero M, Raunio AK, Gahmberg CG, Fagerholm SC. Phosphorylation of the LFA-1 Integrin β2-Chain on Thr-758 Leads to Adhesion, Rac-1/Cdc42 Activation, and Stimulation of CD69 Expression in Human T Cells. *J Biol Chem* (2006) 282:968–75. doi: 10.1074/jbc.M608524200
109. Schiller HB, Fässler R. Mechanosensitivity and Compositional Dynamics of Cell-Matrix Adhesions. *EMBO Rep* (2013) 14(6):509–19. doi: 10.1038/embor.2013.49
110. Winograd-Katz SE, Fässler R, Geiger B, Legate KR. The Integrin Adhesome: From Genes and Proteins to Human Disease. *Nat Rev Mol Cell Biol* (2014) 15:273–88. doi: 10.1038/nrm3769
111. Bachmann M, Kukkurainen S, Hytönen VP, Wehrle-Haller XB. Cell Adhesion by Integrins. *Physiol Rev* (2019) 99:1655–99. doi: 10.1152/physrev.00036.2018
112. Kuo J-C, Han X, Hsiao C-T, Yates JRIII., Waterman CM. Analysis of the Myosin-II-Responsive Focal Adhesion Proteome Reveals a Role for β–Pix in Negative Regulation of Focal Adhesion Maturation. *Nat Cell Biol* (2011) 13 (4):383–93. doi: 10.1038/ncb2216
113. Horton ER, Byron A, Askari JA, Ng DHJ, Millon-Frémillon A, Robertson J, et al. Definition of a Consensus Integrin Adhesome and its Dynamics During Adhesion Complex Assembly and Disassembly. *Nat Cell Biol* (2015) 17:1577–87. doi: 10.1038/ncb3257
114. Calderwood DA, Ginsberg MH. Talin Forges the Links Between Integrins and Actin. *Nat Cell Biol* (2003) 5(8):694–6. doi: 10.1038/ncb0803-694
115. Bledzka K, Bialkowska K, Sossey-Alaoui K, Vaynberg J, Pluskota E, Qin J, et al. Kindlin-2 Directly Binds Actin and Regulates Integrin Outside-in Signaling. *J Cell Biol* (2016) 213:97–108. doi: 10.1083/jcb.201501006
116. Zhang M, March ME, Lane WS, Long EO. A Signaling Network Induced by β2 Integrin Controls the Polarization of Lytic Granulesin Cytotoxic Cells. *Sci Signaling* (2014) 7(346):96. doi: 10.1126/scisignal.2005629
117. Calderwood DA, Zent R, Grant R, Rees DJG, Hynes RO, Ginsberg MH. The Talin Head Domain Binds to Integrin β Subunit Cytoplasmic Tails and Regulates Integrin Activation. *J Biol Chem* (1999) 274:28071–4. doi: 10.1074/jbc.274.40.28071
118. Rio AD, Perez-Jimenez R, Liu R, Roca-Cusachs P, Fernandez JM, Sheetz MP. Stretching Single Talin Rod Molecules Activates Vinculin Binding. *Science* (2009) 323(5914):638–41. doi: 10.1126/science.1162912
119. Yao M, Goult BT, Chen H, Cong P, Sheetz MP, Yan J. Mechanical Activation of Vinculin Binding to Talin Locks Talin in an Unfolded Conformation. *Sci Rep* (2014) 4(4610):7. doi: 10.1038/srep04610
120. Sakai Y, Tsunekawa M, Ohta K, Shimizu T, Pastuhov SI, Hanafusa H, et al. The Integrin Signaling Network Promotes Axon Regeneration via the Src–Ephexin-RhoA GTPase Signaling Axis. *J Neurosci* (2021) 41(22):4754–67. doi: 10.1523/JNEUROSCI.2456-20.2021
121. Haining AWM, Rahikainen R, Cortes E, Lachowski D, Rice A, von Essen M, et al. Mechanotransduction in Talin Through the Interaction of the R8 Domain With DLC1. *PloS Biol* (2018) 16(7):20. doi: 10.1371/journal.pbio.2005599
122. Healy KD, Hodgson L, Kim T-Y, Shutes A, Maddileti S, Juliano RL, et al. DLC-1 Suppresses Non-Small Cell Lung Cancer Growth and Invasion by RhoGAP-Dependent and Independent Mechanisms. *Mol Carcinogenesis* (2008) 47:326–37. doi: 10.1002/mc.20389
123. Moser M, Nieswandt B, Ussar S, Pozgajova M, Fässler R, et al. Kindlin-3 is Essential for Integrin Activation and Platelet Aggregation. *Nat Med* (2008) 14:325–30. doi: 10.1038/nm1722
124. Lu L, Lin C, Yan Z, Wang S, Zhang Y, Wang S, et al. Kindlin-3 Is Essential for the Resting Alpha4beta1 Integrin-Mediated Firm Cell Adhesion Under Shear Flow Conditions. *J Biol Chem* (2016) 291(19):10363–71. doi: 10.1074/jbc.M116.717694
125. Manevich-Mendelson E, Feigelson SW, Pasvolsky R, Aker M, Grabovsky V, Shulman Z, et al. Loss of Kindlin-3 in LAD-III Eliminates LFA-1 But Not VLA-4 Adhesiveness Developed Under Shear Flow Conditions. *Blood* (2009) 114:2344–53. doi: 10.1182/blood-2009-04-218636
126. Klapproth S, Moretti FA, Zeiler M, Ruppert R, Breithaupt U, Mueller S, et al. Minimal Amounts of Kindlin-3 Suffice for Basal Platelet and Leukocyte Functions in Mice. *Blood* (2015) 126(24):2592–600. doi: 10.1182/blood-2015-04-639310
127. Ussar S, Wang H-V, Linder S, Fässler R, Moser M. The Kindlins: Subcellular Localization and Expression Duringmurine Development. *Exp Cell Res* (2006) 312(16):3142–51. doi: 10.1016/j.yexcr.2006.06.030
128. Chatterjee D, Zhiping LL, Tan S-M, Bhattacharjya S. NMR Structure, Dynamics and Interactions of the Integrin β2 Cytoplasmic Tail With Filamin Domain Igflna21. *Sci Rep* (2018) 8(5490):14. doi: 10.1038/s41598-018-23866-6
129. Kiema T, Lad Y, Jiang P, Oxley CL, Baldassarre M, Wegener KL, et al. The Molecular Basis of Filamin Binding to Integrins and Competition With Talin. *Mol Cell* (2006) 21(3):337–47. doi: 10.1016/j.molcel.2006.01.011
130. Takala H, Nurminen E, Nurmi SM, Aatonen M, Strandin T, Takatalo M, et al. β2 Integrin Phosphorylation on Thr758 Acts as a Molecular Switch to Regulate 14-3-3 and Filamin Binding. *Blood* (2008) 112(5):1853–62. doi: 10.1182/blood-2007-12-127795
131. Valmu L, Fagerholm S, Suila H, Gahmberg CG. The Cytoskeletal Association of CD11/CD18 Leukocyte Integrins in Phorbol Ester-Activated Cells Correlates With CD18 Phosphorylation. *Eur J Immunol* (1999) 29:2107–18. doi: 10.1002/(SICI)1521-4141(199907)29:07<2107::AID-IMMU2107>3.0.CO;2-T
132. Loo DT, Kanner SB, Aruffo A. Filamin Binds to the Cytoplasmic Domain of the Beta1-Integrin. Identification of Amino Acids Responsible for This Interaction. *J Biol Chem* (1998) 273:23304–12. doi: 10.1074/jbc.273.36.23304
133. Rosa J-P, Raslova H, Bryckaert M. Filamin A: Key Actor in Platelet Biology. *blood* (2019) 134(16):1279–88. doi: 10.1182/blood.2019000014
134. Calderwood DA, Huttenlocher A, Kiosses WB, Rose DM, Woodside DG, Schwartz MA, et al. Increased Filamin Binding to β-Integrin Cytoplasmic Domains Inhibits Cell Migration. *Nat Cell Biol* (2001) 3:1060–8. doi: 10.1038/ncb1201-1060
135. Rognoni L, Stigler J, Pelz B, Ylänne J, Rief M. Dynamic Force Sensing of Filamin Revealed in Single-Molecule Experiments. *PNAS* (2012) 109 (48):19679–84. doi: 10.1073/pnas.1211274109
136. Nakamura F, Stossel TP, Hartwig JH. The Filamins Organizers of Cell Structure and Function. *Cell Adhesion Migration* (2011) 5(2):160–9. doi: 10.4161/cam.5.2.14401
137. Kumar A, Shutova MS, Tanaka K, Iwamoto DV, Calderwood DA, Svitkina TM, et al. Filamin A Mediates Isotropic Distribution of Applied Force Across the Actin Network. *J Cell Biol* (2019) 218(8):2481–91. doi: 10.1083/jcb.201901086
138. Glogauer M, Pam A, Chou D, Janmey PA, Downey GP, McCulloch CAG. The Role of Actin-Binding Protein 280 in Integrin-Dependent Mechanoprotection. *J Biol Chem* (1998) 273:1689–98. doi: 10.1074/jbc.273.3.1689
139. Ehrlicher AJ, Nakamura F, Hartwig JH, Weitz DA, Stossel TP. Mechanical Strain in Actin Networks Regulates FilGAP and Integrin Binding to Filamin A. *Nature* (2011) 478:260–3. doi: 10.1038/nature10430
140. Ohta Y, Hartwig JH, Stossel TP. FilGAP, a Rho- and ROCK-Regulated GAP for Rac Binds Filamin A to Control Actin Remodelling. *Nat Cell Biol* (2006) 8:803–14. doi: 10.1038/ncb1437
141. Heasman SJ, Ridley AJ. Mammalian Rho GTPases: New Insights Into Their Functions From In Vivo Studies. *Nat Rev Mol Cell Biol* (2008) 9:690–701. doi: 10.1038/nrm2476
142. Algaber A, AlHaidari A, Madhi R, Rahman M, Syk I, Thorlacius H. MicroRNA–340–5p Inhibits Colon Cancer Cell Migration via Targeting of RhoA. *Sci Rep* (2020) 10(16934):1–7. doi: 10.1038/s41598-020-73792-9
143. Moon M-Y, Kim H-J, Kim M-J, Uhm S, Park J-W, Suk K-T. Rap1 Regulates Hepatic Stellate Cell Migration Through the Modulation of RhoA Activity in Response to TGF–β1. *Int J Mol Med* (2019) 44:491–502. doi: 10.3892/ijmm.2019.4215
144. Kim J-M, Kim MY, Lee K, Jeong D. Distinctive and Selective Route of PI3K/PKCa-PKCd/RhoA-Rac1 Signaling in Osteoclastic Cell Migration. *Mol Cell Endocrinol* (2016) p:261–7. doi: 10.1016/j.mce.2016.08.042
145. Worthylake RA, Lemoine S, Watson JM, Burridge K. RhoA is Required for Monocyte Tail Retraction During Transendothelial Migration. *J Cell Biol* (2001) 154(1):147–60. doi: 10.1083/jcb.200103048
146. Sahai E, Marshall CJ. Differing Modes of Tumour Cell Invasion Have Distinct Requirements for Rho/ROCK Signalling and Extracellular Proteolysis. *Nat Cell Biol* (2003) 5:711–9. doi: 10.1038/ncb1019
147. Worthylake RA, Burridge K. RhoA and ROCK Promote Migration by Limiting Membrane Protrusions. *J Biol Chem* (2003) p:13578–84. doi: 10.1074/jbc.M211584200
148. Watanabe S, Okawa K, Miki T, Sakamoto S, Morinaga T, Segawa K, et al. Rho and Anillin-Dependent Control of Mdia2 Localization and Function in

Cytokinesis. *Mol Biol Cell* (2010) 21:3193–204. doi: 10.1091/mbc.e10-04-0324
149. Staus DP, Taylor JM, Mack CP. Enhancement of Mdia2 Activity by Rho-Kinase-Dependent Phosphorylation of the Diaphanous Autoregulatory Domain. *Biochem J* (2011) 439:57–65. doi: 10.1042/BJ20101700
150. Giagulli C, Scarpini E, Ottoboni L, Narumiya S, Butcher EC, Constantin G, et al. RhoA and Zeta PKC Control Distinct Modalities of LFA-1 Activation by Chemokines: Critical Role of LFA-1 Affinity Triggering in Lymphocyte In Vivo Homing. *Immunity* (2004) 20(1):25–35. doi: 10.1016/S1074-7613(03)00350-9
151. Kinashi T. Intracellular Signalling Controlling Integrin Activation in Lymphocytes. *Nat Rev Immunol* (2005) 5:546–59. doi: 10.1038/nri1646
152. Vielkind S, Gallagher-Gambarelli M, Gomez M, Hinton HJ, Cantrell DA. Integrin Regulation by RhoA in Thymocytes. *J Immunol* (2005) 175:350–7. doi: 10.4049/jimmunol.175.1.350
153. Amison RT, Momi S, Morris A, Manni G, Keir S, Gresele P, et al. RhoA Signaling Through Platelet $P2Y_1$ Receptor Controls Leukocyte Recruitment in Allergic Mice. *J Allergy Clin Immunol* (2015) 135(2):528–38. doi: 10.1016/j.jaci.2014.09.032
154. Ridley AJ, Paterson HF, Johnston CL, Diekmann D, Hall A. The Small Gtp-Binding Protein Rac Regulates Growth Factor-Induced Membrane Ruffling. *Cell* (1992) 70:401–10. doi: 10.1016/0092-8674(92)90164-8
155. Nobes CD, Hall A. Rho, Rac, and Cdc42 GTPases Regulate the Assembly of Multimolecular Focal Complexes Associated With Actin Stress Fibers, Lamellipodia, and Filopodia. *Cell* (1995) 81:53–62. doi: 10.1016/0092-8674(95)90370-4
156. Allen WE, Jones GE, Pollard JW. Rho, Rac and Cdc42 Regulate Actin Organization and Cell Adhesion in Macrophages. *J Cell Sci* (1997) 110:707–20. doi: 10.1242/jcs.110.6.707
157. Vincent S, Jeanteur P, Fort P. Growth-Regulated Expression of Rhog, a New Member of the Ras Homolog Gene Family. *Mol Cell Biol* (1992) 12(7):3138–48. doi: 10.1128/MCB.12.7.3138
158. Didsbury J, Weber RF, Bokoch GM, Evans T, Snyderma R. Rac, a Novel Ras-Related Family of Proteins That Are Botulinum Toxin Substrates. *J Biol Chem* (1989) 264(28):16378–82. doi: 10.1016/S0021-9258(19)84716-6
159. Shirsat NV, Pignolo RJ, Kreider BL, Rovera G. A Member of the Ras Gene Superfamily is Expressed Specifically in T, B and Myeloid Hemopoietic Cells. *Oncogene* (1990) 5(5):769–72.
160. Corbetta S, Gualdoni S, Albertinazzi C, Paris S, Croci L, Consalez GG, et al. Generation and Characterization of Rac3 Knockout Mice. *Mol Cell Biol* (2005) 25(13):5763–76. doi: 10.1128/MCB.25.13.5763-5776.2005
161. Haataja L, Groffen J, Heisterkamp N. Characterization of RAC3, a Novel Member of the Rho Family. *J Biol Chem* (1997) 272(33):20384–8. doi: 10.1074/jbc.272.33.20384
162. Fukui Y, Hashimoto O, Sanui T, Oono T, Koga H, Abe M, et al. Haematopoietic Cell-Specific CDM Family Protein DOCK2 is Essential for Lymphocyte Migration. *Nature* (2001) 412:826–31. doi: 10.1038/35090591
163. Pollard TD. Regulation of Actin Filament Assembly by Arp2/3 Complex and Formins. *Annu Rev Biophys Biomolec Structures* (2007) 36:451–77. doi: 10.1146/annurev.biophys.35.040405.101936
164. Atat OE, Fakih A, El-Sibai M. RHOG Activates RAC1 Through CDC42 Leading to Tube Formation in Vascular Endothelial Cells. *cells* (2019) 8(2):17. doi: 10.3390/cells8020171
165. Helden S. Rho GTPase Expression in Human Myeloid Cells. *PLOoS One* (2012) 7(8):14. doi: 10.1371/journal.pone.0042563
166. Dallery E, Galiègue-Zouitina S, Collyn-d'Hooghe M, Quief S, Denis C, Hildebrand MP, et al. TTF, a Gene Encoding a Novel Small G Protein, Fuses to the Lymphoma-Associated LAZ3 Gene by T(3;4) Chromosomal Translocation. *Oncogene* (1995) 10(11):2171–8.
167. Lahousse SB, Smorowski A-L, Denis C, Daniéle L, Kerckaert J-P, Galiégue-Zouitina S. Structural Features of Hematopoiesis-Specific RhoH/ARHH Gene: High Diversity of 5V-UTR in Different Hematopoietic Lineages Suggests a Complex Post-Transcriptional Regulation. *Gene* (2004) 343:55–68. doi: 10.1016/j.gene.2004.08.022
168. Gu Y, Jasti AC, Jansen M, Siefring JE. RhoH, a Hematopoietic-Specific Rho GTPase, Regulates Proliferation, Survival, Migration, and Engraftment of Hematopoietic Progenitor Cells. *blood* (2005) 105(4):1467–75. doi: 10.1182/blood-2004-04-1604
169. Gu Y, Chae H-D, Siefring JE, Jasti AC, Hildeman DA, Williams DA. RhoH GTPase Recruits and Activates Zap70 Required for T Cell Receptor Signaling and Thymocyte Development. *Nat Immunol* (2006) 7(11):1182–90. doi: 10.1038/ni1396
170. Dorn T, Kuhn U, Bungartz G, Stiller S, Bauer M, Ellwart J, et al. RhoH is Important for Positive Thymocyte Selection and T-Cell Receptor Signaling. *Blood* (2007) 109(6):2346–55. doi: 10.1182/blood-2006-04-019034
171. Sanchez-Aguilera A, Rattmann I, Drew DZ, Müller LUW, Summey V, Lucas DM, et al. Involvement of RhoH GTPase in the Development of B-Cell Chronic Lymphocytic Leukemia. *Leukemia* (2010) 24(1):97–104. doi: 10.1038/leu.2009.217
172. Li X, Bu X, Lu B, Avraham H, Flavell RA, Lim B. The Hematopoiesis-Specific GTP-Binding Protein RhoH Is GTPase Deficient and Modulates Activities of Other Rho GTPases by an Inhibitory Function. *Mol Cell Biol* (2002) 22(4):1158–71. doi: 10.1128/MCB.22.4.1158-1171.2002
173. Poh Y-C, Shevtsov SP, Chowdhury F, Wu DC, Na S, Dundr M, et al. Dynamic Force-Induced Direct Dissociation of Protein Complexes in a Nuclear Body in Living Cells. *Nat Commun* (2012) 3(866):10. doi: 10.1038/ncomms1873
174. Swift J, Ivanovska IL, Buxboim A, Harada T, Dingal PCDP, Pinter J, et al. Nuclear Lamin-A Scales With Tissue Stiffness and Enhances Matrix-Directed Differentiation. *Science* (2013) 341. doi: 10.1126/science.1240104
175. Stephens AD, Banigan EJ, Adam SA, Goldman RD, Marko JF. Chromatin and Lamin A Determine Two Different Mechanical Response Regimes of the Cell Nucleus. *Mol Biol Cell* (2017) 28(14):1984–96. doi: 10.1091/mbc.e16-09-0653
176. Lammerding J, Fong LG, Ji JY, Reue K, Stewart CL, Young SG, et al. Lamins A and C But Not Lamin B1 Regulate Nuclear Mechanics. *J Biol Chem* (2006) 281:25768–80. doi: 10.1074/jbc.M513511200
177. Guenther C, Faisal I, Fusciello M, Sokolova M, Harjunpää H, Ilander M, et al. β2-Integrin Adhesion Regulates Dendritic Cell Epigenetic and Transcriptional Landscapes to Restrict Dendritic Cell Maturation and Tumor Rejection. *Cancer Immunol Res* (2021) 9:1354–69. doi: 10.1158/2326-6066.CIR-21-0094
178. Wang P, Dreger M, Madrazo E, Williams CJ, Samaniego R, Hodson NW, et al. WDR5 Modulates Cell Motility and Morphology and Controls Nuclear Changes Induced by a 3D Environment. *PNAS* (2018) 115(34):8581–6. doi: 10.1073/pnas.1719405115
179. Zhang X, Cook PC, Zindy E, Williams CJ, Jowitt TA, Streuli CH, et al. Integrin Alpha4beta1 Controls G9a Activity That Regulates Epigenetic Changes and Nuclear Properties Required for Lymphocyte Migration. *Nucleic Acids Res* (2015) 44(7):3031–44. doi: 10.1093/nar/gkv1348
180. Hamminger P, Marchetti L, Preglej T, Platzer R, Zhu C, Kamnev A, et al. Histone Deacetylase 1 Controls CD4+ T Cell Trafficking in Autoinflammatory Diseases. *J Autoimmun* (2021) 119:13. doi: 10.1016/j.jaut.2021.102610
181. Cougoule C, Van Goethem E, Le Cabec V, Lafouresse F, Dupré L, Mehraj V, et al. Blood Leukocytes and Macrophages of Various Phenotypes Have Distinct Abilities to Form Podosomes and to Migrate in 3D Environments. *Eur J Cell Biol* (2012) 91:938–49. doi: 10.1016/j.ejcb.2012.07.002
182. Leung R, Wang Y, Cuddy K, Sun C, Magalhaes J, Grynpas M, et al. Filamin A Regulates Monocyte Migration Through Rho Small GTPases During Osteoclastogenesis. *J Bone Mineral Res* (2010) 25(5):1077–91. doi: 10.1359/jbmr.091114
183. Honing H, van den Berg TK, van der Pol SMA, Dijkstra CD, van der Kammen RA, Collard JG, et al. RhoA Activation Promotes Transendothelial Migration of Monocytes via ROCK. *J Leukocyte Biol* (2004) 75:6. doi: 10.1189/jlb.0203054
184. Aepfelbacher M, Essler M, Huber E, Czech A, Weber PC. Rho Is a Negative Regulator of Human Monocyte Spreading. *J Immunol* (1996) 157:5070–5.
185. Weber KSC, Klickstein LB, Weber PC, Weber C. Chemokine-Induced Monocyte Transmigration Requires Cdc42-Mediated Cytoskeletal Changes. *Eur J Immunol* (1998) 28:2245–51. doi: 10.1002/(SICI)1521-4141(199807)28:07<2245::AID-IMMU2245>3.0.CO;2-V
186. Worbs T, Hammerschmidt SI, Förster R. Dendritic Cell Migration in Health and Disease. *Nat Rev Immunol* (2017) 17:30–48. doi: 10.1038/nri.2016.116
187. Nitschké M, Aebischer D, Abadier M, Haener S, Lucic M, Vigl B, et al. Differential Requirement for ROCK in Dendritic Cell Migration Within

Lymphatic Capillaries in Steady-State and Inflammation. *Blood* (2012) 120 (11):2249–58. doi: 10.1182/blood-2012-03-417923
188. Cougoule C, Lastrucci C, Guiet R, Mascarau R, Meunier E, Lugo-Villarino G, et al. Podosomes, But Not the Maturation Status, Determine the Protease-Dependent 3d Migration in Human Dendritic Cells. *Front Immunol* (2018) 9:846. doi: 10.3389/fimmu.2018.00846
189. Dieu M-C, Vanbervliet B, Vicari A, Bridon J-M, Oldham E, Aït-Yahia S, et al. Selective Recruitment of Immature and Mature Dendritic Cells by Distinct Chemokines Expressed in Different Anatomic Sites. *J Exp Med* (1998) 188 (2):373–86. doi: 10.1084/jem.188.2.373
190. Saeki H, Moore AM, Brown MJ, Hwang ST. Cutting Edge: Secondary Lymphoid Tissue Chemokine (SLC) and CC Chemokine Receptor 7 (CCR7) Participate in the Emigration Pathway of Mature Dendritic Cells From the Skin to Regional Lymph Nodes. *J Immunol* (1999) 162:2472–5.
191. Braun A, Worbs T, Moschovakis GL, Halle S, Hoffmann K, Bölter J, et al. Afferent Lymph–Derived T Cells and DCs Use Different Chemokine Receptor CCR7-Dependent Routes for Entry Into the Lymph Node and Intranodal Migration. *Nat Immunol* (2011) 12:879–87. doi: 10.1038/ni.2085
192. Jakubzick C, Tacke F, Llodra J, van Rooijen N, Randolph GJ. Modulation of Dendritic Cell Trafficking to and From the Airways. *J Immunol* (2006) 176:3578–84. doi: 10.4049/jimmunol.176.6.3578
193. Morrison VL, James MJ, Grzes K, Cook P, Glass DG, Savinko T, et al. Loss of Beta2-Integrin-Mediated Cytoskeletal Linkage Reprograms Dendritic Cells to a Mature Migratory Phenotype. *Nat Commun* (2014) 5:13. doi: 10.1038/ncomms6359
194. van Goethem E, Poincloux R, Gauffre F, Maridonneau-Parini I, Le Cabec V. Matrix Architecture Dictates Three-Dimensional Migration Modes of Human Macrophages: Differential Involvement of Proteases and Podosome-Like Structures. *J Immunol* (2010) 184:1049–61. doi: 10.4049/jimmunol.0902223
195. Guiet R, Van Goethem E, Cougoule C, Balor S, Valette A, Al Saati T, et al. The Process of Macrophage Migration Promotes Matrix Metalloproteinase-Independent Invasion by Tumor Cells. *J Immunol* (2011) 187(7):3806–14. doi: 10.4049/jimmunol.1101245
196. Guiet R, Vérollet C, Lamsoul I, Cougoule C, Poincloux R, Labrousse A, et al. Macrophage Mesenchymal Migration Requires Podosome Stabilization by Filamin A. *J Biol Chem* (2012) 287:13051–62. doi: 10.1074/jbc.M111.307124
197. Bandaru S, Ala C, Salimi R, Akula MK, Ekstrand M, Devarakonda S, et al. Targeting Filamin A Reduces Macrophage Activity and Atherosclerosis. *Circulation* (2019) 140:67–79. doi: 10.1161/CIRCULATIONAHA.119.039697
198. Cui K, Ardell CL, Podolnikova NP, Yakubenko VP. Distinct Migratory Properties of M1, M2, and Resident Macrophages Are Regulated by αdβ2 and αmβ2 Integrin-Mediated Adhesion. *Front Immunol* (2018) 9. doi: 10.3389/fimmu.2018.02650
199. Allen WE, Zicha D, Ridley AJ, Jones GE. A Role for Cdc42 in Macrophage Chemotaxis. *J Cell Biol* (1998) 141(5):1147–57. doi: 10.1083/jcb.141.5.1147
200. Pradip D, Peng X, Durden DL. Rac2 Specificity in Macrophage Integrin Signaling. *J Biol Chem* (2003) 278(43):41661–9. doi: 10.1074/jbc.M306491200
201. Wells CM, Walmsley M, Ooi S, Tybulewicz V, Ridley AJ. Rac1-Deficient Macrophages Exhibit Defects in Cell Spreading and Membrane Ruffling But Not Migration. *J Cell Sci* (2003) 117(7):1259–68. doi: 10.1242/jcs.00997
202. Yamauchi A, Kim C, Li S, Marchal CC, Towe J, Atkinson SJ, et al. Rac2-Deficient Murine Macrophages Have Selective Defects in Superoxide Production and Phagocytosis of Opsonized Particles. *J Immunol* (2004) 173:5971–9. doi: 10.4049/jimmunol.173.10.5971
203. Wheeler AP, Wells CM, Smith SD, Vega FM, Henderson RB, Tybulewicz VL, et al. Rac1 and Rac2 Regulate Macrophage Morphology But are Not Essential for Migration. *J Cell Sci* (2006) 119:2749–57. doi: 10.1242/jcs.03024
204. Harry GJ. Microglia During Development and Aging. *Pharmacol Ther* (2013) 139(3):313–26. doi: 10.1016/j.pharmthera.2013.04.013
205. Marshall GP, Demir M, Steindler DA, Laywell ED. Subventricular Zone Microglia Possess a Unique Capacity for Massive In Vitro Expansion. *GLIA* (2008) 56(16):1799–808. doi: 10.1002/glia.20730
206. Kurpius D, Wilson N, Fuller L, Hoffman A, Dailey ME. Early Activation, Motility, and Homing of Neonatal Microglia to Injured Neurons Does Not Require Protein Synthesis. *Glia* (2006) 54:58–70. doi: 10.1002/glia.20355
207. Haapaniemi H, Tomita M, Tanahashi N, Takeda H, Yokoyama M, Fukuuchi Y. Non-Amoeboid Locomotion of Cultured Microglia Obtained From Newborn Rat Brain. *Neurosci Lett* (1995) 193:121–4. doi: 10.1016/0304-3940(95)11683-N
208. Carbonell WS, Murase S-I, Horwitz AF, Mandell JW. Migration of Perilesional Microglia After Focal Brain Injury and Modulation by CC Chemokine Receptor 5: An In Situ Time-Lapse Confocal Imaging Study. *J Neurosci* (2005) 25(30):7040–7. doi: 10.1523/JNEUROSCI.5171-04.2005
209. Neumann J, Gunzer M, Gutzeit HO, Ullrich O, Reymann KG, Dinkel K. Microglia Provide Neuroprotection After Ischemia. *FASEB J* (2006) 20:714–6. doi: 10.1096/fj.05-4882fje
210. Hyun Y-M, Hong C-W. Deep Insight Into Neutrophil Trafficking in Various Organs. *J Leukocyte Biol* (2017) 102:617–29. doi: 10.1189/jlb.1RU1216-521R
211. Kienle K, Lämmermann T. Neutrophil Swarming: An Essential Process of the Neutrophil Tissue Response. *Immunol Rev* (2016) 273:76–93. doi: 10.1111/imr.12458
212. Lämmermann T, Afonso PV, Angermann BR, Wang JM, Kastenmüller W, Parent CA, et al. Neutrophil Swarms Require LTB4 and Integrins at Sites of Cell Death In Vivo. *Nature* (2013) 498(7454):371–5. doi: 10.1038/nature12175
213. Yamahashi Y, Cavnar PJ, Hind LE, Berthier E, Bennin DA, Beebe D, et al. Integrin Associated Proteins Differentially Regulate Neutrophil Polarity and Directed Migration in 2D and 3D. *Biomed Microdevices* (2015) 17(100):9. doi: 10.1007/s10544-015-9998-x
214. Yago T, Petrich BG, Zhang N, Liu Z, Shao B, Ginsberg MH, et al. Blocking Neutrophil Integrin Activation Prevents Ischemia–Reperfusion Injury. *J Exp Med* (2015) 212(8):1267–81. doi: 10.1084/jem.20142358
215. Roth H, Samereier M, Begandt D, Pick R, Salvermoser M, Brechtefeld D, et al. Filamin A Promotes Efficient Migration and Phagocytosis of Neutrophil-Like HL-60 Cells. *Eur J Cell Biol* (2017) 96(6):553–66. doi: 10.1016/j.ejcb.2017.05.004
216. Sun C, Forster C, Nakamura F, Glogauer M. Filamin-A Regulates Neutrophil Uropod Retraction Through RhoA During Chemotaxis. *PloS One* (2013) 8 (10):8. doi: 10.1371/journal.pone.0079009
217. Uotila LM, Guenther C, Savinko T, Lehti TA, Fagerholm SC. Filamin A Regulates Neutrophil Adhesion, Production of Reactive Oxygen Species, and Neutrophil Extracellular Trap Release. *J Immunol* (2017) 199(210):3644–53. doi: 10.4049/jimmunol.1700087
218. Sun CX, Downey GP, Zhu F, Koh ALY, Thang H, Glogauer M. Rac1 is the Small GTPase Responsible for Regulating the Neutrophil Chemotaxis Compass. *Blood* (2004) 104(12):3758–65. doi: 10.1182/blood-2004-03-0781
219. Roberts AW, Kim C, Zhen L, Lowe JB, Kapur R, Petryniak B, et al. Deficiency of the Hematopoietic Cell-Specific Rho Family GTPase Rac2 Is Characterized by Abnormalities in Neutrophil Function and Host Defense. *Immunity* (1999) 10:183–96. doi: 10.1016/s1074-7613(00)80019-9
220. Boutboul D, Kuehn HS, Van de Wyngaert Z, Niemela JE, Callebaut I, Stoddard J, et al. Dominant-Negative IKZF1 Mutations Cause a T, B, and Myeloid Cell Combined Immunodeficiency. *J Clin Invest* (2018) 128 (7):3071–87. doi: 10.1172/JCI98164
221. Szczur K, Xu H, Atkinson S, Zheng Y, Filippi M-D. Rho GTPase CDC42 Regulates Directionality and Random Movement via Distinct MAPK Pathways in Neutrophils. *Blood* (2006) 108(13):4205–13. doi: 10.1182/blood-2006-03-013789
222. Yang HW, Collins SR, Meyer T. Locally Excitable Cdc42 Signals Steer Cells During Chemotaxis. *Nat Cell Biol* (2015) 18(2):191–201. doi: 10.1038/ncb3292
223. Kumar S, Xu J, Perkins C, Guo F, Snapper S, Finkelman FD, et al. Cdc42 Regulates Neutrophil Migration via Crosstalk Between WASp, CD11b, and Microtubules. *Blood* (2012) 120(17):3563–74. doi: 10.1182/blood-2012-04-426981
224. Iikura M, Ebisawa M, Yamaguchi M, Tachimoto H, Ohta K, Yamamoto K, et al. Transendothelial Migration of Human Basophils. *J Immunol* (2004) 173:5189–95. doi: 10.4049/jimmunol.173.8.5189
225. Dahlin JS, Hallgren J. Mast Cell Progenitors: Origin, Development and Migration to Tissues. *Mol Immunol* (2015) 63:9–17. doi: 10.1016/j.molimm.2014.01.018
226. Okayama Y, Kawakami T. Development, Migration, and Survival of Mast Cells. *Immunol Res* (2006) 34(2):97–115. doi: 10.1385/IR:34:2:97
227. Rosenkranz AR, Coxon A, Maurer M, Gurish MF, Austen KF, Friend DS, et al. Cutting Edge: Impaired Mast Cell Development and Innate Immunity in Mac-1 (CD11b/CD18, CR3)-Deficient Mice. *J Immunol* (1998) 161:6463–7.

228. Klein O, Krier-Burris RA, Lazki-Hagenbach P, Gorzalczany Y, Mei Y, Ji P, et al. Mammalian Diaphanous-Related Formin 1 (Mdia1) Coordinates Mast Cell Migration and Secretion Through its Actin-Nucleating Activity. *J Allergy Clin Immunol* (2019) 144(4):1074–90. doi: 10.1016/j.jaci.2019.06.028
229. Gruber BL, Marchese MJ, Kew R. Angiogenic Factors Stimulate Mast-Cell Migration. *Blood* (1995) 86(7):2488–93. doi: 10.1182/blood.V86.7.2488.2488
230. Azizkhan RG, Azizkhan JC, Zetter BR, Folkman J. Mast Cell Heparin Stimulates Migration Of Capillary Endothelial Cells In Vitro. *J Exp Med* (1980) 152:931–44. doi: 10.1084/jem.152.4.931
231. Lee BJ, Mace EM. From Stem Cell to Immune Effector: How Adhesion, Migration, and Polarity Shape T-Cell and Natural Killer Cell Lymphocyte Development In Vitro and In Vivo. *Mol Biol Cell* (2020) 31(10):981–91. doi: 10.1091/mbc.E19-08-0424
232. Beuneu H, Deguine J, Breart B, Mandelboim O, Di Santo JP, Bousso P. Dynamic Behavior of NK Cells During Activation in Lymph Nodes. *Blood* (2009) 114(15):3227–34. doi: 10.1182/blood-2009-06-228759
233. Bajénoff M, Breart B, Huang AYC, Qi H, Cazareth J, Braud VM, et al. Natural Killer Cell Behavior in Lymph Nodes Revealed by Static and Real-Time Imaging. *J Exp Med* (2006) 203(3):619–31. doi: 10.1084/jem.20051474
234. Mace EM, Gunesch JT, Dixon A, Orange JS. Human NK Cell Development Requires CD56-Mediated Motility and Formation of the Developmental Synapse. *Nat Commun* (2016) 7(12171):13. doi: 10.1038/ncomms12171
235. Lee BJ, Mace EM. Acquisition of Cell Migration Defines NK Cell Differentiation From Hematopoietic Stem Cell Precursors. *Mol Biol Cell* (2017) 28:3573–81. doi: 10.1091/mbc.e17-08-0508
236. Timonen T. Natural Killer Cells: Endothelial Interactions, Migration, and Target Cell Recognition. *J Leukocyte Biol* (1997) 62(6):693–701. doi: 10.1002/jlb.62.6.693
237. Worbs T, Mempel TR, Bölter J, von Andrian UH, Förster R. CCR7 Ligands Stimulate the Intranodal Motility of T Lymphocytes In Vivo. *J Exp Med* (2007) 204(3):489–95. doi: 10.1084/jem.20061706
238. Morrison VL, MacPherson M, Savinko T, Lek HS, Prescott A, Fagerholm SC. The β2 Integrin–Kindlin-3 Interaction is Essential for T-Cell Homing But Dispensable for T-Cell Activation In Vivo. *Blood* (2013) 122(8):1428–36. doi: 10.1182/blood-2013-02-484998
239. Smith A, Carrasco YR, Stanley P, Kieffer N, Batista FD, Hogg N. A Talin-Dependent LFA-1 Focal Zone is Formed by Rapidly Migrating T Lymphocytes. *J Cell Biol* (2005) 170(1):141–51. doi: 10.1083/jcb.200412032
240. Luo J, Li D, Wei D, Wang X, Wang L, Zeug X. RhoA and RhoC are Involved in Stromal Cell-Derived Factor-1-Induced Cell Migration by Regulating F-Actin Redistribution and Assembly. *Mol Cell Biochem* (2017) 436:13–21. doi: 10.1007/s11010-017-3072-3
241. Garcı´a-Bernal D, Wright N, Sotillo-Mallo E, Nombela-Arrieta C, Stein JV, Bustelo XR, et al. Vav1 and Rac Control Chemokine-Promoted T Lymphocyte Adhesion Mediated by the Integrin Alpha4 Beta1. *Mol Biol Cell* (2005) 16:3223–5. doi: 10.1091/mbc.e04-12-1049
242. Banon-Rodriguez I, de Guinoa JS, Bernardini A, Ragazzini C, Fernandez E, Carrasco YR, et al. WIP Regulates Persistence of Cell Migration and Ruffle Formation in Both Mesenchymal and Amoeboid Modes of Motility. *PloS One* (2013) 8(8):14. doi: 10.1371/journal.pone.0070364
243. Guinoa J, Barrio L, Mellado M, Carrasco YR. CXCL13/CXCR5 Signaling Enhances BCR-Triggered B-Cell Activation by Shaping Cell Dynamics. *Blood* (2011) 118(6):1560–9. doi: 10.1182/blood-2011-01-332106
244. Liu X, Carman CV, Springer TA. Quantitative Analysis of B-Lymphocyte Migration Directed by CXCL13. *Integr Biol* (2016) 8:894–903. doi: 10.1039/c6ib00128a
245. Pan Y-R, Chen C-C, Chan Y-T, Wang H-J, Chien F-T, Chen Y-L, et al. STAT3-Coordinated Migration Facilitates the Dissemination of Diffuse Large B-Cell Lymphomas. *Nat Commun* (2018) 9(3696):16. doi: 10.1038/s41467-018-06134-z
246. Sharma P, Siddiqui BA, Anandhan S, Yadav SS, Subudhi SK, Gao J, et al. The Next Decade of Immune Checkpoint Therapy. *Cancer Discov* (2021) 11 (4):838–57. doi: 10.1158/2159-8290.CD-20-1680
247. Bonaventura P, Shekarian T, Alcazer V, Valladeau-Guilemond J, Valsesia-Wittmann S, Amigorena S, et al. Cold Tumors: A Therapeutic Challenge for Immunotherapy. *Front Immunol* (2019) 10. doi: 10.3389/fimmu.2019.00168
248. Peranzoni E, Lemoine J, Vimeux L, Feuillet V, Barrin S, Kantari-Mimoun C, et al. Macrophages Impede CD8 T Cells From Reaching Tumor Cells and Limit the Efficacy of Anti–PD-1 Treatment. *PNAS* (2018) 115(17):E4041–50. doi: 10.1073/pnas.1720948115
249. Boissonnas A, Licata F, Poupel L, Jacquelin S, Fetler L, Krumeich S, et al. CD8+ Tumor-Infiltrating T Cells Are Trapped in the Tumor-Dendritic Cell Network. *Neoplasia* (2013) 15(1):85–94. doi: 10.1593/neo.121572
250. Engelhardt JJ, Boldajipour B, Beemiller P, Pandurangi P, Sorensen C, Werb Z, et al. Marginating Dendritic Cells of the Tumor Microenvironment Cross-Present Tumor Antigens and Stably Engage Tumor-Specific T Cells. *Cell* (2012) 21(3):402–17. doi: 10.1016/j.ccr.2012.01.008
251. Mi Y, Guo N, Luan J, Cheng J, Hu Z, Jiang P, et al. The Emerging Role of Myeloid-Derived Suppressor Cells in the Glioma Immune Suppressive Microenvironment. *Front Immunol* (2020) 11. doi: 10.3389/fimmu.2020.00737
252. Karin N. The Development and Homing of Myeloid-Derived Suppressor Cells: From a Two-Stage Model to a Multistep Narrative. *Front Immunol* (2020) 11. doi: 10.3389/fimmu.2020.557586
253. Liu L, Zhang L, Zhao S, Zhao X-Y, Min P-X, Ma Y-D, et al. Non-Canonical Notch Signaling Regulates Actin Remodeling in Cell Migration by Activating PI3K/AKT/Cdc42 Pathway. *Front Pharmacol* (2019) 10. doi: 10.3389/fphar.2019.00370
254. Redmond L, Ghosh A. The Role of Notch and Rho GTPase Signaling in the Control of Dendritic Development. *Curr Opin Neurobiol* (2001) 11:111–7. doi: 10.1016/S0959-4388(00)00181-1
255. Liu LY, Wang H, Xenakis JJ, Spencer LA. Notch Signaling Mediates Granulocyte-Macrophage Colony-Stimulating Factor Priming-Induced Transendothelial Migration of Human Eosinophils. *Allergy* (2015) 70:805–12. doi: 10.1111/all.12624
256. Noren NK, Niessen CM, Gumbiner BM, Burridge K. Cadherin Engagement Regulates Rho Family GTPases. *J Biol Chem* (2001) 276(36):33305–8. doi: 10.1074/jbc.C100306200
257. Nelson CM, Pirone DM, Tan JL, Chen CS. Vascular Endothelial-Cadherin Regulates Cytoskeletal Tension, Cell Spreading, and Focal Adhesions by Stimulating RhoA. *Mol Biol Cell* (2004) 15:2943–53. doi: 10.1091/mbc.e03-10-0745
258. Siddiqui KRR, Laffont S, Powrie F. E-Cadherin Marks a Subset of Inflammatory Dendritic Cells That Promote T Cell-Mediated Colitis. *Immunity* (2010) 32(4):557–67. doi: 10.1016/j.immuni.2010.03.017
259. Vafaei S, Zekiy AO, Khanamir RA, Zaman BA, Ghayourvahdat A, Azimizonuzi H, et al. Combination Therapy With Immune Checkpoint Inhibitors (ICIs); a New Frontier. *Cancer Cell Int* (2022) 22(2):27. doi: 10.1186/s12935-021-02407-8
260. Yamaguchi O, Kaira K, Hashimoto K, Mouri A, Miura Y, Shiono A, et al. Radiotherapy is an Independent Prognostic Marker of Favorable Prognosis in non-Small Cell Lung Cancer Patients After Treatment With the Immune Checkpoint Inhibitor, Nivolumab. *Thorac Cancer* (2019) 10(4):992–1000. doi: 10.1111/1759-7714.13044

Conflict of Interest: The author declares that the research was conducted in the absence of any commercial or financial relationships that could be construed as a potential conflict of interest.

frontiers | Frontiers in Immunology

ORIGINAL RESEARCH
published: 26 May 2022
doi: 10.3389/fimmu.2022.867082

Modification of Extracellular Matrix by the Product of DHA Oxidation Switches Macrophage Adhesion Patterns and Promotes Retention of Macrophages During Chronic Inflammation

*Jared L. Casteel[1], Kasey R. Keever[1,2], Christopher L. Ardell[1], David L. Williams[2,3], Detao Gao[4], Eugene A. Podrez[4], Tatiana V. Byzova[5] and Valentin P. Yakubenko[1,2]**

[1] Department of Biomedical Sciences, Quillen College of Medicine, East Tennessee State University, Johnson City, TN, United States, [2] Center of Excellence in Inflammation, Infectious Disease and Immunity, Quillen College of Medicine, East Tennessee State University, Johnson City, TN, United States, [3] Department of Surgery, Quillen College of Medicine, East Tennessee State University, Johnson City, TN, United States, [4] Department of Inflammation and Immunity, Lerner Research Institute, Cleveland Clinic, Cleveland, OH, United States, [5] Department of Neurosciences, Lerner Research Institute, Cleveland Clinic, Cleveland, OH, United States

OPEN ACCESS

Edited by:
Zhichao Fan,
UCONN Health, United States

Reviewed by:
Rongrong Liu,
Northwestern University, United States
Dennis Wolf,
University of Freiburg, Germany
Craig T. Lefort,
Rhode Island Hospital, United States

***Correspondence:**
Valentin P. Yakubenko
yakubenko@etsu.edu
orcid.org/0000-0002-0242-3061

Specialty section:
This article was submitted to Autoimmune and Autoinflammatory Disorders, a section of the journal Frontiers in Immunology

Received: 31 January 2022
Accepted: 27 April 2022
Published: 26 May 2022

Citation:
Casteel JL, Keever KR, Ardell CL, Williams DL, Gao D, Podrez EA, Byzova TV and Yakubenko VP (2022) Modification of Extracellular Matrix by the Product of DHA Oxidation Switches Macrophage Adhesion Patterns and Promotes Retention of Macrophages During Chronic Inflammation. Front. Immunol. 13:867082. doi: 10.3389/fimmu.2022.867082

Oxidation of polyunsaturated fatty acids contributes to different aspects of the inflammatory response due to the variety of products generated. Specifically, the oxidation of DHA produces the end-product, carboxyethylpyrrole (CEP), which forms a covalent adduct with proteins *via* an ϵ-amino group of lysines. Previously, we found that CEP formation is dramatically increased in inflamed tissue and CEP-modified albumin and fibrinogen became ligands for $\alpha_D\beta_2$ (CD11d/CD18) and $\alpha_M\beta_2$ (CD11b/CD18) integrins. In this study, we evaluated the effect of extracellular matrix (ECM) modification with CEP on the adhesive properties of M1-polarized macrophages, particularly during chronic inflammation. Using digested atherosclerotic lesions and *in vitro* oxidation assays, we demonstrated the ability of ECM proteins to form adducts with CEP, particularly, DHA oxidation leads to the formation of CEP adducts with collagen IV and laminin, but not with collagen I. Using integrin $\alpha_D\beta_2$-transfected HEK293 cells, WT and $\alpha_D^{-/-}$ mouse M1-polarized macrophages, we revealed that CEP-modified proteins support stronger cell adhesion and spreading when compared with natural ECM ligands such as collagen IV, laminin, and fibrinogen. Integrin $\alpha_D\beta_2$ is critical for M1 macrophage adhesion to CEP. Based on biolayer interferometry results, the isolated α_D I-domain demonstrates markedly higher binding affinity to CEP compared to the "natural" $\alpha_D\beta_2$ ligand fibrinogen. Finally, the

presence of CEP-modified proteins in a 3D fibrin matrix significantly increased M1 macrophage retention. Therefore, CEP modification converts ECM proteins to $\alpha_D\beta_2$-recognition ligands by changing a positively charged lysine to negatively charged CEP, which increases M1 macrophage adhesion to ECM and promotes macrophage retention during detrimental inflammation, autoimmunity, and chronic inflammation.

Keywords: macrophage, adhesion, migration, integrin $\alpha_D\beta_2$, CD11d/CD18, carboxyethylpyrrole (CEP), ECM, inflammation

INTRODUCTION

Low-grade chronic inflammation is a key component in the development of metabolic and autoimmune diseases such as diabetes, atherosclerosis, obesity, and rheumatoid arthritis (1–3). A critical step in the progression of the disease is the accumulation of classically activated pro-inflammatory (M1-like) macrophages in the extracellular matrix (ECM) of inflamed tissues (4, 5). The failure of pro-inflammatory macrophages to emigrate from the inflamed tissue leads to excessive leukocyte recruitment, metabolic imbalance, and damage of healthy tissue, which all together promote the development of chronic inflammation (1, 6). The mechanism and key components of macrophage retention within the site of inflammation are not yet well understood, although this information can improve the treatment of a variety of different pathologies. Enhanced adhesion that prevents macrophage migration is a potential central mechanism of chronic inflammation development. The cell adhesion force is regulated by the density of adhesive receptors, ligand availability, and receptor-ligand affinity (7). The major adhesive receptors on macrophages are integrins. β_1 integrins ($\alpha_1\beta_1$, $\alpha_2\beta_1$, $\alpha_3\beta_1$, etc.) have a moderate expression on macrophages (8, 9) and support adhesion/migration to major ECM proteins, such as collagens and laminins. The role of high-density expressed β_2 integrins ($\alpha_M\beta_2$, $\alpha_D\beta_2$, etc.) in macrophage migration/retention in tissue is thought to be limited by lack of binding to major ECM proteins (10, 11).

Nevertheless, we recently demonstrated that macrophage receptor integrin $\alpha_D\beta_2$ (CD11d/CD18) contributes to the development of atherosclerosis and diabetes due to the generation of strong adhesion of pro-inflammatory macrophages to the inflamed ECM, thereby promoting the retention of macrophages at the site of chronic inflammation (12). Integrin $\alpha_D\beta_2$ is the most recently discovered leukocyte integrin (13, 14), that contributes to an inflammatory response (12, 15–17) and infection in different pathological conditions (18–21). Interestingly, integrin $\alpha_D\beta_2$ is upregulated on pro-inflammatory macrophages, which makes it potentially important for macrophage retention (12). However, the critical $\alpha_D\beta_2$ ligand in the inflamed tissue is not yet defined.

We recently discovered a potential mechanism that could explain the presence of inflammation-specific ligands in the ECM for integrin $\alpha_D\beta_2$. We revealed that during acute inflammation, the oxidation of docosahexaenoic acid (DHA) leads to the generation of the end-product carboxyethylpyrrole (CEP), which forms an adduct with proteins *via* an ϵ-amino group of lysines (22, 23). *In vitro* analysis with BSA demonstrated that 10-20 lysines can be modified by CEP in one protein molecule. Notably, positively charged lysines are substituted to the pyrroles with exposed negatively charged carboxyl groups. (**Figure 1**). Based on our recent data, a carboxyl group in the CEP structure is specifically responsible for the binding to integrins $\alpha_D\beta_2$ and $\alpha_M\beta_2$ (23). Accordingly, CEP-modification significantly changes the surface charge of the targeted protein and its binding properties.

In our previous study, we found that during peritoneal inflammation at least two proteins are modified with CEP in the peritoneal cavity - fibrinogen and albumin. Most importantly, we found that CEP-modified proteins support the migration of non-polarized macrophages to the site of acute inflammation due to interaction with macrophage integrins $\alpha_D\beta_2$ and $\alpha_M\beta_2$ (23). Integrins $\alpha_D\beta_2$ and $\alpha_M\beta_2$ are adhesive receptors, which interact with many ligands and transduce a signal to the actin cytoskeleton that regulates cell adhesion, migration, and other cell responses (24, 25). $\alpha_D\beta_2$ possesses a high homology and similar ligand-binding specificity to $\alpha_M\beta_2$ (11); however, these two integrins demonstrate different roles in chronic inflammatory diseases. As discussed above, α_D supports the development of atherosclerosis (12) and diabetes (26), while integrin α_M protects against these metabolic diseases (27, 28). Apparently, the different surface densities of these integrins on primary monocytes (29) and distinct subsets of macrophages (12, 18, 26), determine their diverse roles in cell migration and chronic inflammation. Interestingly, the analysis of $\alpha_D\beta_2$ and $\alpha_M\beta_2$ binding to CEP demonstrated that α_D has a 5-folds higher affinity to CEP (23), which may have a physiological importance for macrophage adhesion.

The goal of the current project is to evaluate how the modification of ECM proteins with CEP affects their binding properties and the strength of macrophage adhesion, which is critical for macrophage retention during chronic inflammation.

MATERIAL AND METHODS

Reagents and Antibodies

Reagents were purchased from Sigma-Aldrich (St. Louis, MO) and Thermo Fisher Scientific (Waltham, MA). Recombinant mouse IFNγ, CCL2, and CCL5 were purchased from

Abbreviations: CEP, carboxyethylpyrrole; ECM, Extracellular matrix; EDTA, Ethylenediaminetetraacetic acid; FACS, Fluorescence-activated cell sorting; IFNγ, interferon-γ; CCL2, C-C motif chemokine ligand 2 (MCP-1); CCL5, C-C motif chemokine ligand 5 (RANTES); TG, thioglycollate; WT, wide type; 2D, 2 dimensional; 3D, 3 dimensional.

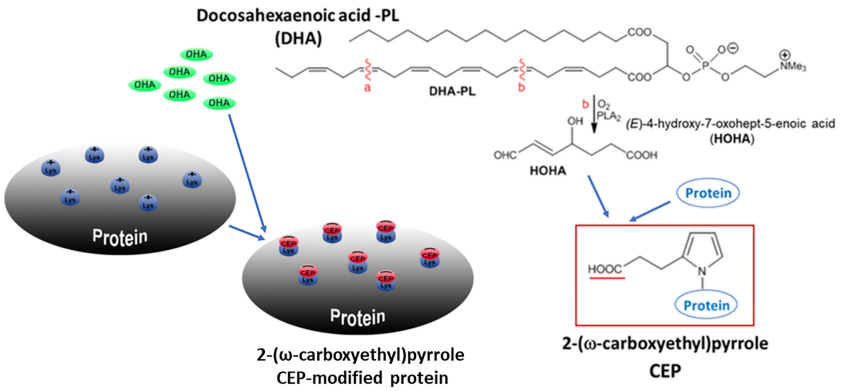

FIGURE 1 | Schematic representation of CEP formation. PLA_2-catalyzed hydrolysis of DHA generates 4-hydroxy-7-oxo-hept-5-eonate (HOHA), which, in turn, produces 2-ω-Carboxyethylpyrrole (CEP)-protein derivatives through condensation with the primary amino groups of protein lysyl residues. A positively charged lysine is modified by pyrrole with a negatively charged carboxyl group. Multiple lysines can be modified by CEP in one protein molecule.

Invitrogen Corporation (Carlsbad, CA). Human fibrinogen and thrombin were obtained from Enzyme Research Laboratories (South Bend, IN). Collagen IV, collagen I, and laminin were purchased from Corning (Corning, NY). CEP-BSA (21:1 molar ratio) and CEP-Fg (29:1 molar ratio) were prepared through a Paar-Knorr pyrrole synthesis with (9H-fluoren-9-ylmethyl ester 4,7-dioxo-heptanoic acid) DOHA-Fm as described previously (28). Anti-CD68 mAb was from eBioscience. Polyclonal antibody against the α_D I-domain was described previously (11). The antibody recognizes both human and mouse α_D I-domains and has no cross-reactivity with recombinant human and mouse α_M, α_X, and α_L I-domains. The antibody was isolated from rabbit serum by affinity chromatography using α_D I-domain-Sepharose. Anti-macrophage antibody F4/80 was from eBioscience (San Diego, CA). A polyclonal antibody against CEP and monoclonal IgM anti-CEP antibody were described previously (30, 31). Blocking IgG anti-CEP antibody (Clone 3C9) was generated in Dr. Tatiana Byzova's laboratory (23).

Animals

Wild type (C57BL/6J, stock # 000664) and integrin α_D-deficient (B6.129S7-*Itgad*^{tm1Bll}/J, stock # 005258) mice were bought from Jackson Laboratory (Bar Harbor, ME). α_D-deficient have been backcrossed to C57BL/6 for at least ten generations. All procedures were performed according to animal protocols approved by East Tennessee State University IACUC.

Generation of Classically Activated (M1) Macrophages

Notably, the terms M1 and M2 macrophages are artificial and do not represent all variabilities of macrophage subsets *in vivo*. We used the term M1 in our manuscript to refer to *in vitro* polarized macrophages activated by IFN-γ which serve as a model for pro-inflammatory macrophages *in vivo*. Therefore, peritoneal macrophages from 8-12-week-old mice (WT and $\alpha_D^{-/-}$) were harvested by lavage of the peritoneal cavity with 5 ml of sterile PBS 3 days after intraperitoneal (IP) injection of 4% thioglycollate (TG; 0.5ml). The cells were washed twice with PBS and resuspended in RPMI media supplemented with 10% FBS, 0.1 mg/ml streptomycin, and 0.1 unit/ml penicillin. The cell suspension was transferred into 100mm Petri dishes and incubated for 2h at 37°C in humidified air containing a 5% CO_2 atmosphere. Nonadherent cells were washed out with PBS, and the adherent macrophages were replenished with complete RPMI media. The macrophages were differentiated to M1 phenotypes by treatment with recombinant mouse interferon-γ (IFN-γ) (100 U/ml, Thermo Fisher) for 4 days. Medium with IFN-γ was changed every 2 days or as required. Macrophages were dissociated from the plates using 5mM EDTA in PBS and used for the experiments thereafter.

Generation of $\alpha_D\beta_2$-Transfected HEK293 Cells

The HEK293 cells stably expressing human integrin $\alpha_D\beta_2$ were generated as described previously (11) and maintained in DMEM/F-12 (Invitrogen) supplemented with 10% FBS, 2 mM glutamine, 15 mM HEPES, 0.1 mg/ml streptomycin, and 0.1 unit/ml penicillin.

Isolation of Recombinant α_D I-Domain in an Active Conformation

The construct for the α_D I-domain was generated and recombinant protein was isolated as described in our previous paper (23). Briefly, α_D in the active conformation (Pro^{128}-Lys^{314}) was inserted in the pET15b vector, expressed in E. Coli as a His-tag fusion protein, and purified using affinity chromatography on Ni-chelating agarose (Qiagen Inc., Valencia, CA).

Flow Cytometry Analysis

Flow cytometry analysis was performed to assess the expression of integrin α_D on mouse peritoneal macrophages and $\alpha_D\beta_2$-transfected HEK293 cells. Cells were harvested and pre-incubated with 4% normal goat serum for 30 min at 4°C, then $2x10^6$ cells were incubated with a specific antibody for 30 min at 4°C. Non-conjugated antibodies required additional incubation with Alexa 488 or Alexa 647-donkey anti-mouse IgG (at a 1:1000

dilution) for 30 min at 4°C. Finally, the cells were washed and analyzed using a Fortessa X-20 (Becton Dickinson).

Cell Adhesion Assay

The adhesion assay was performed as described previously (23) with modifications. Briefly, 96-well plates (Immulon 2HB, Cambridge, MA) were coated with different concentrations of fibrinogen, collagen IV, collagen I, or laminin for 3 h at 37°C. The wells were post-coated with 0.5% polyvinyl alcohol for 1 h at room temperature. Mouse peritoneal macrophages or HEK293 cells transfected with integrin $\alpha_D\beta_2$ were labeled with 10 μM Calcein AM (Molecular Probes, Eugene, OR) for 30 min at 37°C and washed with HBSS and resuspended in the same medium at a concentration of 1×10^6 cells/mL. $\alpha_D\beta_2$-transfected HEK 293 cells were also supplemented with 2mM $MnCl_2$. Aliquots (50 μL) of the labeled cells were added to each well. After 30 minutes of incubation at 37°C in a 5% CO_2 humidified atmosphere, the nonadherent cells were removed by washing with PBS. The fluorescence was measured in a Synergy H1 fluorescence plate reader (BioTek, Winooski, VT), and the number of adherent cells was determined from a labeled control.

Cell Spreading Assay

Glass coverslips were coated with fibrinogen (20 μg/ml), Collagen IV (5 μg/ml) or CEP-BSA (750 μM) for 3 hours at 37°C and post-coated with 0.5% polyvinylpyrrolidone for 1 hour at 37°C. To determine cell spreading, inflammatory macrophages isolated from the WT and $\alpha_D^{-/-}$ mice were allowed to adhere to coverslips for 1 hour at 37°C. Macrophages were fixed with 4% paraformaldehyde, permeabilized with 0.1% Triton X-100, and incubated with Phalloidin-iFluor 555 and DAPI. Fluorescent images were obtained with EVOS FL auto cell fluorescent imaging system using 20x objective with multi-frame automatic setup (9-fields). The cell areas were calculated using Imaris 8.0 software.

Migration of Macrophages in 3D Fibrin Gel

Migration assay was performed as described previously (26). Polarized M1 macrophages were labeled with PKH26 red fluorescent dye. Cell migration assay was performed for 48 hours at 37°C in 5% CO_2 in a sterile condition. An equal number of WT macrophages was evaluated by cytospin of mixed cells before the experiment and at the starting point before migration. Labeled WT ($1.5x10^5$) activated macrophages were plated on the membranes of transwell inserts with a pore size of 8 μm and 6.5 mm in diameter (Costar, Corning, NY) precoated with fibrinogen (Fg). Fibrin gel (100 μl/sample) was generated by mixing 0.75mg/ml Fg containing 1% FBS and 1% P/S and 0.5 U/ml thrombin. In some samples 9 μM CEP was incorporated into the gel during polymerization. 30 nM of MCP-1 was added on top of the gel to initiate the migration. Migrating cells were detected by Leica Confocal microscope (Leica-TCS SP8), and the results were analyzed and reconstructed using IMARIS 8.0 software.

Biolayer Interferometry

The binding parameters of the interaction between the α_D I-domain with CEP or fibrinogen were determined using an Octet K2 instrument (FortéBio, Sartorius Group). CEP-BSA or fibrinogen was immobilized on the Amine Reactive Second-generation (AR2G) biosensor using the amine coupling kit according to the manufacturer's protocol. Different concentrations of the active forms of α_D I-domain (50-1000 nM) were applied in the mobile phase, and the association between the immobilized and flowing proteins was detected. Experiments were performed in 20 mm HEPES, 150 mm NaCl, 1 mM $CaCl_2$, 1 mM $MgCl_2$, 0.02% (v/v) Tween-20, 0.02% BSA, pH 7.5. The protein-coated biosensors were regenerated with 25 mm NaOH and 2M NaCl. Analyses of the binding kinetics were performed using DataAnalysis HT11.0 software (ForteBio). The value of the equilibrium dissociation constant (K_D) was obtained by fitting a plot of response at equilibrium (Req) against the concentration.

Immunostaining

Cryosections (10 μm) of aorta roots (from WT and $ApoE^{-/-}$ mice after five weeks on a western diet) were warmed to room temperature for 30 minutes prior to immunofluorescence staining. Tissue sections were fixed in ice-cold acetone for 10 minutes followed by permeabilizing with 0.2% Tween-20 for 10 min to increase the signal of intracellular binding sites. Tissue sections were washed in PBS and incubated with SuperBlock (PBS) Blocking buffer (Thermo Scientific, Rockford, IL, USA) for 45 min to block nonspecific binding. Tissues were then incubated at 4°C overnight with the primary antibody (rabbit polyclonal anti-CEP and rat anti-mouse CD68 (macrophage marker). After washing several times with PBS, the sections were incubated with Alexa Fluor 488-conjugated donkey anti-rabbit IgG and Alexa Fluor 568-conjugated donkey anti-rat for 1 hour at room temperature. The sections were subsequently washed and sealed. The tissue sections were examined by Leica Confocal microscope (Leica-TCS SP8). Control sections without the primary antibody were also performed at the same time.

Analysis of CEP Formation in Atherosclerotic Lesions of $ApoE^{-/-}$ Mice by Western Blot

Male ApoE-deficient mice were kept on a Western diet for 16 weeks. After that, $ApoE^{-/-}$ and the same age WT C57BL/6 mice (as the control) were euthanized, their vascular system was perfused with 10 ml PBS, and the aortas were cleaned from the outer layers of connective tissue and removed. The isolated aortas were digested with Collagenase type I, type XI, Hyaluronidase, and DHAase I according to the published protocol (12). The cells were separated by centrifugation. The non-cellular supernatant was high speed centrifugated to exclude aggregates and cell traces, and used for Western Blot analysis.

The same concentration of proteins isolated from $ApoE^{-/-}$ and WT aortas was loaded on SDS-electrophoresis analyzed by 7% SDS-PAGE electrophoresis and Western blotting. The Immobilon-P membranes (Millipore) were incubated with rabbit polyclonal anti-CEP antibody, followed by incubation with goat anti-rabbit secondary antibody conjugated to horseradish peroxidase and developed using enhanced SuperSignal Chemiluminescent Substrate (Pierce).

Generation of CEP-Modified ECM Proteins

The evaluation of CEP-modified proteins was performed as described previously (23). Collagen I, collagen IV, and laminin were coated on a 96-well plate at a concentration of 20 µg/ml overnight at 4°C. Wells were post-coated with 0.5% polyvinyl alcohol for 1 h at 37°C. 20 µM DHA in 20mM Hepes, 150 mM NaCl, 0.01% H_2O_2, and 1mM $CaCl_2$ were added to the wells and incubated in an oxygen-free environment (under argon) for 18 hours at 37°C. After incubation, the plate was washed out with PBS supplemented with 0.05% Tween-20 3 times and incubated with anti-CEP polyclonal antibody (0.9 µg/ml) for 2 hours at 37°C. After washing, wells were incubated with goat-anti-rabbit HRP conjugated antibody for 1 h at 37°C and the binding was developed using TMB-ELISA substrate solution (Pierce). The result was detected by a plate reader using a wavelength of 450 nm.

Statistical Analysis

Statistical analyses were performed using a Student's t-test or Student's paired t-tests where indicated in the text using SigmaPlot 13. A value of $p<0.05$ was considered significant. Error bars represent the SEM of experiments.

RESULTS

DHA Oxidation Generates CEP Adducts With ECM Proteins in Atherosclerotic Lesions and *In Vitro*

We and others have demonstrated the presence of CEP in different inflammatory tissues using immunohistochemistry (23, 30–34). Particularly, anti-CEP antibody detected strong immunostaining in the sections of atherosclerotic lesions of ApoE$^{-/-}$ mice on a Western diet (**Figure 2A**). However, the direct formation of CEP-protein adducts was shown previously only in the peritoneal cavity, but not in the tissue (23). To demonstrate the link between CEP immunostaining and the formation of CEP-modified proteins in the inflamed tissue during chronic inflammation, we evaluated CEP-protein adduct formation in atherosclerotic lesions (**Figure 2B**). Male ApoE-deficient mice were kept on a Western diet for 16 weeks (n=3). After that, ApoE$^{-/-}$ and the same age WT C57BL/6 mice (as the control) were euthanized, their vascular system was perfused and aortas were removed. The isolated aortas were digested according to the published protocol (12) and cells were separated by centrifugation. The non-cellular supernatant was high speed centrifugated to exclude aggregates and cell traces, and used for Western Blot analysis.

The same concentration of proteins isolated from ApoE$^{-/-}$ and WT aortas was loaded on SDS-electrophoresis (**Figure 2B**, left panel) and analyzed using an anti-CEP antibody (**Figure 2B**, right panel). We found a dramatic difference in anti-CEP staining of proteins isolated from the atherosclerotic lesions of ApoE-deficient and WT mice. While only one weak band was spotted in the sample isolated from WT mice, several intensive bands were detected in the ApoE$^{-/-}$ mice samples that represent several CEP-modified proteins. Notably, the faded CEP signal from the WT mice corresponds to the concept that the natural oxidation of PUFA in a healthy organism can lead to a low level of adduct formation. We detected such signal previously in commercial fibrinogen that we used in our experiments as a control (23).

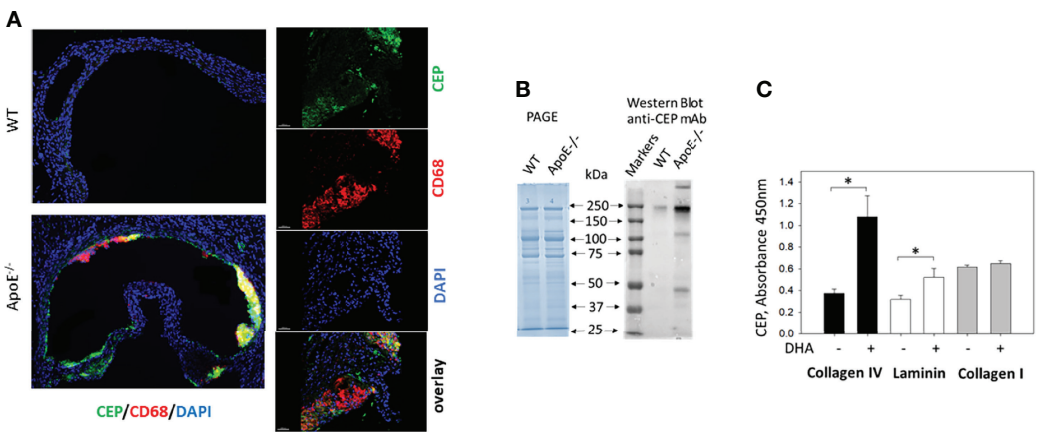

FIGURE 2 | CEP forms adducts with ECM proteins during inflammation and oxidation of DHA. **(A)** CEP deposition in atherosclerotic lesions. Aortic sinuses were isolated from the ApoE-deficient mice after five weeks on a western diet. The sections were prepared and immunostained with anti-CEP (green) and anti-CD68 (red) antibodies. The crosssection of entire aorta roots (right) and 200x magnified inlet (left) are shown (scale bar 200 µm). **(B)** Electrophoresis (PAGE) and Western blot analysis with anti-CEP antibody of digested aortas. Aortas of ApoE-/- and WT mice were digested, cells were separated and the non-cellular contest was analyzed by electrophoresis with Coomassie Blue and Western Blot (7% PAGE) with anti-CEP antibody (representative experiment from 4 performed). **(C)** Generation of CEP-modified ECM proteins. Collagen IV, collagen I, and laminin were coated on a 96-well plate and incubated in the presence (or absence) of 2 µM DHA in 20 mM HEPES, 150 mM NaCl, 0.01% H_2O_2, and 1mM $CaCl_2$ in an oxygen-free environment (under argon atmosphere) for 18 hours at 37°C. After incubation, the plate was incubated with an anti-CEP polyclonal antibody (0.9 µg/ml) followed by goat-anti-rabbit HRP conjugated antibody. The binding was developed using a TMB-ELISA substrate solution (Pierce). The result was detected by plate reader using wavelength 450 nm. Statistical analyses were performed using Student's paired *t*-tests from 3 independent experiments. *P < 0.05.

To confirm the ability of CEP to form the covalent adduct with ECM proteins, we tested the formation of CEP modification in collagen I, laminin, and collagen IV using *in vitro* DHA oxidation assay that we developed previously (23). ECM proteins were incubated with DHA and 0.01% H_2O_2 for 18 h at 37°C. After incubation, CEP formation was detected by ELISA with an anti-CEP antibody (**Figure 2C**). We found that DHA oxidation led to the formation of CEP-collagen IV adduct and CEP-laminin adduct, while collagen I was not modified.

These experiments clearly demonstrated that ECM proteins are modified by CEP, and inflamed tissue (e.g. atherosclerotic lesions) can be a source of specific adhesive substrate for macrophages.

M1 Macrophages Demonstrate Stronger Adhesion and Spreading to CEP-Modified Proteins

Pro-inflammatory, M1-like macrophages, are the major source of inflammatory stimuli during chronic inflammation. We tested how protein modification with CEP affects M1 macrophage adhesion to ECM proteins such as collagen IV, laminin, and fibrinogen (which leaks from blood to the ECM through the damaged endothelial monolayer during inflammation). Different concentrations of collagen IV, laminin, CEP-modified BSA, and BSA alone as a control were immobilized on the 96-well plate and tested as substrates for M1 macrophage adhesion (**Figure 3A**). We found that the adhesion of pro-inflammatory macrophages to CEP-modified BSA dramatically overreached the adhesion of macrophages to natural ECM ligands. Notably, BSA alone does not support the adhesion of macrophages. In a separate experiment, we compared the adhesion of fibrinogen-modified by CEP and native fibrinogen. Clearly, CEP modification dramatically increased macrophage adhesion to fibrinogen (**Figure 3B**).

To verify these results macrophage spreading on CEP, collagen IV, and fibrinogen was evaluated. Cells were labeled with phalloidin-PE, examined by fluorescent microscopy, and analyzed using the ImarisCell module (Imaris 8.0). Corresponding to the adhesion data, the results demonstrate stronger spreading to CEP with larger cell areas and focal adhesion complexes (**Figures 3C, D**).

The Presence of CEP in a 3D Matrix Inhibits M1 Macrophage Migration

To evaluate the effect of CEP modification in ECM on cell motility we performed a 3D migration assay by comparing M1 macrophage migration in a polymerized fibrin matrix and polymerized fibrin matrix supplemented with 9 μM CEP. Based on our previous result the migration of M1 macrophages in a fibrin matrix is lower compared to non-activated or M2 macrophages (26). The goal of this experiment was to evaluate the additional effect of CEP on this migration. Cells were plated on one side of the gel and migration was initiated by CCL2 and CCL5 added to the other side of the gel (**Figure 4A**). We found that migration of M1 macrophages was dramatically reduced in fibrin gel supplemented with CEP (**Figures 4B–D**), which corresponds to strong adhesion events and promotion of macrophage retention at the site of chronic inflammation.

To more critically evaluate these results, we tested the morphology of macrophages in a 3D matrix supplemented with CEP. 3D gels were generated using polymerized fibrin and polymerized fibrin/9 uM CEP. The same macrophages

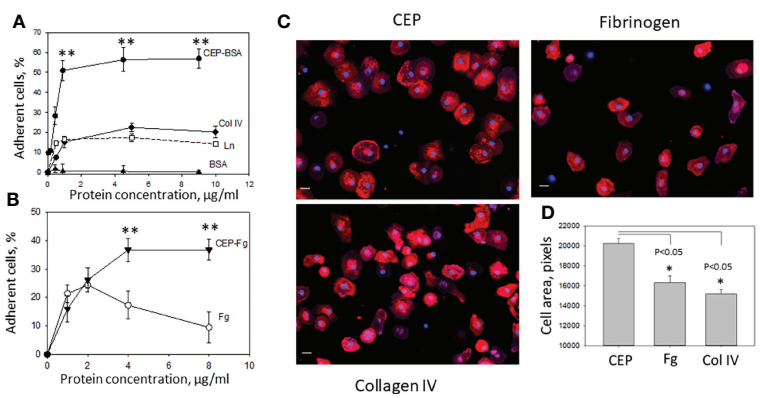

FIGURE 3 | Adhesion of M1-polarized macrophages to CEP and ECM proteins. **(A)** Different concentrations of CEP-BSA, collagen IV (Col IV), laminin (Ln) and BSA were immobilized on a 96-well plate for 3 h at 37°C. Fluorescently labeled macrophages were added to the wells and cell adhesion was determined after 30 min in a fluorescence plate reader. CEP-BSA is presented based on the concentration of BSA. 1μg BSA contains 250 nM CEP. A representative experiment from 4 performed. Data are presented as mean ± SEM **p < 0.01. **(B)** Different concentrations of CEP-fibrinogen (CEP-Fg) and fibrinogen (Fg) were immobilized and tested in an adhesion assay as described above. A summary result from 3 experiments. CEP-Fg is shown based on the concentration of Fg. 1μg Fg contains 87 nM CEP Data are presented as mean ± SEM **p < 0.01. **(C)** Macrophages were allowed to adhere to glass coverslips coated with fibrinogen, Collagen IV or CEP-BSA for 1 hour at 37°C. Macrophages were fixed with 2% paraformaldehyde, permeabilized with 0.1% Triton X-100, and incubated with Alexa Fluor 555-conjugated phalloidin and DAPI. Fluorescent images were obtained with EVOS FL auto cell fluorescent imaging system using 20x objective with mosaic 9-fields setup. **(D)** The cell area was calculated using Imaris 8.0 software. Data are presented as mean ± SEM *p < 0.05.

were incorporated into both matrixes during polymerization and migration was stimulated with a gradient of CCL2. After 18 hours, the cells inside the gel (at least 80 μM from the gel surface) were analyzed using the confocal microscope. We found that cells in the fibrin matrix present a more elongated shape when compared with the more rounded cells in the matrix with supplemented CEP (**Figure 4E**) The difference between the length-to-diameter ratio was extremely significant (P<0.0001, n=30-35/group) (**Figure 4F**). According to published data, elongated cell morphology in a 3D matrix corresponds to migrating cells.

Therefore, our results demonstrate that modification with CEP affects M1 macrophage adhesion, spreading, and migration-dependent morphology.

Integrin $\alpha_D\beta_2$ Is Critical for M1 Macrophage Adhesion and Spreading to CEP-Modified Proteins

The major adhesive receptors for CEP on macrophages are integrins $\alpha_D\beta_2$ and $\alpha_M\beta_2$. Integrin α_D is upregulated on M1 macrophages (12), (**Figure 5A**), while α_M maintains the same level of expression. This difference determines the distinct roles of these β_2 integrins in inflammation. While $\alpha_M\beta_2$ supports macrophage migration and demonstrates some protective function during chronic inflammation (27, 35), integrin $\alpha_D\beta_2$ inhibits M1 macrophage migration and contributes to the development of chronic inflammation (12, 26). We hypothesized that integrin $\alpha_D\beta_2$ is critical for M1 macrophage adhesion to CEP-modified proteins. To test this hypothesis, we compared the adhesion of M1 macrophages isolated from the WT and α_D-deficient mice to CEP. The adhesion assay demonstrated a dramatic reduction in macrophage adhesion in α_D-deficient mice (**Figure 5B**). Moreover, macrophage spreading to CEP was significantly affected in $\alpha_D^{-/-}$ M1 macrophages, the total cell areas were reduced as well as cell shapes were irregular (**Figures 5C, D**).

Therefore, our data demonstrate that α_D-deficiency significantly reduced adhesion and spreading of M1 macrophages on CEP, which confirmed the critical role of $\alpha_D\beta_2$ in macrophage adhesion and potential retention in CEP-modified substrate.

The Binding Properties of CEP Exceed the Binding Properties of Natural $\alpha_D\beta_2$ Ligands

Macrophages are a complex system with a variety of adhesive receptors that have overlapping ligand binding properties. To verify the role of CEP as a strong $\alpha_D\beta_2$ ligand, we tested $\alpha_D\beta_2$-transfected HEK293 cells (**Figure 6A**). HEK293 cells do not express any receptors that interact with CEP such as integrin $\alpha_M\beta_2$, CD36, or TLRs (23, 34). Adhesion of $\alpha_D\beta_2$-transfected HEK293 cells was tested to CEP-BSA versus BSA and CEP-fibrinogen versus fibrinogen. As we expected $\alpha_D\beta_2$-cells do not adhere to BSA, but demonstrate the strong concentration-dependent adhesion to CEP-BSA. (**Figure 6B**, upper).

Fibrinogen is a natural ligand for integrin $\alpha_D\beta_2$ and a common element of the ECM during inflammation. Markedly, CEP modification significantly improves the adhesive properties of fibrinogen to $\alpha_D\beta_2$-HEK293 transfected

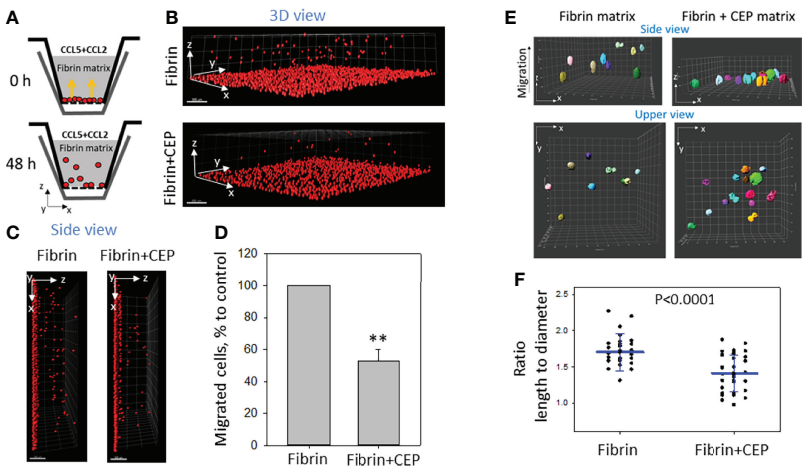

FIGURE 4 | The presence of CEP in the matrix inhibits the 3D migration of M1 macrophages. **(A)** Sketch diagram of the migrating cells in Boyden transwell chamber. Before migration (upper panel) and after 48h migration (lower panel). **(B)** WT M1 macrophages were labeled with red PKH26 fluorescent dye. Labeled WT ($1.5x10^5$) activated macrophages were plated on the membranes of transwell inserts (Boyden chamber) with a pore size of 8 μm and 6.5 mm in diameter (Costar, Corning, NY) precoated with fibrinogen (Fg). Fibrin gel (100 μl/sample) was generated by mixing 0.75mg/ml Fg containing 1% FBS and 1% P/S and 0.5 U/ml thrombin with or without 9uM CEP. Migration of macrophages was stimulated by 30 nM CCL2 and 100nM CCL5 added to the top of the gel. After 48 hours, migrating cells were detected by a Leica Confocal microscope **(B, C)**. **(D)** The results were analyzed by IMARIS 8.0 software, and statistical analyses were performed using Student's paired t-tests (n = 5 per group). Scale bar= 300 μm. Data are presented as mean ± SEM. **P < 0.01. **(E)** The morphology of non-labeled macrophages was evaluated after gel staining with CytoPainet Phalloidinin-iFluor 555 in fibrin matrix (left panel) and Fibrin matrix supplemented with CEP (right panel). The ratio length/diameter was calculated using the ImarisCell module (IMARIS 8.0). **(F)** Statistical analyses were performed using Student's t-tests, n = 30 (fibrin gel) 36 (fibrin+CEP gel). P < 0.0001.

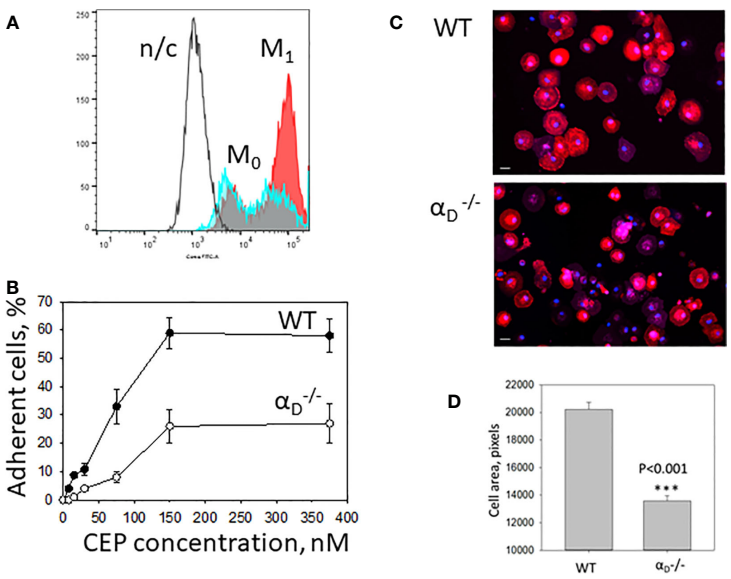

FIGURE 5 | Integrin $\alpha_D\beta_2$ is critical for M1 macrophage adhesion to CEP-modified proteins. **(A)** The expression of integrin α_D is upregulated on M1 macrophages. Peritoneal macrophages were isolated and plated for 4 days in the presence of IFNg in complete RPMI media (Red). M1 macrophages were collected using cell dissociation buffer and stain with anti-α_D polyclonal antibody, followed by staining with donkey-anti-rabbit Alexa 647secondary antibody. Freshly isolated peritoneal macrophages were used as a control (M0)(Blue). Integrin α_D expression was tested using flow cytometry (Fortessa X-20). N/c-negative control. **(B)** Adhesion of WT and $\alpha_D^{-/-}$ M1 macrophages to CEP-BSA. Isolated M1 macrophages were fluorescently labeled with Calcein AM and added to the well coated with CEP-BSA. cell adhesion was determined after 30 min in a fluorescence plate reader. **(C)** Macrophages were allowed to adhere to glass coverslips coated with CEP-BSA for 1 hour at 37°C. After fixation with 2% paraformaldehyde and permeabilization with 0.1% Triton X-100, cells were incubated with CytoPainet Phalloidinin-iFluor 555 and DAPI. Fluorescent images were obtained with EVOS FL auto cell fluorescent imaging system using 20x objective with mosaic 9-fields setup. **(D)** The cell area was calculated using Imaris 8.0 software. Data are presented as mean ± SEM ***$p < 0.001$.

cells similar to the result, which was obtained for M1 macrophages (**Figure 3B**). Notably, it has been shown previously that cell adhesion to fibrinogen achieved maximum at fibrinogen concentration 2-3 μg/ml and is significantly reduced at higher concentrations (10, 36). The mechanism is not known but may depend on the surface-induced lateral aggregation of fibrinogen (37). This result demonstrated that CEP modification in different proteins provides a similar augmentation of cell adhesive properties.

To evaluate a difference in the binding of $\alpha_D\beta_2$ to CEP and fibrinogen, we isolated $\alpha_D\beta_2$ ligand-binding motif – I-domain (**Figure 6C**) and examined its binding properties using BioLayer Interferometry. CEP and fibrinogen were immobilized on amino coupling biosensors and tested with different concentrations of α_D I-domain using two approaches such as kinetic titration (single cycle kinetics) (**Figure 6D**) and equilibrium analysis (steady-state analysis) (**Figures 6E, F**). The binding affinity was analyzed using DataAnalysis HT11.0 software (ForteBio). We found that the affinity of α_D binding to CEP (K_D=1.0x10^{-7}M) is 2-fold stronger than the α_D interaction with fibrinogen (K_D=2.2x10^{-7}).

Therefore, $\alpha_D\beta_2$ generates a more powerful adhesion to CEP-modified proteins due to a higher affinity mediated by a negative charge of a carboxyl group in CEP's structure. This result suggests the unique role of CEP-modified ECM proteins in macrophage adhesion that generates strong $\alpha_D\beta_2$-dependent adhesion *via* CEP that can be critical for macrophage retention.

DISCUSSION

In our previous project, we found that CEP, the product of DHA oxidation, is a ligand for integrins $\alpha_M\beta_2$ and $\alpha_D\beta_2$ (23). In the current study, we tested how the modification of the ECM proteins with CEP affects macrophage adhesion. Now we found that 1) Polyunsaturated fatty acid oxidation generates the formation of adducts between CEP and ECM proteins *in vitro*. 2) The development of atherosclerosis promotes a CEP formation in proteins within the atherosclerotic lesions. 3) Pro-inflammatory M1 macrophages demonstrate a stronger adhesion to CEP-modified proteins compared to natural ECM ligands. 4) M1 macrophage adhesion to CEP inhibits cell migration. 5) The adhesion of M1 macrophages to CEP-modified proteins is driven by integrin $\alpha_D\beta_2$.

The previous experiments using immunostaining with the anti-CEP antibody demonstrated the deposition of CEP in tissue during inflammation including myocardial infarction (38), peritoneal inflammation (23), atherosclerosis (38), and macular degeneration (32, 39). Our published data revealed that neutrophil-mediated oxidation led to the formation of CEP-

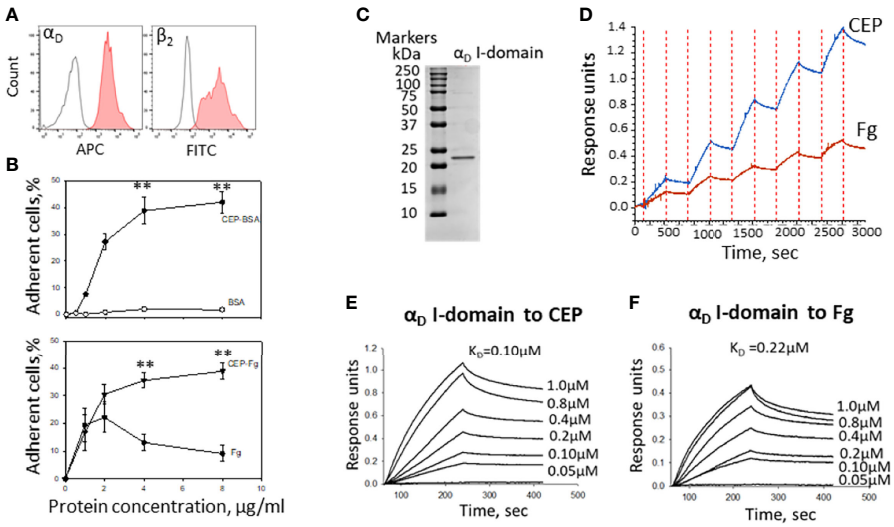

FIGURE 6 | The binding properties of CEP exceed the binding properties of natural $\alpha_D\beta_2$ ligands. **(A)** The expression of integrins α_D and β_2 on the surface of HEK293-transfected cells. After isolation, cells were stained with anti-α_D polyclonal antibody and anti-β_2 monoclonal antibody, followed by staining with donkey-anti-rabbit Alexa 647 and donkey-anti-mouse Alexa 488 secondary antibodies. Control is shown in open histogram. **(B)** Different concentrations of CEP-BSA and BSA (Upper panel) or CEP-fibrinogen (CEP-Fg) and Fg (lower panel) were immobilized on a 96-well plate for 3 h at 37°C. Fluorescently labeled $\alpha_D\beta_2$ HEK293-transfected cells were added to the wells and cell adhesion was determined after 30 min in a fluorescence plate reader. A summary result from 4-6 experiments. Data are presented as mean ± SEM **$p < 0.01$. **(C)** Isolated α_D I-domain binds to CEP in biolayer interferometry assays. SDS-PAGE of generated I-domain. α_D active (D^{122}-K^{314}) I-domain was isolated from soluble fractions of **(E)** coli lysates and purified using affinity chromatography. The protein purity was assessed by SDS-PAGE on 4-15% gradient gel under non-reducing conditions followed by staining with Coomassie Blue. Representative profiles of the biolayer interferometry responses for α_D binding to the immobilized CEP-BSA and Fibrinogen (Fg). **(D)** Single cycle kinetic of α_D I-domain binding (concentrations ranging from 24-750 nM) to CEP-BSA and Fg coupled to AR2G biosensor. **(F)** Steady state analysis of α_D I-domain binding to CEP **(E)** and Fg **(F)** (concentrations ranging from 50-1000 nM). The K_D of binding was calculated using DataAnalysis HT11.0 software (ForteBio).

fibrinogen and CEP-BSA adducts (23). We hypothesize that PUFA oxidation can lead to the modification of different ECM proteins that contain an exposed lysine on a protein's surface. We do expect some limitations, which can depend on special tertiary structures, post-translational modifications, or cross-linkage through lysines. Our concern was primarily based on the absence of CEP adduct formation with the E-fragment of fibrin (23), which has a strong triple-coiled helix structure. (The triple-coiled helix is also a major component of laminin and collagen fibrils). In addition to a triple-coiled structure, collagens IV, V, and VI contain flexible globular domains, which are absent in collagens I and III (40). In our current experiments, we found that *in vitro* oxidation of DHA generates CEP-collagen IV adduct formation, while collagen I is not modified by CEP, which confirms our hypothesis regarding the potential role of the globular domains in CEP adducts formation.

Previously we demonstrated that non-activated peritoneal macrophages can bind CEP *via* $\alpha_M\beta_2$ and $\alpha_D\beta_2$. However, we did not compare the level of macrophage adhesion to natural adhesive ligands and CEP-modified ligands. Moreover, we did not test the effect of CEP modification on the adhesion and migration of M1 macrophages, which is critical for the development of inflammatory response. In this paper, we are particularly focused on integrin $\alpha_D\beta_2$ since it is upregulated on pro-inflammatory M1-like macrophages and our previous data demonstrated that the α_D I-domain showed 5 folds stronger affinity to CEP compared to the α_M I domain (23, 41). This difference most likely is mediated by clusters of positively charged amino acids on the surface of the α_D I-domain. The increased binding activity to negatively charged ligands was described previously for integrin $\alpha_X\beta_2$ which has a significantly lower expression on macrophages but has a high level of homology with integrin $\alpha_D\beta_2$ (42).

In our previous project, we found that $\alpha_D\beta_2$ on the surface of pro-inflammatory M1 macrophages contributed to the retention of macrophages at the site of atherosclerotic lesions due to strong cell adhesion (12). It has been shown that $\alpha_D\beta_2$ is a multiligand protein that can bind to ICAM-3, VCAM-1, fibrinogen, fibronectin, and vitronectin (11). However, these proteins are cell surface receptors or plasma proteins, which are sporadic in the interstitium, while the major ECM proteins such as collagens and laminins do not support $\alpha_D\beta_2$ -mediated adhesion (26). This raises the question regarding the potential ECM ligands for $\alpha_D\beta_2$ -mediated macrophage retention. The modification of collagen IV and laminin with CEP (**Figure 2C**) demonstrates the protein modification in ECM and resolves this issue. This mechanism presents the formation of the universal ligand for $\alpha_D\beta_2$-mediated adhesion. Notably, in our previous project, we found that a carboxyl group in CEP's structure is critical for integrin binding since another product of DHA oxidation, ethylpyrole, has a similar structure, but does not have a carboxyl group and loses the ability to interact with integrins $\alpha_M\beta_2$ and $\alpha_D\beta_2$ (23).

Therefore, the positively charged lysines in different proteins can be modified with negatively charged CEP, which converts these proteins to the $\alpha_D\beta_2$-dependent substrate.

We found that adhesion and spreading of M1 macrophages to the CEP-modified proteins is much stronger compared to native collagen IV, laminin, or fibrinogen (**Figure 3**). The adhesion to collagens and laminins is mediated *via* β_1 integrins such as $\alpha_1\beta_1$, $\alpha_2\beta_2$, etc. The level of β_1 integrins is lower on macrophages compared to β_2 integrins (8, 9). Therefore, the switch of binding from classical collagen/β_1-dependent to CEP-modified collagen/β_2-dependent increased cell adhesion. Moreover, we demonstrated that M1 macrophage adhesion to CEP is integrin $\alpha_D\beta_2$-dependent since it is dramatically reduced in α_D-deficient macrophages (**Figure 5B**). Notably, α_D-deficiency does not affect the expression of other major adhesive receptors on the macrophage surface (26). We verified this result on several systems including $\alpha_D\beta_2$-transfected cells and isolated α_D I-domain. $\alpha_D\beta_2$-transfected cells generated lower adhesion compared to M1 macrophages (**Figures 5B**, **6B**) since the expression of $\alpha_D\beta_2$ on these cells is lower (**Figures 5A**, **6A**). Nevertheless, these cells demonstrate a specific effect of integrin $\alpha_D\beta_2$ on cell adhesion. The results of the adhesion assay are confirmed by BioLayer Interferometry, which measures the direct protein-protein interaction between α_D I-domain and CEP or fibrinogen.

I-domain is a region of $\alpha_D\beta_2$ that contains most of the ligand-binding sites for β_2 integrins (43). We previously showed that binding sites for CEP and fibrinogen are located within the I-domain (23). In our earlier study regarding the ligand binding properties of integrin $\alpha_D\beta_2$, we compared α_D I-domain binding to all previously identified ligands including fibrinogen, fibronectin, ICAM-3, VCAM-1, plasminogen, vitronectin, and CYR61 using the surface plasmon resonance (Biacore 3000) (11). These studies demonstrated a K_D for α_D I-domain/fibrinogen binding $7.6x10^{-7}$ M. In another project we tested α_D I-domain binding to CEP by Biacore and calculated constant dissociation for this binding as K_D $1.8x10^{-7}$ M (23). However, we did not compare α_D I-domain binding to fibrinogen and CEP in the same experiment. Previously, the Biacore results for α_D binding to fibrinogen and to CEP were obtained from different α_D I-domain isolations, using different ligand densities on sensor chips and were performed several years apart (11, 23). Therefore, it was critical to analyze these interactions in one experiment to verify this result. Based on Biolayer Interfereometry results, which were performed on one α_D I-domain isolation using the same I-domain concentrations, we found that the calculated affinity of α_D I-domain/CEP interaction ($1.0x10^{-7}$M) is 2 folds stronger compared to the α_D I-domain/fibrinogen binding ($2.2x10^{-7}$M). These results are slightly different from our previous Biocare results. We explain this difference by the difference in the experimental platforms between surface plasmon resonance (Biocore) and biolayer interferometry (Octet). Nevertheless, both methods provides a similar result and demonstrates the stronger binding of α_D I-domain to CEP compared to fibrinogen.

All α_D ligands analyzed by Biacore previously (11) showed a K_D for α_D I-domain binding in the range $0.2\text{-}8x10^{-6}$ M. The strongest binding was found for α_D I-domain interaction with the rare ECM protein CYR61 (CCN1) with the K_D $2.9x10^{-7}$ M. This affinity is still weaker than α_D I-domain/CEP binding that we detected. Most importantly, the binding to "classical" $\alpha_D\beta_2$ ligands such as ICAM-3 ($1.89x10^{-6}$ M), VCAM-1 ($8.13x10^{-6}$ M), and fibrinogen ($0.76x10^{-6}$ M) (11) are significantly less compared to CEP. These data together demonstrate that CEP modification generates preferential ligands for $\alpha_D\beta_2$-mediated macrophage adhesion during inflammation. Therefore, inflammation and oxidation generate the improved conditions for $\alpha_D\beta_2$-dependent macrophage adhesion.

The theory of mesenchymal cell migration postulates that optimal migration occurs with an intermediate level of receptor expression and substrate density, while the high density of receptors and corresponding substrates generate very strong adhesion, preventing cell motility (7, 26, 44–46).

Previously we found that non-activated macrophages demonstrated an improved migration in a CEP-supplemented matrix (23). Non-activated macrophages express an intermediate level of $\alpha_D\beta_2$ and $\alpha_M\beta_2$ integrins (26). We and others have shown experimentally that intermediate levels of integrin expression support cell migration (7, 26, 47, 48).

We propose that upregulation of $\alpha_D\beta_2$ on M1 macrophages and modification of ECM proteins with CEP promotes the conditions for the formation of an excessive number of receptor-ligand pairs with a high binding affinity. Accordingly, this high level of macrophage adhesion can prevent macrophage migration. In agreement with this concept, we found that migration of M1 macrophages in a 3D fibrin matrix supplemented with CEP is significantly reduced compared to migration in a pure fibrin matrix. Interestingly, we found that the morphology of M1 macrophages in a 3D matrix is affected by the presence of CEP (**Figure 4D**). Particularly, we revealed, that M1 macrophages in CEP supplemented matrix have a more rounded shape compared to macrophages in fibrin gel. It has been shown previously that migrated macrophages have an elongated shape and accordingly a greater length-to-diameter ratio (49, 50). The length-to-diameter ratio of macrophages in a CEP supplemented matrix is statistically significantly lower compared to control, which is in agreement with the reduced macrophage migration that we detected (**Figure 4A**).

To summarize, we propose a potential mechanism that affects macrophage adhesion and migration in inflamed tissue. Oxidation of DHA, which is a common structural component of cell membranes, leads to the formation of adducts between ECM proteins and CEP. Experimental data demonstrated that 20-30 modifications can occur in one protein molecule (23, 30, 32, 51). These modifications substitute a lysine-mediated positive charge for a CEP-mediated negative charge, which affects the conformation and ligand-binding properties of modified proteins. CEP is recognized by integrins $\alpha_M\beta_2$ and $\alpha_D\beta_2$. Accordingly, CEP modification can transform random proteins in integrin-related ligands. Freshly differentiated non-activated macrophages possess an intermediate level of $\alpha_M\beta_2$ and $\alpha_D\beta_2$ expression that supports CEP-mediated migration to the site of inflammation. Polarized pro-inflammatory (M1-like) macrophages express a high level of $\alpha_D\beta_2$, generating a high adhesion to CEP-modified proteins in the inflamed tissue that prevents M1 macrophage migration and leads to the development

of chronic inflammation. The high affinity between $\alpha_D\beta_2$ and CEP additionally intensifies the potential effect. This model proposes that targeting the binding between $\alpha_D\beta_2$ and CEP can provide benefits against macrophage retention in the inflamed tissue and the development of chronic inflammation during metabolic and autoimmune diseases.

DATA AVAILABILITY STATEMENT

The original contributions presented in the study are included in the article/supplementary material. Further inquiries can be directed to the corresponding author.

ETHICS STATEMENT

The animal study was reviewed and approved by East Tennessee State University IACUC.

AUTHOR CONTRIBUTIONS

JC performed the experiments, analyzed the data, and edited the manuscript; KK, DG, CA, performed the experiments and analyzed the data; DW, EP, TB analyzed the data and edited the manuscript; VY designed the research, performed the experiments, analyzed the data, and wrote the manuscript. All authors contributed to the article and approved the submitted version.

FUNDING

These studies were supported by the American Heart Association 20AIREA35150018 (VY); and partially supported by the National Institutes of Health grants R15HL157836 (VY), R01GM119197 (DW), R01GM083016 (DW), R01HL071625 (TB), R01HL145536 (TB) and by the National Institute of Health grant C06RR0306551 for East Tennessee State University.

REFERENCES

1. Parisi L, Gini E, Baci D, Tremolati M, Fanuli M, Bassani B, et al. Macrophage Polarization in Chronic Inflammatory Diseases: Killers or Builders? *J Immunol Res* (2018) 2018:8917804. doi: 10.1155/2018/8917804
2. Groh L, Keating ST, Joosten LAB, Netea MG, Riksen NP. Monocyte and Macrophage Immunometabolism in Atherosclerosis. *Semin Immunopathol* (2018) 40(2):203–14. doi: 10.1007/s00281-017-0656-7
3. Ross EA, Devitt A, Johnson JR. Macrophages: The Good, the Bad, and the Gluttony. *Front Immunol* (2021) 12:708186. doi: 10.3389/fimmu.2021.708186
4. Koltsova EK, Hedrick CC, Ley K. Myeloid Cells in Atherosclerosis: A Delicate Balance of Anti-Inflammatory and Proinflammatory Mechanisms. *Curr Opin Lipidol* (2013) 24(5):371–80. doi: 10.1097/MOL.0b013e328363d298
5. Locati M, Curtale G, Mantovani A. Diversity, Mechanisms, and Significance of Macrophage Plasticity. *Annu Rev Pathol* (2020) 15:123–47. doi: 10.1146/annurev-pathmechdis-012418-012718
6. Moore KJ, Sheedy FJ, Fisher EA. Macrophages in Atherosclerosis: A Dynamic Balance. *Nat Rev Immunol* (2013) 13(10):709–21. doi: 10.1038/nri3520
7. Palecek SP, Loftus JC, Ginsberg MH, Lauffenburger DA, Horwitz AF. Integrin-Ligand Binding Properties Govern Cell Migration Speed Through Cell-Substratum Adhesiveness. *Nature* (1997) 385:537–40. doi: 10.1038/385537a0
8. Ammon C, Meyer SP, Schwarzfischer L, Krause SW, Andreesen R, Kreutz M. Comparative Analysis of Integrin Expression on Monocyte-Derived Macrophages and Monocyte-Derived Dendritic Cells. *Immunology* (2000) 100(3):364–9. doi: 10.1046/j.1365-2567.2000.00056.x
9. Ou Z, Dolmatova E, Lassegue B, Griendling KK. β1- and β2-Integrins: Central Players in Regulating Vascular Permeability and Leukocyte Recruitment During Acute Inflammation. *Am J Physiol Heart Circ Physiol* (2021) 320(2):H734–H9. doi: 10.1152/ajpheart.00518.2020
10. Yakubenko VP, Lishko VK, Lam SC-T, Ugarova TP. A Molecular Basis for Integrin $\alpha_M\beta_2$ in Ligand Binding Promiscuity. *J Biol Chem* (2002) 277:48635–42. doi: 10.1074/jbc.M208877200
11. Yakubenko VP, Yadav SP, Ugarova TP. Integrin $\alpha_D\beta_2$, an Adhesion Receptor Up-Regulated on Macrophage Foam Cells, Exhibits Multiligand-Binding Properties. *Blood* (2006) 107:1643–50. doi: 10.1182/blood-2005-06-2509
12. Aziz MH, Cui K, Das M, Brown KE, Ardell CL, Febbraio M, et al. The Upregulation of Integrin $\alpha_D\beta_2$ (CD11d/CD18) on Inflammatory Macrophages Promotes Macrophage Retention in Vascular Lesions and Development of Atherosclerosis. *J Immunol* (2017) 198(12):4855–67. doi: 10.4049/jimmunol.1602175
13. Danilenko DM, Rossito PV, van der Vieren M, Le Tring H, Mc Donagh SP, Affolter VK, et al. A Novel Canine Leukointegrin, Alpha D Beta 2, is Expressed by Specific Macrophage Subpopulations in Tissue and a Minot CD8+ Lymphocyte Subpopulation in Peripheral Blood. *J Immunol* (1995) 155:35–44.
14. Van der Vieren M, Le Trong H, St.John T, Staunton DE, Gallatin WM. A Novel Leukointegrin, $\alpha_D\beta_2$, Binds Preferentially to ICAM-3. *Immunity* (1995) 3:683–90. doi: 10.1016/1074-7613(95)90058-6
15. Bao F, Brown A, Dekaban GA, Omana V, Weaver LC. CD11d Integrin Blockade Reduces the Systemic Inflammatory Response Syndrome After Spinal Cord Injury. *Exp Neurol* (2011) 231(2):272–83. doi: 10.1016/j.expneurol.2011.07.001
16. Thomas AP, Dunn TN, Oort PJ, Grino M, Adams SH. Inflammatory Phenotyping Identifies CD11d as a Gene Markedly Induced in White Adipose Tissue in Obese Rodents and Women. *J Nutr* (2011) 141(6):1172–80. doi: 10.3945/jn.110.127068
17. Weaver LC, Bao F, Dekaban GA, Hryciw T, Shultz SR, Cain DP, et al. CD11d Integrin Blockade Reduces the Systemic Inflammatory Response Syndrome After Traumatic Brain Injury in Rats. *Exp Neurol* (2015) 271:409–22. doi: 10.1016/j.expneurol.2015.07.003
18. Miyazaki Y, Bunting M, Stafforini DM, Harris ES, McIntyre TM, Prescott SM, et al. Integrin $\alpha_D\beta_2$ Is Dynamically Expressed by Inflamed Macrophages and Alters the Natural History of Lethal Systemic Infections. *J Immunol* (2008) 180(1):590–600. doi: 10.4049/jimmunol.180.1.590
19. de Azevedo-Quintanilha IG, Vieira-de-Abreu A, Ferreira AC, Nascimento DO, Siqueira AM, Campbell RA, et al. Integrin $\alpha_D\beta_2$ (CD11d/CD18) Mediates Experimental Malaria-Associated Acute Respiratory Distress Syndrome (MA-ARDS). *Malar J* (2016) 15(1):393. doi: 10.1186/s12936-016-1447-7
20. Nascimento DO, Vieira-de-Abreu A, Arcanjo AF, Bozza PT, Zimmerman GA, Castro-Faria-Neto HC. Integrin $\alpha_D\beta_2$ (CD11d/CD18) Modulates Leukocyte Accumulation, Pathogen Clearance, and Pyroptosis in Experimental Salmonella Typhimurium Infection. *Front Immunol* (2018) 9:1128. doi: 10.3389/fimmu.2018.01128
21. Bailey WP, Cui K, Ardell CL, Keever KR, Singh S, Rodriguez-Gil DJ, et al. The Expression of Integrin $\alpha_D\beta_2$ (CD11d/CD18) on Neutrophils Orchestrates the Defense Mechanism Against Endotoxemia and Sepsis. *J Leukoc Biol* (2021) 109(5):877–90. doi: 10.1002/JLB.3HI0820-529RR.
22. Yakubenko VP, Byzova TV. Biological and Pathophysiological Roles of End-Products of DHA Oxidation. *Biochim Biophys Acta* (2017) 1862(4):407–15. doi: 10.1016/j.bbalip.2016.09.022
23. Yakubenko VP, Cui K, Ardell CL, Brown KE, West XZ, Gao D, et al. Oxidative Modifications of Extracellular Matrix Promote the Second Wave of

Inflammation *via* β_2 Integrins. *Blood* (2018) 132(1):78–88. doi: 10.1182/blood-2017-10-810176
24. Blythe EN, Weaver LC, Brown A, Dekaban GA. Beta2 Integrin CD11d/CD18: From Expression to an Emerging Role in Staged Leukocyte Migration. *Front Immunol* (2021) 12:775447. doi: 10.3389/fimmu.2021.775447
25. Shi C, Simon DI. Integrin Signals, Transcription Factors, and Monocyte Differentiation. *Trends Cardiovasc Med* (2006) 16(5):146–52. doi: 10.1016/j.tcm.2006.03.002
26. Cui K, Ardell CL, Podolnikova NP, Yakubenko VP. Distinct Migratory Properties of M1, M2, and Resident Macrophages Are Regulated by $\alpha_D\beta_2$ and $\alpha_M\beta_2$ Integrin-Mediated Adhesion. *Front Immunol* (2018) 9:2650. doi: 10.3389/fimmu.2018.02650
27. Szpak D, Izem L, Verbovetskiy D, Soloviev DA, Yakubenko VP, Pluskota E. Alphambeta2 Is Antiatherogenic in Female But Not Male Mice. *J Immunol* (2018) 200(7):2426–38. doi: 10.4049/jimmunol.1700313
28. Wolf D, Bukosza N, Engel D, Poggi M, Jehle F, Anto MN, et al. Inflammation, But Not Recruitment, of Adipose Tissue Macrophages Requires Signalling Through Mac-1 (CD11b/CD18) in Diet-Induced Obesity (DIO). *Thromb Haemost* (2017) 117(2):325–38. doi: 10.1160/TH16-07-0553
29. Miyazaki Y, Vieira-de-Abreu A, Harris ES, Shah AM, Weyrich AS, Castro-Faria-Neto HC, et al. Integrin $\alpha_D\beta_2$ (CD11d/CD18) Is Expressed by Human Circulating and Tissue Myeloid Leukocytes and Mediates Inflammatory Signaling. *PloS One* (2014) 9(11):e112770. doi: 10.1371/journal.pone.0112770
30. Gu X, Meer SG, Miyagi M, Rayborn ME, Hollyfield JG, Crabb JW, et al. Carboxyethylpyrrole Protein Adducts and Autoantibodies, Biomarkers for Age-Related Macular Degeneration. *J Biol Chem* (2003) 278(43):42027–35. doi: 10.1074/jbc.M305460200
31. West XZ, Malinin NL, Merkulova AA, Tischenko M, Kerr BA, Borden EC, et al. Oxidative Stress Induces Angiogenesis by Activating TLR2 With Novel Endogenous Ligands. *Nature* (2010) 467(7318):972–6. doi: 10.1038/nature09421
32. Ebrahem Q, Renganathan K, Sears J, Vasanji A, Gu X, Lu L, et al. Carboxyethylpyrrole Oxidative Protein Modifications Stimulate Neovascularization: Implications for Age-Related Macular Degeneration. *Proc Natl Acad Sci USA* (2006) 103(36):13480–4. doi: 10.1073/pnas.0601552103
33. Hoff HF, O'Neil J, Wu Z, Hoppe G, Salomon RL. Phospholipid Hydroxyalkenals: Biological and Chemical Properties of Specific Oxidized Lipids Present in Atherosclerotic Lesions. *Arterioscler Thromb Vasc Biol* (2003) 23(2):275–82. doi: 10.1161/01.ATV.0000051407.42536.73
34. Kim YW, Yakubenko VP, West XZ, Gugiu GB, Renganathan K, Biswas S, et al. Receptor-Mediated Mechanism Controlling Tissue Levels of Bioactive Lipid Oxidation Products. *Circ Res* (2015) 117(4):321–32. doi: 10.1161/CIRCRESAHA.117.305925
35. Wolf D, Anto-Michel N, Blankenbach H, Wiedemann A, Buscher K, Hohmann JD, et al. A Ligand-Specific Blockade of the Integrin Mac-1 Selectively Targets Pathologic Inflammation While Maintaining Protective Host-Defense. *Nat Commun* (2018) 9(1):525. doi: 10.1038/s41467-018-02896-8
36. Lishko VK, Burke T, Ugarova T. Antiadhesive Effect of Fibrinogen: A Safeguard for Thrombus Stability. *Blood* (2007) 109(4):1541–9. doi: 10.1182/blood-2006-05-022764
37. Yermolenko IS, Gorkun OV, Fuhrmann A, Podolnikova NP, Lishko VK, Oshkadyerov SP, et al. The Assembly of Nonadhesive Fibrinogen Matrices Depends on the alphaC Regions of the Fibrinogen Molecule. *J Biol Chem* (2012) 287(50):41979–90. doi: 10.1074/jbc.M112.410696
38. Kerr BA, Ma L, West XZ, Ding L, Malinin NL, Weber ME, et al. Interference With Akt Signaling Protects Against Myocardial Infarction and Death by Limiting the Consequences of Oxidative Stress. *Sci Signal* (2013) 6(287):ra67. doi: 10.1126/scisignal.2003948
39. Hollyfield JG, Bonilha VL, Rayborn ME, Yang X, Shadrach KG, Lu L, et al. Oxidative Damage-Induced Inflammation Initiates Age-Related Macular Degeneration. *Nat Med* (2008) 14(2):194–8. doi: 10.1038/nm1709
40. Shoulders MD, Raines RT. Collagen Structure and Stability. *Annu Rev Biochem* (2009) 78:929–58. doi: 10.1146/annurev.biochem.77.032207.120833
41. Cui K, Podolnikova NP, Bailey W, Szmuc E, Podrez EA, Byzova TV, et al. Inhibition of Integrin $\alpha_D\beta_2$-Mediated Macrophage Adhesion to End-Product of DHA Oxidation Prevents Macrophage Accumulation During Inflammation. *J Biol Chem* (2019) 294(39):14370–82. doi: 10.1074/jbc.RA119.009590
42. Vorup-Jensen T, Carman CV, Shimaoka M, Schuck P, Svitel J, Springer TA. Exposure of Acidic Residues as a Danger Signal for Recognition of Fibrinogen and Other Macromolecules by Integrin $\alpha_X\beta_2$. *Proc Natl Acad Sci USA* (2005) 102(5):1614–9. doi: 10.1073/pnas.0409057102
43. Luo BH, Carman CV, Springer TA. Structural Basis of Integrin Regulation and Signaling. *Annu Rev Immunol* (2007) 25:619–47. doi: 10.1146/annurev.immunol.25.022106.141618
44. Wiesner C, Le-Cabec V, El AK, Maridonneau-Parini I, Linder S. Podosomes in Space: Macrophage Migration and Matrix Degradation in 2D and 3D Settings. *Cell Adh Migr* (2014) 8(3):179–91. doi: 10.4161/cam.28116
45. DiMilla PA, Barbee K, Lauffenburger DA. Mathematical Model for the Effects of Adhesion and Mechanics on Cell Migration Speed. *Biophys J* (1991) 60:15–37. doi: 10.1016/S0006-3495(91)82027-6
46. DiMilla PA, Stone JA, Quinn JA, Albelda SM, Lauffenburger DA. Maximal Migration of Human Smooth Muscle Cells on Fibronectin and Type IV Collagen Occurs at an Intermediate Attachment Strength. *J Cell Biol* (1993) 122:729–37. doi: 10.1083/jcb.122.3.729
47. Lishko VK, Yakubenko VP, Ugarova TP. The Interplay Between Integrins $\alpha_M\beta_2$ and $\alpha_5\beta_1$ During Cell Migration to Fibronectin. *Exp Cell Res* (2003) 283:116–26. doi: 10.1016/S0014-4827(02)00024-1
48. Yakubenko VP, Belevych N, Mishchuk D, Schurin A, Lam SC, Ugarova TP. The Role of Integrin Alpha D Beta2 (CD11d/CD18) in Monocyte/Macrophage Migration. *Exp Cell Res* (2008) 314:2569–78. doi: 10.1016/j.yexcr.2008.05.016
49. Cougoule C, Van GE, Le C, Lafouresse F, Dupre L, Mehraj V, et al. Blood Leukocytes and Macrophages of Various Phenotypes Have Distinct Abilities to Form Podosomes and to Migrate in 3D Environments. *Eur J Cell Biol* (2012) 91(11-12):938–49. doi: 10.1016/j.ejcb.2012.07.002
50. McWhorter FY, Wang T, Nguyen P, Chung T, Liu WF. Modulation of Macrophage Phenotype by Cell Shape. *Proc Natl Acad Sci USA* (2013) 110(43):17253–8. doi: 10.1073/pnas.1308887110
51. Salomon RG. Carboxyethylpyrroles: From Hypothesis to the Discovery of Biologically Active Natural Products. *Chem Res Toxicol* (2017) 30(1):105–13. doi: 10.1021/acs.chemrestox.6b00304

Conflict of Interest: The authors declare that the research was conducted in the absence of any commercial or financial relationships that could be construed as a potential conflict of interest.

Publisher's Note: All claims expressed in this article are solely those of the authors and do not necessarily represent those of their affiliated organizations, or those of the publisher, the editors and the reviewers. Any product that may be evaluated in this article, or claim that may be made by its manufacturer, is not guaranteed or endorsed by the publisher.

frontiers | Frontiers in Immunology

ORIGINAL RESEARCH
published: 02 June 2022
doi: 10.3389/fimmu.2022.888612

HAPLN1 Affects Cell Viability and Promotes the Pro-Inflammatory Phenotype of Fibroblast-Like Synoviocytes

Yong Chen[1], Baojiang Wang[2], Yanjuan Chen[3], Qunyan Wu[2], Wing-Fu Lai[4,5], Laiyou Wei[1], Kutty Selva Nandakumar[6†] and Dongzhou Liu[1†]*

[1] Division of Rheumatology and Research, The Second Clinical Medical College, Jinan University (Shenzhen People's Hospital), Shenzhen, China, [2] Institute of Maternal and Child Medicine, Affiliated Shenzhen Maternity and Child Healthcare Hospital, Southern Medical University, Shenzhen, China, [3] School of Basic Medicine, Jinan University, Guangzhou, China, [4] Department of Urology, Zhejiang Provincial People's Hospital, Hangzhou Medical College, Zhejiang, China, [5] Department of Applied Biology and Chemical Technology, Hong Kong Polytechnic University, Wanchai, Hong Kong SAR, China, [6] Southern Medical Universit - Karolinska Institute (SMU-KI) United Medical Inflammation Center, School of Pharmaceutical Sciences, Southern Medical University, Guangzhou, China

OPEN ACCESS

Edited by:
Hao Sun,
University of California, San Diego, United States

Reviewed by:
Thomas N. Wight, Benaroya Research Institute, United States
Ganesan Ramamoorthi, Moffitt Cancer Center, United States
Xiao-Feng Li, Anhui Medical University, China

***Correspondence:**
Dongzhou Liu
liu_dz2001@sina.com

†These authors have contributed equally to this work

Specialty section:
This article was submitted to Autoimmune and Autoinflammatory Disorders, a section of the journal Frontiers in Immunology

Received: *03 March 2022*
Accepted: *04 May 2022*
Published: *02 June 2022*

Citation:
Chen Y, Wang B, Chen Y, Wu Q, Lai W-F, Wei L, Nandakumar KS and Liu D (2022) HAPLN1 Affects Cell Viability and Promotes the Pro-Inflammatory Phenotype of Fibroblast-Like Synoviocytes. Front. Immunol. 13:888612. doi: 10.3389/fimmu.2022.888612

HAPLN1 maintains aggregation and the binding activity of extracellular matrix (ECM) molecules (such as hyaluronic acid and proteoglycan) to stabilize the macromolecular structure of the ECM. An increase in HAPLN1 expression is observed in a few types of musculoskeletal diseases including rheumatoid arthritis (RA); however, its functions are obscure. This study examined the role of HAPLN1 in determining the viability, proliferation, mobility, and pro-inflammatory phenotype of RA- fibroblast-like synoviocytes (RA-FLSs) by using small interfering RNA (siHAPLN1), over-expression vector ($HAPLN1^{OE}$), and a recombinant HAPLN1 (rHAPLN1) protein. HAPLN1 was found to promote proliferation but inhibit RA-FLS migration. Metformin, an AMPK activator, was previously found by us to be able to inhibit FLS activation but promote HAPLN1 secretion. In this study, we confirmed the up-regulation of HAPLN1 in RA patients, and found the positive relationship between HAPLN1 expression and the AMPK level. Treatment with either si-HAPLN1 or $HAPLN1^{OE}$ down-regulated the expression of AMPK-α gene, although up-regulation of the level of p-AMPK-α was observed in RA-FLSs. si-HAPLN1 down-regulated the expression of proinflammatory factors like TNF-α, MMPs, and IL-6, while $HAPLN1^{OE}$ up-regulated their levels. qPCR assay indicated that the levels of TGF-β, ACAN, fibronectin, collagen II, and Ki-67 were down-regulated upon si-HAPLN1 treatment, while $HAPLN1^{OE}$ treatment led to up-regulation of ACAN and Ki-67 and down-regulation of cyclin-D1. Proteomics of si-HAPLN1, rHAPLN1, and mRNA-Seq analysis of rHAPLN1 confirmed the functions of HAPLN1 in the activation of inflammation, proliferation, cell adhesion, and strengthening of ECM functions. Our results for the first time demonstrate the function of HAPLN1 in promoting the proliferation and pro-inflammatory phenotype of RA-FLSs, thereby contributing to RA pathogenesis. Future in-depth studies are required for better understanding the role of HAPLN1 in RA.

Keywords: rheumatoid arthritis, hyaluronan and proteoglycan link protein 1, fibroblast-like synoviocytes, cell viability, cell migration, pathogenesis

1 INTRODUCTION

Rheumatoid arthritis (RA) is a chronic autoimmune disease characterized by destructive, chronic, debilitating arthritis. Pannus formation is one of the main features of the disease (1). During RA development, the number of fibroblast-like synoviocytes (FLSs), one of the key effector cells (2), increases significantly, leading to the transformation of the synovial lining from a delicate structure into an invasive hyperplastic tissue mass known as pannus (3). The pannus tissue contributes to the chronic inflammatory milieu in the arthritic joint, resulting in an expansion of the synovial membrane and the occurrence of a complex interplay among different dendritic cell (DC) subtypes, T cells, macrophages, B cells, neutrophils, fibroblasts, and osteoclasts (4). FLSs transform the synovium into a hyperplastic invasive pannus by producing various mediators such as cytokines and proteases, leading to the destruction of the extracellular matrix (ECM), cartilages, and bones (5). The cell phenotype of RA-FLSs mimics cancer cells in terms of invasion, proliferation, and apoptosis (6). The presence of functionally distinct arthritis-associated fibroblast subsets in human synovial tissues, along with the identification of fibroblast subsets that mediate either inflammation or bone/cartilage damage in arthritis, suggests that targeting FLSs is an attractive therapeutic approach to treat RA (7).

Hyaluronan and proteoglycan link protein 1 (HAPLN1), also known as cartilage link protein, was originally identified from the proteoglycan component extracted from the bovine articular cartilage (8). Our previous study confirmed the secretion of HAPLN1by RA-FLSs (9). Physiologically, HAPLN1 is a component of the ECM required for normal cartilage development. It maintains stable aggregation and the binding activity of two important ECM macromolecules [hyaluronic acid (HA) and proteoglycan] which, along with other molecules present in the joint, contribute not only to the maintenance of the stable macromolecular structure but also to the compression resistance of the joint (10). The vital role played by HAPLN1 in regulating bone/cartilage growth was documented previously. HAPLN1-deficient mice showed a series of cardiac malformations (e.g., atrial septal and myocardial defects) along with a remarkable reduction in the level of multifunctional proteoglycans (11). The most classic disease first reported to be associated with HAPLN1 is juvenile rheumatoid arthritis (12), but the mechanisms were not yet fully known. Nevertheless, genomics research has enabled the clarification of the relation of HAPLN1 with various rheumatic disorders [including spinal degeneration, osteoarthritis (OA), ankylosing spondylitis (AS), and RA] (13–17). The HAPLN1 gene is present adjacent to the ankylosing spondylitis-associated single nucleotide polymorphism (SNP) (rs4552569) (18). Compared to subjects with the CC or CT genotype, those with the TT genotype for the SNP at rs179851 were found to be significantly overrepresented among the subjects with higher scores for osteophyte formation and disc space narrowing (13). Importantly, HAPLN1 showed a significant correlation with the severity of RA (17). We found that one of the most significantly up-regulated genes in RA-FLSs, contrary to osteoarthritis (OA)-FLSs, is HAPLN1, whose protein level increases in the plasma and synovium of RA patients (9). Recently, the oncogenic phenotype of HAPLN1 was reported to be able to contribute to cellular hyperactivity and remodeling of collagen matrices (19, 20). The exact role of HAPLN1 in RA and its interaction with other matrix molecules under disease conditions are still unclear. The objective of this study is, therefore, to explore the potential role played by HAPLN1 in RA-FLS-mediated disease pathogenesis.

2 RESULTS

2.1 Increased HAPLN1 Expression in the Synovium and Plasma of RA Patients

The HAPLN1 expression in the synovium of RA (n=20) was found by immunohistochemical assays to be significantly higher than that of OA patients (n=17) (**Figure 1A** and **Supplementary Table S1** for participants' details). Similarly, the HAPLN1 level in the plasma of RA patients (n=61) was higher than that of OA patients (n=20) and healthy control subjects (HC, n=12) (**Figure 1B** and **Supplementary Table S2** for participants' details). These results agree with our earlier mRNA sequencing analysis, which showed that the level of HAPLN1 expression in RA-FLSs is higher than that in OA FLSs (**Figure 1C**) (9).

The AMP-activated protein kinase (AMPK) pathway contributes to cell viability, metabolism, and inflammation during the onset and progression of RA (21, 22). Treatment of RA-FLSs with an AMPK activator, metformin, up-regulates HAPLN1 expression (9). Therefore, changes in AMPK expression could help elucidate the functions of HAPLN1. In this study, the AMPK level in healthy people was found to be significantly higher than OA and RA patients and had a significant positive correlation with the HAPLN1 level in the plasma of RA patients ($n = 48$; $r = 0.693$, $p < 0.0001$) (**Figure 1C**). In addition, the plasma HAPLN1 level negatively correlated with the course of the arthritis disease ($n = 46$, $r = -0.311$, $p = 0.038$). HAPLN1 in RA patients having less than 3 years of disease activity ($n = 20$) was higher than that in patients having disease symptoms for more than 3 years ($n = 41$) (**Figure 1D** and **Supplementary Figure S1**). A moderate positive correlation between HAPLN1 and the rheumatoid factor was noted ($n = 24$, $r = 0.431$, $p < 0.05$) (**Figure 1E**). However, no correlation between the HAPLN1 level and other indexes of disease activity (such as ESR and CRP) was revealed by the data in this study (**Figures 1F, G**). The elevated AMPK level was consistent with our previous observations (9). It is plausible that HAPLN1 participates in AMPK-regulated metabolic pathways.

2.2 HAPLN1 Increased the Proliferation But Inhibited the Mobility of RA-FLSs

To dissect the role of HAPLN1 in determining the viability of RA-FLSs, three small interfering RNA (si-RNA HAPLN1) molecules and an over-expression plasmid vector ($HAPLN1^{OE}$) were used to study the proliferation and migration ability of RA-FLSs. All of the tested siRNA molecules in this study effectively down-regulated the mRNA level of HAPLN1, while transfecting

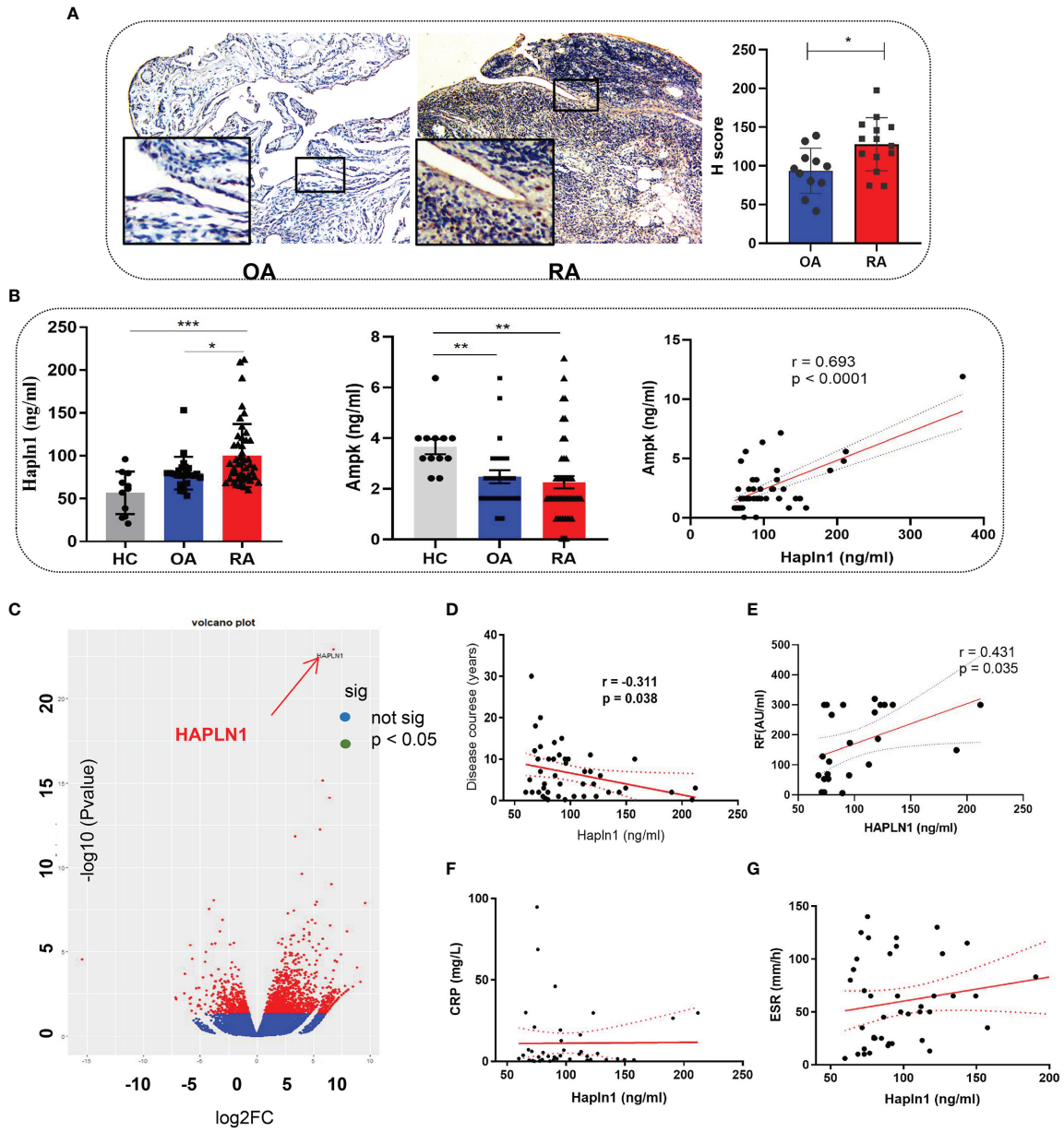

FIGURE 1 | HAPLN1 is up-regulated in RA patients and positively correlated with AMPK. **(A)** Increased HAPLN1 expression, quantified by the H score, in RA (n=20) than OA (n=17) synovium (magnification of gross looking, 10×5; magnification of foci in the framed, 10×20). **(B)** Plasma HAPLN1 levels examined by ELISA were significantly enhanced in RA (n=61) patients than OA (n=20) patients and HC (n=12), while AMPK levels were decreased in both OA and RA patients compared to HC. Plasma HAPLN1 and AMPK levels were significantly positively correlated (r = 0.693, p < 0.0001). **(C)** Volcano plot showing higher expression of the HAPLN1 gene in FLSs from RA than OA patients (n=3 in each group). **(D, E)** Plasma HAPLN1 levels negatively correlated with the disease course (r = -0.311, p = 0.038) and showed a moderately positive correlation with RF levels (r = 0.431, p = 0.038) of RA patients. **(F, G)** No significant correlation between the HAPLN1 level and ESR and CRP. *$p < 0.05$; **P < 0.01; ***$p < 0.001$.

RA-FLSs with HAPLN1^{OE} up-regulated the expression of HAPLN1 (**Supplementary Figure S2**). Recombinant HAPLN1 (rHAPLN1) at different concentrations was also added to RA-FLSs to study its functions.

Transfection with si-HAPLN1 did not affect the proliferation of RA-FLSs (**Figure 2A** and **Supplementary Figure S3**), though a significant increase in the apoptotic ratio of RA-FLSs was revealed by the results of our TUNEL assay (**Figure 2B**). The wound healing assay and the transwell assay showed an increase in the migration ability of RA-FLSs after transfection with si-HAPLN1 (**Figures 2C, D**), and the effect was reversed after the addition of rHAPLN1 (50 ng/ml) (**Figure 2D**). Conversely, after

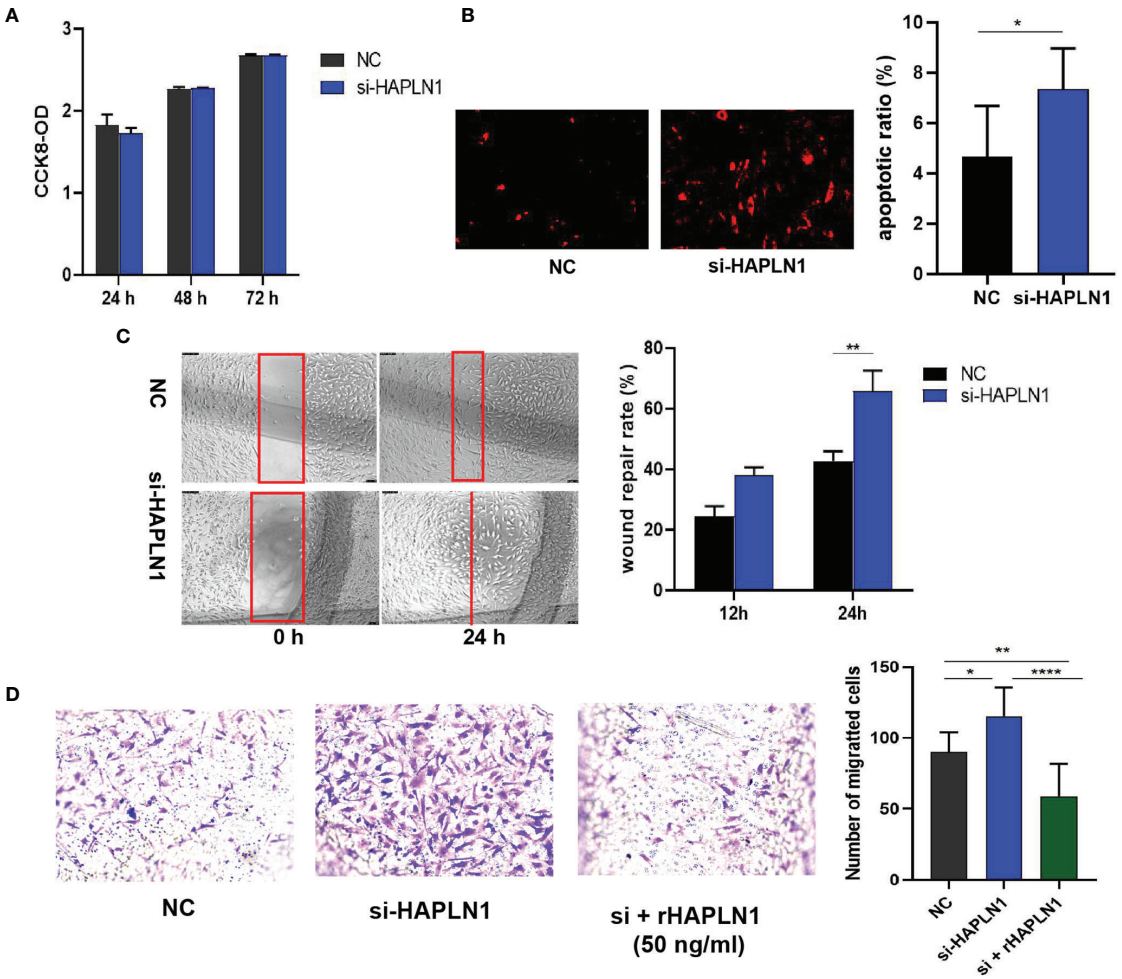

FIGURE 2 | Effects of si-HAPLN1 on RA-FLS activity. Transfection of siHAPLN1 in RA-FLSs did not significantly affect the **(A)** proliferation but significantly increased **(B)** apoptosis (magnification: 10×10) and **(C, D)** migration ability of RA-FLSs. Wound healing **(C**, magnification: 10×5**)** and transwell assays **(D**, magnification: 10×5**)** were used to measure the migration capacity of FLSs. Recombinant HAPLN1 (50 ng/ml) attenuated the increased migration ability induced by si-HAPLN1 in the transwell assay. *$p < 0.05$; **$p < 0.01$; ****$p < 0.0001$. NC, negative control is control siRNA of si-HAPLN1.

transfection with HAPLN1^{OE}, RA-FLSs showed enhanced proliferation and a decline in the apoptotic ratio (**Figures 3A, B** and **Supplementary Figure S4**). Results of the wound healing assay showed a decrease in the level of migration exhibited by HAPLN1^{OE}-transfected RA-FLSs (**Figure 3C**), whereas rHAPLN1 confirmed the effects of HAPLN1 on RA-FLSs which showed a significant increase in the proliferation activity (**Figure 4A** and **Supplementary Figure S5**) and a reduction in apoptosis, especially during the early phase (**Figures 4B, C**). The wound healing assay and the transwell assay demonstrated that rHAPLN1 inhibited the migration ability of RA-FLSs (**Figures 4D, E**). It is known that cell mobility is elevated in cancer cells as well as in activated RA-FLSs (6). However, our experiments with si-HAPLN1, HAPLN1^{OE}, and rHAPLN1 demonstrated that HAPLN1 shows an inhibitory effect on the mobility of RA-FLSs although it could activate RA-FLS proliferation.

2.3 Expression of HAPLN1 Affects the Cell Cycle, Structure Molecules and Cytokines Secretion of RA-FLSs

2.3.1 The mRNA Level of Ki-67 Was Up-Related by HAPLN1

In cancer research, Ki-67 expression can indicate the effect of a treatment on cell proliferation (23), and is proved to be able to predict the activity of RA-FLSs (24). Transfection with si-HAPLN1 decreased Ki-67 mRNA expression significantly, while transfection with HAPLN1^{OE} increased its expression in RA-FLSs (**Figures 5A, B**). We also checked the expression of Cyclin D1, which is an important regulator of cell cycle, with many carcinomas being characterized by Cyclin D1 overexpression that induces uncontrolled cell proliferation (25). Changes of Cyclin D1 are not consistent with the changes observed in the MTT assay, CCK8 assay, and Ki-67 expression in the current study. It was significantly reduced by HAPLN1^{OE}

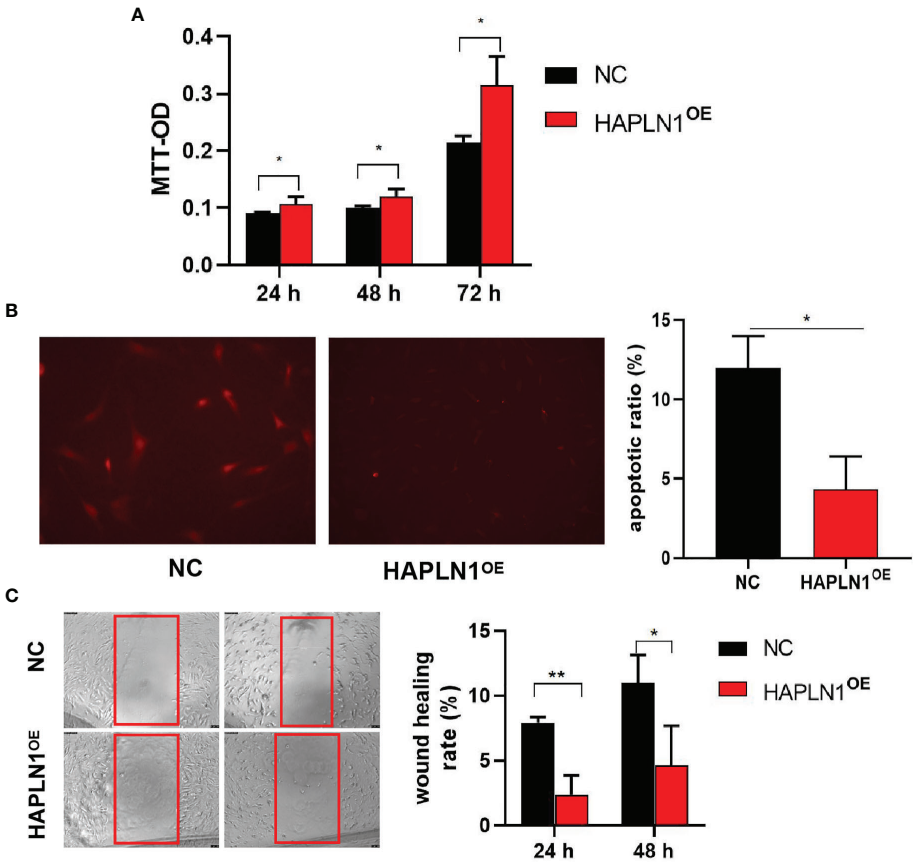

FIGURE 3 | Effects of HAPLN1 over-expression on RA-FLSs activity. Over-expression of HAPLN1 (HAPLN1^{OE}) in RA-FLSs significantly increased the **(A)** proliferation but reduced **(B)** apoptosis (magnification: 10×10) and **(C)** migration (magnification: 10×5) of RA-FLSs. *$p < 0.05$; **$p < 0.01$. NC, negative control is control plasmid vector of HAPLN1^{OE}.

transfection (**Figures 5A, B, 6C, D**). It seems Cyclin D1 could not validate HAPLN1 promotes cell viability, but inhibits cell mobility function could be explained as Cyclin D1 is reported to target roles in cytoskeletal modelling, cell adhesion, and motility. Cyclin D1 loss is associated with reduced cellular migration in response to different stimuli (25).

2.3.2 Cell Structure Molecules Were Up-Regulated by HAPLN1

ACAN is a well-documented chaperone of HAPLN1, playing a significant role in regulating the ECM structure (26). mRNA of ACAN was significantly down-regulated by si-HAPLN1 while up-regulated by HAPLN1^{OE} transfection. Other structure molecules such as TGF-β, fibronectin, and collagen II were also down-regulated by si-HAPLN1 treatment (**Figures 5C, D**). These targets play key roles in ECM formation, wound healing, and fibrosis in different pathological conditions. A strengthened ECM architecture is a way to restrain cancer cell progression (27). Thus, changes in these targets as led by HAPLN1 validated the role of HAPLN1 in controlling cell migration of RA-FLSs. Pearson correlation coefficient analysis was applied to analyze the relative mRNA levels from the si-control group. A strong positive correlation (r = 0.66, 95%CI [0.13, 0.90], $p < 0.05$) between TGF-β and HAPLN1 was observed (**Figure 5E**). TGF-β signaling events are known to control diverse processes and responses, such as cell proliferation, differentiation, apoptosis, and migration. Besides limited cell migration in pre-malignant cells (28), it cross-talks with multiple inflammation pathways (29).

2.3.3 Inflammatory Cytokines Were Promoted by HAPLN1

Previously we reported an increase in the expression of HAPLN1 in RA-FLSs after stimulation of the AMPK pathway (9). We further confirmed the inter-dependence of the positive correlation between HAPLN1 and AMPK by using clinical RA plasma samples as mentioned above (**Figure 1B**). The role of AMPK as a regulator of metabolism and inflammation is well known (30, 31). Therefore, we investigated how HAPLN1 affects RA-FLSs in the expression of AMPK-α and related cytokines, such as TNF-α, IL-6, and MMPs, involved in inflammation.

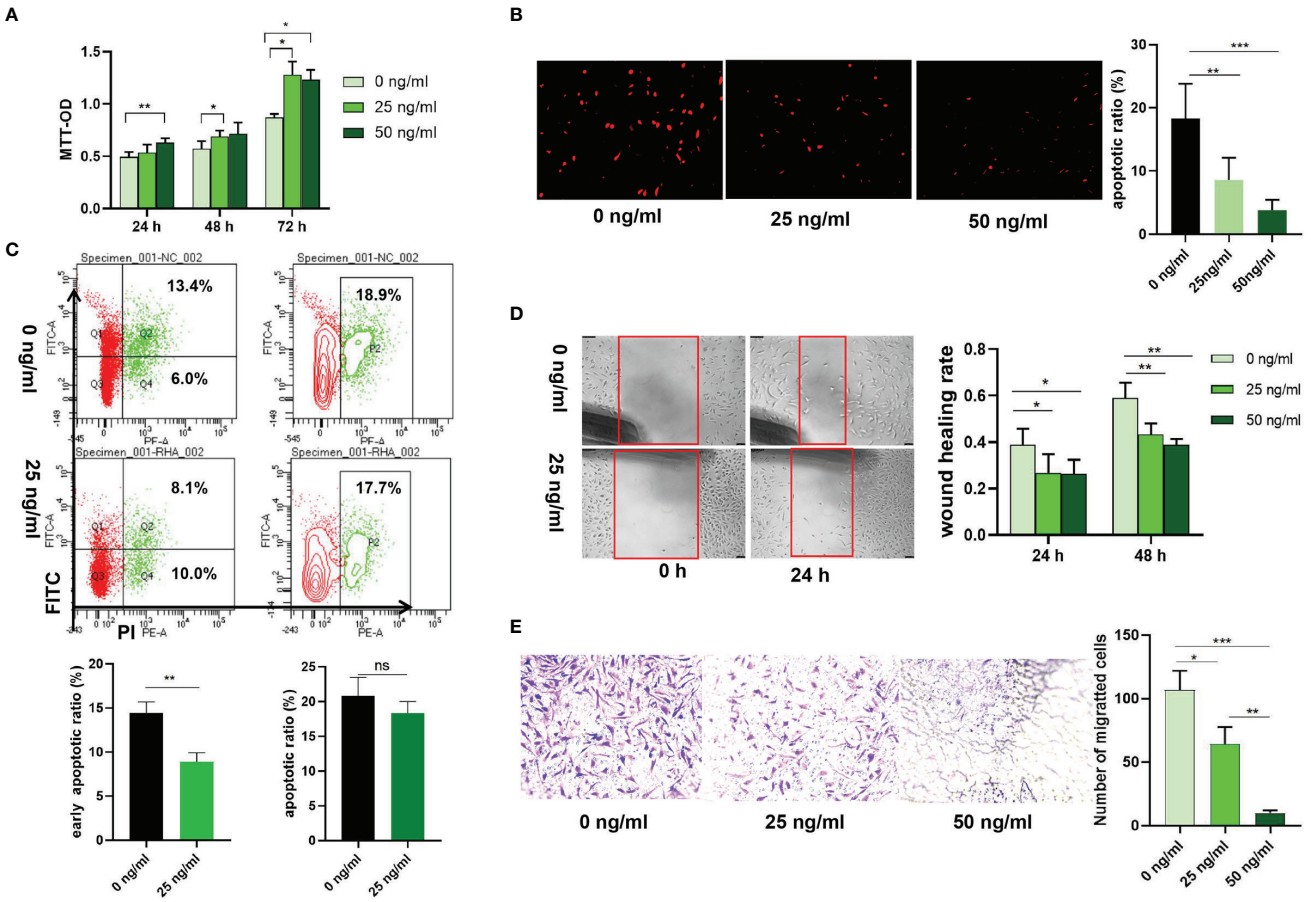

FIGURE 4 | Effects of rHAPLN1 on RA-FLSs activity. **(A)** Treatment of RA-FLSs with rHAPLN1 significantly enhanced the **(A)** proliferation but reduced **(B, C)** apoptosis of RA-FLSs (magnification: 10×10), especially during the early phase and **(D, E)** migration. Wound healing **(D)** and transwell **(E)** assays were used to evaluate the migration capacity of FLSs (magnification:10×5). ns, not significant; *$p < 0.05$; **$p < 0.01$; ***$p < 0.001$.

Transfection of si-HAPLN1 into RA-FLSs inhibited the expression of mRNAs of AMPK-α, TNF-α, IL-6, and MMP1, MMP3, and MMP9 (**Figure 6A**). Results of the automated WB assay confirmed successful silencing of HAPLN1. The expression of TNF-α, MMP1, MMP3, and MMP9 was inhibited in a way similar to the expression of the corresponding mRNAs (**Figure 6B**). However, the expression of AMPK-α and pAMPK-α at the protein level, unlike its mRNA expression, was found to be up-regulated. $HAPLN1^{OE}$ transfection in RA-FLSs up-regulated the expression of TNF-α, IL-6, and MMP9, while AMPK-α was down-regulated (**Figure 6C**). Unlike the expression of mRNA, the expression of AMPK-α and pAMPK-α was also up-regulated when TNF-α, IL-6, MMP1, and MMP3 showed a trend of up-regulation (**Figure 6D**).

To better understand the potential interactions between these molecules, we collected multiple expression data of relative mRNA levels from control groups of si-HAPLN1 (si-Control), and applied the Pearson correlation coefficient analysis. HAPLN1 levels showed a strong positive correlation with the level of AMPK-α (**Figure 6E**), which is in accordance with its plasma levels and also with our previous findings using metformin treatment (9). AMPK-α also positively correlated to TGF-β and ACAN (**Figures 6F, G**). Importantly, HAPLN1 levels had a positive correlation with the inflammatory cytokines such as IL-6 (**Figure 6H**) and the modulators of the ECM structure, including TGF-β and fibronectin (**Figures 6I, J**). Thus, HAPLN1 promotes the production of inflammatory cytokines, which plausibly could provide a molecular basis for its contribution to cell viability and mobility. In RA-FLSs, AMPK activation results in up-regulation of HAPLN1 levels and vice versa. Based on the effect of HAPLN1 on AMPK expression, along with the possible regulation of the HAPLN1 expression through the cAMP-PKA-(possibly, AMPK)-RUNX1/2 pathway in granulosa cells (32), we proposed that a negative feedback loop between HAPLN1 and AMPK expression exists.

2.4 Proteome and mRNA-Seq Analysis of HAPLN1 Functions in RA-FLSs

As the current molecular interaction network of HAPLN1 is barely barren, to get acquaintance with HAPLN1 functions in

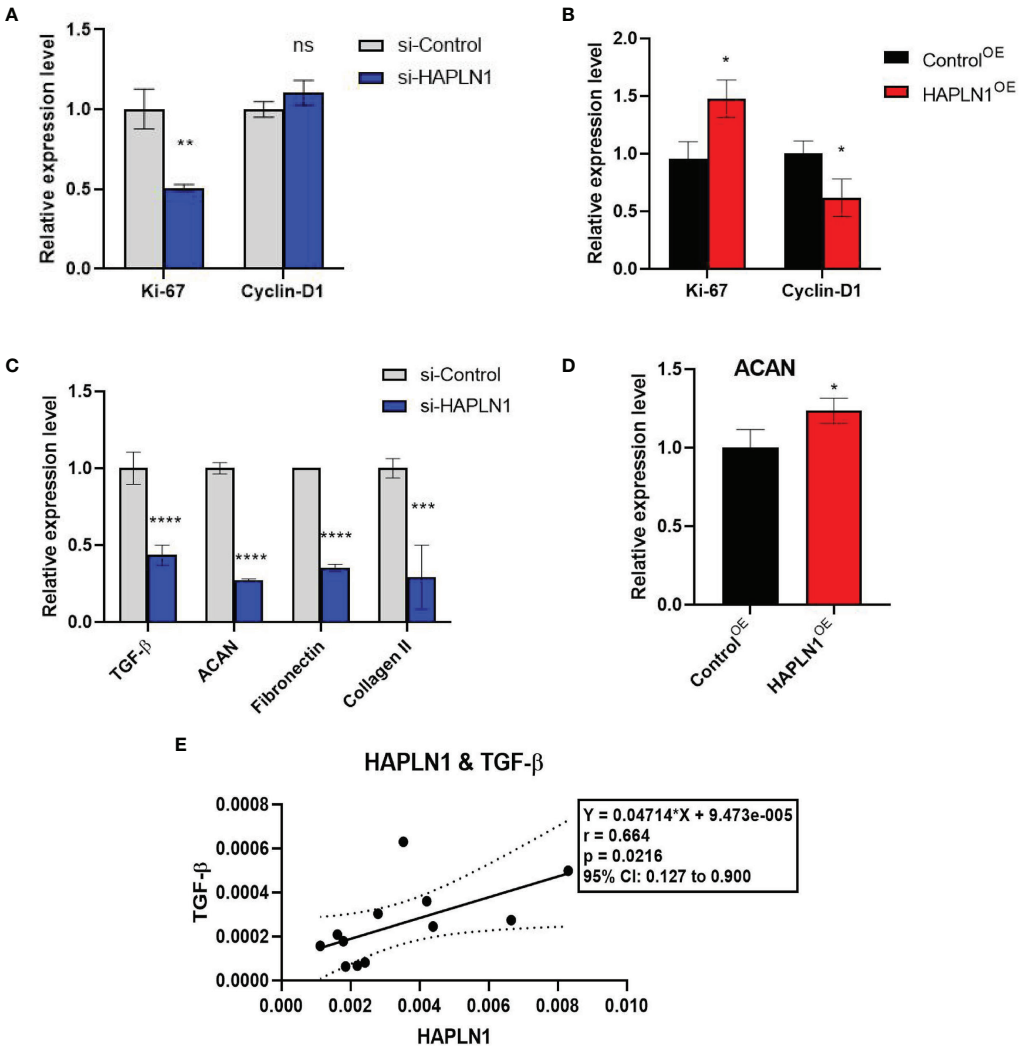

FIGURE 5 | The effects of si-HAPLN1 and HAPLN1^{OE} on RA-FLS-derived cell-cycle and structure molecules. **(A)** si-HAPLN1 transfection decreased Ki-67 mRNA expression significantly, **(B)** HAPLN1^{OE} transfection increased Ki-67 but down-regulated Cyclin D1 expression in RA-FLSs. **(C)** Expression of mRNA of TGF-β, ACAN, fibronectin, and collagen II were down-regulated by si-HAPLN1 treatment in RA-FLSs, while **(D)** ACAN was significantly up-regulated by HAPLN1^{OE} transfection. **(E)** Pearson correlation coefficient analysis showed relative mRNA levels from the si-control group, with a strong positive correlation (r = 0.66, 95%CI [0.13, 0.90], $p < 0.05$) between TGF-β and HAPLN1. *$p < 0.05$; **$p < 0.01$; ***$p < 0.001$; ****$p < 0.0001$; ns, not significant.

RA-FLSs from a more comprehensive view, proteomics and transcriptome analyses were done with rHAPLN1 treated or si-HAPLN1 transfected RA-FLSs to further investigate HAPLN1 functions in RA-FLSs.

2.4.1 Proteomics Analysis

We identified 443,973 matched spectra and 4184 quantifiable proteins in RA-FLSs from NC, si-HAPLN1, and rHAPLN1 groups (**Supplementary Table S5**). Principal component analysis (PCA) indicated a high level of aggregation between duplicated samples, demonstrating the quantitative reproducibility of experiments (**Supplementary Figure S6**). Among the identified proteins, 14 were up-regulated and 47 were down-regulated after si-HAPLN1 transfection. Besides, 101 proteins were up-regulated and 82 were down-regulated after rHAPLN1 treatment as compared to NC (**Figures 7A, B**). Compared to the control siRNA-treated RA-FLSs (NC group) and as shown by KEGG enrichment analysis, differentially enriched proteins (DEPs) in si-HAPLN1-treated RA-FLSs were enriched in pathways including *Staphylococcus aureus* infection, systemic lupus erythematous (SLE), cardiomyopathy, COVID-19, and ribosome (**Figure 7C**). RA-FLSs treated with rHAPLN1 were enriched in pathways including protein digestion, *S. aureus* infection, ECM-receptor interaction, RA, p53 signaling pathway, cholesterol metabolism, PI3K-Akt signaling pathway, JAK-STAT signaling pathway, and pathways for various cancers (**Figure 7D**). More specifically, through clustering analysis, the down-regulated DEPs of the si-HAPLN1 group were enriched in

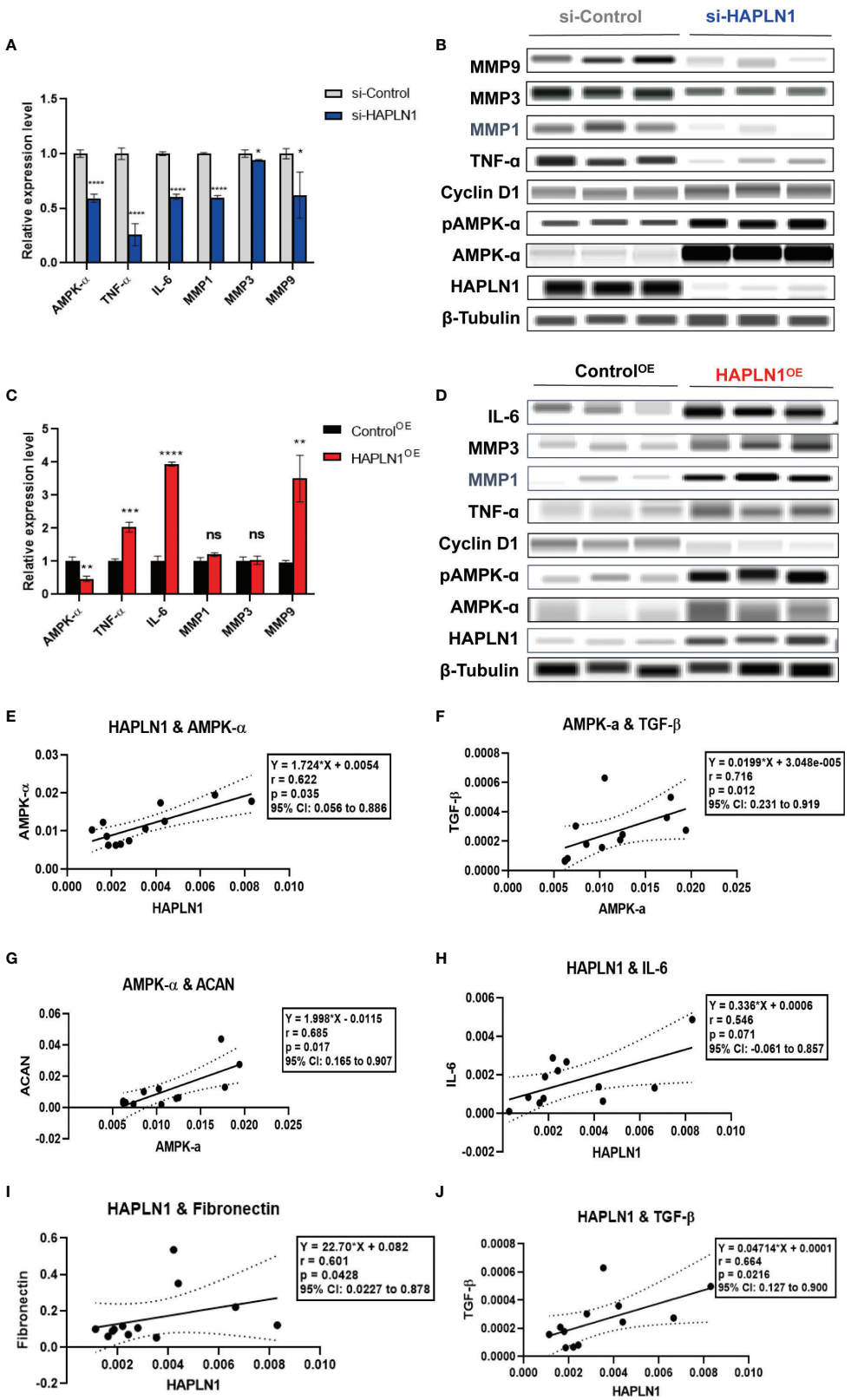

FIGURE 6 | Continued

FIGURE 6 | The effects of si-HAPLN1 and HAPLN1^{OE} on RA-FLS-derived cytokines. **(A, B)** si-HAPLN1 transfection to RA-FLSs inhibited TNF-α, IL-6, MMP1, MMP3, and MMP9 mRNA and protein expression; the mRNA level of AMPK-α was reduced, but AMPK-α and pAMPK-α were up-regulated in the protein level. Expression of Cyclin D1 seems unaffected by si-HAPLN1 transfection. **(C, D)** After over-expression of HAPLN1 in RA-FLSs, TNF-α, IL-6, and MMP9 mRNA and protein expressions were up-regulated while AMPK-α was down-regulated at the mRNA level but AMPK-α and pAMPK-α were up-regulated at the protein level. Cyclin D1 proved to be down-regulated in the protein level by HAPLN1^{OE} transfection. **(E)** In control si-RNA-treated RA-FLSs form multiple tests, **(E–G)** AMPK-α mRNA positively correlated with HAPLN1, TGF-β, and ACAN. **(H-J)** HAPLN1 mRNA shows positive correlations with fibronectin, TGF-β, and IL-6 expression. $^{*}p < 0.05$; $^{**}p < 0.01$; $^{***}p < 0.001$; $^{****}p < 0.0001$; ns, not significant. si-Control, negative control management of si-HAPLN1 transfection; Control^{OE}, negative control management of HAPLN1^{OE} transfection.

S. aureus infection, SLE, TNF signaling pathway, COVID-19, and ribosome. Therefore, si-HAPLN1 treatment mostly results in DEPs that participate in down-regulating proteins related to inflammation. On the other hand, in the rHAPLN1-treated RA-FLSs, the down-regulated DEPs involved are in cellular senescence, drug metabolism, p53 signaling pathway, glutathione metabolism, RA, and cytokine-cytokine receptor interactions; the up-regulated DEPs involved are in cytochrome P450, malaria, platelet activation, JAK-STAT signaling pathway, PI3K-Akt signaling pathway, PPAR signaling pathway, human papillomavirus infection, relaxin signaling pathway, chemical carcinogenesis, microRNAs in cancer, cholesterol metabolism, amoebiasis, focal adhesion, and ECM-receptor interaction (**Supplementary Figure S7**). Based on these results, it is clear that rHAPLN1 treatment mainly leads to pro-inflammation, activation of metabolism, and carcinogenesis. However, pathway enrichment analysis also indicated cell adhesion reinforcement that confirms our transwell and wound healing assays.

As an example, we took the TNF signaling pathway affected by si-HAPLN1 transfection for description of our proteomics results. Tumor necrosis factor receptor type 1-associated death domain protein (TRADD) and mitogen activated protein kinases (MKK3/6), known for their role in apoptosis and cell survival were found to be down-regulated (**Figure 7E**). In rHAPLN1-treated RA-FLSs, up-regulation of MMPs and down-regulation of CyclinD1 were observed (**Figure 7F**). This is in accordance with our results obtained with HAPLN1^{OE} transfection in RA-FLSs (**Figures 5B, 6C, D**). An up-regulated multifunctional matrix glycoprotein thrombospondin-1 (TSP-1) together with matrix metalloproteinases (MMPs) suggest an increased level of angiogenesis, which is a classical pathology feature of pannus in RA (33). Up-regulated expression of collagen within the ECM-receptor interaction pathway (**Supplementary Figure S7**) is in accordance with the reduced expression of collagen II gene after transfection with si-HAPLN1 and with up-regulated expression of ACAN after transfection with HAPLN1^{OE} (**Figures 5C, D**). Proteomics results indicate upregulation of the expression of collagen, laminin, and thrombospondin (**Supplementary Figure S8**), which are associated with cell migration (34, 35).

Notably, rHAPLN1 up-regulated DEPs within various metabolism pathways. High demands for energy and biosynthetic precursors are well known in the pathogenic nature of RA (36). CYP1B1, glutathione S-alkyltransferase (EC: 2.5.1.18), cytochrome P450 (EC: 1.14.14.1), and aldehyde dehydrogenase (EC: 1.2.1.5) were up-regulated in the metabolism of xenobiotics *via* the cytochrome P450 pathway (**Supplementary Figure S9**). These four enzymes were reported to participate in the development of various cancers (37–40). Although these targets have not been well investigated in RA, detection of a higher metabolic level, along with the up-regulated expression of pro-inflammatory DEPs, suggest the effects of rHAPLN1 on the viability of RA-FLSs.

2.4.2 mRNA Sequencing Analysis

mRNA sequencing analysis was done with rHAPLN1- or PBS-treated RA-FLSs. Principal component analysis (PCA) showed a high level of aggregation between duplicated samples, suggesting the quantitative reproducibility of experiments (**Supplementary Figure S10**). Among the 504 differentially expressed genes (DEGs), 439 were up-regulated with the top 6 genes being RP11-231C14.4 (an uncharacterized gene), ANKRD36, NPIPB11, NPIPB4, BRCA2, and GOLGA6L4. At the same time, 65 genes such as KRT81, PXMP2, JHDM1D-AS1, and IL33 were down-regulated (**Figures 8A, B**). Two DEGs (up-regulated LRP1 and down-regulated CRIP1) were in accordance with the results found in our proteome analysis (**Figure 8B**). Metascape pathway analysis of 439 up-regulated DEGs treated by rHAPLN1 showed main enrichment of genes in the GTPase cycle, cell cycle, and regulation of cell division (**Figure 8C**). KEGG analysis showed enrichment in herpes simplex virus 1 infection, hypertrophic cardiomyopathy, and others (**Supplementary Figure S11**). Moreover, GSEA analysis was performed to compare rHAPLN1 and PBS groups. The rHAPLN1 group was found to positively associate with the pathways of extracellular matrix structural constituents, alpha actin binding, metalloaminopeptidase activity, proteoglycan binding, focal adhesion, regulation of protein exit from endoplasmic reticulum, lipid translocation, regulation of androgen receptor signaling pathway, retrograde axonal transport, dendritic spine development, peptide cross linking, and insulin-like growth factor receptor signaling pathway (**Supplementary Figure S12**). Although only 2 overlapping targets were identified in our proteomics study, these enriched functional pathways were in accordance with proteomics analysis and could potentially explain the effects of HAPLN1 on the proliferation, migration, and apoptosis of RA-FLSs.

3 DISCUSSION

HAPLN1, discovered 50 years ago, has a wide range of physiological effects with an important contribution to cartilage formation and homeostasis as well as to the

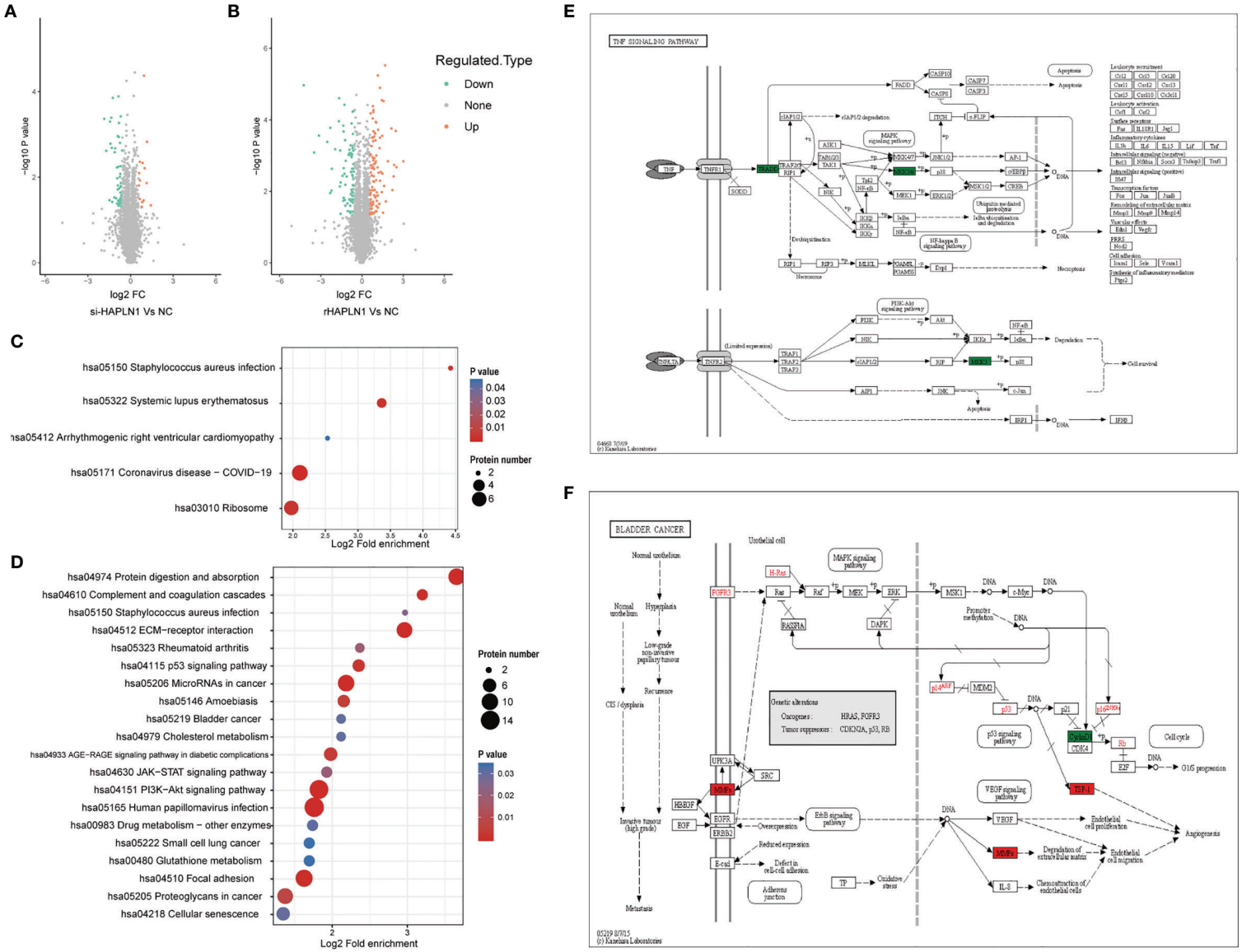

FIGURE 7 | Proteomic analysis of si-HAPLN1- and rHAPLN1-treated RA-FLSs. **(A, B)** Among the quantifiable proteins, 14 were up-regulated and 47 were down-regulated by si-HAPLN1 transfection. There were 101 proteins up-regulated, and 82 were down-regulated by rHAPLN1 treatment compared to NC. **(C)** KEGG enrichment analysis shows the pathways associated with DEPs of si-HAPLN1-treated RA-FLSs. **(D)** KEGG enrichment analysis shows the top 20 pathways associated with DEPs of rHAPLN1-treated RA-FLSs. **(E)** DEPs of si-HAPLN1-treated RA-FLSs enriched in the TNF signaling pathway. **(F)**. DEPs of rHAPLN1-treated RA-FLSs enriched in the bladder cancer pathway. Targets in red blocks represent up-regulation, in green blocks represent down-regulation.

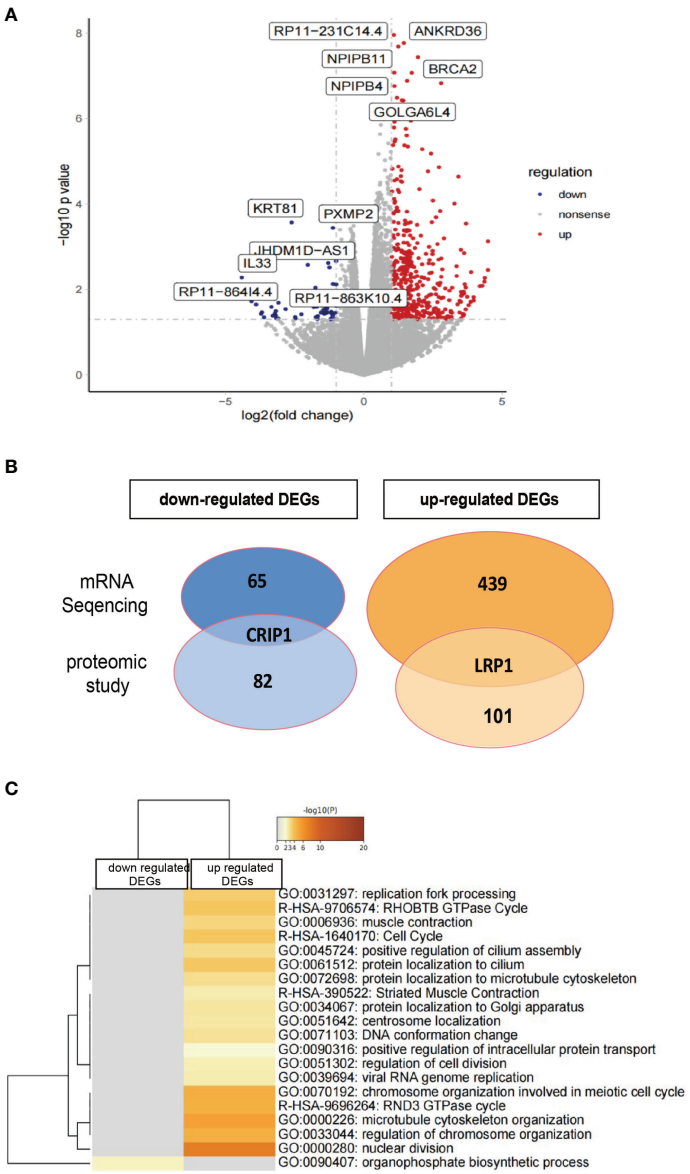

FIGURE 8 | Transcriptome analysis of rHAPLN1-treated RA-FLSs. **(A)** Among the 504 DEGs detected, 439 were up-regulated and 65 were down-regulated. **(B)** Two DEGs detected (up-regulated LRP1 and down-regulated CRIP1) were in accordance with the proteomic studies. **(C)** Metascape analysis of DEGs demonstrated an enrichment of various pathways including replication fork processing, GTPase cycle, cell cycle, and cell division.

regulation of the development of the central nervous system (41). Besides HAPLN1, the HAPLN family includes paralogs of HAPLN2, HAPLN3, and HAPLN4, all of which related pathways are Phospholipase-C Pathway and Integrin Pathway. Annotations related to these genes include extracellular matrix structural constituent and hyaluronic acid binding. They constitute a HAPLN family (42, 43). HAPLN1 interacts with the globular domains of hyaluronic acid and proteoglycans, such as aggrecan, versican, and α-trypsin inhibitor in the ECM, to form a stable ternary complex and contributes to the compression resistance and shock absorption of the joints (44). During the process of chondrogenesis and differentiation of human mesenchymal stem cells (hMSCs), HAPLN1 expression reached its peak level between 6 and 12 days (45). Perinatal mice with inactivated HAPLN1 developed lethal achondroplasia, with their extremities and vertebral cartilage lacking proteoglycan deposition and having a reduced number of hypertrophic chondrocytes (46). In addition, HAPLN1 was shown to have the properties of an oncogene contributing to an increased susceptibility to lung cancer (47), aggressiveness of hepatocellular carcinomas (48), and drug resistance to multiple myeloma (49).

We have reported HAPLN1 as one of the most obviously up-regulated DEGs in RA-FLSs and upon activation of AMPK by metformin HAPLN1 secretion has increased in RA-FLSs (9). Based on AMPK functions and the use of metformin in RA, we hypothesized that an increase in the levels of HAPLN1 in RA-FLSs could help protect the joints (9). In this study, we demonstrated an increase in HAPLN1 expression in the synovium and plasma samples from RA patients. Over-expression of HAPLN1 with a plasmid vector or treatment with rHAPLN1 increased the proliferation but decreased apoptosis of RA-FLSs. Although si-HAPLN1 transfection did not show any effect on proliferation, it induced apoptosis of RA-FLSs significantly. So, HAPLN1 seems to be an oncogenic gene, and it could activate the viability of RA-FLSs.

Apart from hyaluronic acid and proteoglycans, interactions between HAPLN1 and other molecules have been investigated. For example, TNF-α-activated mitogen-activated kinase (MEK) in chondrocytes regulates the expression of HAPLN1, and controls the catabolism and anabolism of the extracellular matrix of chondrocytes (50). In multiple myeloma cells, HAPLN1 can activate the NF-ƙB pathway to acquire resistance to bortezomib (49). In granulosa cells, HAPLN1 can potentially promote the PKA-RUNX1/RUNX2 pathway (9, 32). In this study, upon silencing HAPLN1, pro-inflammatory factors such as TNF-α, MMPs, and IL-6 as well as structure-related molecules such as TGF-β, fibronectin, and ACAN were down-regulated. Conversely, $HAPLN1^{OE}$-treated RA-FLSs showed up-regulation of TNF-α, MMPs, IL-6, and ACAN expression. In untreated RA-FLSs, the relative mRNA expression of HAPLN1 was positively associated with that of TGF-β and IL-6. The Ki-67 has been widely used as a proliferation marker for most human tumor cells (51). Its expression was decreased after si-HAPLN1 transfection but increased after $HAPLN1^{OE}$ treatment. Based on these findings and the current knowledge, HAPLN1 is expected to be able to promote pro-inflammatory secretory phenotypes and to contribute to the regulation of structural molecules in cells.

AMPK and its related pathway have been broadly investigated with participation in glucose metabolism and inflammation reaction, generally in an inhibitory way (31), specifically, inflammatory cytokines such as TNF-α, IL-6, IL-17, NF-ƙB, and MMPs are directly or indirectly inhibited (52, 53). Relative mRNA expression of AMPK-α and HAPLN1 in untreated RA-FLSs showed a positive correlation, which is consistent with the observation made on plasma samples from RA patients. Thus, in this study, we intended to examine whether AMPK is affected by HAPLN1 expression to clarify its effect on inflammation. However, both si-HAPLN1- and $HAPLN1^{OE}$-treated RA-FLSs down-regulated AMPK-α expression at the mRNA level, but not the protein level, of pAMPK-α. This suggests the presence of a complex feedback circle between AMPK-α and HAPLN1. AMPK and its phosphorylation levels are recognized to be especially vulnerable to variations in the metabolism status such as the AMP/ATP ratio (54). Based on our omics study, we proposed that HAPLN1 turns cells into a more hyperactive and hypermetabolism status. So, after silencing HAPLN1, a lower metabolic status of higher AMP/ATP ratio results in an increased level of pAMPK-α. However, a higher metabolic status accompanied by inflammation lowered the AMP/ATP ratio as represented by up-regulated pAMPK-α. Such a hypothesis needs further experimental validation.

Furthermore, Cyclin D1 is involved in the regulation of cell proliferation during the G1 phase of the cell cycle. Given the frequent over-expression of Cyclin D1 in cancer cells, its expression appears to be closely linked with carcinogenesis (55). Cyclin D1 has a central role in mediating invasion and metastasis of cancer cells by controlling Rho/ROCK signaling and matrix deposition of thrombospondin-1 (56). We designed to check this target to verify possible promotion of cell viability by HAPLN1. In this study, however, the mRNA expression levels of Cyclin D1 in RA-FLSs was significantly decreased by $HAPLN1^{OE}$ treatment, which might possibly explain its inhibitory ability on RA-FLS migration. There is a dilemma in clarifying the role of HAPLN1 in RA-FLSs viability by functional studies in the cancer research field because an increased level of HAPLN1 seems to be associated with a higher degree of aggressiveness, leading to stemness of various cancers (47, 48, 57) while achieving robust ECM restrictions on metastasis of cancer cells (19, 20).

Proteomic and mRNA-seq results showed the function of HAPLN1 in RA-FLSs from a holistic view. With highly significant changes observed in the expression of DEPs and DEGs, it is plausible to consider the involvement of HAPLN in a complex network of signaling pathways. Proteomic analysis suggested si-HAPLN1-transfected RA-FLSs were enriched in pro-inflammatory pathways with down-regulated DEPs. It is not strange that the mRNA level and the protein level seem to have a low correlation, as the multi-step process of gene expression involves transcription, translocation, and turnover of mRNAs and proteins (58). Although only 2 targets overlapped with proteomic and transcriptional studies with rHAPLN1-treated RA-FLSs, the omics study reflected activation of inflammation, proliferation, an increase in cell adhesion, and strengthening of ECM functions. These findings were confirmed by the molecular network consisting of MMPs, IL-6, Ki-67, TGF-β, and cyclin D1 as shown by qPCR and Western blot analysis. Genes such as ANKRD36 (59), BRCA2 (60), and GOLGA6L4 (61), which were most up-regulated upon rHAPLN1 treatment, were all reported as oncogenic targets. In consistence with the reported close relation between HAPLN1 and AMPK levels, HAPLN1 seems to be involved in the metabolism of RA-FLSs. Spontaneously resolving joint inflammation in RA was reported to be dependent on the metabolic agility of FLS (62), and increased levels of SUMOylation links metabolic and aggressive phenotype of RA-FLSs (63). Therefore, altering metabolic changes might be a key to developing joint-protective strategies in RA-FLSs (64) and more research is required to decipher the complex network of HAPLN1 functions contributing to the altered metabolic status of RA-FLSs.

In conclusion, HAPLN1 accelerates proliferation and reduces apoptosis of RA-FLSs to form a pathological pannus, mimicking the aggressive feature of cancer cells. Based on physiological

development and oncology studies, HAPLN1 seems to be an oncogene but having an opposing feature on cell adhesion and inhibition of migration. By combining biological experiments and the observations made from proteomics and mRNA sequencing analysis, our results suggest HAPLN1 as a pathogenic factor in RA. Future in-depth studies, especially those related to animal experiments, are mandatory for better understanding of the role of HAPLN1 in RA.

4 MATERIAL AND METHODS

4.1 Patients' Characteristics and Samples

We used blood samples from 61 RA and 20 OA patients and 12 age- and gender-matched healthy controls (HC) for measuring HAPLN1 levels by ELISA. The mean disease course of RA patients was 6.39 years (ranging from 0.2 to 30.0 years). Synovium samples were collected by arthroscopic surgery done with 20 RA and 17 OA patients and used for immunohistochemical (IHC) staining of HAPLN1. The inclusion and exclusion criteria and general information such as age, gender, disease activity, and disease course reported earlier (9) are summarized in **Supplementary Tables S1, 2**.

4.2 Enzyme Linked Immunosorbent Assay (ELISA)

Blood samples of HC, OA, and RA patients were centrifuged after standing at room temperature for 2 h, at 1500 g for 10 min to collect the plasma. The HAPLN1 levels were detected by ELISA (RayBiotech, US). Plasma AMPK levels in RA patients were also evaluated by ELISA according to the manufacturer's protocol (Jianglaibio, China). The SuPerMax 3000FA absorbance microplate reader (Flash Co. Ltd., China) was used to read the optical density (OD) values at 450 nm and concentrations of specific proteins were calculated based on the standard curve.

4.3 Immunohistochemical (IHC) Staining for HAPLN1

Synovium samples collected from 20 RA and 17 OA patients for IHC staining of HAPLN1 were prepared as reported earlier (9). Rabbit monoclonal anti-HAPLN1 antibody (Abcam, US) was added as the primary antibody (1:50) and incubated for 2 h at 37°C. Biotin-conjugated goat anti-rabbit antibodies (ZSGB-Bio, China), streptavidin-peroxidase conjugate, and diaminobenzidine were used as the detecting system. IHC-stained sections were semi-quantified under a microscope. The staining intensity was counted as none (0 points), weak positive (1+), moderate positive (2+), and strong positive (3+). The percentage of positive cells was obtained to calculate the H-Score. The range of H score for each slice was between 0 and 300. The formula of the H-Score is as follows (65):

$$\begin{aligned} H\ \ sore = &(\%\ \ at\ \ weak\ \ positve)\ \ \times 1 \\ &+ (\%\ \ at\ \ morderate\ \ positve) \times 2 \\ &+ (\%\ \ at\ \ strong\ \ positve)\ \ \times 3 \end{aligned}$$

4.4 Isolation and Culture of RA-FLSs

Primary RA-FLSs were acquired from 3 untreated RA patients. Isolation and culture of RA-FLSs were reported as before (9). Briefly, FLSs were isolated by enzyme digestion and subsequently cultured in Dulbecco's modified essential medium (DMEM) containing 10% fetal bovine serum (FBS, Invitrogen) and antibiotics (penicillin and streptomycin) at 37° C with 5% CO_2. Cells cultured between passages 4 and 9 were used in this study.

4.5 Small Interfering RNA (siRNA) HAPLN1 Preparation and Transfection

RA-FLSs at 60-70% confluency were transfected with siRNAs (Ribobio Company, China) at 50 nM with Lipofectamine™ 3000 reagent (Invitrogen, US). The following siRNA sequences were used: control siRNA (confidential sequence information) and 3 siRNAs of HAPLN1, si-1 (5'-AGGGTAGAGTGTTTCTGAA-3'), si-2 (5'-CCTGGAAAATTCTCGGATA), and si-3 (5'-ACCTCACTCTGGAAGATTA-3'). The three siRNAs effectively silenced HAPLN1 expression (**Supplementary Figure S2A**), and si-1 was selected randomly and used in subsequent studies. The negative control (NC) group denoted control siRNA transfection of RA-FLSs in the experiment.

4.6HAPLN1 Over-Expression Vector Preparation and Transfection

For $HAPLN1^{OE}$ RA-FLSs experiments, HAPLN1 over-expression plasmid and its control were constructed and packaged by Ubigene Biosciences (Guangzhou, China). The stbl3 strain plasmid cytomegalovirus vector-infected cells were cultured in LB medium (QDRS Biotec, China) with 100 g/ml of ampicillin under 37°C, 225 rpm for 24 h. The $HAPLN1^{OE}$ plasmid vector and its negative control (NC) were then isolated with the Genopure Plasmid Maxi Kit (Roche, US). RA-FLS at 60-70% confluency was transfected with $HAPLN1^{OE}$ vector or its negative control with Lipofectamine™ 3000 reagent (Invitrogen). The effects of $HAPLN1^{OE}$ plasmid vector are shown in **Supplementary Figure S2B**.

4.7 MTT Assay

MTT assay was used to ascertain FLSs viability transfected with si-HAPLN1, $HAPLN1^{OE}$, or their corresponding NC, or treated with rHAPLN1 (recombinant human HAPLN1 protein, Abcam, US) at different concentrations (0, 25, and 50 ng/ml). FLSs samples (si-HAPLN1 vs. its negative control, $HAPLN1^{OE}$ vs. its negative control, or treated with different concentrations of rHAPLN1) digested using 0.25% pancreatin were transferred to 96-well plates with $3\text{-}5 \times 10^3$ cells/well. At different time points (24, 48, and 72 h), the viability of the cells was measured using the MTT assay kit (Abcam).

4.8 CCK-8 Assay

Cell viability after transfection with si-HAPLN1, $HAPLN1^{OE}$, or their respective controls, or treated with different concentrations of rHAPLN1, was determined using the Cell Counting Kit-8 (CCK-8, Molecular Technology, Japan) assay.

4.9 TUNEL Assay

RA-FLSs transfected with si-HAPLN1, HAPLN1^{OE}, or their corresponding controls, or treated with rHAPLN1 (0 or 50 ng/ml), were digested and transferred to 6-well plates with 2-3 × 10^5 cells/well, cultured for 48 h, and stained by the One Step TUNEL Apoptosis Assay Kit (Beyotime, China). The apoptosis rate was calculated under a fluorescence microscope (Leica, Germany) with the excitation wavelength at 550 nm (Cy3) and the emission wavelength at 570 nm (red fluorescence).

4.10 Flow Cytometry for FLSs Apoptosis

FLSs apoptosis treated with rHAPLN1 was measured using the Annexin V-FITC/PI Cell Apoptosis Detection Kit (Vazyme, China) by flow cytometry. After treatment of FLSs with rHAPLN1 (0 or 50 ng/ml) for 48 h in 6-well plates, the cells were collected (3×10^5/well), washed twice with PBS, re-suspended in 500 µl 1 × binding buffer, mixed with Annexin-V-fluorescein isothiocyanate (FITC, 5 µl) and propidium iodide (PI, 5 µl), and analyzed using a flow cytometer (BD FACSCantoTM II, US). The scatter diagram was distributed as follows: Q3, healthy cells (FITC-/PI-); Q2, apoptotic cells at an advanced stage (FITC+/PI+); and Q4, apoptotic cells at an early stage (FITC+/PI-). The apoptosis rate was calculated as a ratio of apoptotic cells in P2 (Q4 + Q2).

4.11 Wound Healing Assay

Wound healing assay was conducted to evaluate the migration capacity of FLSs transfected either with si-HAPLN1, HAPLN1^{OE}, or their corresponding controls, or treated with different concentrations (0, 25, and 50 ng/ml) of rHAPLN1. FLS samples (si-HAPLN1 vs. its negative control, HAPLN1^{OE} vs. its negative control, or treated with different concentrations of rHAPLN1) were transferred to 6-well plates with 3 × 10^5 cells/well and cultured with serum free-RPMI 1640 medium. At different time points, the migrating ability of the cells was measured by using the wound healing assay as previously reported (9).

4.12 Transwell Assay

Transwell assay was performed to evaluate the migration capacity of FLSs transfected with si-HAPLN1, HAPLN1^{OE}, or their respective controls, or treated with rHAPLN1. FLSs in each set of experiments were re-suspended after culturing for 24 h. Transwell assay was conducted as previously described (9).

4.13 Quantitative Real-Time Polymerase Chain Reaction (qPCR)

Total RNA from FLSs transfected with si-HAPLN1, HAPLN1^{OE}, or their respective controls, or treated with rHAPLN1, was prepared using TRIzol® Reagent (Thermo Scientific, US) and quantified using Qubit (Thermofisher, US). RNA was reverse transcribed into cDNA using PrimeScript™ RT Master Mix (Takara, Japan). The reaction mixture contained 5 ml of 2 × TB Green Premix Ex Taq II (Takara, Japan), 3 ml of nuclease-free water, 1 ml of cDNA, 0.4 ml of each gene-specific primer, and 0.2 l of ROX reference dye. The qRT-PCR analysis was performed using the Applied Biosystems ViiA™ 7 Real-Time PCR System (Thermofisher, US). Each value represented an average from three independent biological replicates. GAPDH gene expression was used for data standardization. The fold change was calculated using the 2-ΔΔCt method. Primers of GAPDH, AMPK-α, TNF-α, IL-6, TGF-β, ACAN, fibronectin, collagen II, MMP1, MMP3, MMP9, Cyclin-D1, and Ki-67 are given in **Supplementary Table S3**.

4.14 Automated Western Blot Analysis

Total proteins from FLSs transfected with si-HAPLN1, HAPLN1^{OE}, or their respective controls for 48 h were extracted with Cell Lysis Buffer (Cell Signaling, US). Their concentration was measured using the BCA Protein Assay Kit (Merck, US). Relative changes in HAPLN1, pAMPK-α, IL-6, TNF-α, MMP1, MMP3, and MMP9 protein levels were determined. Expression of β-tubulin was selected as an internal reference. Capillary electrophoresis and Western blot analysis were carried out using reagents provided in the kit in accordance to the instructions provided by the user manual (ProteinSimple WES, US) as previously reported (9). Rabbit anti-HAPLN1 antibody (Abcam, US), rabbit anti-TNF-α, AMPK-α, pAMPK-α, MMP-1, MMP-3, IL-6, Cyclin D1, and β-tubulin specific mAbs (Cell Signaling, US) were used (1:100). Goat anti-rabbit secondary antibodies were provided by the ProteinSimple WES kit and applied as instructed. Data were analyzed using an in-built Compass software SW 4.0. The truncated and full-length target protein intensities (area under the curve) were normalized to that of the tubulin peak. In most of the figures, electropherograms were represented as pseudo-blots, generated using Compass software.

4.15 Statistical Analysis

Statistical analysis was performed using GraphPad Prism 8.0 software. All the data were given as mean ± SD. Differences between two groups were evaluated for statistical significance using Student's t-test. One-way ANOVA with Tukey's multiple comparisons test was used to evaluate the differences among three or more groups. Correlations were evaluated using Liner regression and correlation test. $p < 0.05$ was considered statistically significant.

4.16 Proteomics Analysis

Label-free proteomics study was applied to FLSs transfected with si-HAPLN1 or treated with rHAPLN1 (50 ng/ml) and their controls for 48 h (management of each group is given in **Supplementary Table S4**) by PTMBiolabs, Inc. (Hangzhou, China). Each concentration was tested with 3 biological replicates. Cell samples were processed as reported earlier (66). LC–MS/MS proteomics analysis was performed on an EASY-nLC 1000 ultra-performance liquid chromatography (UPLC) system, followed by MS/MS using Q Exactive Plus (ThermoFisher Scientific, US) coupled online to the UPLC system. The MS/MS data were retrieved by the Maxquant search engine (v1.6.6.0). A human database was searched (Swiss-Prot). The decoy database anti-library was used to reduce the false positive rate (FDR). The FDR was adjusted to < 1%, and the minimum score for modified peptides was set > 40. Proteins with a fold-change ≥1.50 or ≤0.67 between si-HAPLN1, rHAPLN1, and their controls were considered as expression significant. Based on the protein sequence alignment method, the protein domain functions were defined by InterProScan (http://www.ebi.ac.uk/

interpro/). Functional annotation enrichment of DEPs was performed by KEGG analysis. The enrichment significance was identified as $p < 0.05$ in the Fisher's exact test and $q < 0.05$ in the Benjamini-Hochberg procedure.

4.17 High-Throughput mRNA Sequencing Analysis

High-throughput RNA sequencing was performed using FLSs after treatment with rHAPLN1 (0 and 50 ng/ml) for 48 h. Each concentration was tested three times. RNA-seq analysis was performed by Seqhealth Technology Co., Ltd (Wuhan, China). Total RNA (2 g) was used for stranded RNA sequencing library preparation using KCTM Stranded mRNA Library Prep Kit for Illumina® (Seqhealth Co., Ltd. China). PCR products corresponding to 200-500 bps were enriched, quantified, and sequenced with Novaseq 6000 sequencer (Illumina), PE150 model. Raw sequencing data were first filtered by Trimmomatic (v. 0.36). Low-quality reads were discarded. The reads contaminated with adaptor sequences were trimmed. Clean data were mapped to the human reference genome from UCSC (https://genome.ucsc.edu/) using STRA software (v. 2.5.3a) with default parameters. Reads mapped to the exon regions of each gene were counted by feature Counts (Subread-1.5.1; Bioconductor) and then RPKMs were calculated. DEGs between groups were identified using the edgeR package (v. 3.12.1) in R studio software (version 3.6). A p-value cut-off of 0.05 and fold-change cut-off of 2.0 were used to judge the statistical significance of gene expression differences. The volcano plot was drawn with the ggplot2 package in R studio. Heatmaps of pathway enrichment analysis of DEGs were generated using Metascape (http://metascape.org) and a *P*-value less than 0.05 was statistically significant. KEGG enrichment analysis for DEGs was performed using KOBAS software (v. 2.1.1) with a p-value cut-off of 0.05. To compare transcriptome characteristics of rHAPLN1 with PBS groups, GSEA software (version 4.0.0) was used. Annotated pathway files (c5.go.bp.v7.4.symbols.gmt) were downloaded in the MSigDB database (http://www.gsea-msigdb.org/gsea/msigdb/collections.jsp). Pathways with a *P*-value less than 0.05 and false discovery rate (FDR) less than 0.2 were significantly enriched.

DATA AVAILABILITY STATEMENT

The RNA-seq data presented in this study have been deposited in the the NCBI Gene Expression Omnibus (GEO) database (https://www.ncbi.nlm.nih.gov/), under accession code GSE200597. The mass spectrometry proteomics data have been deposited to the ProteomeXchange Consortium (http://proteomecentral.proteomexchange.org) via the iProX partner repository with the dataset identifier PXD033131.

ETHICS STATEMENT

The studies involving human participants were reviewed and approved by Ethics Committee of Shenzhen Peoples' Hospital. The patients/participants provided their written informed consent to participate in this study.

AUTHOR CONTRIBUTIONS

Concept and design: YC and DZL. Experiment performance: YC, LYW, BJW, QYW. Acquisition, analysis and interpretation of data: YC, YJC and KSN. Drafting and revising the manuscript: YC, KSN, W-FL and BJW. All authors contributed to the article and approved the submitted version.

FUNDING

The study was funded by the China Postdoctoral Science Foundation Project (No. 2021M701438); National Natural Science Foundation of China No. 81971464) and the National Key Research and Development Program (2019YFC0840600).

ACKNOWLEDGMENTS

We are grateful for the time and effort from all the investigators, doctors, study nurses, and research assistants at the study centers for their invaluable contribution to this study.

SUPPLEMENTARY MATERIAL

The Supplementary Material for this article can be found online at: https://www.frontiersin.org/articles/10.3389/fimmu.2022.888612/full#supplementary-material

REFERENCES

1. Lin YJ, Anzaghe M, Schulke S. Update on the Pathomechanism, Diagnosis, and Treatment Options for Rheumatoid Arthritis. *Cells-Basel* (2020) 9(4):880. doi: 10.3390/cells9040880
2. Bartok B, Firestein GS. Fibroblast-Like Synoviocytes: Key Effector Cells in Rheumatoid Arthritis. *Immunol Rev* (2010) 233:233–55. doi: 10.1111/j.0105-2896.2009.00859.x
3. Bottini N, Firestein GS. Duality of Fibroblast-Like Synoviocytes in RA: Passive Responders and Imprinted Aggressors. *Nat Rev Rheumatol* (2013) 9:24–33. doi: 10.1038/nrrheum.2012.190
4. Smolen JS, Aletaha D, McInnes IB. Rheumatoid Arthritis. *Lancet* (2016) 388:2023–38. doi: 10.1016/S0140-6736(16)30173-8
5. Nygaard G, Firestein GS. Restoring Synovial Homeostasis in Rheumatoid Arthritis by Targeting Fibroblast-Like Synoviocytes. *Nat Rev Rheumatol* (2020) 16:316–33. doi: 10.1038/s41584-020-0413-5
6. Caire R, Audoux E, Courbon G, Michaud E, Petit C, Dalix E, et al. YAP/TAZ: Key Players for Rheumatoid Arthritis Severity by Driving Fibroblast Like Synoviocytes Phenotype and Fibro-Inflammatory Response. *Front Immunol* (2021) 12:791907. doi: 10.3389/fimmu.2021.791907
7. Mizoguchi F, Slowikowski K, Wei K, Marshall JL, Rao DA, Chang SK, et al. Functionally Distinct Disease-Associated Fibroblast Subsets in

Rheumatoid Arthritis. *Nat Commun* (2018) 9:789. doi: 10.1038/s41467-018-02892-y
8. Swann DA, Powell S, Broadhurst J, Sordillo E, Sotman S. The Formation of a Stable Complex Between Dissociated Proteoglycan and Hyaluronic Acid in the Absence of a Link Protein. *Biochem J* (1976) 157:503–6. doi: 10.1042/bj1570503
9. Chen Y, Qiu F, Yu B, Chen Y, Zuo F, Zhu X, et al. Metformin, an AMPK Activator, Inhibits Activation of FLSs But Promotes HAPLN1 Secretion. *Mol Ther Methods Clin Dev* (2020) 17:1202–14. doi: 10.1016/j.omtm.2020.05.008
10. Evanko SP, Gooden MD, Kang I, Chan CK, Vernon RB, Wight TN. A Role for HAPLN1 During Phenotypic Modulation of Human Lung Fibroblasts *In Vitro*. *J Histochem Cytochem* (2020) 68:797–811. doi: 10.1369/0022155420966663
11. Wirrig EE, Snarr BS, Chintalapudi MR, O'Neal JL, Phelps AL, Barth JL, et al. Cartilage Link Protein 1 (Crtl1), an Extracellular Matrix Component Playing an Important Role in Heart Development. *Dev Biol* (2007) 310:291–303. doi: 10.1016/j.ydbio.2007.07.041
12. Danieli MG, Markovits D, Gabrielli A, Corvetta A, Giorgi PL, van der Zee R, et al. Juvenile Rheumatoid Arthritis Patients Manifest Immune Reactivity to the Mycobacterial 65-kDa Heat Shock Protein, to its 180-188 Peptide, and to a Partially Homologous Peptide of the Proteoglycan Link Protein. *Clin Immunol Immunopathol* (1992) 64:121–8. doi: 10.1016/0090-1229(92)90189-u
13. Urano T, Narusawa K, Shiraki M, Sasaki N, Hosoi T, Ouchi Y, et al. Single-Nucleotide Polymorphism in the Hyaluronan and Proteoglycan Link Protein 1 (HAPLN1) Gene is Associated With Spinal Osteophyte Formation and Disc Degeneration in Japanese Women. *Eur Spine J* (2011) 20:572–7. doi: 10.1007/s00586-010-1598-0
14. Erwin WM, DeSouza L, Funabashi M, Kawchuk G, Karim MZ, Kim S, et al. The Biological Basis of Degenerative Disc Disease: Proteomic and Biomechanical Analysis of the Canine Intervertebral Disc. *Arthritis Res Ther* (2015) 17:240. doi: 10.1186/s13075-015-0733-z
15. Zheng J, Wu C, Ma W, Zhang Y, Hou T, Xu H, et al. Abnormal Expression of Chondroitin Sulphate N-Acetylgalactosaminyltransferase 1 and Hapln-1 in Cartilage With Kashin-Beck Disease and Primary Osteoarthritis. *Int Orthop* (2013) 37:2051–9. doi: 10.1007/s00264-013-1937-y
16. Layh-Schmitt G, Lu S, Navid F, Brooks SR, Lazowick E, Davis KM, et al. Generation and Differentiation of Induced Pluripotent Stem Cells Reveal Ankylosing Spondylitis Risk Gene Expression in Bone Progenitors. *Clin Rheumatol* (2017) 36:143–54. doi: 10.1007/s10067-016-3469-5
17. Galligan CL, Baig E, Bykerk V, Keystone EC, Fish EN. Distinctive Gene Expression Signatures in Rheumatoid Arthritis Synovial Tissue Fibroblast Cells: Correlates With Disease Activity. *Genes Immun* (2007) 8:480–91. doi: 10.1038/sj.gene.6364400
18. Lin Z, Bei JX, Shen M, Li Q, Liao Z, Zhang Y, et al. A Genome-Wide Association Study in Han Chinese Identifies New Susceptibility Loci for Ankylosing Spondylitis. *Nat Genet* (2011) 44:73–7. doi: 10.1038/ng.1005
19. Ecker BL, Kaur A, Douglass SM, Webster MR, Almeida FV, Marino GE, et al. Age-Related Changes in HAPLN1 Increase Lymphatic Permeability and Affect Routes of Melanoma Metastasis. *Cancer Discov* (2019) 9:82–95. doi: 10.1158/2159-8290.CD-18-0168
20. Kaur A, Ecker BL, Douglass SM, Kugel CR, Webster MR, Almeida FV, et al. Remodeling of the Collagen Matrix in Aging Skin Promotes Melanoma Metastasis and Affects Immune Cell Motility. *Cancer Discov* (2019) 9:64–81. doi: 10.1158/2159-8290.CD-18-0193
21. Wen Z, Jin K, Shen Y, Yang Z, Li Y, Wu B, et al. N-Myristoyltransferase Deficiency Impairs Activation of Kinase AMPK and Promotes Synovial Tissue Inflammation. *Nat Immunol* (2019) 20:313–25. doi: 10.1038/s41590-018-0296-7
22. Samimi Z, Kardideh B, Zafari P, Bahrehmand F, Roghani SA, Taghadosi M. The Impaired Gene Expression of Adenosine Monophosphate-Activated Kinase (AMPK), a Key Metabolic Enzyme in Leukocytes of Newly Diagnosed Rheumatoid Arthritis Patients. *Mol Biol Rep* (2019) 46:6353–60. doi: 10.1007/s11033-019-05078-x
23. Sobecki M, Mrouj K, Colinge J, Gerbe F, Jay P, Krasinska L, et al. Cell-Cycle Regulation Accounts for Variability in Ki-67 Expression Levels. *Cancer Res* (2017) 77:2722–34. doi: 10.1158/0008-5472.CAN-16-0707
24. Takahashi S, Saegusa J, Sendo S, Okano T, Akashi K, Irino Y, et al. Glutaminase 1 Plays a Key Role in the Cell Growth of Fibroblast-Like Synoviocytes in Rheumatoid Arthritis. *Arthritis Res Ther* (2017) 19:76. doi: 10.1186/s13075-017-1283-3
25. Montalto FI, De Amicis F. Cyclin D1 in Cancer: A Molecular Connection for Cell Cycle Control, Adhesion and Invasion in Tumor and Stroma. *Cells-Basel* (2020) 9(12):2648. doi: 10.3390/cells9122648
26. Todhunter RJ, Garrison SJ, Jordan J, Hunter L, Castelhano MG, Ash K, et al. Gene Expression in Hip Soft Tissues in Incipient Canine Hip Dysplasia and Osteoarthritis. *J Orthop Res* (2019) 37:313–24. doi: 10.1002/jor.24178
27. Dalton CJ, Lemmon CA. Fibronectin: Molecular Structure, Fibrillar Structure and Mechanochemical Signaling. *Cells-Basel* (2021) 10(9):2443. doi: 10.3390/cells10092443
28. Xie F, Ling L, van Dam H, Zhou F, Zhang L. TGF-Beta Signaling in Cancer Metastasis. *Acta Biochim Biophys Sin (Shanghai)* (2018) 50:121–32. doi: 10.1093/abbs/gmx123
29. Nolte M, Margadant C. Controlling Immunity and Inflammation Through Integrin-Dependent Regulation of TGF-Beta. *Trends Cell Biol* (2020) 30:49–59. doi: 10.1016/j.tcb.2019.10.002
30. Hou T, Sun X, Zhu J, Hon KL, Jiang P, Chu IM, et al. IL-37 Ameliorating Allergic Inflammation in Atopic Dermatitis Through Regulating Microbiota and AMPK-mTOR Signaling Pathway-Modulated Autophagy Mechanism. *Front Immunol* (2020) 11:752. doi: 10.3389/fimmu.2020.00752
31. Lyons CL, Roche HM. Nutritional Modulation of AMPK-Impact Upon Metabolic-Inflammation. *Int J Mol Sci* (2018) 19(10):3092. doi: 10.3390/ijms19103092
32. Liu J, Park ES, Curry TJ, Jo M. Periovulatory Expression of Hyaluronan and Proteoglycan Link Protein 1 (Hapln1) in the Rat Ovary: Hormonal Regulation and Potential Function. *Mol Endocrinol* (2010) 24:1203–17. doi: 10.1210/me.2009-0325
33. Colville-Nash PR, Scott DL. Angiogenesis and Rheumatoid Arthritis: Pathogenic and Therapeutic Implications. *Ann Rheum Dis* (1992) 51:919–25. doi: 10.1136/ard.51.7.919
34. Huang C, Chen J. Laminin332 Mediates Proliferation, Apoptosis, Invasion, Migration and Epithelialtomesenchymal Transition in Pancreatic Ductal Adenocarcinoma. *Mol Med Rep* (2021) 23(1):11. doi: 10.3892/mmr.2020.11649
35. Halper J, Kjaer M. Basic Components of Connective Tissues and Extracellular Matrix: Elastin, Fibrillin, Fibulins, Fibrinogen, Fibronectin, Laminin, Tenascins and Thrombospondins. *Adv Exp Med Biol* (2014) 802:31–47. doi: 10.1007/978-94-007-7893-1_3
36. Weyand CM, Goronzy JJ. Immunometabolism in Early and Late Stages of Rheumatoid Arthritis. *Nat Rev Rheumatol* (2017) 13:291–301. doi: 10.1038/nrrheum.2017.49
37. Ahmed LA, Younus H. Aldehyde Toxicity and Metabolism: The Role of Aldehyde Dehydrogenases in Detoxification, Drug Resistance and Carcinogenesis. *Drug Metab Rev* (2019) 51:42–64. doi: 10.1080/03602532.2018.1555587
38. Li C, Long B, Qin X, Li W, Zhou Y. Cytochrome P1B1 (CYP1B1) Polymorphisms and Cancer Risk: A Meta-Analysis of 52 Studies. *Toxicology* (2015) 327:77–86. doi: 10.1016/j.tox.2014.11.007
39. Chatterjee A, Gupta S. The Multifaceted Role of Glutathione S-Transferases in Cancer. *Cancer Lett* (2018) 433:33–42. doi: 10.1016/j.canlet.2018.06.028
40. Stipp MC, Acco A. Involvement of Cytochrome P450 Enzymes in Inflammation and Cancer: A Review. *Cancer Chemother Pharmacol* (2021) 87:295–309. doi: 10.1007/s00280-020-04181-2
41. Szarvas D, Gaal B, Matesz C, Racz E. Distribution of the Extracellular Matrix in the Pararubral Area of the Rat. *Neuroscience* (2018) 394:177–88. doi: 10.1016/j.neuroscience.2018.10.027
42. Oohashi T, Edamatsu M, Bekku Y, Carulli D. The Hyaluronan and Proteoglycan Link Proteins: Organizers of the Brain Extracellular Matrix and Key Molecules for Neuronal Function and Plasticity. *Exp Neurol* (2015) 274:134–44. doi: 10.1016/j.expneurol.2015.09.010
43. Spicer AP, Joo A, Bowling RJ. A Hyaluronan Binding Link Protein Gene Family Whose Members are Physically Linked Adjacent to Chondroitin Sulfate Proteoglycan Core Protein Genes: The Missing Links. *J Biol Chem* (2003) 278:21083–91. doi: 10.1074/jbc.M213100200
44. Hirashima Y, Kobayashi H, Gotoh J, Terao T. Inter-Alpha-Trypsin Inhibitor Is Concentrated in the Pericellular Environment of Mouse Granulosa Cells

Through Hyaluronan-Binding. *Eur J Obstet Gynecol Reprod Biol* (1997) 73:79–84. doi: 10.1016/S0301-2115(96)02689-9
45. Xu J, Wang W, Ludeman M, Cheng K, Hayami T, Lotz JC, et al. Chondrogenic Differentiation of Human Mesenchymal Stem Cells in Three-Dimensional Alginate Gels. *Tissue Eng Part A* (2008) 14:667–80. doi: 10.1089/tea.2007.0272
46. Watanabe H, Yamada Y. Mice Lacking Link Protein Develop Dwarfism and Craniofacial Abnormalities. *Nat Genet* (1999) 21:225–9. doi: 10.1038/6016
47. Jones CC, Bradford Y, Amos CI, Blot WJ, Chanock SJ, Harris CC, et al. Cross-Cancer Pleiotropic Associations With Lung Cancer Risk in African Americans. *Cancer Epidemiol Biomark Prev* (2019) 28:715–23. doi: 10.1158/1055-9965.EPI-18-0935
48. Mebarki S, Désert R, Sulpice L, Sicard M, Desille M, Canal F, et al. *De Novo* HAPLN1 Expression Hallmarks Wnt-Induced Stem Cell and Fibrogenic Networks Leading to Aggressive Human Hepatocellular Carcinomas. *Oncotarget* (2016) 7:39026–43. doi: 10.18632/oncotarget.9346
49. Huynh M, Pak C, Markovina S, Callander NS, Chng KS, Wuerzberger-Davis SM, et al. Hyaluronan and Proteoglycan Link Protein 1 (HAPLN1) Activates Bortezomib-Resistant NF-kappaB Activity and Increases Drug Resistance in Multiple Myeloma. *J Biol Chem* (2018) 293:2452–65. doi: 10.1074/jbc.RA117.000667
50. Rockel JS, Bernier SM, Leask A. Egr-1 Inhibits the Expression of Extracellular Matrix Genes in Chondrocytes by TNFalpha-Induced MEK/ERK Signalling. *Arthritis Res Ther* (2009) 11:R8. doi: 10.1186/ar2595
51. Sun X, Kaufman PD. Ki-67: More Than a Proliferation Marker. *Chromosoma* (2018) 127:175–86. doi: 10.1007/s00412-018-0659-8
52. Li WD, Li NP, Song DD, Rong JJ, Qian AM, Li XQ. Metformin Inhibits Endothelial Progenitor Cell Migration by Decreasing Matrix Metalloproteinases, MMP-2 and MMP-9, *via* the AMPK/mTOR/autophagy Pathway. *Int J Mol Med* (2017) 39:1262–8. doi: 10.3892/ijmm.2017.2929
53. Ma F, Hao H, Gao X, Cai Y, Zhou J, Liang P, et al. Melatonin Ameliorates Necrotizing Enterocolitis by Preventing Th17/Treg Imbalance Through Activation of the AMPK/SIRT1 Pathway. *Theranostics* (2020) 10:7730–46. doi: 10.7150/thno.45862
54. Yan Y, Mukherjee S, Harikumar KG, Strutzenberg TS, Zhou XE, Suino-Powell K, et al. Structure of an AMPK Complex in an Inactive, ATP-Bound State. *Science* (2021) 373:413–9. doi: 10.1126/science.abe7565
55. Casimiro MC, Arnold A, Pestell RG. Kinase Independent Oncogenic Cyclin D1. *Aging (Albany NY)* (2015) 7:455–6. doi: 10.18632/aging.100773
56. Li Z, Wang C, Prendergast GC, Pestell RG. Cyclin D1 Functions in Cell Migration. *Cell Cycle* (2006) 5:2440–2. doi: 10.4161/cc.5.21.3428
57. Ivanova AV, Goparaju CM, Ivanov SV, Nonaka D, Cruz C, Beck A, et al. Protumorigenic Role of HAPLN1 and its IgV Domain in Malignant Pleural Mesothelioma. *Clin Cancer Res* (2009) 15:2602–11. doi: 10.1158/1078-0432.CCR-08-2755
58. Schwanhausser B, Busse D, Li N, Dittmar G, Schuchhardt J, Wolf J, et al. Corrigendum: Global Quantification of Mammalian Gene Expression Control. *Nature* (2013) 495:126–7. doi: 10.1038/nature11848
59. Iqbal Z, Absar M, Akhtar T, Aleem A, Jameel A, Basit S, et al. Integrated Genomic Analysis Identifies ANKRD36 Gene as a Novel and Common Biomarker of Disease Progression in Chronic Myeloid Leukemia. *Biol (Basel)* (2021) 10(1):1182. doi: 10.3390/biology10111182
60. Esposito MV, Minopoli G, Esposito L, D'Argenio V, Di Maggio F, Sasso E, et al. A Functional Analysis of the Unclassified Pro2767Ser BRCA2 Variant Reveals its Potential Pathogenicity That Acts by Hampering DNA Binding and Homology-Mediated DNA Repair. *Cancers (Basel)* (2019) 11(10):1454. doi: 10.3390/cancers11101454
61. Strausberg RL, Feingold EA, Grouse LH, Derge JG, Klausner RD, Collins FS, et al. Generation and Initial Analysis of More Than 15,000 Full-Length Human and Mouse cDNA Sequences. *Proc Natl Acad Sci USA* (2002) 99:16899–903. doi: 10.1073/pnas.242603899
62. Falconer J, Pucino V, Clayton SA, Marshall JL, Raizada S, Adams H, et al. Spontaneously Resolving Joint Inflammation is Characterised by Metabolic Agility Of Fibroblast-Like Synoviocytes. *Front Immunol* (2021) 12:725641. doi: 10.3389/fimmu.2021.725641
63. Wang C, Xiao Y, Lao M, Wang J, Xu S, Li R, et al. Increased SUMO-Activating Enzyme SAE1/UBA2 Promotes Glycolysis and Pathogenic Behavior of Rheumatoid Fibroblast-Like Synoviocytes. *JCI Insight* (2020) 5(18):e135935. doi: 10.1172/jci.insight.135935
64. Bustamante MF, Garcia-Carbonell R, Whisenant KD, Guma M. Fibroblast-Like Synoviocyte Metabolism in the Pathogenesis of Rheumatoid Arthritis. *Arthritis Res Ther* (2017) 19:110. doi: 10.1186/s13075-017-1303-3
65. Pierceall WE, Wolfe M, Suschak J, Chang H, Chen Y, Sprott KM, et al. Strategies for H-Score Normalization of Preanalytical Technical Variables With Potential Utility to Immunohistochemical-Based Biomarker Quantitation in Therapeutic Response Diagnostics. *Anal Cell Pathol (Amst)* (2011) 34:159–68. doi: 10.3233/ACP-2011-014
66. Zhang Z, Xie H, Zuo W, Tang J, Zeng Z, Cai W, et al. Lysine 2-Hydroxyisobutyrylation Proteomics Reveals Protein Modification Alteration in the Actin Cytoskeleton Pathway of Oral Squamous Cell Carcinoma. *J Proteomics* (2021) 249:104371. doi: 10.1016/j.jprot.2021.104371

Conflict of Interest: The authors declare that the research was conducted in the absence of any commercial or financial relationships that could be construed as a potential conflict of interest.

Advantages of publishing in Frontiers

OPEN ACCESS
Articles are free to read for greatest visibility and readership

FAST PUBLICATION
Around 90 days from submission to decision

HIGH QUALITY PEER-REVIEW
Rigorous, collaborative, and constructive peer-review

TRANSPARENT PEER-REVIEW
Editors and reviewers acknowledged by name on published articles

Frontiers
Avenue du Tribunal-Fédéral 34
1005 Lausanne | Switzerland

Visit us: www.frontiersin.org
Contact us: frontiersin.org/about/contact

REPRODUCIBILITY OF RESEARCH
Support open data and methods to enhance research reproducibility

DIGITAL PUBLISHING
Articles designed for optimal readership across devices

FOLLOW US
@frontiersin

IMPACT METRICS
Advanced article metrics track visibility across digital media

EXTENSIVE PROMOTION
Marketing and promotion of impactful research

LOOP RESEARCH NETWORK
Our network increases your article's readership